UNIVERSIDAD NACIONAL AUTÓNOMA DE MÉXICO

Maestría y Doctorado en Ciencias Bioquímicas

Rol Biológico de la subunidad ζ como un inhibidor unidireccional de la F_1F_O-ATPasa de *Paracoccus denitrificans*

TESIS

QUE PARA OPTAR POR EL GRADO DE:

Doctor en Ciencias

PRESENTA:
QFB. Francisco Guillermo Mendoza Hoffmann

TUTOR PRINCIPAL
Dr. José de Jesús García Trejo
Facultad de Química, UNAM

MIEMBROS DEL COMITÉ TUTOR

Dra. Xóchitl Pérez Martínez
Instituto de Fisiología Celular, UNAM

Dr. Miguel Ángel Cevallos Gaos
Centro de Ciencias Genómicas, UNAM

Ciudad de México. Octubre, 2018

Agradecimientos

A mi tutor el Dr. José de Jesús García Trejo, le agradezco que me tuvo mucha paciencia cuando llegué al laboratorio y que pasó muchas horas enseñándome a hacer experimentos. Y le agradezco aún más esos días en los que brincó conmigo de emoción cuando los experimentos salieron, así como compartió conmigo los momentos de frustración y tristeza cuando éstos no salieron.

Al Dr. Miguel Ángel Cevallos Gaos quién me recibió dos veces en su laboratorio para que avanzara a toda máquina con los experimentos de biología molecular. Le agradezco que cuando los experimentos no me salían y me frustraba, que siempre me motivó y que además, más que un tutor fue un compañero de laboratorio con quien podía platicar de la ciencia y de la vida.

A la Dra. Xóchitl Pérez Martínez, por siempre mostrarme que existían cosas que no sabía, encaminarme a la actualización constante y a ser autocrítico.

Al Dr. Salvador Uribe Carvajal, por permitirme realizar algunos experimentos en su laboratorio, por formar parte de mi comité tutoral de la maestría, los buenos consejos y por las platicas de ciencia.

Al Dr. Diego Gonzalez Halphen, por ser un investigador tan ameno que, aunque nunca formó parte de mi comité tutoral de maestría o doctorado, siempre estuvo al tanto de mi y me dio buenos consejos.

A la Dra. Marietta Tuena Sangri, por todo el apoyo, consejos, la oportunidad de formar parte de sus seminarios y por ser un gran ejemplo como investigadora.

A la memoria del Dr. Armando Gómez Puyou, por sus sabias palabras y excelentes preguntas en los seminarios. Además, nunca olvidaré las palabras motivacionales que me brindó después de mi primer seminario.

Se agradece sobremanera el apoyo técnico de la Mtra. Ángeles Péres Oseguera, técnico del Dr. Miguel Ángel Cevallos Gaos. Sin tu apoyo no hubiera logrado nada en la biología molecular, agrazesco que, aunque tenías mucho trabajo siempre estuviste dispuesta a enseñarme y a platicar conmigo.

Se agradece el apoyo técnico de Mtra. Raquel Ortega técnico del Dr. García Trejo. Porque más allá de los experimentos, es el alma del laboratorio.

Al Dr. Heliodoro Celis Sandoval, por tantas pláticas amenas, por enseñarme a preparar cromatóforos y por ilustrarme sobre las bacterias fotosintéticas.

Se reconoce la colaboración de la Dra. Leticia Ramírez del departamento de Bioquímica de la facultad de Medicina, por su apoyo con los experimentos de Dicroismo Circular y además por las excelentes preguntas en los seminarios que me ayudaron a mejorar como estudiante.

Se reconoce la colaboración de la Dra. Georgina Garza Ramoz del departamento de Bioquímica de la Facultad de Medicina, por permitirnos utilizar su equipo para llevar a cabo los experimentos de potencial de membrana.

A todos los miembros del Laboratorio Nacional de Citometría por su apoyo incondicional en la realización de los experimentos de potencial de membrana en células.

A la Dra. Mariel Zarco Zavala, porque fue mi sensei en el laboratorio cuando ingresé al posgrado y fue muy paciente conmigo, además de enseñarme ha realizar muchos experimentos. Yo no habría llegado a donde llegué si ella no hubiera sido mi sensei.

Al QFB. y casi Mtro. Carlos Chávez, porque al igual que Mariel me tomó bajo su ala cuando llegué al laboratorio. Gracias por los buenos momentos vividos en el laboratorio.

A mi compañero de laboratorio Adán Martínez Torrez, por hacer la vida del laboratorio más amena y por intentar ser tan molesto como yo lo he sido contigo. You are fired!!! Vas a ver que me vas a extrañar.

Al Mtro. Emilio Espinosa Simón, por su ayuda con los experimentos de cuantificación de ATP intracelular y sobre todo por las pláticas de ciencia.

A mis compañeros de laboratorio Alan, porque lo considero como mi hijo pródigo y estoy seguro de que logrará todo lo que se ponga en mente. A Gilberto, quien es un estudiante brillante y acelerado, y por último a Manuel quién es el nuevo miembro de la familia del laboratorio.

A mis compañeros de laboratorio de Cuernavaca: Gabriel, por estar a mi lado cuando los experimentos no salían y motivarme. A Abraham, Semiramis, Lorena, Alejandro de Tijuana, Lozano y Santiago (sigo esperando mi clase de filogénias) por su apoyo incondicional y por haberme aguantado en su laboratorio durante los meses que los acompañé.

A todos los compañeros de posgrado del edificio F: Pablo, Mónica, Carlos, Bere, Telma, Valeria, Gaby, Francisco, Erick, Pablo de Tijuana, Christian, Rosy, Kika, Diego, etc., muchas gracias por las pizzas y las convivencias.

A mis amigos Lucio, Elenae, Omar, Roberto, Ángel, Claudia, por las grandes pláticas de ciencia, por los seminarios que se ponenían tan buenos y ante todo por su amistad.

A todo el personal del Posgrado de Ciencias Bioquímicas, Lety, Norma, Julio y Lilia, quienes han hecho de mi estancia en el posgrado algo que nunca olvidaré.

A todo el personal del edificio F, Lalo, Ale, Karla, Otilia, Iris, Mica, Ana, Halpa y Verito, muchas gracias por todo. Sin el apoyo y las sonrisas de ustedes nada es posible.

A la Facultad de Química, por haberme permitido disfrutar de sus intalaciones y habernos otorgado un laboratorio nuevo el cual pude estrenar y que he disfrutado tanto.

A la memoria de José Jaime Barrera Moreno, quien fue un gran trabajador y que siempre fue en demasía atento con todos los que laboramos en el edificio F.

Al Consejo Naconal de Ciencia y Tecnología (CONACYT), por haberme apoyado durante 6 años con una beca de masetría y luego con una de doctorado (277245) y por el apoyo para el laboratorio en forma del proyecto CB-2011-01-167622. Gracias a dichos apoyos yo pude disfrutar de 6 años maravillosos que fueron mis estudios de posgrado.

Al proyecto de DGAPA IN221216 por permitirnos adquirir todo lo necesario para llevar a cabo los experimentos y por haberme apoyado con una beca para la titulación.

Al programa de Apoyo para Estudios del Posgrado (PAEP), que me apoyó con recursos para asistir a un congreso nacional en la maestría y a cuatro más durante mi doctorado (dos nacionales y dos internacionales).

Dedicatorias

A mis papás por haberme traído a este mundo y por haber sido tan buenos conmigo. Los quiero hoy más más que nunca.

A mi hermana Fernanda, gracias por hacerme una persona más fuerte y por consolarme cuando más lo he necesitado. Nunca olvidaré el día que me enseñaste a hacer mi tarea cuando estaba en primero de primaria.

A mi sobrinito Alex, eres un regalo que ha hecho de mi vida más agradable, ha sido muy duro para mi no estar cerca de ti estos años, pero espero regresar pronto y tratar de ser para ti lo que han sido para mis tíos Billy, Gunter y Héctor.

A mis abuelitas y todos mis tíos, tías y primos (ustedes saben que no los puedo nombrar uno por uno porque serían más nombres que tesis). Gracias por ser parte de mi familia.

A mi mejor amigo José, por aguantarme y por haberme acompañado al cine más de 88 veces en un año. Si algo he extrañado más que nada es ir al cine tres veces en un día y estar sentados en el malecón de Playas sin hacer nada platicando de cualquier cosa.

A mi segunda familia Pinedo García, por haberme aceptado como un hijo y por haberme alentado a seguir adelante. Muchas gracias Sra. Sandra García y al Profe Pinedo que en paz descanse y a mi hermano Jorge.

A mi otra segunda familia Mendoza Gonzalez, que me adoptaron un tiempo y me han apoyado incondicionalmente.

A mis tíos Billy y Gunter. Billy porque desde que tengo memoria ha estado para apoyarme en todo lo que he necesitado. Ante mis ojos eres el ejemplo a seguir como persona. A Gunter, gracias porque durante la universidad fuiste más que un tío mi amigo.

A mi otra segunda familia Olmedo Nieva, gracias por aceptarme como un miembro más de su familia. Me ha causado mucha felicidad formar parte de su familia y se los agradezco muchísimo.

A mi prometida Leslie Olmedo Nieva, sabes que te amo con locura, eres el principal motivo de mi felicidad y ante mis ojos eres la persona más bella y brillante que conozco. Sólo espero que algo de tu brillantez se me pegue porque me hace falta. Te agradezco mucho porque lo poco o mucho que logré en el posgrado fue gracias a que me ayudaste a mejorarlo.

Índice

1 Resumen

El papel biológico de los tres inhibidores naturales de la F_1F_O-ATPasa: IF_1, ε y ζ en siguen siendo controvertidos. La subunidad ζ es un modelo útil para los estudios de eliminación génica, ya que imita a la IF_1 mitocondrial, pero en la F_1F_O-ATPasa de *Paracoccus denitrificans* (*P. denitrificans*) (PdF_1F_O), además es una subunidad monogénica y súpernumeraria. En este trabajo, obtuvimos una cepa derivada de *P. denitrificans* 1222 denominada PdΔζ a la cual se le eliminó el gen que codifica para la subunidad ζ y se determinó su papel en el crecimiento y en la bioenergética celular. Se midió la velocidad de crecimiento celular de la cepa silvestre y la cepa mutante en dos condiciones, en medio nutritivo y en medio mínimo. Subsecuentemente, se midió la velocidad de síntesis de ATP y de hidrólisis de ATP en partículas sub-bacterianas y se compararon ambas actividades en muestras preparadas de ambas cepas. Posteriormente se evaluó el potencial de membrana en partículas sub-bacterianas y en células completas. Se evaluó la expresión del complejo succinato deshidrogenasa en la cepa silvestre en ambas condiciones de cultivo. Finalmente, se purificó la enzima F_1-ATPasa de ambas cepas y se evaluó la actividad de hidrólisis de ATP en tres condiciones diferentes. Los resultados muestran que la falta del gen ζ in vivo restringe fuertemente el crecimiento respiratorio de *P. denitrificans* y éste se restablece mediante la complementación en trans con un gen ζ exógeno. La eliminación del gen ζ aumentó la actividad acoplada de F_1F_O-ATPasa sin afectar la actividad de PdF_1F_O-ATP sintasa, y esta última no se vio afectada en absoluto por la reconstitución *in vitro*. Por lo tanto, ζ funciona como el trinquete de una matraca siendo un inhibidor unidireccional del nanomotor PdF_1F_O-ATPasa que favorece la renovación de la síntesis de ATP para mejorar el crecimiento de las células respiratorias y la bioenergética. Adicionalmente, se estudió la función, presencia y ausencia de la subunidad ζ en otras α-proteobacterias.

2 Abstract

The biological roles of the three natural F_1F_O-ATPase inhibitors, ε, ζ, and IF_1, on cell physiology remain controversial. The ζ subunit is a useful model for deletion studies since it mimics mitochondrial IF_1, but in the F_1F_O-ATPase of *Paracoccus denitrificans* (PdF_1F_O), it is a monogenic and supernumerary subunit. Here, we constructed a *P. denitrificans* 1222 derivative (PdΔζ) with a deleted ζ gene to determine its role in cell growth and bioenergetics. The cell growth rate of the wild strain and the mutant strain were measured under two conditions, in a nutritive medium and in a minimal medium. Subsequently, the rate of synthesis of ATP and hydrolysis of ATP in sub-bacterial particles was measured and both activities were compared in samples prepared from both strains. Then, the membrane potential was evaluated in sub-bacterial particles and in whole cells. The expression of the succinate dehydrogenase complex in the wild strain was evaluated under both culture conditions. Finally, the enzyme F1-ATPase was purified from both strains and the hydrolysis activity of ATP was evaluated in three different conditions. The results show that the lack of ζ in vivo strongly restricts respiratory *P. denitrificans* growth, and this is restored by complementation in trans with an exogenous ζ gene. Removal of ζ increased the coupled F_1F_O-ATPase activity without affecting the PdF_1F_O-ATP synthase turnover, and the latter was not affected at all by ζ reconstitution in vitro. Therefore, ζ works as a unidirectional pawl-ratchet inhibitor of the PdF_1F_O-ATPase nanomotor favoring the ATP synthase turnover to improve respiratory cell growth and bioenergetics. Additionally, we studied the function, presence and absence of the ζ subunit in other α-proteobacteria.

3 Introducción

El adenosín trifosfato (ATP) es la moneda energética utilizada por todos los organismos para llevar a cabo procesos biológicos (1-3). Para sintetizar al ATP, los organismos necesitan condensar al adenosín difosfato (ADP) con fosfato inorgánico (Pi). Existen varias rutas metabólicas que sintetizan ATP a nivel sustrato, tales como la glucólisis (conocida también como vía de Embden-Myerhof-Parnas) (4-6), la vía Entner-Doudoroff (7,8), el ciclo de los ácidos tricarboxílicos (conocida también como ciclo de Krebs) (6,9,10), etc. Sin embargo, la fosforilación oxidativa y la fotofosforilación son las rutas que producen más ATP (11). Estas dos rutas metabólicas utilizan la ATP sintasa para sintetizar al ATP (12-15). Esta enzima sintetiza ATP aprovechando un gradiente electroquímico ($\Delta\mu$) de protones (H^+) o de sodio (Na^+) (16). El gradiente electroquímico es generado por los complejos de la cadena transportadora de electrones ya que bombean protones a través de la membrana mientras llevan a cabo reacciónes de oxido-reducción (16). Una vez generado el gradiente electroquímico, los iones pueden fluir del lado con mayor concentración (lado P) hacia el lado con menor concentración (lado N) pasando por dos hemicanales que se encuentran en la parte membranal de la enzima (17).

Tipos de ATP sintasas

Hay dos tipos de ATP sintasa, la tipo F y la tipo A (18). La ATP sintasa de tipo F está presente en dos dominios de la vida, Eukarya y Bacteria, mientras que la tipo A está presente principalmente en el tercer dominio de la vida: Archaea y en algunos casos raros, en el dominio Bacteria (19,20). Aunque la ATP sintasa de tipo A y de tipo F tienen la misma función y una estructura similar, poseen algunas características que las distinguen (18). La ATP sintasa tipo A tiene un número mayor de subunidades que la tipo F (21).

Composición de las ATP sintasas de tipo F

La ATP sintasa tipo F está compuesta por dos fracciones: F_1 y F_O. La fracción F_1 es soluble en agua y es la porción catalítica de la enzima (22). En bacterias esta porción está expuesta hacia al citoplasma celular, mientras que en eucariontes se encuentra expuesta hacia la matriz mitocondrial o el estroma de los cloroplastos. La fracción F_O es hidrofóbica y se encuentra embebida en la membrana citoplásmica de bacteria o en la membrana interna de las mitocondrias y la membrana tilacoidal de los cloroplastos (17).

Ocho subunidades canónicas están presentes en todas las F_1F_O-ATP sintasas (Tabla 1 y Figura 1A) y forman la estructura más simple encontrada tanto en bacterias (23,24) como en cloroplastos (25). Las ATP sintasas F bacterianas más estudiadas hasta ahora son la de *Escherichia coli* (*E. coli*) y *Geobacillus stearothermophilus* (*G*. *stearothermophilus*) (anteriormente conocida como *Bacillus* PS3), ambas se componen sólo por las 8 subunidades canónicas (24,26). donde la fracción F_1 posee 5 subunidades (α, β, γ, δ y ε) y la fracción F_O 3 (*a*, *b* y *c*) (Tabla 1 y Figura 1A).

Por otro lado, se ha descrito recientemente una subunidad adicional en una clase específica de bacterias, las α-proteobacterias. En esta clase, la fracción F_1 tiene una subunidad adicional llamada ζ por lo que poseen en total 9 subunidades en su enzima (Tabla 1, Figura 1B) (27,28).

Las ATP sintasas de tipo F mitocondriales son estructuralmente más complejas ya que están compuestas por las 8 subunidades canónicas y 8 o más subunidades adicionales denominadas supernumerarias, las cuales ayudan en la dimerización y oligomerización de la enzima (Tabla 1) (23,29).

Subunidades que comprenden a la F_1F_O-ATP sintasa de diferentes organismos.

	Bacteria	Cloroplasto	α-proteobacteria	Mitocondria
F_1	α_3	α_3	α_3	α_3
	β_3	β_3	β_3	β_3
	γ	γ	γ	γ
	δ	δ	δ	OSCP
	***ε**	***ε**	ε	δ
				ε
			***ζ**	***IF$_1$**
F_O	a	IV	a	a or Sub. 6
	b_2	I, II	b_2	b
	$c_{9\text{-}12}$	$III_{9\text{-}12}$	c_{12}	$C_{8\text{-}12}$
				A6L, d, e, f, g, F6.

Tabla 1. Composición de las ATP sintasas. La enzima proveniente de bacterias y de cloroplastos tiene 8 subunidades, la de α-proteobacterias tiene 9 subunidades, y la enzima mitocondrial tiene 16 o más subunidades. Las subunidades se acomodan de acuerdo con sus homólogos correspondientes en las otras enzimas. La subunidad OSCP mitocondrial es el homólogo de δ, y la subunidad δ mitocondrial es homóloga de la subunidad ε de las otras enzimas. La subunidad ε mitocondrial no tiene homólogo en las otras enzimas. Las subunidades inhibidorias están marcadas con un asterisco. La estequiometría de las subunidades se indica en el número en subíndice y cuando la subunidad no tiene número, entonces su estequiometría es uno. Los colores de las subunidades de la Tabla 1 coincide con los colores de las estructuras de la Figura 1.

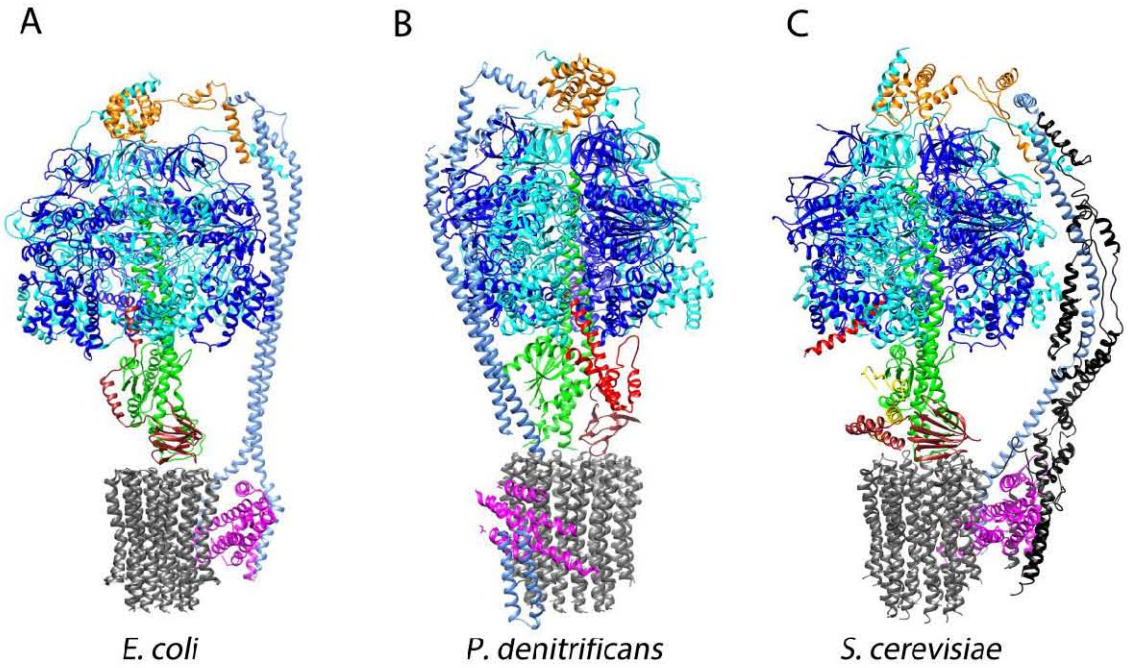

Figura 1. Estructura de la F_1F_O-ATP sintasa de *E. coli*, *P. denitrificans* y *S. cerevisiae*. La F_1F_0-ATP sintasa bacteriana está representada por la enzima de *E. coli* (PDB ID 5T4O). La enzima de *E. coli* se encuentra inhibida por la subunidad ε (marrón). La enzima de las α-proteobacterias está representada por la de *P. denitrificans* (30). La enzima de *P. denitrificans* es se encuentra inhibida por su subunidad ζ (rojo). La enzima mitocondrial está representada por la de *S. cerevisiae* (PDB ID 6CP6) y la subunidad IF_1 de *S. cerevisiae* (PDB ID 3ZIA). La enzima de *S. cerevisiae* se encuentra inhibida por la subunidad IF_1 (roja). La estructura F_1-IF_1 de *S. cerevisiae* (PDB ID 3ZIA) se alineó con la estructura F_1F_0 de *S. cerevisiae*. Luego se eliminó la fracción F_1 de *S. cerevisiae* 3ZIA y se dejó la IF_1 superpuesta sobre la estructura F_1F_0 de *S. cerevisiae*. La alineación se hizo usando el programa PyMol (31). Las imágenes de las estructuras de las tres enzimas se obtuvieron usando el programa UCSF Chimera (32). Los colores de las subunidades de las estructuras coinciden con los colores utilizados de las subunidades de la Tabla 1.

3.1 Síntesis de ATP por la F_1F_O-ATP sintasa

3.2 La Fracción F_O

La F_1F_O-ATP sintasa utiliza el gradiente electroquímico para llevar a cabo su mecanismo de síntesis de ATP (11,16). Ésta va a permitir el paso de iones (H^+ o Na^+) del lado P al lado N de la membrana, funcionando como un molino de agua (Figura 2).

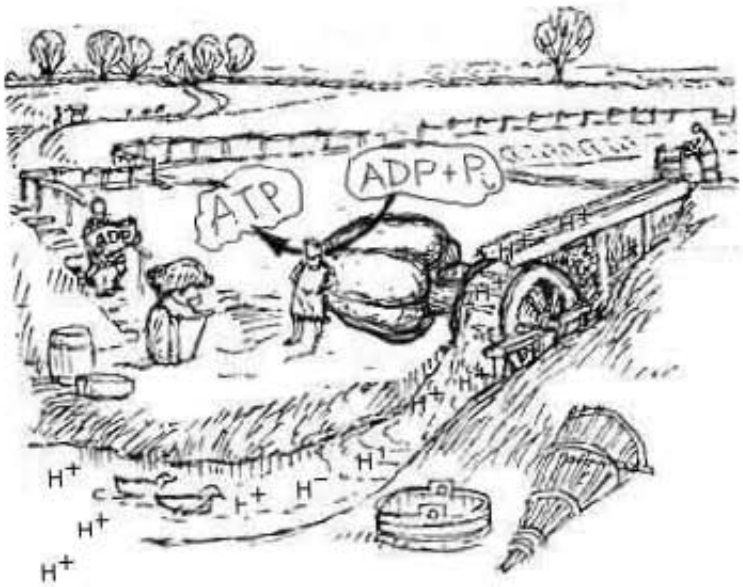

Figura 2. La ATP sintasa es impulsada por el gradiente electroquímico. Caricatura representativa del funcionamiento de la ATP sintasa. La enzima asemeja un molino de agua y el gradiente de protones está representado por el flujo de agua. Figura tomada del libro Bioenergetics 2 (33).

El flujo de los protones de iones (H^+ o Na^+) a través de la membrana, se lleva a cabo a través de los dos hemicanales de la fracción F_O (17,34). Estos hemicanales están en la interfase del anillo *c* y la subunidad *a* (Figura 3). Un hemicanal está en la parte inferior de la interfase y la otra está en la parte superior (observado desde la parte inferior de la F_1F_O). En la interfase del anillo *c* y la subunidad *a* hay una interacción entre una carga negativa y una carga positiva (17,34). La carga negativa de la subunidad *c* proviene de un carboxilato perteneciente a la cadena lateral de un residuo de aspartato o de glutamato (35,36). La carga positiva de la subunidad *a* proviene de un grupo guanidino perteneciente a la cadena lateral de un residuo conservado de arginina (37,38). Los iones (H^+ o Na^+) pasarán a través del hemicanal

inferior y el carboxilato de la subunidad *c* será protonado (17,34). Esta protonación disipa la carga negativa del carboxilato por lo que hay un cambio conformacional de esta cadena lateral (39) y ya no hay interacción con la carga del guanidinio. Ahora, la subunidad *c* protonada se alejará de la carga del guanidino de la subunidad *a* y la subunidad *c* aledaña que se encuentra desprotonada interactuará con la carga del guanidino de la subunidad *a* (17,34). Una vez que todas las subunidades *c* están protonadas, el anillo *c* habrá rotado 360º en la dirección de las manecillas del reloj (visto desde la parte inferior de F_O) (Figura 3). Una vez que el anillo *c* ha girado 360º, la subunidad *c* liberará al protón y éste pasará a través del hemicanal superior y llegará al lado N de la membrana (Figura 3). La subunidad *c* recién desprotonada interactuará de nuevo con la carga de la asparagina de la subunidad *a* y posteriormente recibirá otro protón, repitiéndose el mecanismo. El anillo de subunidades c se mantendrá en constante rotación mientras exista un gradiente electroquímico. El anillo *c* pasará este movimiento de rotación a la subunidad γ de la fracción F_1 a través de las interacciones que hay entre ellas en su interfase. La interfase entre el anillo de subunidades *c* y la subunidad γ es estabilizada por la subunidad ε, la cual aumenta la superficie de contacto entre ellas (Figura 1) (14,40,41). La ausencia de la subunidad ε da lugar a una disociación de la fracción F_1 de la F_O (42,43). Dado que el anillo de subunidades *c* y las subunidades γ y ε giran en unísono, este conjunto de subunidades es conocido como **el rotor** de la ATP sintasa (Figuras 3 y 5). Una vez que la subunidad γ comienza a girar en el sentido de las manecillas del reloj, ésta va a pasar la energía mecánica generada por el anillo de subunidades *c* a las subunidades α y β (Figura 3 y Figura 4) (13).

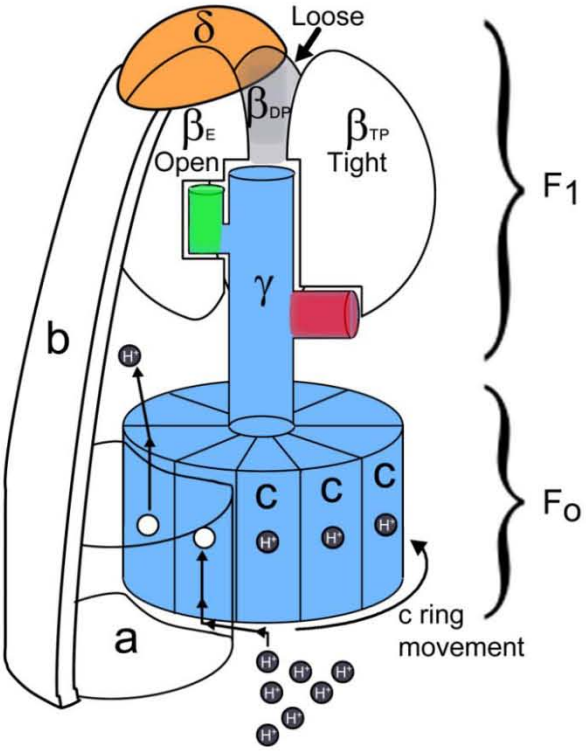

Figura 3. Representación del giro del anillo de subunidades *c* de la ATP sintasa. Los iones (H^+ o Na) pasan a través del hemicanal inferior de la interfase entre la subunidad *a* y el anillo de subunidades *c* (azul), protonando a cada una de éstas. Las subunidades *c* protonadas se alejan de la subunidad *a*. Una vez las subunidades *c* protonadas han girado casi 360º, liberan el protón hacia el hemicanal superior permitiendo el paso de los protones al lano N de la membrana. El anillo de subunidades *c* transmitirá el giro a la subunidad γ (azul) y ésta ocasionará cambios conformacionales en las subunidades β. La asimetría de la subunidad γ está representada por su N-terminal (verde) y su dominio globular (rojo). El N-terminal de la subunidad γ dará lugar al estado conformacional Abierto de la subunidad β y el dominio globular dará lugar al estado Cerrado. Las subunidades del rotor están representadas en azul. La subunidad β en que interactúa con la subunidad β en estado Relajado se representa en gris. Las subunidades α y ε no están incluidas en esta representación. La figura está adaptada de (34).

3.3 La Fracción F_1

La subunidad γ al interactúar con las subunidades α y β da lugar a tres estados conformacionales de ellas, esto se debe a que γ tiene una estructura asimétrica. La asimetría de γ se debe a que la α-hélice de su N-terminal tiene una menor extensión

que la de su C-terminal (Figura 4 color verde y azúl respectivamente). Además, la subunidad γ en su parte inferior tiene un dominio globular (Figura 4 color rojo).

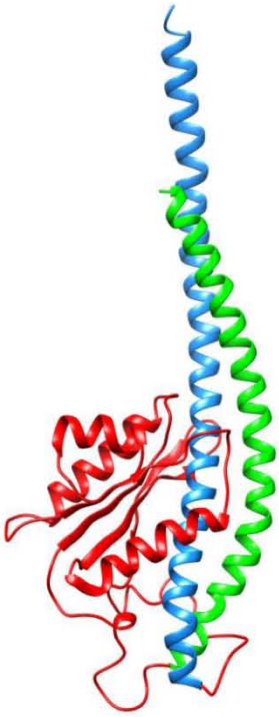

Figura 4. Asimetría estructural de la subunidad γ. Modelo estructural de la subunidad γ de la α-proteobacteria *Sinorhizobium meliloti* (*S. meliloti*), en verde el N-terminal, en rojo el dominio globular y en azul el C-terminal. La subunidad γ de *S. meliloti* se modeló sobre la estructura de la subunidad γ de la F_1F_O de *P. denitrificans* (PDB ID 5DN6) utilizando el programa Swiss Model (44). La imagen de la estructura de la subunidad γ se obtuvo utilizando el programa UCSF Chimera (32).

La posición de γ determinará los estados conformacionales de α y β (Figura 3, Figura 4 y Figura 5). Las subunidades α y β se ensamblan en la forma de un anillo hexamérico que alterna a 3 subunidades α con tres subunidades β (denominado hexámero α_3/β_3). Dado que este hexámero α_3/β_3 se mantiene fijo se le denomina **estator** de la ATP sintasa (Figura 5). La subunidad γ es el eje del hexámero α_3/β_3 (Figura 5), por ello, cuando γ gira su N-terminal y su dominio globular interactúan con diferentes subunidades del hexámero (Figuras 3 y 6).

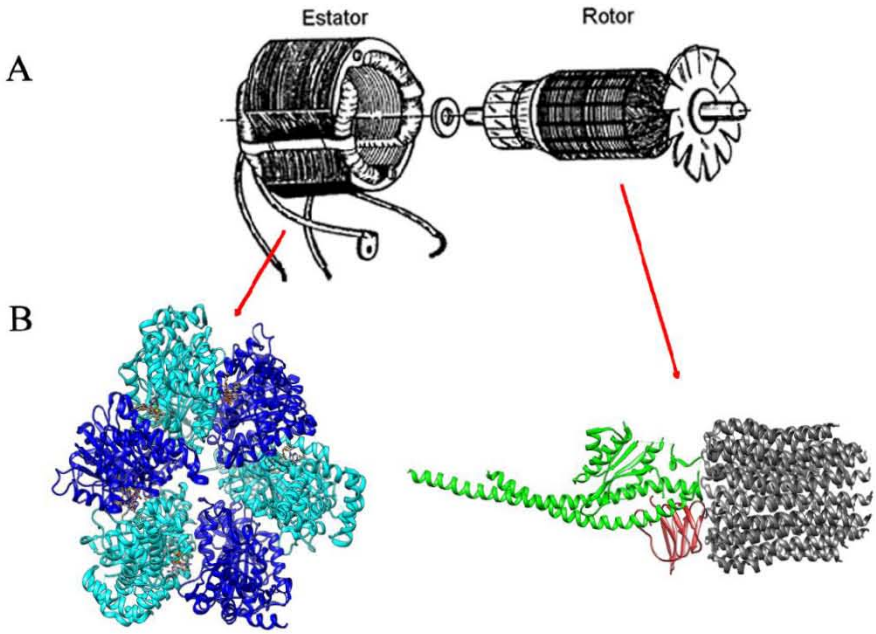

Figura 5. Estructura del Estator y del Rotor de la F_1F_O-ATP sintasa. Comparación de la estructura del Estator y del Rotor de la ATP sintasa con un dibujo de un motor eléctrico separado en sus componentes Estator y Rotor. A) Dibujo de un motor eléctrico, en el que se separa el Estator del Rotor. B) Modelo estructural del hexámero de subunidades α_3/β_3 denominado como el Estator de la enzima (en cian las subunidades α, en azul las subunidades β). B) Modelo estructural de las subunidades γ, ε y el anillo de subunidades *c* (en verde la subunidad γ, en marrón la subunidad ε y en gris el anillo de subunidades *c*). El rotor y el estator del panel B se tomaron del PDB ID 5DN6. La imagen en el panel B de la estructura del estator y del rotor se obtuvo utilizando el programa UCSF Chimera (32).

El hexámero α_3/β_3 tiene seis interfases entre las subunidades α y β. Las seis interfases unen cada una un nucleótido, sin embargo, sólo tres interfases son catalíticas. Cada interfase catalítica estará interacutando con una parte diferente de la subunidad γ, por lo que existen tres estados conformacionales. Para simplificar la explicación, los estados conformacioanles de las interfases catalíticas serán denominadas estados conformacionacionales de la subunidad β. Existen tres estados conformacionales de la subunidad β: **Abierto** (β_E), **Relajado** (β_{DP}) y **Cerrado** (β_{TP}) (Figura 3 y Figura 6) (14,22,45-47). Cuando el estado conformacional de β se encuentra **Abierto**, su sitio de unión a nucleótidos está vacío porque acaba de liberar ATP+Mg y este sitio **Abierto** ahora puede unir ADP+Pi+Mg^{+2} (Figura 3 y

Figura 6). Cuando el estado conformacional de β se encuentra **Relajado**, su sitio de unión a nucleótidos se encuentra uniendo ADP+Pi+Mg^{+2} (Figura 3 y Figura 6). Por último, cuando el estado conformacional de β se encuentra **Cerrado**, su sitio de unión a nucleótidos ha condensado el ADP+Pi en ATP, por lo que este sitio **Cerrado** ahora tiene unido un ATP+Mg (Figura 3 y Figura 6) (46). Como los estados conformacionales de β dependen de las interacciones asimétricas con la subunidad γ, cuando el dominio N-terminal de γ se encuentra interactuando con la subunidad β más cercana, esta interacción obligará a que la subunidad β se encuentre en el estado conformacional **Abierto** (Figura 3 y Figura 6). En ese mismo momento, el dominio globular de γ interactuará con una subunidad β diferente, y esta interacción obligará que la subunidad β se encuentre en el estado conformacional **Cerrado** (Figura 3 y Figura 6). Simultáneamente, la parte de la subunidad γ que no es el dominio N-terminal o globular estará interactuando con la tercera subunidad β. Esta interacción con la parte de la subunidad γ que no es el dominio N-terminal o globular permitirá que la subunidad β se encuentre en el estado conformacional **Relajado** (Figura 3 y Figura 6) (48). Por lo tanto, en un instante en el que la subunidad γ se encuentra en una posición específica, habrá 3 estados conformacionales diferentes para cada una de las tres subunidades β: **Abierto**, **Cerrado** y **Relajado** (Figura 3 y Figura 6) (22). Consecuentemente, cuando γ rota 360° cada subunidad β habrá pasado los tres estados conformacionales. Por ello, cada subunidad β habrá condensado un ATP, significando tres ATP sintetizados por cada rotación completa de γ.

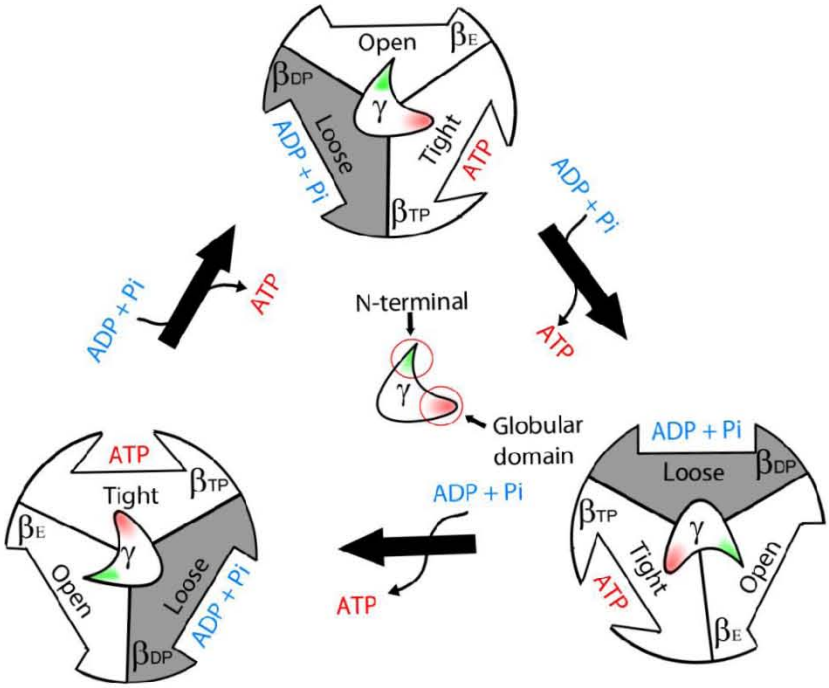

Figura 6. Modelo del mecanismo rotacional de síntesis de ATP de la ATP sintasa. Los tres diferentes estados conformacionales de las subunidades β se muestran: **Abierto**, **Relajado** y **Cerrado**. El estado conformacional **Abierto** de β se encuentra vacío. El estado conformacional **Relajado** de β (gris) tiene unido ADP + Pi. El estado conformacional **Cerrado** de β ha condensado el ADP + Pi en un ATP (rojo). La subunidad γ se representa en el centro de las subunidades β y su asimetría se representa por su N-terminal (verde) y su dominio globular (rojo). Cuando la subunidad γ comienza a rotar, su dominio N-terminal y globular darán paso a los estados conformacionales de las subunidades β. Su N-terminal estará más cerca del estado **Abierto** y el dominio globular será el más cercano al estado **Cerrado**. El estado **Abierto** también se conoce como β_E, el estado **Relajado** también se conoce como β_{DP}, y el estado **Cerrado** también se conoce como β_{TP} (22). La figura está adaptada de (45,47).

3.4 El brazo periférico de la F_1F_O-ATP sintasa

El brazo periférico mantiene fijo en su posición al estator α_3/β_3 y no le permite que siga el arrastre del movimiento del rotor. El brazo periférico conecta a la subunidad *a* con la subunidad δ. El brazo periférico se compone de diferentes subunidades dependiendo si la enzima es bacteriana, de cloroplasto o de mitocondria (49). En el caso de la enzima bacteriana, el brazo periférico está compuesto por una subunidad *a*, un dímero de subunidades *b* y una subunidad δ (Figura 3 y Figura 5).

3.5 Hidrólisis de ATP por la F_1F_O-ATP sintasa

En ausencia de un aceptor final de electrones, la cadena transportadora de electrones dejará de bombear protones (Figura 7B). Ésto ocasionará que el gradiente electroquímico disminuya y entonces que la ATP sintasa lleve a cabo la reacción inversa: la hidrólisis de ATP (13). Cuando la ATP sintasa se encuentra hidrolizando ATP se le denomina ATPasa (50). Cuando las subunidades β hidrolizan ATP, éstas sufren los mismos cambios conformacionales que durante la síntesis. Por ello, cuando las subunidades β hidrolizan al ATP, los cambios conformacionales generados por ellas van a impulsar a la subunidad γ la cual rotará en el sentido opuesto (en contra de las manecillas del reloj visto desde F_O "CCW"). La subunidad γ al rotar en el sentido CCW va a impulsar la rotación del anillo de subunidades *c* en dicho sentido. El anillo de subunidades *c* al girar en el sentido CCW bombea a los iones en dirección contraria al de la síntesis de ATP, sostienendo el gradiente electroquímico (Figura 7). La hidrólisis de ATP es por la F_1F_O-ATPasa es una reacción adversa en la mayoría de los organismos (51). El consumo total del ATP intracelular lleva a la muerte celular. Por ello, esta reacción de la enzima se encuentra regulada.

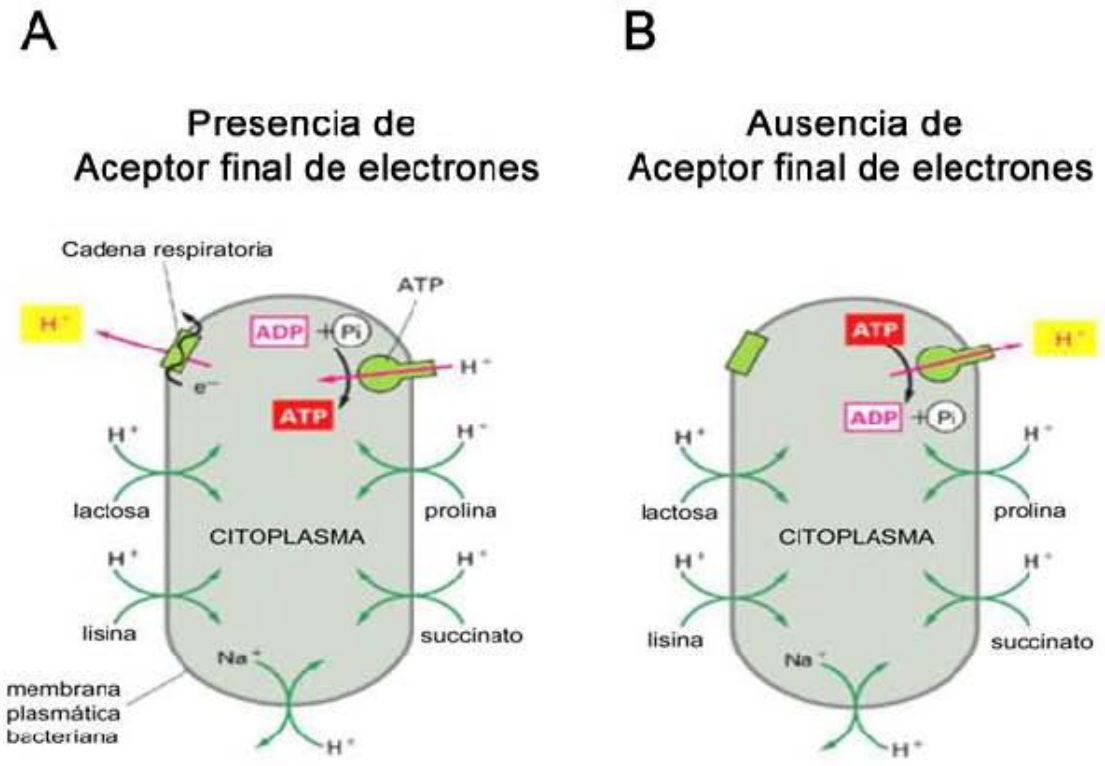

Figura 7. Condiciones de síntesis e hidrólisis de ATP por la F_1F_O-ATP sintasa. A) En presencia de un aceptor final de electrones, la cadena transportadora de electrones (CTE) bombea protones al espacio periplásmico y estos protones son aprovechados por la ATP sintasa para sintetizar ATP. B) En ausencia de aceptor final de electrones, la CTE no bombea protones al espacio periplásmico y para sostener el gradiente electroquímico la ATP sintasa gira en el sentido opuesto. La ATP sintasa, ahora en modalidad ATPasa bombea protones y sostiene al gradiente electroquímico. Modificado de (52).

3.6 Subunidades reguladoras de la F_1F_O-ATPasa

3.7 Mecanismo de inhibición de la subunidad ε

La subunidad ε es una subunidad estructural que mantiene a la fracción F_1 unida con la fracción F_O (42,43). La estructura terciaria de la subunidad ε contiene un dominio β-plegado en su N-terminal y dos α-hélices en su C-terminal (Figura 8). Adicional a su función estructural, en la ATPasa bacteriana, la subunidad ε inhibe el giro del rotor en el sentido de la hidrólisis de ATP (53). Esta función inhibidora de la subunidad ε sobre la enzima se ha descrito en bacterias como *Escherichia coli* (*E. coli*) (54) y *Geobacillus stearothermophilus* (*G. stearothermophilus*) (anteriormente

conocida como *Bacillus* PS3) (26). El mecanismo de regulación de la subunidad ε es mediado por la capacidad de ésta para asociar una molécula de ATP (Figura 8).

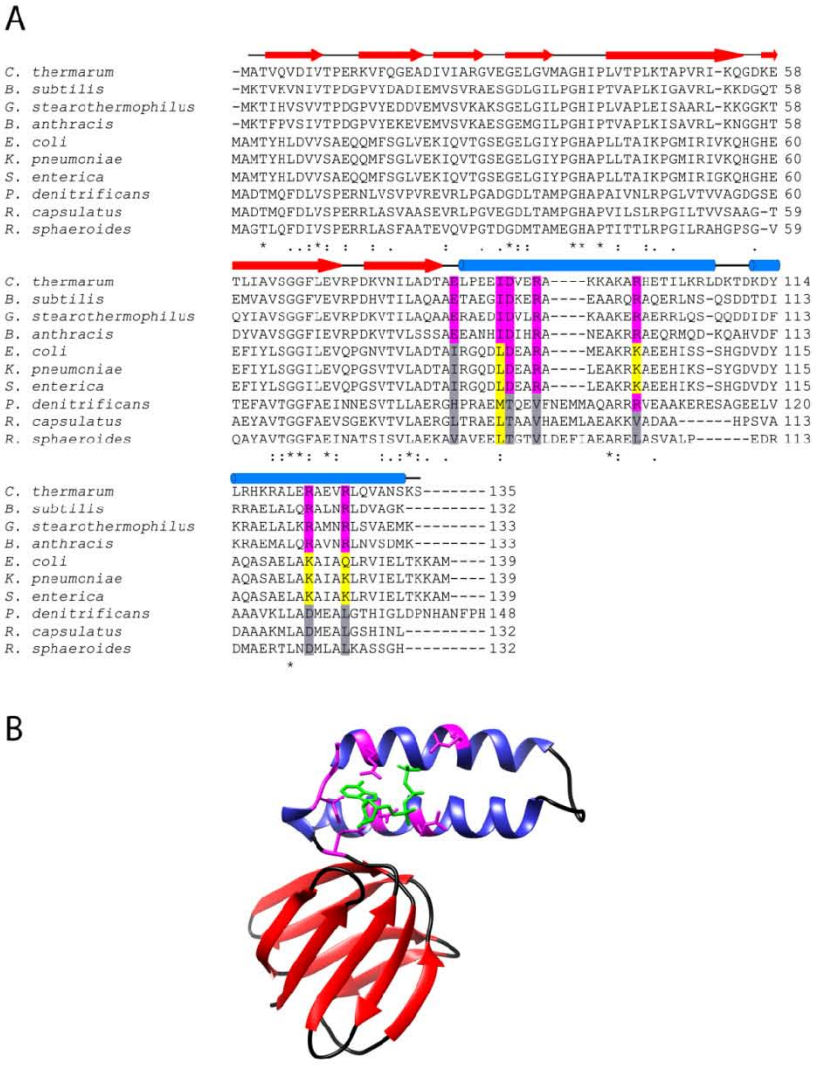

Figura 8. Sitio de unión de ATP de la subunidad ε. El sitio de unión de ATP considerado aquí es el de la subunidad ε de *Caldalkalibacillus thermarum* (*C. thermarum*) (PDB ID 5IK2). A) Alineamiento de la secuencia de aminoácidos de la subunidad ε de diferentes bacterias; de la clase de Bacillus: *C. thermarum, B. subtilis, G. stearothermophilus, B. anthracis*. De la clase de las γ-proteobacteria: *E. coli, K. pneumoniae, S. enterica*. De la clase de las α-proteobacteria: *P. denitrificans, R. capsulatus, R. sphaeroides.* Se destacan los residuos que interactúan con la molécula de ATP (verde). Los residuos idénticos (magenta). Los residuos conservados (amarillo). Los residuos no conservados (gris). La flecha roja indica la parte N-terminal de la secuencia que es β-laminar. El cilindro azul indica la parte C-terminal de la secuencia que es α-hélice. Las líneas negras indican los bucles. El asterisco (*) indica posiciones

en el alineamiento que tienen un residuo idéntico. Los dos puntos (:) indican posiciones en el alineamiento que se conservan (similar). El punto (.) indica posiciones en el alineamiento que están débilmente conservadas (débilmente similar). Finalmente, ningún símbolo ( ) indica posiciones en el alineamiento que no se conservan en absoluto. La alineación se hizo usando CLUSTAL-Omega. B) Estructura de la subunidad ε de *C. thermarum*. En rojo, el N-terminal (β laminar), en azul el C-terminal (α-hélice), en magenta las cadenas laterales que interactúan con la molécula de ATP, y en verde la molécula de ATP. La imagen de la estructura se obtuvo usando el programa UCSF Chimera.

Cuando hay una alta concentración de ATP en el citoplasma, la subunidad ε une una molécula de ATP lo cual conlleva a que esta subunidad sufra un cambio conformacional y se encuentre compacta (Figura 8B y Figura 9). Cuando disminuye la concentración de ATP, la subunidad ε no puede unir ninguna molécula de ATP y esto conlleva a que su C-terminal se encuentre extendido (Figura 9). La conformación compacta de ε permite que el rotor de la ATPasa pueda rotar en ambos sentidos (Figura 9). Mientras que la conformación extendida de ε no permite que el rotor de la ATPasa pueda rotar en el sentido CCW (Figura 9). Sin embargo, la conformación extendida de ε permite la giro del rotor en el sentido de la síntesis de ATP (55). Por ello, se propone que ε funciona como un trinquete de una matraca (55). En su conformación extendida, el C-terminal de la subunidad ε interactúa con la interfase α_{DP}/β_{DP} y con la subunidad γ (Figura 9) (26,54).

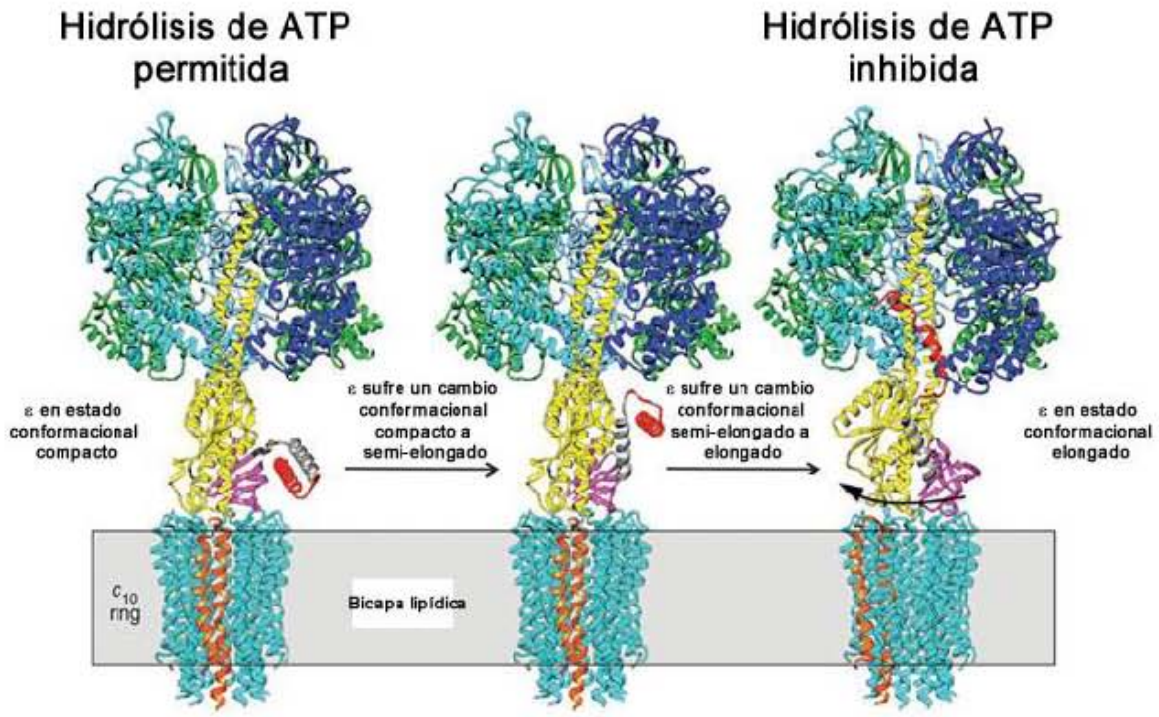

Figura 9. Mecanismo de inhibición de la subunidad ε bacteriana. Modelo de transición de la subunidad ε del estado conformacional compacto al estado conformacional estirado de *E. coli*. De lado izquierdo, la subunidad ε se encuentra en el estado conformacional compacto. En el estado conformacional compacto, la subunidad ε es capaz de unir una molécula de ATP y el rotor de la F_1F_0-ATP sintasa puede rotar en ambos sentidos. En el centro, la subunidad ε ha sufrido en el estado conformacional semi-elongado. De lado derecho, la subunidad ε en el estado conformacional estirado. El rotor de la F_1F_0-ATP sintasa sólo puede girar en el sentido de la síntesis de ATP. El N-terminal de la subunidad ε se encuentra en color magenta y la segunda α-hélice del C-terminal se encuentra en color rojo. Modificado de (54).

3.8 Mecanismo de inhibición de la subunidad IF_1 mitocondrial

En la ATP sintasa mitocondrial, el C-terminal de la subunidad δ (homóloga a la subunidad ε bacteriana) no tiene capacidad de extenderse (Figura 10, panel derecho) (56). Adicionalmente, esta subunidad no conserva el sitio de unión al ATP. Debido a que la subunidad δ no tiene función inhibidora, ocurrió un evento de evolución convergente surgiedo la subunidad inhibidora IF_1 (57). La subunidad IF_1 se estructura en una sola α-hélice (Figura 11 A).

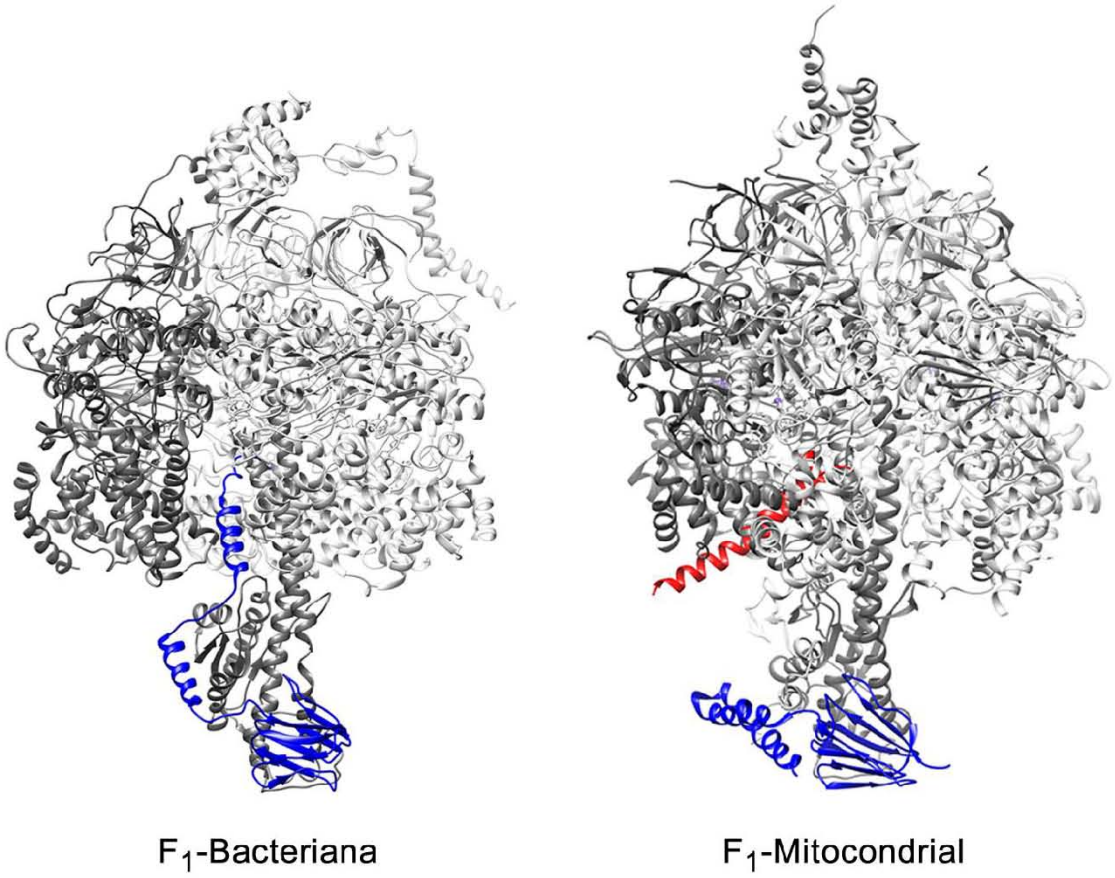

Figura 10. La subunidad δ en la F_1-ATPasa mitocondrial no tiene conformación extendida. En azul la subunidad δ mitocondrial y ε bacteriana. De lado izquierdo la subunidad ε en estado conformacional elongado en la F_1 Bacteriana (tomado de la figura 1 A). De lado derecho la subunidad δ en estado conformacional compacto dentro del complejo F_1 mitocondrial de levadura (tomado de la Figura 1 C). Las estructuras fueron modeladas utilizando el programa UCSF Chimera.

El mecanismo de inhibición de la subunidad IF_1 depende del pH de la matriz mitocondrial. A pH <7 (6.0-6.8) la subunidad es capaz de inhibir la actividad ATPasa (Figura 11 A). El dominio C-terminal de la IF_1 (amarillo en la Fig 11 A) induce la formación de homodímeros de la IF_1 *in vitro*, lo cual favorece la formación de dímeros de la ATP sintasa en la mitocondria (58) que le dan forma a las crestas mitocondriales (59,60). Adicionalmente, la IF_1 cuando se encuentra formando homodímeros ayuda a la dimerización del complejo ATP sintasa de la mitocondria (Figura 11 D) (58,61).

La estructura de IF_1 se ha determiando a partir del residuo 20 del N-terminal y es una α-hélice (Figura 11 A). Los residuos 10 al 19 del N-terminal de IF_1 tienen alta movilidad debido a que es un dominio intrínsecamente desordenado, por ello no se ha podido determinar su estructura mediante cristalografía de rayos X. Los primeros residuos del dominio N-terminal de IF_1 sólo se estructuran en α-hélice conforme va interactuando con la interfase de las subunidades α/β (Figura 11 B y C) (62). Al reconstituir un exceso de IF_1 con la F_1-ATPasa, la IF_1 ocupa las tres interfases α/β. En la interfase **Abierta**, el N-terminal de IF_1 se encuentra intrínsecamente desordenado ya que la α-hélice N-terminal de IF_1 comienza a partir del residuo Glutamato-31 (Figura 11 C panel izquierdo). La subunidad γ rota 120º y la interfase **Abierta** cambia a la **Relajada**, y la α-hélice del N-terminal de IF_1 está estructurada a partir del residuo Glicina-23 (Figura 11 C panel central). La subunidad γ rota nuevamente 120º cambiando la interfase **Relajada** a **Cerrada** y la α-hélice del N-terminal comienza a partir del residuo Serina-11 (Figura 11 B y C panel derecho) (62). Cuando IF_1 se encuentra en la interfase **Cerrada** su N-terminal se encuentra más estructurado y logrando atravesar la interfase α_{DP}/β_{DP} e interactuando con la subunidad γ. Cuando el N-terminal de IF_1 interactua con γ evita que el rotor gire en el sentido CCW y la F_1F_O-ATPasa deja de hidrolizar ATP (62,63).

A

B

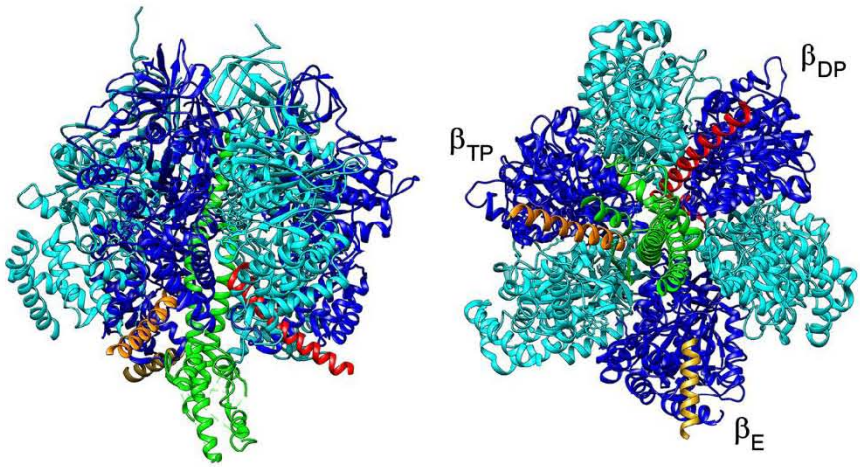
β_{DP}
β_{TP}
β_{E}

C

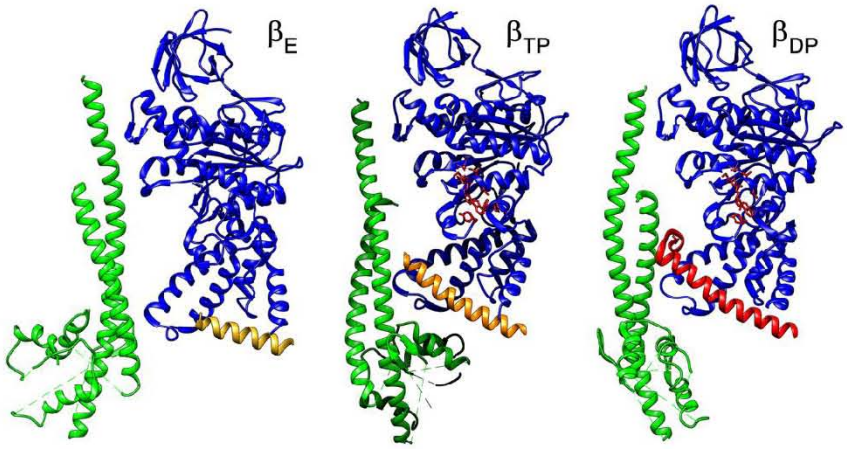
β_{E}
β_{TP}
β_{DP}

D

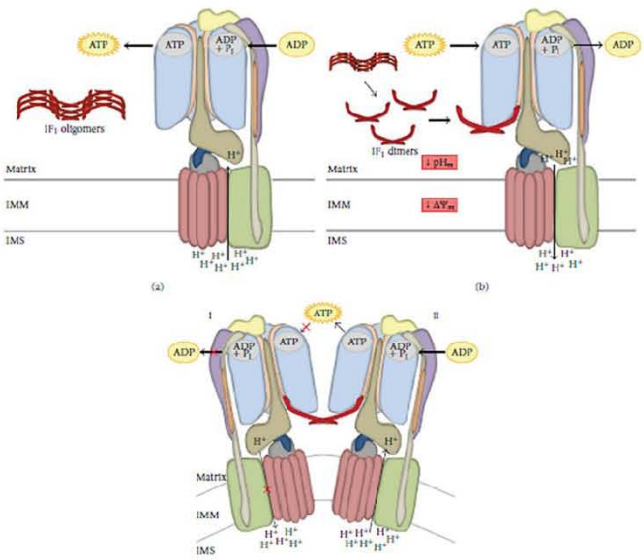
ATP
ADP + P_i
ADP
IF_1 oligomers
IF_1 dimers
Matrix
IMM
IMS
(a)
(b)
I
II

Figura 11. Estructura y mecanismo inhibitorio de la subunidad inhibidora IF_1 de la F_1F_O-ATPasa mitocondrial. A) Estructura de la subunidad IF_1 formando un homodímero, en rojo el N-terminal y en amarillo el C-terminal. El N-terminal de IF_1 sólo se encuentra resuelto a partir del residuo Glicina 19. B) Mecanismo de inhibición de la subunidad IF_1 sobre la fracción F_1-ATPasa, visto de abajo hacia arriba. Tres subunidades IF1 se encuentran atravesando las interfases α/β, en dorado, la estructura resuelta del N-terminal de la subunidad IF_1 a partir del residuo Glutamato 31. En anaranjado, la estructura del N-terminal de la subunidad IF_1 a partir del residuo Glicina 23. En rojo, el N-terminal de la subunidad IF_1 a partir del residuo Serina 13. C) Visualización de la F_1-ATPasa inhibida por la subunidad IF_1. Se muestra la fracción F_1 desde un costado y sólo se muestra la subunidad β, γ e IF_1. La subunidad β que se muestra está interactuando con IF_1. Se muestra como IF_1 se va estructurando gracias a los giros parciales de 120º de γ. En dorado, IF_1 interactúa con la interfase abierta α_E/β_E. En naranja, IF_1 interactúa con la interfase relajada α_{TP}/β_{TP}. En rojo, IF_1 interactúa con la interfase cerrada α_{DP}/β_{DP}. D) Esquema del mecanismo de dimerización de los complejos F_1F_O-mitocondriales mediado por la subunidad IF_1. La IF_1 a pH >7 se oligomeriza y a pH <7 se dimeriza. IF_1 dimerizada por su C-terminal permite que sus N-terminales interactúen con una F_1F_O promoviendo la dimerización del complejo. A) Modificado de (64) (PDB ID IGMJ) B) y C) Modificado de (65) (PDB ID 4TT3). D) Tomado de (61).

3.9 Mecanismo de inhibición por la subunidad ζ de las α-proteobacterias.

En la F_1F_O-ATPasa perteneciente a la clase de las α-proteobacterias, la subunidad ε no mantiene la función inhibidora (28). Debido a que ε no tiene función inhibidora, la enzima de estas bacterias obtuvo a la subunidad inhibidora ζ mediante un evento de evolución convergente (27,28,30). La subunidad ζ en solución se estructura en cuatro α-hélices (Figura 12, panel izquierdo) y su dominio inhibitorio se encuentra en el extremo N-terminal (residuos 1-14) (28). La secuencia del dominio N-terminal de ζ guarda cierta similitud con el N-terminal de IF_1 (28) y de manera similar al ser determinado por RMN se encuentra intrínsecamente desordenado (Figura 12, panel izquierdo en color morado) (66,67). La similaridad del N-terminal de IF_1 y ζ puede ser el motivo por el cual ambas subunidades se unen a la interfase α_{DP}/β_{DP} para inhibir a la ATPasa, lo cual se ha mostrado por modelado basado en homología (68) y subsecuentemente por una estructura resuelta mediante cristalografía de rayos X (69). Se ha propuesto que la subunidad ζ interactúa con la F_1F_O-ATPasa por un

mecanismo de entrada, rotación, unión y candado (en inglés “Entrance, Rotation, α-helix, Lock” abreviado ERAHL) acoplado a la rotación de ζ, y al mismo tiempo a una transición del N-terminal intrínsecamente desordenado a una estructura secundaria de α-hélice (68,70,71).

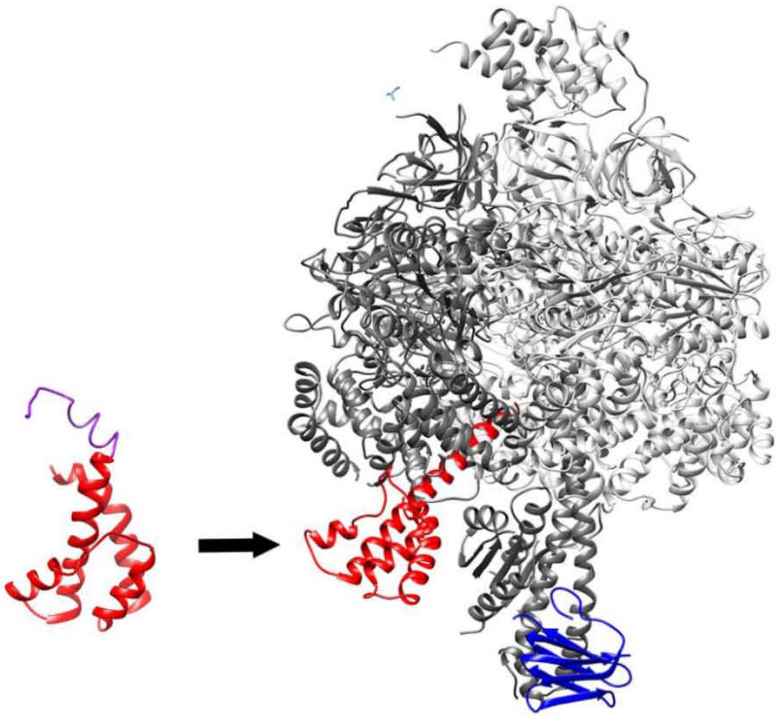

Figura 12. Estructura y mecanismo de inhibición de la subunidad ζ de la F_1-ATPasa de *P. denitrificans*. De lado izquierdo, la estructura de la subunidad ζ resuelta por Resonancia Magnética Nuclear (PDB ID 2LL0). De lado derecho, la F_1-ATPasa inhibida por la subunidad ζ, modificado de (30).

3.10 Rol fisiológico de las subunidades reguladoras

Las subunidades reguladoras ε, IF_1 y ζ tienen en principio un papel central en el metabolismo celular debido a que inhiben la actividad F_1F_O-ATPasa. Sirve recalcar que la hidrólisis de ATP por la F_1F_O-ATPasa no es su rol fisiológico (aunque hay excepciones (72)) y por ende su inhibición es determinante para el metabolismo celular. Sin embargo, este papel de las subunidades inhibidoras no se ha demostrado de manera contundente. Se ha eliminado el gen (knockout) que codifica para la subunidad ε al igual que para IF_1 en diversos organismos, no obstante, no

se ha observado un fenotipo diferente al de los organismos silvestres, por lo que los resultados de organismos knockout han resultado controversiales.

Rol fisiológico de la subunidad ε bacteriana

Para estudiar el papel fisiológico de la subunidad inhibidora ε sobre el metabolismo de una bacteria, se eliminó el gen que codifica para ésta en *E. coli* (42). Al eliminar a la subunidad ε, la fracción F_1 se disoció de la F_O. La disociación de F_1 de F_O da lugar a la perdida de la capacidad de sintetizar ATP y, adicionalmente, la F_1 tiene una actividad F_1-ATPasa deshibibida (42). Para evitar la disociación de F_1F_O, se eliminó el C-terminal inhibitorio de ε en *E. coli* (73). Sin embargo, la cepa mutante no tuvo diferencias en el crecimiento celular, potencial de membrana y concentración de ATP intracelular que la cepa silvestre (73). De manera inesperada, al eliminar los primeros cinco residuos del C-terminal de ε, la subunidad ahora inhibe el giro del rotor en el sentido de la síntesis de ATP (CW). Ésta cepa mutante muestra un fenotipo diferente al de la cepa silvestre (74). Sin embargo, no se ha podido dilucidar el rol fisiológico de la subunidad ε en una bacteria.

3.11 Rol fisiológico de la subunidad IF_1 mitocondrial

Las enfermedades cardiovasculares son la principal causa de muerte en el mundo de acuerdo a la Federación Mundial del Corazón (75) y los niveles de expresión de la subunidad IF_1 se han relacionado con dichas patologías, así como, con los niveles del colesterol de alta densidad (HDL) (76). Por ello, la subunidad IF_1 es relevante para la medicina. La IF_1 promueve un mejor estado de energía en los corazones de ratas que han sido sometidas a episodios de isquemia prolongada, esto se asocia a la capacidad de IF_1 para inhibir el consumo de ATP por la actividad F_1F_O-ATPasa (77,78). Esta asociación se debe a que la F_1F_O-ATPasa consume más de la mitad de ATP celular durante la isquemia (79). Para evitar el consumo de ATP durante la isquemia, hay un aumento en la expresión de IF_1 en el tejido cardiaco de ratones expuestos a una isquemia prolongada (80). El aumento en la expresión de IF_1 se asocia a una protección al tejido cardiaco en respuesta a la isquémia (81).

Para determinar el rol fisiológico de la subunidad IF_1 mitocondrial, se han realizado silenciamientos de la subunidad IF_1 en líneas celulares. El silenciamiento de la IF_1 disminuye la forma dimérica de la F_1F_O-ATP sintasa y la formación de las crestas mitocondriales (81). Además, la disminución de las crestas mitocondriales promueve la apoptosis por la liberación del citrocromo *c* (82). También, el silenciamiento de IF_1 aumenta la autofagia y la producción de especies reactivas de oxígeno (83). Sin embargo, los estudios de silenciamiento en líneas celulares no han establecido un rol claro de IF_1 en el metabolismo celular.

Se ha eliminado el gen que codifica para la subunidad IF_1 en *Saccharomyces cerevisiae* (levaduras) (84,85), *Caenorhabditis elegans* (gusanos) (86) y *Mus musculus* (ratones) (87,88). En los ratones knockout hubo un aumento en la actividad F_1F_O-ATPasa, una disminución dímeros del complejo (88) y una menor cantidad de crestas mitocondriales que en las mitocondrias de los ratones silvestres (87). Por último, la IF_1 en los ratones knockout protege al corazón de la hipertrofia por sobrecarga de presión (80). Sin embargo, no se detectó un fenotipo en los ratones knockout, ya éstos podían crecer y reproducirse igual que los ratones silvestres (88). En *C. elegans* al remover el gen IF_1 (MAI-2), los gusanos mutantes y silvestres tenían el mismo tiempo de vida y capacidad reproductiva en condiciones normales. Pero en condiciones de estrés, los gusanos mutantes muerieron más rápido que los gusanos silvestres. De manera contrastante, los gusanos mutantes y silvestres tenían la misma concentración de ATP intracelular lo que es un resultado difícil de interpretar. Otro dato complicado de interpretar es la menor actividad F_1F_O-ATPasa en muestras solubilizadas de la cepa mutante respecto a la silvestre, ya que ésto es contradictorio a lo reportado tanto en estudios *in vitro* como en estudios *in vivo* (86). En *S. cerevisiae* se han identificado dos factores de estabilización (stf1 y stf2) que pueden funcionar como la IF_1. Por ello, se obtuvo una levadura sin los tres genes (IF_1, stf1 y stf2). En la levadura triple knockout, la actividad de F_1F_O-ATPasa fue mayor que en la enzima de la silvestre. Además, en condiciones limitadas la levadura mutante consume el ATP intracelular más rápido que la levadura silvestre, correlacionando con el aumento en la actividad F_1F_O-ATPasa de

la cepa mutante. Sin embargo, no hubo diferencias en el crecimiento celular de las levaduras mutantes y silvestres (84).

La identificación de los genes stf1 y stf2 en levadura, anudado con la presencia varias copias del gen IF_1 en el genoma de organismos eucariontes, hacen notorio que para poder estudiar el rol fisiológico de IF_1 en eucariontes, se requiere obtener organismos knockout de IF_1 más la eliminación de las copias adicionales de IF_1, así como de stf1 y stf2.

4 Planteamiento del problema

La principal función biológica de la F_1F_O-ATP sintasa es la síntesis de ATP. Por ello, la inhibición de la función contraria de la enzima (hidrólisis de ATP) es fundamental para el correcto funcionamiento metabólico del organismo. Debido a que se encargan de inhibir la actividad F_1F_O-ATPasa, las subunidades reguladoras ε, IF_1 y ζ tienen un papel central en el metabolismo celular. La ausencia de la subunidad inhibidora de la F_1F_O-ATPasa en un organismo, debe de dar lugar a un aumento en la actividad de hidrólisis de ATP, efecto que debe repercutir en la concentración de ATP intracelular y como consecuencia, dar lugar a un efecto adverso en el crecimiento celular del organismo. Por ello, para estudiar el papel fisiológico de las subunidades reguladoras en el metabolismo celular se han eliminado los genes codificantes de IF_1 y ε de los genomas de *E. coli*, *C. elegans* y *M. muluscus*. Como se mencionó, la eliminación de la subunidad ε no dio resultados concluyentes debido a que se disoció la fracción F_1 de la F_O. La eliminación de la subunidad IF_1 tampoco dio resultados concluyentes debido a que el gen de la IF_1 (ATPIF1) tiene varias copias en los organismos eucariontes, además de que existen proteínas adicionales que pueden suplir el mecanismo inhibitorio de la IF_1 (stf1 y stf2). Considerando todo lo anterior, debido a que la subunidad reguladora ζ tiene una sola copia de su gen en las α-proteobacterias, como es el caso de *P. denitrificans*, y esta bacteria puede cultivarse en condiciones aeróbicas similares a las condiciones mitocondriales, proponemos a la subunidad ζ y a *P. denitrificans* para dilucidar el papel fisiológico de la subunidad reguladora ζ en el metabolismo celular de un organismo.

5 Hipótesis

En *P. denitrificans* la ausencia de la subunidad inhibidora ζ ocasionará un aumento en la actividad F_1F_O-ATPasa, resultando en una disminución de ATP intracelular, lo que a su vez dará lugar a una disminución en la velocidad de crecimiento celular.

6 Objetivo general

Evaluar el papel fisiológico de la subunidad ζ en la α-proteobacteria *P. denitrificans*.

6.1 Objetivos particulares

- Eliminar el gen que codifica para la subunidad inhibidora ζ en una cepa de *P. denitrificans* (PdΔζ).
- Evaluar la velocidad de crecimiento de la cepa PdΔζ y la silvestre en un medio de cultivo rico en nutrientes (LB) y otro mínimo respiratorio (succinato).
- Evaluar la expresión de la F_1F_O-ATP sintasa de la cepa silvestre y mutante en un medio de cultivo rico en nutrientes (LB) y en medio mínimo respiratorio (succinato).
- Evaluar la actividad de síntesis e hidrólisis de ATP a partir de PSB de ambas cepas.
- Evaluar el potencial de membrana en partículas sub-bacterianas (PSB) y en células vivas.
- Cuantificar la concentración de ATP intracelular de PdWT y PdΔζ en diferentes condiciones.

7 Materiales y Métodos

7.1 Medios de cultivo, enzimas y sistemas comerciales de biología molecular.

7.1.1 Medios de cultivo

Se utilizaron los medios de cultivo LB-Miller (LB) y succinato. El medio LB se preparó utilizando extracto de levadura (BD de Becton, Dickson and Company., Sparks, Maryland, USA.), Tryptona y NaCl (SIGMA-ALDRICH, Co., St. Louis, Missouri, USA.). El medio succinato se preparó conforme lo especificado anteriormente en (89). Los medios de cultivo líquidos de 2 ml se utilizaron en tubos de 15 ml de tamaño (marca Falcon de la compañía Thermo Fisher Scientific Inc., Waltham, Massachusetts, USA.) y los medios de 50 ml en matraces de 250 ml de tamaño marca PIREX (Corning Incorporated, Nueva York, USA). Los medios de cultivo sólidos con agar al 1.5 % p/v (AMRESCO, LLC., Solon, Ohio, USA) se utilizaron en cajas Petri (VWR, Radnor, Pennsylvania, USA.).

7.1.2 Preparación del medio succinato

El medio de cultivo succinato se preparó de la siguiente manera según el protocolo de (89):

Fosfato de potasio monobásico (KH_2PO_4) 50 mM
Cloruro de amonio (NH_4Cl) 75 mM
Sulfato de Sodio (Na_2SO_4) 11.5 mM
Cloruro de Magnesio ($MgCl_2$) 1.25 mM
Ácido cítrico 1 mM
Ácido succínico 10 g/L
Disolución de sales concentradas 1 ml/L

La disolución de sales concentradas se prepara con:

Cloruro de calcio ($CaCl_2$) 100 mM
Cloruro de hierro ($FeCl_2$) 90 mM
Cloruro de manganeso ($MnCl_2$) 50 mM
Cloruro de zinc ($ZnCl_2$) 25 mM
Cloruro de cobalto ($CoCl_2$) 10 mM

Cloruro de cobre ($CuCl_2$) 5 mM
Ácido bórico (H_3BO_3) 5 mM
Molibdato de sodio (Na_2MoO_4) 10 mM

Para que las sales de la disolución de sales concentradas no precipiten, se requiere añadir HCl diluído 1:1 con agua.

7.1.3 Enzimas

Para amplificar secuencias de ADN se utilizó la enzima polimerasa High Fidelity Pol (número de catálogo PCR-204S) (Jena Bioscience, Jena, Thüringen, Alemania). Para manipular las secuencias de ADN amplificadas, se utilizaron las enzimas de restricción NdeI y BamHI y para ligar la enzima ligasa T4; todas las enzimas de la marca New England Bio Labs Inc. (números de catálogo: R0145S, R0156S, R0111S, R0142S, R0101S y M0202S) (Ipswich, Massachusetts, USA.). La enzima polimerasa venía con su amortiguador de reacción 10X y su mezcla de desoxinucleótidos a una concentración de 10 mM. Todas las enzimas se utilizaron con forme el protocolo especificado por el fabricante para cada una de ellas.

7.1.4 Sistemas comerciales de biología molecular

El ADN genómico se extrajo utilizando el sistema comercial Genomic DNA purification (número de catálogo A1120) (Promega Corporation, Madison, Wisconsin, USA.). Todas las secuencias amplificadas se ligaron en el plásmido pJET con el sistema comercial cloneJET PCR Cloning (número de catálogo K1232) (Thermo Fisher Scientific Inc., Waltham, Massachusetts, USA.). El ADN plasmídico se extrajo utilizando el Sistema comercial High Pure Plasmid Isolation (número de catálogo 11754777001) (Roche, Mannheim, Alemania). El ADN se purificó a partir de geles de agarosa utilizando el sistema comercial QIAquick Gel Extraction (número de catálogo 28704) (Quiagen, Hilden, Alemania). Todos los sistemas comerciales se utilizaron conforme el protocolo especificado por el fabricante para cada uno de ellos.

7.1.5 Condiciones de crecimiento de las bacterias

Todas las cepas de *E. coli* se cultivaron a 37 ºC durante 24 h en matraces con medio LB líquido o en cajas Petri con medio LB sólido. Al medio LB sólido se le añadió 10 % p/v de sacarosa cuando fue requerido. Las cepas de *P. denitrificans* se cultivaron a 30 °C durante 24 h en matraces con medio LB o succinato líquido o en cajas Petri con medio LB sólido. Cuando se requriío, las cepas de *P. denitrificans* se cultivaron hasta por 48 h. Se utilizaron antibióticos en los medios de cultivo y cuando fue necesario se utilizaron a las siguientes concentraciones (µg/ml): rifampicina, 50; kanamicina, 50; gentamicina, 30; y ampicilina, 100 (Todos los antibióticos se compraron con SIGMA (SIGMA-ALDRICH Co., St. Louis, Missouri, USA.).

7.2 Eliminación del gen que codifica para la subunidad ζ

El gen que codifica para la subunidad inhibidora ζ se eliminó en *P. denitrificans* (*Pd* 1222). Para eliminar al gen ζ, se llevaron a cabo las técnicas de biología molecular que se describen a continuación.

Cepa o plásmido	Propiedades relevantes	Referencias
Cepa		
Escherichia coli		
DH5α	Cepa hospedera para plásmidos	Hanahan *et al*. (1983)
	F$^-$ *hsdR17 thi-1 gyrA Δ*(*lacZYA-argF*) *supE44 recA1*(φ80d*ΔlacZ*M15) *relA*	
S17-1	Sm^R, *pro*, res$^-$, mod$^+$, RP4-2 integrado (Tc::Mu) (Km::Tn7), donador de plásmidos en las conjugaciones.	Simon *et al.* (1983)
Paracoccus denitrificans		
1222	Rif^R, Spc^R, mod$^+$, m$^-$, frecuencia de conjugación alta.	de Vries *et al.* (1989)
Δζ	PD 1222, Km^R, ζ$^-$	Mendoza-Hoffmann *et al.* 2018
Δζ+ζ	Δζ, pFMMCJG+ζ (pBBR+ζ)	Mendoza-Hoffmann *et al.* 2018
Plásmido		
pJQ200SK	Gm^R, sacB, mob$^+$,	Quandt *et al.* (1993)

pFMMCJG-Δζ	pJQ200SK, GmR, sacB, marcador de Km^R flanqueado por las secuencias de 997 pb río arriba del gen ζ y 870 pb río abajo del gen ζ.	Mendoza-Hoffmann *et al.* 2018
pBBR1 MCS-5	GmR, rep, mob^+.	Kovach *et al.* (1995)
pFMMCJG+ζ	pBBR1 MCS-5, Gm^R, ζ con su propio promotor de 200 pb insertado como un fragmento EcoRI-KpnI.	Mendoza-Hoffmann *et al.* 2018

Tabla 2. Cepas bacterianas y plásmidos utilizados en esta tesis.

7.3 Extracción de ADN genómico

Las cepas de *P. denitrificans* o de *E. coli* se cultivaron en 2 ml de medio LB (dentro de un tubo de 15 ml) durante 24 h a 37 ^oC con agitación constante en una incubadora modelo DNI-10 (MRC, Cambridge, Reino Unido). Posteriormente las células se cosecharon mediante centrifugación, el sobrenadante se desechó y la pastilla formada por las células se conservó. El ADN genómico se extrajo a partir de la pastilla formada por las células bacterianas utilizando el sistema comercial de extracción de ADN genómico mencionado anteriormente, siguiendo el protocolo de éste.

7.4 Reacción en cadena de la polimerasa (PCR)

Varias secuencias de ADN se amplificaron mediante PCR utilizando oligonucleótidos específicos para cada secuencia de ADN (Saiki, R. K., et al. 1988), los detalles de los oligonucleótidos se muestran en la tabla 1. En un tubo de 0.2 ml (Eppendorf, Hamburg, Alemania) se mezclaron los siguientes reactivos para poder llevar acabo la reacción de amplificación: ADN molde a una concentración que dependió de la secuencia a amplificar, oligonucleótidos sentido y anti-sentido específicos para cada secuencia a amplificar (tabla 1), una mezcla de desoxinucleótidos, amortiguador de reacción de la enzima polimerasa, sulfato de magnesio ($MgSO_4$), polimerasa de alta fidelidad y un volumen de agua necesario hasta llevar el volumen final de la mezcla a 50 µl. La mezcla se llevó a cabo en hielo

para mantener la temperatura a 4 ºC. La reacción se llevó a cabo en un aparato termociclador modelo Verity marca Applied Biosystems (Thermo Fisher Scientific Inc., Waltham, Massachusetts, USA.).

7.5 Electroforesis en gel de agarosa

Los tamaños de las secuencias amplificadas se determinaron al separarlos en una electroforesis en gel de agarosa (Aaij, C. y Borst, P., 1972). Los tamaños de las secuencias se compararon con dos marcadores de tamaño molecular (número de catálogo N3231 y N3232) (New Englan Bio Labs Inc., Ipswich, Massachusetts, USA.). El gel se preparó al 2 % de agarosa p/v en una disolusión amortiguadora TBE (ácido bórico 89 mM, EDTA 2 mM y tris 89 mM a pH 7.6). Se calentó la mezcla de agarosa con TBE hasta disolverla completamente. Posteriormente, la mezcla se polimerizó y el gel resultante se colocó en una cámara de electroforesis marca Bio-Rad modelo Mini-Sub Cell GT Cell (Berkeley, California, USA) con amortiguador TBE. Cada secuencia amplificada se mezcló con con mezcla de carga (glicerol al 10 %, rojo de cresol al 0.083 % p/v) y al igual que los marcadores de tamaño molecular, posteriormente se colocaron cada uno en un pozo. La cámara se programó a 80 V durante 1.5 h. Al finalizar la electroforesis el gel se tiñó con Bromuro de etidio durante 10 min en agitación constante. A continuación, el gel se destiñó y se observar las secuencias de ADN amplificadas en un equipo transiluminador modelo MINILUMI (DNR Bio-Imaging Systems, Neve Yamin, Israel). A excepción de los marcadores de tamaño, todos los reactivos se compraron en Sigma-Aldrich Co. (St. Louis, Missouri, USA.) y los marcadores de tamaño con New England (número de catálogo N3231 y N3232) (Berkeley, California, USA).

7.6 Eliminación del gen que codifica para la subunidad ζ en *P. denitrificans* (PdΔζ).

Para eliminar el gen que codifica para la subunidad ζ de *P. denitrificans* 1222 (Pd1222), se reemplazó el gen ζ con un con un marcador de resistencia a kanamicina mediante recombinación homóloga (Figura 13). Primero se amplificaron por PCR las regiones flanqueadoras del gen ζ. La región río arriba (RAR) a partir del codón de inicio que se amplificó fue de 997 pb. La región río abajo (RAB) a partir

del codón de finalización que se amplificó fue de 870 pb. Se utilizaron los oligonucleótidos ZFlarJJ1 y ZRlarJJ2, así como los oligonucleótidos F100915JJ3 y R100915JJ4, respectivamente (Tabla 3). La secuencia del cassette de resistencia a kanamicina (Km) que se amplificó fue de 1019 pb utilizando los oligonucleótidos FKmJJ1 y RKmJJ2 (Tabla 3) y el ADN molde utilizado fue el plásmido pDON221. Cada producto de PCR se ligó en un plásmido pJET y se transformó en células de *E. coli* DH5α competentes, seleccionando las clonas postivas en placas LB con ampicilina. Las clonas positivas se cultivaron en LB a 37 ºC durante 24 h. Se confirmó la presencia de los insertos deseados en el plásmido pJET, usando reacciones de restricción específicas que cortan los límites de las inserciones: XbaI-SacI para insertos de RAR y RAB y NdeI-KpnI para Km. Los plásmidos con inserto pJET / RAR y pJET / RAB se digirieron con SacI y luego se ligaron juntos (Figura 13). Después, la ligadura se transformó, se seleccionó, y se cultivaron las clonas positivas tal como se describió anteriormente. La presencia del inserto deseado de RAR + RAB (1867 pb) en el plásmido pJET se confirmó como se describió anteriormente digiriendo con la enzima XbaI. A continuación, el pJET / RAR + RAB y el pJET / Km se digirieron con las enzimas NdeI y KpnI. El pJET / Km^R se separó en una electroforesis y la banda de Km se extrajo del gel. Seguidamente, el pJET / RAR + RAB y el Km se ligaron entre ellos y así se obtuvo una construcción pJET / RAR + Km + RAB (Figura 13). Esta construcción se transformó, se seleccionaron las clonas positivas como se describió anteriormente. La presencia del inserto deseado de RAR + Km + RAB en los plásmidos se confirmó como se describió anteriormente digiriéndolo con la enzima XbaI. Posteriormente, la construcción digerida de RAR + Km + RAB con XbaI se ligó en un vector suicida pJQ200SK que también se había digerido con XbaI. La construcción pJQ200SK / RAR + Km + RAB se transformó en células de *E. coli* S17 competentes (90) y se cultivó en placas LB con kanamicina y gentamicina a 37 ºC 24 h. Posteriormente, las clonas que eran resistentes positivas se cultivaron en LB a 37 ºC durante 24 h, el vector positivo + inserto se denominó $\Delta\zeta$ y se confirmaron mediante digestiones con XbaI. Finalmente, las cepas de *E. coli* S17-1 / $\Delta\zeta$ y Pd1222 (WT) se conjugaron entre ellas. Las cepas conjugadas se cultivaron en medio LB líquido libre de antibiótico hasta

alcanzar la fase estacionaria. Posteriormente se sembraron en una placa de Petri LB, en una proporción de 1:1. Las cepas conjugadas se incubaron a 37 ºC durante 24 h y a continuación se resuspendieron en medio LB. Las diluciones seriadas se plaquearon en LB con gentamicina y rifampicina para seleccionar las células Pd1222 que contenían el plásmido pJQ200SK / ∆ζ (denominado pFMMCJG-Δζ). Ulteriormente, se seleccionaron las bacterias que habían llevado el evento de recombinación. En el evento de recombinación, el gen ζ se transfirió del cromosoma al plásmido y el cassette de resistencia a kanamicina se transfirió del plásmido al cromosoma. Después, se seleccionaron las bacterias que ya no tenían plásmido + gen ζ. Para asegurarnos que las bacterias no tenían plásmido + gen ζ, las bacterias se crecieron en LB con kanamicina y 10% de sacarosa como se describió anteriormente (91). A las clonas capaces de crecer en presencia de sacarosa y kanamicina, pero incapaces de crecer en gentamicina, se les denominó Pd∆ζ y se les extrajo el ADN total. Utilizando el ADN total de la cepa Pd∆ζ, se realizaron reacciones de PCR con los oligonucleótidos del gen ζ (ZFNeIJJ y ZRpromJJ2) (Tabla 3) (Figura 14). También se confirmó la presencia del cassette de resistencia a kanamicina en la cepa Pd∆ζ. Se amplificó el cassette de resistencia a kanamicina usando los oligonucleótidos ZFlarJJ1 y RKmJJ2 (Figura 15).

Blanco	Oligonucleotidos	Secuencia	Sitios de restricción
Río arriba a partir del codón de inicio del gen ζ (997 bp)	Sentido (ZFlarJJ1)	5'- **TCT AGA** CCA AGC GCG TGC CGG ATC GCC TC – 3'	XbaI
	Antisentido (ZRlarJJ2)	5'- **GAG CTC CAT ATG** GGC CTC CGG CTT GGG ATT ATC -3'	NdeI - SacI

Río abajo a partir del codoón de paro del gen ζ (870 bp)	Sentido (F100915JJ3)	5'- **GAG CTC GGT ACC** GCT TTC GCA AGA CGG CGA CGC CCC GGA ATC - 3 '	SacI - KpnI
	Antisentido (R100915JJ4)	5'- **TCT AGA** TGC TGG TGC TGC AAC TGC TGA TGA ACG GGC TGA ACA TC - 3'	XbaI
Resistencia a Kanamycin (1019 bp)	Sentido (FKmJJ1)	5'- **CAT ATG** GTT GCA ACG AAC AGG TCA CTA TC - '3	NdeI
	Antisentido (RKmJJ2)	5'- **GGT ACC** TTA GAA AAA CTC ATC GAG CAT C-3	KpnI
Gen ζ con su propio promotor (200 pb a partir del codón de inicio del gel ζ) (514pb)	Sentido (ZFpromJJ1)	5'- **GAA TTC** GCG TGC CGG GCT CGG TGC CTT C -3	EcoRI
	Antisentido (ZRpromJJ2)	5'- **GGT ACC GAG CTC** TCA GAT CTC GCT GAT GAT CTG TTC GCG CGC -3 '	SacI - KpnI
Gen ζ (314 pb)	Sentido (ZFNdeIJJ)	5 '-**CAT ATG** ACC ACA TTT GAC GAC CGC GAG CGC -3'	NdeI

Tabla 3. Oligonucleótidos utilizados en esta tesis.

7.7 Complementación de la cepa mutante *P. denitrificans* Δζ (PdΔζ)

El gen ζ con su propio promotor se amplificó utilizando el ADN de Pd1222 (PdWT) y los oligonucleótidos ZFpromJJ1 y ZRpromJJ2 (Tabla 3). Este producto de amplificación se clonó en el plásmido pJET y se transformó en células de *E. coli* DH5α competentes, seleccionando en placas LB complementadas con ampicilina. La presencia del inserto en el vector de las clonas positivas se corroboró digiriendo con el ADN plasmídico con las enzimas de restricción EcoRI y SacI. El inserto de uno de estos plásmidos se clonó en un plásmido pBBR1MCS-5 (92) y el plásmido pFMMCJG + ζ resultante se transformó luego en células de *E. coli* S17-1 competentes. Finalmente, esta construcción se introdujo por conjugación en células de la cepa PdΔζ como se describió anteriormente. La cepa complementada se denominó PdΔζ + ζ.

7.8 Curvas de crecimiento

Las cepas de *P. denitrificans*: Pd1222 (PdWT), la PdΔζ (mutante) y la PdΔζ+ζ (mutante complementada) se cultivaron en 2 ml de medio LB a 30 ºC hasta que alcanzaron 0.6 unidades de absorbancia (UA) a 600 nm. De las cepas que estaban a 0.6 UA, se tomó 1 ml de cada una de ellas y se inoculó por separado en 60 ml de medio líquido (LB o succinato) contenido en un matraz de 250 ml. Los medios inoculados se incubaron a 30 ºC durante 48 h a 175 rpm. Durante las 48 h que las cepas se incubaron, cada dos horas se tomaron alícuotas de 200 μl de cada cepa. Los 200 μl tomados de cada cepa se diluyeron hasta 1 ml con el correspondiente medio LB o succinato, y la absorbancia se midió a 600 nm en un espectrofotómetro WPA Biowave (Biochrom, Cambridge, RU) (Figura 19).

7.9 Preparaciones de lisado celular

Las cepas Pd1222 y PdΔζ se cultivaron en medio LB a 30 ºC durante 24 o 48 h. Las células de cada cepa se cosecharon luego por centrifugación y se resuspendieron en una **disolución denominada A+** con un contenido 10% de glicerol, 50 mM de

sacarosa, 1 mM de EDTA, 1 mM de ATP, 1 mM de benzamidina, 1 mM de PMSF, 4 tabletas por litro de los inhibidores de proteasa (Roche, Mannheim, Alemania) (número de catálogo 05056489001) y 20 mM de Tris ajustado a pH 7.6. Las células de cada cepa se sonicaron en un baño de agua con hielo y se obtuvieron extractos de células para cada cepa. Se sonicó durante 10 segundos y se dejó enfriar 1 minuto, este proceso se repitió 10 veces. El minuto entre cada sonicado es para evitar que las muestras se calienten demasiado.

7.10 Cuantificación de proteína por el método Lowry-TCA

La concentración de proteína de los lisados celular, de la F_1 y de la F_1F_O se cuantificó mediante el método Lowry-TCA (93,94). Se preparan una mezcla de dos disoluciones, la primera disolución de Na_2CO_3 al 2% en agua (disolución A), la segunda disolución lleva CuSO4 al 1%, Tartrato de Na y K al 2% en NaOH a 0.1N (disolución B). La mezcla de ambas disoluciones lleva 50 veces más de la disolución A que de la disolución B (50 A : 1 B). Se prepara otra disolución a partir del reactivo de Folin & Ciocalteu's phenol (Sigma Aldrich Co., St. Louis, Missouri, USA.), mezclando 50% del reactivo de Folin con 50% de agua. Tanto las muestras y la curva estándar (preparada con albúmina) se colocan en tubos de 1.5 ml y se llevan a un volumen de 1 ml. Se les añade 100 μl del detergente Desoxicolato, se mezcla y se incuba 10 min a temperatura ambiente, para que se solubilicen todas las proteínas que se encuentran en la membrana. A continuación, se añade 100 μl de ácido tricloroacético al 72 %, se mezcla y se incuba en baño de hielo durante 10 min para que se precipiten todas las proteínas. Los tubos en los que se encuentran las muestras se centrifugan durante 15 min y se elimina el sobrenadante. En seguida, se resuspende el precipitado (las proteínas) en 97.5 μl de agua con 2.5 μl de NaOH 2N. Una vez resuspendidas las muestras y la curva estándar, se procede a añadir 800 μl de la mezcla de disolución 50 A : 1 B, se mezcla y se incuba 10 minutos a temperatura ambiente. A continuación, se le añade a cada tubo que contiene muestra o curva estándar 100 μl de la mezcla de disolución Folin con agua, se mezcla y se incuba 30 minutos a temperatura ambiente. Se procede a tomar lectura de las muestras y la curva estándar en un espectrofotómetro a una longitud de onda

de 660 nm. Se grafican los datos y se calcula la concentración de proteína de las muestras interpolando las absorbancias a partir de la curva estándar.

7.11 Electroforesis desnaturalizantes en gel de poliacrilamida (SDS-PAGE)

Para identificar las proteínas de interés se realizó la técnica de SDS-PAGE Von Jagow (95). Los lisados celulares, las partículas sub-bacterianas (PSB), las fracciones obtenidas de las columnas, las fracciones F_1 purificadas y la subunidad ζ purificada se confirmaron o se seleccionaron dependiendo el caso de cada una de ellas a partir de separarlas mediante electroforesis en geles de poliacrilamida en condiciones desnaturalizantes. Primero se prepararon las siguientes disoluciones, **disolución para geles 3X**: Tris 3 M (pH 8.45), HCl 1 M, dodecilsulfato de sodio (SDS) 0.3 % (p/v); **disolución de ánodo**: Tris 100 mM (pH 8.9) y HCl (22.5 mM); **disolución cátodo**: Tris 100 mM (pH 8.25), Tricina 100 mM, SDS 0.1 %; **disolución de carga**: glicerol 15 %, SDS 2 %, bromofenol 0.02 %, disolución para geles 3X 12.5 %, DTT 1 mM, β-mercaptoetanol 5 %, todo disuelto en agua. Para poder separar las proteínas mediante la electroforesis se prepararon dos geles, el concentrador y el separador. **El gel concentrador** (4 %) se preparó con: disolución para geles 3X 33 %, del reactivo 30 % Acrylamide/Bis solution (37.5:1) 14.5 % (Bio-Rad, Berkeley, California, USA) (número de catálogo 161-0158), de una disolución de Persulfato de Amonio (PSA) al 10 % se utilizó 0.85 % (Sigma Aldrich Co., St. Louis, Missouri, USA), del reactivo tetrametiletilendiamina (TEMED) 0.17 % (Sigma Aldrich Co., St. Louis, Missouri, USA). **El gel separador** (12 %) se preparó con: disolución para geles 3X 33 %, del reactivo 30 % Acrylamide/Bis solution (37.5:1) 39.76 %, de una disolución de glicerol al 80 % se utilizó 8.24 % (Sigma Aldrich), de una disolución de PSA al 10 % se utilizó 0.5 %, del reactivo TEMED 0.1 %. Las disoluciones preparadas para ambos geles se colocan entre los vidrios del sistema Mini-protean Tetra Cell (Bio-Rad). La disolución del gel separador se coloca primero, esto es en la parte inferior de los vidrios, se añade 0.5 ml de isopropanol y se espera 15 min a que se polimerice la poliacrilamida. Una vez polimerizado el gel separador, se añade la disolución del gel concentrador, se colocan los peines que van a dar

forma a los pozos y se espera 15 min para que polimerice la poliacrilamida. Una vez que se polimerizan ambos geles, se cargan las muestras y el marcador de peso molecular (MPM) (Precision Plus Protein Standars: Unstained, Kaleidoscope o Western C) (Bio-Rad) se mezclan con la disolución de carga en una cantidad de 1:1. Las muestras o el MPM mezcladas con la disolución de carga se colocan cada una en pozo diferente del gel. A continuación, el gel se coloca en la cámara de electroforesis, colocando también las disoluciones de ánodo y cátodo y posteriormente se conecta la fuente de poder. La electroforesis se programa de 100 a 130 V durante 1 a 2.5 h a temperatura ambiente. Concluido el tiempo de la electroforesis, se procede a teñir los geles en disolución teñidora. La disolución teñidora está compuesta de Coomassie 0.1 % (Sigma Aldrich), metanol 40 %, ácido acético 10 %. Finalmente, los geles se destiñen con la disolución desteñidora. La disolución desteñidora está compuesta de metanol 50 % y ácido acético 7.5 %. Una vez desteñidos los geles, se analiza el patrón de las bandas.

7.12 Western blot

Para identificar las proteínas de interés se realizó la técnica de Western blot (96). En algunos de los casos, las proteínas que se encontraban en los geles en lugar de ser teñidas con la disolución teñidora se transfirieron a una membrana de polifluoruro de vinilideno (PVDF) con poros de 0.2 μm inmobilion P-SQ (Millipore). Para llevar a cabo la transferencia de las proteínas del gel de pliacrilamida hacia la membrana, se dispuso la membrana sobre el gel y a continuación se colocaron en el sistema de transferencia Mini-TransBlot Cell (Bio-Rad). La cámara de transferencia se llenó con la disolución de transferencia, se conectó la fuente de poder y se programó a 100 mA durante dos horas. La disolución de transferencia se preparó con: ácido N-ciclohexil-3-aminopropanesulfonico (CAPS) 10 mM (pH 11) y metanol 20 %. Terminando el tiempo de la transferencia, la membrana que ahora contiene a las proteínas se colocó en una disolución salina con detergente (PBS-Tween 20) que contenía leche baja en grasa al 5 % Svelty (Nestlé, Vevey, Suecia) y se incubó 2 horas a temperatura ambiente o toda la noche a 4 ^{o}C, en ambas ocasiones se dejó en agitación constante. La disolución PBS-Tween 20 se preparó con NaCl 136 mM, KCl 2.68 mM, Na2HPO4 10 mM, KH2PO4 1.76 mM y Tween-20

0.1 % (Sigma Aldrich). Una vez que se incubó la membrana en el PBS-Tween 20 con leche, se enjuagó la membrana con 30 ml de la disolución PBS-Tween 20. En seguida, se colocó la membrana en la misma disolución que contenía al anticuerpo primario y se incubó durante 2 horas a temperatura ambiente en agitación constante. Terminando la incubación con el anticuerpo primario, la membrana se lavó con disolución PBS-Tween 20 tres veces de 10 minutos cada una. Al finalizar los lavados, la membrana se colocó en disolución anterior que contenía la concentración pertinente del anticuerpo secundario y se incubó durante 1 hora a temperatura ambiente en agitación constante. Terminando la incubación con el anticuerpo secundario, la membrana se lavó con disolución PBS-tween tres veces de 10 minutos cada una. Después, a la membrana se le añadió el reactivo de revelado Inmobilon Western Chemiluminescent HRP Substrate (Millipore), se dejó 3 minutos, se removió el excedente del reactivo de revelado. Finalmente, la membrana se colocó en un equipo transiluminador modelo MICROCHEMI (DNR Bio-Imaging Systems) y se programó para que se tomaran imágenes después de diferentes tiempos de exposición (Figura 17 y Figura 21).

7.13 Preparación de partículas sub-bacterianas (PSB)

Células de las cepas PdWT y Pd$\Delta\zeta$ que se cultivaron en medio LB o medio succinato, se colectaron a través de centrifugación a 6,000 rpm durante 10 minutos. A las células colectadas, se les añadió lisozima para remover la pared celular y obtener esferoplastos. A partir de los esferoplastos de ambas cepas y se prepararon membranas invertidas mediante choque osmótico. A las membranas invertidas se les removió el ADN añadiendo DNAsa y $MgCl_2$ 10 mM. A continuación, las membranas invertidas se sonicaron durante 10 segundos y se dejó enfriarse 1 minuto, este proceso se repitió 10 veces. Este procedimiento se llevó a cabo mientras las membranas invertidas se encontraban en un recipiente con hielo para evitar que se calentaran durante la sonicación. Posteriormente, las membranas sonicadas se les centrifugó a 13,000 rpm durante 1 hora. Se descartó el sobrenadante y se recuperó la pastilla obtenida. A la pastilla se le añadió un pequeño volumen de **disolución A+** y se resuspendió sólo la parte superior rojiza

utilizando un pincel. La parte resuspendida son las partículas sub-bacterianas (PSB), las cuales contienen los complejos respiratorios funcionales.

7.14 Ensayo de síntesis de ATP por la F_1F_O-ATP sintasa

A las PSB se les midió actividad de síntesis de ATP utilizando un ensayo acoplado. El ensayo acoplado utiliza las enzimas hexocinasa y glucosa-6-fosfato deshidrogenasa. Se utilizan estas dos enzimas debido a que una cataliza la fosforilación de la glucosa a glucosa 6-fosfato, y la segunda enzima cataliza la deshidrogenación de la glucosa 6-fosfato en 6-fosfogluconolactona. En la primera reacción se utiliza un fosfato para fosforilar a la glucosa, dicho fosfato proviene de una molécula de ATP, quedando una molécula de ADP disponible en el medio. Dicha molécula de ADP es transformada por la F_1F_O-ATP sintasa en ATP y la molécula de ATP nuevamente se utiliza para fosforilar otra molécula de glucosa por la hexocinasa. En la segunda reacción se reduce una molécula de $NADP^+$ en NADPH. Por ello, este sistema de dos enzimas se acopla para mantener la concentración de ADP constante y en el segundo paso para reducir una molécula de $NADP^+$ por cada ATP sintetizado. La acumulación de NADPH se va siguiendo a 340 nm a una temperatura de 37 ºC. La mezcla de reacción del sistema acoplado se preparó con Tris / HCl 20 mM (pH 7,4), sacarosa 250 mM, ADP 1 mM, $MgCl_2$ 5 mM, Pi 20 mM, AP5A 100 µM, $NADP^+$ 0.5 mM, glucosa 10 mM y 30 U / ml de G6PDH y hexocinasa. La mezcla de reacción del sistema acoplado se preincubó durante 10 minutos a 37ºC y posteriormente se añadieron las PSB, seguido de la adición de succinato 10 mM para iniciar la reacción de síntesis de ATP. La pendiente lineal del aumento de la absorbancia a 340 nm se tomó para estimar la velocidad de síntesis de ATP. Se realizaron trazos en presencia de desacoplante (FCCP) y venturicidina para descartar cualquier actividad de síntesis de ATP que no fuese mediada por la ATP sintasa. Posteriormente, se restaron los trazos con FCCP y venturicidina a los trazos de actividad sin ellos (Figura 20 y Figura 22).

7.15 Ensayo de hidrólisis de ATP por la F_1F_O-ATPasa

A las PSB o a la fración F_1 se les midió actividad de hidrólisis de ATP utilizando un ensayo acoplado. El ensayo acoplado utiliza las enzimas piruvato cinasa y lactato deshidrogenasa. Se utilizan estas dos enzimas debido a que una cataliza la defosforilación del fosfoenolpiruvato, y la segunda enzima cataliza la hidrogenación del piruvato para dar lugar al lactato. En la primera reacción se utiliza el fosfato liberado del fosfoenolpiruvato para fosforilar una molécula de ADP y obtener una molécula de ATP. Dicha molécula de ATP es hidrolizada por la F_1F_O-ATPasa en ADP y Pi, por lo que la molécula de ADP nuevamente se fosforila y se genera otro ATP. En la segunda reacción se oxida una molécula de NADH a NAD^+. Por ello, este sistema de dos enzimas se acopla para mantener la concentración de ATP constante y en el segundo paso para oxidar una molécula de NADH por cada ATP hidrolizado. La oxidación del NADH se va siguiendo a 340 nm a una temperatura de 37 ºC. La mezcla de reacción del sistema acoplado contenía 50 mM de Tris / acetato (pH 8.0), 250 mM de sacarosa, 3 mM de Mg + 2 acetato, 30 mM de K + 1 acetato, 1.5 mM de PEP, 3 mM de ATP, 200 µM de NADH, 4 U / ml de PK, 4 U / ml de LDH. Para las mediciones realizadas con PSBs, se añadieron inhibidores de la cadena transportadora de electrones 2 µg / ml de rotenona o 5 mM de cianuro (NaCN) como (complejo I o complejo IV, respectivamente) para evitar la oxidación respiratoria de NADH; las reacciones de ATPasa se iniciaron mediante la adición de PSBs a las celdas. Se preincubó una reacción blanco que contenía el inhibidor venturicidina (4 µg / ml) el cual es específico de la F_1F_O-ATPasa durante 10 minutos. La actividad residual insensible a venturicidina se restó de la actividad en ausencia del inhibidor. Algunas mediciones se llevaron a cabo utilizando LDAO 0.15% como activador de la actividad ATPasa, estas medidas incluyeron cianuro sódico 5 mM para bloquear la oxidación respiratoria de NADH, pero no venturicidina ya que el detergente altera la membrana bacteriana; en este caso, se utilizó otro blanco que incluía 5 mM de azida de sodio (NaN_3) y la actividad residual se restó de la actividad total en ausencia del inhibidor. Para las muestras F_1-ATPasa o F_1F_O-ATPasa, las reacciones se iniciaron mediante la adición de estas enzimas a la celda de reacción.

7.16 Purificación de la Fracción F_1

La fracción F_1 se extrajo a partir de membranas invertidas utilizando cloroformo. Se separó la parte hidrofóbica de la soluble centrifugando a 15,600 RCF (fuerza centrífuga relativa) durante 15 minutos a temperatura ambiente. La fase acuosa se recuperó y en seguida se centrifugó a 143,791 RCF durante 1 hora a 15 ^{o}C. Se recuperó el sobrenadante y posteriormente el sobrenadante que contenía a la F_1 se unió en una columna de cromatografía de líquidos HiTrap Q Sepharose (Q HP) (5 ml, GE Healthcare, Little Chalfont, Reino Unido). Posteriormente, la enzima se disoció de la columna usando un gradiente de NaCl (0 a 1M), las fracciones que contenían la F_1 se seleccionaron mediante ensayos de ATPasa y SDS-PAGE. Las fracciones seleccionadas se desalaron centrifugando en un Amicon Ultra-15 de corte de 10 kDa (Millipore, Darmstadt, Alemania). A continuación, la muestra que contiene a la F_1 se une a una columna de afinidad etil aminohexil (EAH) (Amersham Biosciences, Uppsala, Suecia). La F_1 se eluye mediante un gradiente de NaCl (100 a 500 mM) y las fracciones se seleccionaron como se describió anteriormente para la columna HiTrap. Finalmente, la F_1 se concentró y se inyectó en una columna de exclusión molecular Superdex 200 (GE Healthcare, Little Chalfont, RU). Las fracciones que contenían la F_1 se seleccionaron como se describió anteriormente. La F_1 purificada de ambas cepas se observó después de realizar un SDS-PAGE y un WB (Figura 24).

7.17 Sobreexpresión y purificación de la subunidad recombinante ζ de *P. denitrificans*

En el laboratorio se contaba con células de *E. coli* BL21 (DE3) pLys S codon plus transformadas con el plásmido pT7-7 / ζ Pd. Estas células se cultivaron en medio LB y se cosecharon mediante centrifugación. Las células cosechadas se lisaron mediante sonicación (10 veces de 30 s intercaladas con 1 minuto de intervalo de descanso). Se removió el ADN añadiendo DNAsa y $MgCl_2$ 10 mM. La parte membranal se separó mediante centrifugación y se recuperó el sobrenadante. Al sobrenadante se le añadió 50 % de sulfato de amonio (314 mg / ml de muestra), el sulfato de amonio se añadió lentamente mientras que la muestra se estaba agitando

en un baño de hielo. La muestra se centrifugó a 14,000 rpm durante 15 minutos a 4 ^{o}C. Al sobrenadante se le vuelvió a añadir sulfato de amonio hasta alcanzar 80 % de saturación (210 mg / ml de muestra) y se repitió el paso de centrifugación. Se colectó el precipitado, se resuspendió en una disolución que contenía 20 mM de fosfato de potasio monobásico (KH_2PO_4) (pH 7), 1mM de EDTA y 1mM de PMSF (denominada disolución B). Se desaló la muestra colocándola dentro de una membrana para diálisis de poro de 3.5 kDa y la membrana se colocó en un recipiente que contenía 1 litro de la disolución B. Se dejó aproximadamente 24 h en agitación suave a 4 ^{o}C. Una vez desalada la muestra, ésta se unió a una columna de intercambio iónico de sefarosa dietil amino etil (DEAE) (Pharmacia Biotech, Estocolmo, Suecia). La subunidad ζ se eluyó de la columna utilizando un gradiente de KH_2PO_4 (0 a 500 mM). Se colectaron las fracciones como se describió en la purificación de la F_1. Las fracciones seleccionadas se concentraron y se pasaron por una columna de exclusión molecular superdex 75 (GE Healthcare, Little Chalfont, RU). Las fracciones que salieron de la columna superdex 75 se colectaron y posteriormente se seleccionaron como se describió anteriormente. Las fracciones seleccionadas se unieron y se concentraron, se cuantificó la proteína y se realizó un SDS-PAGE (Figura 24).

7.18 Ensayos de inhibición de la F_1 por reconstitución homóloga con la subunidad ζ recombinante.

Para medir la capacidad de inhibición de la subunida ζ sobre la actividad F-ATPasa, a la F_1 purificada de la cepa PdWT y PdΔζ se le incubó con la subunidad ζ recombinante a las concentraciones indicadas durante 20 min a temperatura ambiente (Figura 25). Las incubaciones se llevaron a cabo en una disolución que contenía Tris-HCl 20 mM (pH 8), sacarosa 250 mM, ATP 1 mM y $MgCl_2$ 1 mM, sulfito 60 mM. Después de la incubación, se midió la actividad en una celda de 1 ml y que contenía la dilución del ensayo acoplado para medir la actividad ATPasa (descrita anteriormente). La concentración de sulfito al llevarla al volumen de 1 ml quedó a 1.5 mM, para evitar la inhibición de las enzimas por el sulfito, se añadió 3 veces más de piruvato cinasa y de lactato deshidrogenasa a la mezcla de reacción. Además,

cuando se requirió, el sistema acoplado contenía al detergente lauril dimetilamina N-oxido (LDAO) al 0.015 % como activador de la enzima (Figura 25).

7.19 Potencial de membrana a partir de PSB

Para estimar el potencial de membrana generado por la hidrólisis de ATP mediada por la F_1F_O-ATPasa, se utilizaron PSB de la cepa PdWT y Pd$\Delta\zeta$. Las PSB de ambas cepas por separado se colocaron en una celda que contenía una disolución con 20 mM de ácido 3-morfolinopropano-1-sulfónico (MOPS) (pH 7.5), 125 mM de cloruro de potasio (KCl), 5 mM de cloruro de magnesio ($MgCl_2$), 100 μM de EGTA, 3.6 μM de valinomicina y 1 μM de 9-amino-6-cloro-2-metoxiacridina (ACMA). El fluoróforo ACMA al ser irradiado con luz a 419 nm emite fluorescencia a 483 nm. Además, el ACMA disminuye su fluorescencia debido a su acumulacion dentro de las vesículas en respuesta al gradiente de protones. Así que, cuando los protones se acumulan en el interior de las PSB, el ACMA pasará al interior de las PSB, se protonará y adquirirá una carga positiva, y disminuirá la fluorescencia emitida. La celda con las PSB y con la disolución que contiene al ACMA se colocó en el fluorómetro ISS PC1 con agitación constante a 37 ^oC, la fluorescencia emitida por el ACMA se midió y se graficó normalizada en porcentaje. Posteriormente se añadió a la celda succinato (5 mM), el succinato es reducido por el complejo succinato deshidrogenasa y se transfieren electrones a los siguientes complejos de la CTE y el complejo III y IV bombean protones al interior de las PSB. Se midió la disminución de la fluorescencia emitida por el ACMA. A continuación, se disipó el gradiente electroquímico añadiendo cianuro de sodio (NaCN) (5 mM) y se midió la recuperación de la fluorescencia emitida por el ACMA. De manera subsecuente, se añadió ATP/Mg (2 mM) y la F_1F_O-ATPasa generó un gradiente electroquímico y se midió la disminución de la fluorescencia emitida por el ACMA. Por último, las PSB fueron desacopladas añadiendo mesoxalonitrilo 4-trifluorometoxi fenilhidrazona (FCCP) (5 mM) y se midió el aumento de la fluorescencia emitida por el ACMA (Figura 22) tal como se describe en (97).

7.20 Potencial de membrana a partir de células vivas por citometría de flujo.

Para estimar el potencial de membrana en células vivas, se llevó a cabo una tinción con el sistema comercial de potencial de membrana BacLight (Molecular Probes por Thermo Fisher Scientific, Waltham, Massachusetts, USA) (Número de catálogo B34950) y se estimó el potencial de membrana mediante citometría de flujo. Se utilizó el colorante 3,3'-dietiloxicarbocianuro 3-clorofenilhidrazona ($DiOC_2(3)$), el cual atraviesa la membrana celular de las bacterias y tiene afinidad por aquellas membranas con potencial de membrana. El colorante $DiOC_2(3)$ a pequeñas concentraciones es capaz de emitir fluorescencia en el espectro verde (530 nm) y a mayores concentraciones es capaz de emitir fluorescencia en el espectro rojo a 610 nm. Por lo que las células con mayor potencial de membrana acumularán una mayor concentración del $DiOC_2(3)$ y emitirán mayor señal a 610 nm. El cociente 610 nm / 530 nm indicará un mayor potencial de membrana. Las células de diluyeron en su propio medio de cultivo hasta alcanzar 1 de absorbancia a 600 nm y posteriormente se tomaron aproximadamente 100 μL y se diluyeron a 1 ml en una disolución que contenía Tris 10 mM (pH 7.4), glucosa 10 mM y EDTA 1 mM. Posteriormente, a las células PdWT, PdΔζ y PdΔζ+ζ disueltas se les añadió 30 μM del $DiOC_2(3)$ durante 30 min a temperatura ambiente. El EDTA se utilizó para permeabilizar la pared celular de éstas bacterias gram-negativas para que el $DiOC_2(3)$ pudiera atravesarla y acumularse dentro de la célula (98,99). Dos controles se llevaron a cabo, el primero fue añadir FCCP a las células para desacoplar la membrana y subsecuentemente se les incubó con el $DiOC_2(3)$. Este control permitió eliminar la señal emitida por la acumulación del colorante en células sin potencial de membrana. El segundo control fue medir la fluorescencia de las células que no llevaban colorante ni desacoplante, para restar la señal de fluorescencia de las células sin teñir. La fluorescencia emitida por las células teñidas con el colorante $DiOC_2(3)$, con FCCP y sin colorante ni desacoplante se midió mediante en un citómetro de flujo CytoFLEX S (Beckman Coulter Life Sciences, Indianapolis, Indiana, USA) (Figura 23).

7.21 Estimación de ATP intracelular

La concentración de ATP intracelular se estimó utilizando el sistema comercial Adenosine 5'-triphosphate (ATP) Bioluminescent Assay (SIGMA-ALDRICH, St. Louis, MO, USA) (Número de catálogo FLAA). Se tomó 50 μL de células a una absorbancia de 1 a 600 nm en 450 μL de una disolución que contenía Tris-HCl 100 mM (pH 7.8) y EDTA 4 mM. Se lisaron las células colocando los 500 μL en agua hirviendo durante 2 minutos. Después, las células hervidas se incubaron en hielo durante 5 minutos. A continuación, los restos de membrana se eliminaron de los lisados celulares por centrifugación a 15,160 RCF. Al lisado celular se le añadió el reactivo luciferin/luciferasa, este sistema emite bioluminiscencia proporcional a la cantidad de ATP que se encuentra en la muestra. Para calcular la concentración de ATP intracelular, se preparó una curva de calibración de ATP como se describe por el fabricante del sistema comercial Adenosine 5'-triphosphate (ATP) Bioluminescent Assay. Se detectó la bioluminiscencia en un luminómetro POLARstar Omega (BGM LABTECH, Offenburg, Alemania) (Figura 26).

8 Resultados

8.1 Diseño de la cepa mutante de *P. denitrificans* sin el gen que codifica para la subunidad ζ.

Para obtener una cepa de *P. denitrificans* sin el gen que codifica la subunidad ζ, se diseñó una construcción que contenía la secuencia aledaña río arriba del codón de inicio del gen ζ y una secuencia aledaña río abajo del codón de paro. Entre ambas secuencias se ligará una secuencia de resistencia al antibiótico kanamicina (Km) y mediante recombinación homóloga se reemplazará el gen que codifica para la subunidad ζ por el gen de resistencia a Km del genoma de *P. denitrificans*.

Diseño de la construcción Δζ. Se amplificaron mediante PCR las secuencias aledañas al gen ζ, río arriba (RAR) (997 pb) y río abajo (RAB) (870 pb) (Figura 14 A y B); además se amplificó la secuencia de resistencia a Km (1,019 pb) (Figura 14 C). Para cada amplificación se utilizaron los oligonucleótidos pertinentes (tabla 3) (Figura 13).

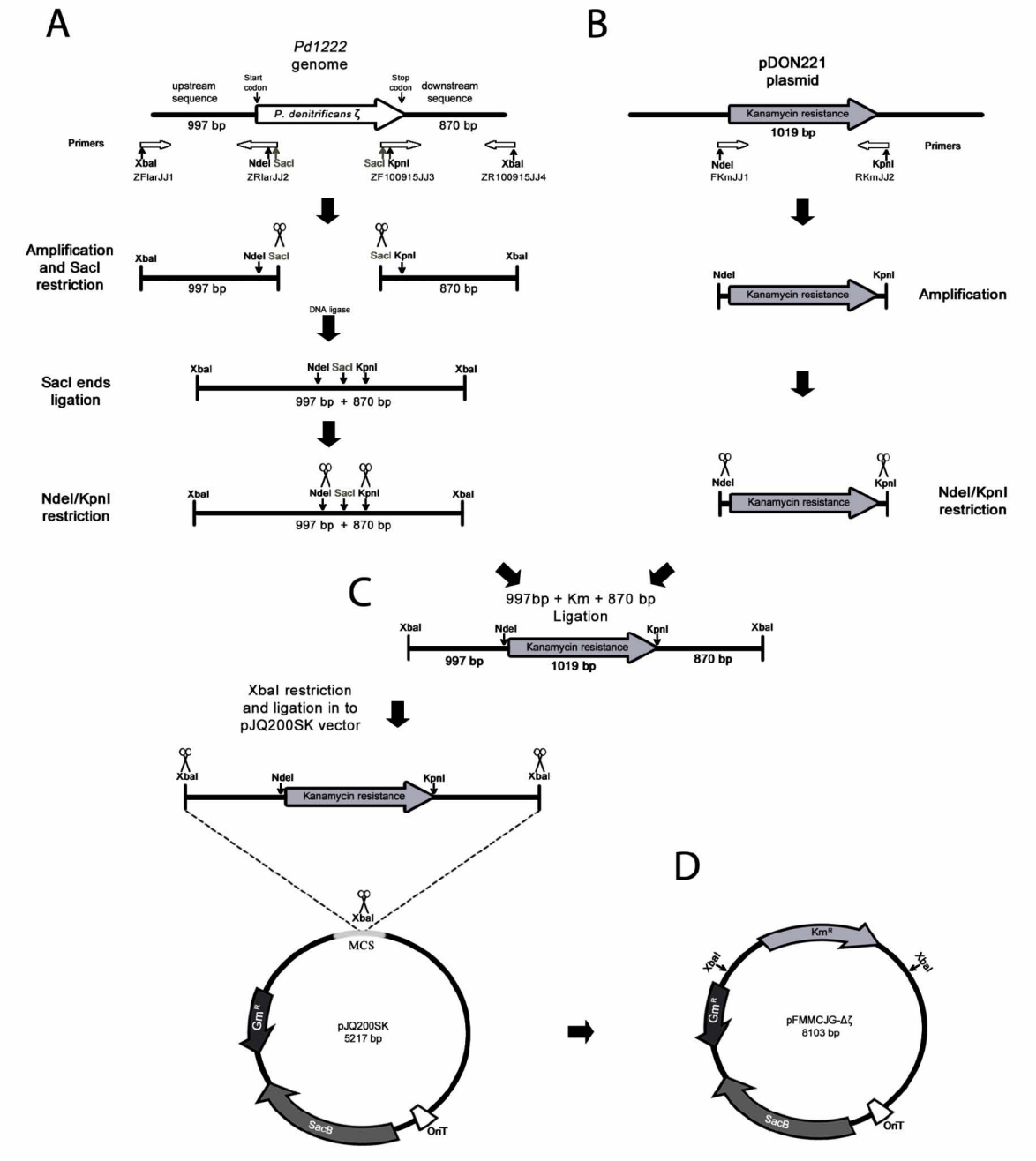

Figura 13. Diseño de la cepa mutante de *P. denitrificans* sin el gen que codifica para la subunidad ζ. A) Los oligonucleótidos sentido y antisentido utilizados para la amplificación de dos fragmentos diferentes del genoma Pd1222 se muestran en flechas blancas. Estos oligonucleótidos se usaron para amplificar la secuencia río arriba de 997 pb a partir del codón de inicio del gen ζ y la secuencia río abajo de 870 pb a partir del codón de paro del gen ζ. Se añadieron diferentes sitios de restricción a las secuencias de los oligonucleótidos y las enzimas de restricción se muestran en la figura. Uno de

estos sitios de restricción (sitio SacI) se usó para generar un fragmento de fusión que contiene ambas amplificaciones (997 y 870 pb). Las secuencias río arriba y río abajo se digirieron con SacI y a continuación se ligaron entre ellas. Posteriormente, las secuencias se digirieron con NdeI y KpnI. B) Los oligonucleótidos sentido y antisentido usados para la amplificación del marcador de resistencia a kanamicina (Km^R) del plásmido pDON221 se muestran en flechas blancas. Estos oligonucleótidos tenían dos sitios de restricción, en el extremo 5' prima de la secuencia Km^R se añadió el sitio de restricción NdeI y en el extremo 3' prima un sitio de restricción KpnI. Una vez amplificada la secuencia Km^R, se digirió con las enzimas NdeI y KpnI. C) La secuencia río arriba–río abajo y la secuencia Km^R se ligaron entre ellas. Se obtuvo la construcción río arriba–Km^R–río abajo. Esta construcción se digirió con XbaI y en seguida se ligó al plásmido pJQ200SK previamente digerido con XbaI. D) Mapa del vector plásmido pJQ200Δζ final (pFMMCJG- Δζ).

Ligación de las secuencias río arriba – Km – río abajo. Las secuencias amplificadas: río arriba (RAR), río abajo (RAB) y Km, se ligaron todas a un plásmido de subclonación pJET y se transformaron en células de la cepa *E. coli* DH5α competentes. Las clonas positivas fueron seleccionadas mediante el uso del antibiótico ampicilina y se les extrajo el ADN plasmídico. Posteriormente, el ADN plasmídico que contenía a las secuencias RAR y RAB se digirió con la enzima SacI y se ligaron ambas secuencias (Figura 13). A continuación, la construcción pJET / RAR - RAB se transformó en células competentes *E. coli* DH5α. La construcción pJET / RAR - RAB se extrajo de las clonas positivas y se confirmó digiriendo el vector + inserto con la enzima de restricción XbaI (Figura 14 B). Confirmada la construcción pJET / RAR - RAB, se digirió con las enzimas de restricción NdeI y KpnI. De la misma manera, el plásmido pJET / Km se digirió con las enzimas NdeI y KpnI. La secuencia de Km se separó del pJET mediante una electroforesis en gel de agarosa. El inserto Km se purificó a partir del gel de agarosa y se ligó con la construcción pJET / RAR - RAB (secuencia que previamente se digirió con NdeI y KpnI). La ligación se transformó en células competentes *E. coli* DH5α y a las clonas positivas se les extrajo el ADN plasmídico. Para confirmar la presencia de la construcción **RAR – Km – RAB**, el ADN plasmídico se digirió con las enzimas de restricción XbaI, KpnI y NdeI + KpnI. Las digestiones se separaron en un gel de agarosa y se analizó la separación del inserto deseado (Figura 15). El pJET / **RAR – Km – RAB** digerido con la enzima XbaI dio lugar a dos bandas de ~3,000 pb. Una

banda corresponde al plásmido pJET que mide 2,974 pb y la otra banda corresponde a la construcción **RAR – Km – RAB** de 2886 pb. Dado que ambas bandas 2,974 pb y 2,886 pb miden casi igual se ven sobrelapadas (Figura 15, tercer carril de izquierda a derecha). El pJET / **RAR – Km – RAB** digerido con la enzima KpnI dio lugar a una banda de ~6,000 pb. La banda corresponde al plásmido **pJET / RAR – Km – RAB** linearizado que mide 5,860 pb (Figura 15, cuarto carril de izquierda a derecha). El pJET / **RAR – Km – RAB** digerido con las enzimas NdeI y KpnI dio lugar a dos bandas. Una banda corresponde al plásmido pJET / **RAR – RAB** que mide 4,441 pb y la otra banda corresponde a la secuencia de Km de 1,019 pb (Figura 15, cuarto carril de izquierda a derecha). Con estas restricciones enzimáticas se confirmó el ensamblaje correcto de la construcción **RAR – Km – RAB** la cual se denominó Δζ. Una vez ligada la construcción Δζ, la digestión con la enzima XbaI se ligó con el plásmido pJQ200SK (previamente digerido con XbaI). La ligación se transformó en células competentes *E. coli* DH5α, se extrajo el ADN plasmídico y se digirió con la enzima XbaI. La digestión se separó en una electroforesis en gel de agarosa (Figura 16), en donde se pueden distinguir dos bandas, una de 5,217 pb correspondiente al plásmido pJQ200SK y otra banda de 2,886 pb correspondiente a la construcción Δζ (Figura 16). Al plásmido modificado pJQ200SK / Δζ se le denominó pFMMCJG-Δζ (Tabla 2, Figura 13).

8.2 Conjugación de la cepa *E. coli* S17-1 / pFMMCJG-Δζ con la cepa *P. denitrificans* 1222.

El plásmido pFMMCJG-Δζ se transformó en células competentes de la cepa *E. coli* S17-1. Las clonas positivas se seleccionaron mediante ensayos de restricción con las respectivas enzimas y ADN plasmídicos. Una clona positiva de la cepa *E. coli* S17-1 / pFMMCJG-Δζ se conjugó con la cepa *P. denitrificans* 1222 (Pd1222) como se describe en materiales y métodos. Una vez que el plásmido pFMMCJG-Δζ se encontraba dentro de la cepa Pd1222, mediante recombinación homóloga el gen de la subunidad ζ encontrado en el genoma bacteriano fue sustituido por la secuencia de resistencia a Km que se encontraba en el plásmido pFMMCJG-Δζ . De la misma

manera, el gen de la subunidad ζ que se encontraba en el genoma pasó al plásmido. El plásmido pFMMCJG-Δζ no se puede replicar en *P. denitrificans*, por lo que se pierde conforme las células de *P. denitrificans* se dividen. La cepa *P. denitrificans* 1222 / pFMMCJG-Δζ se denominó PdΔζ. La cepa PdΔζ se seleccionó cultivándola en medio LB con gentamicina, Km y rifampicina y subsecuentemente se cultivó nuevamente en medio LB añadiendo sacarosa al 10 %.

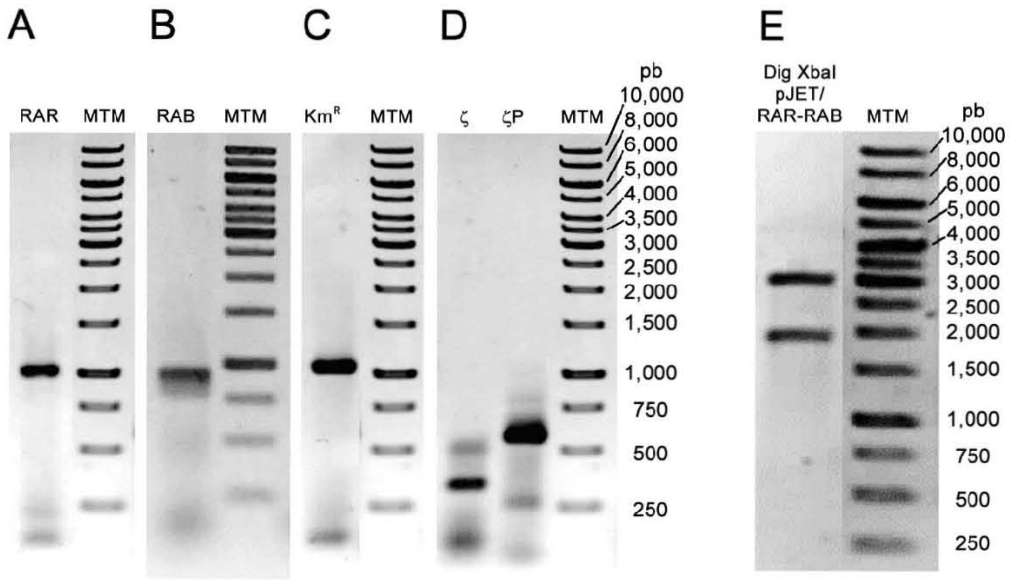

Figura 14. Amplificaciones para la obtención de la construcción Δζ y ligación de las secuencias río arriba–río abajo. En A), B), C), D) y E) se muestra imágenes de los geles de agarosa al 2% teñidos con bromuro de etidio. Los tamaños de los productos de PCR y la digestión se resolvieron mediante una electroforesis en gel de agarosa. A) PCR de la secuencia río arriba (RAR) (997 pb). B) PCR de la secuencia río abajo (RAB) (870 pb). C) PCR de la secuencia de resistencia a kanamicina (Km^R) (1019 pb). E) El pJET / RAR-RAB fue digerido con la enzima de restricción XbaI. El pJET corresponde a la banda de 2,974 pb y el RAR-RAB corresponde a la banda de 1889 pb. El marcador de tamaño molecular (MTM) se corrió en el siguiente carril en cada uno de los geles. En el gel E) la imagen del gel se cortó para mostrar el MTM a lado de la digestión.

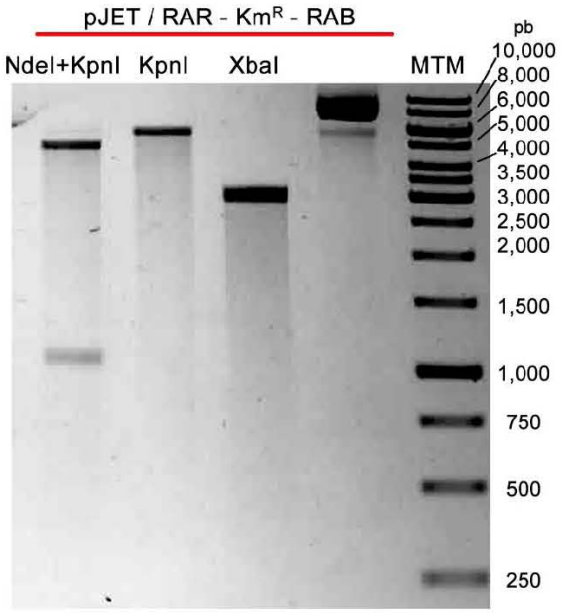

Figura 15. Confirmación del correcto ligamiento de la construcción pJET / RAR – KmR – RAB (ΔζΔζ). Se muestra la imagen de un gel de agarosa al 2% teñido con bromuro de etidio. Para confirmar la correcta ligación de la construcción pJET / RAR – Km^R – RAB, se le realizaron varias digestiones para confirmar el correcto tamaño de los diversos productos de las digestiones. Los tamaños de los productos de las digestiones se resolvieron mediante una electroforesis en gel de agarosa. La línea roja indica que todos los carriles que se encuentran debajo de la misma fueron cargados con la construcción pJET / RAR – Km^R – RAB y debajo de la línea roja se indica con que enzimas se digirió. En el caso del carril que no tiene indicada ninguna enzima no fue digerida y se corrió sin ningún tipo de digestión. El marcador de tamaño molecular (MTM) se corrió en el último carril. La construcción pJET / RAR – Km^R – RAB digerida con las enzimas de restricción NdeI+KpnI da lugar a dos bandas de tamaños diferentes, una banda de 4,841 pb correspondiente al pJET / RAR – RAB y la otra banda de 1,019 pb correspondiente a la Km^R. La construcción pJET / RAR – Km^R – RAB digerida con la enzima de restricción KpnI da lugar a una banda de tamaño de 5,860 pb correspondiente a la construcción pJET / RAR – Km^R – RAB linealizada. La construcción pJET / RAR – Km^R – RAB digerida con XbaI da lugar a dos bandas, una banda de tamaño de 2,974 pb correspondiente al plásmido pJET linealizado, la segunda banda de tamaño de 2,886 pb correspondiente a RAR – Km^R – RAB. La banda del plásmido pJET y la banda del RAR – Km^R – RAB al tener un tamaño similar corrieron a la misma altura por lo que sólo se ve una banda en dicho carril.

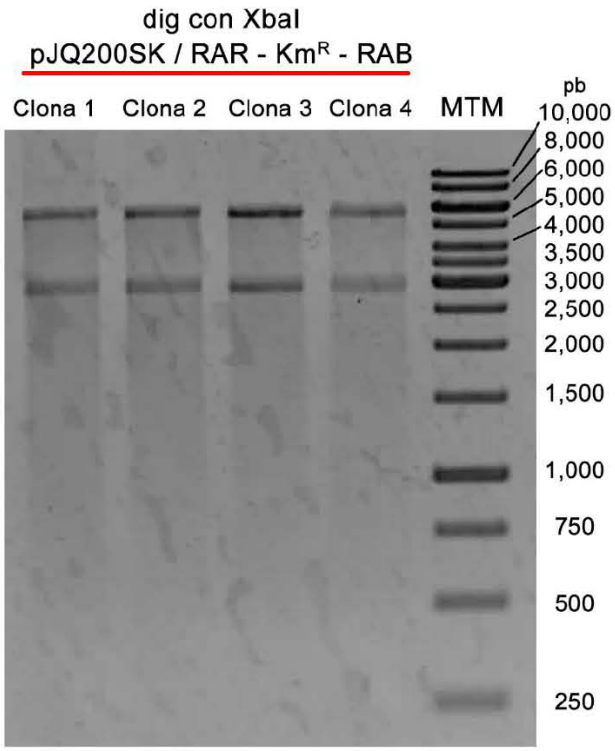

Figura 16. Confirmación del correcto ligamiento de la construcción pJQ200SK / RAR – KmR – RAB (Δζ). Se muestra la imagen de un gel de agarosa al 2% teñido con bromuro de etidio. Para confirmar la correcta ligación de la construcción pQ200SK / RAR – Km^R – RAB, se les realizó una digestión al ADN plasmídico extraído de varias clonas. La digestión se realizó con la enzima de restricción XbaI. Los tamaños de los productos de las digestiones se resolvieron mediante una electroforesis en gel de agarosa. La línea roja indica que todos los carriles que se encuentran debajo de la misma fueron cargados con la construcción pJQ200SK / RAR – Km^R – RAB y debajo de la línea roja se indica que se digirió con la enzima XbaI. El marcador de tamaño molecular (MTM) se corrió en el último carril. La construcción pQ200SK / RAR – Km^R – RAB digerida con la enzima de restricción XbaI da lugar a dos bandas de tamaños diferentes, una banda de 5,217 pb correspondiente al pJQ200SK y la otra banda de 2,886 pb correspondiente a RAR – Km^R – RAB.

8.3 Obtención de la cepa mutante complementada PdΔζ+ζ.

Para confirmar que los efectos observados en la cepa PdΔζ se deban a la ausencia de la subunidad ζ y no a efectos secundarios derivados del proceso de recombinación homóloga, se obtuvo una cepa mutante complementada denominada PdΔζ+ζ. Para obtener la cepa PdΔζ+ζ, se amplificó la secuencia de la subunidad ζ con su propio promotor (ζP), esto es, los 314 pb de la secuencia de la subunidad ζ con los primeros 200 pb aledaños río arriba a su codón de inicio (514

pb) (Figura 14 D). Una vez amplificada la secuencia de ζP, se ligó a un plásmido pJET y se llevó a cabo el mismo procedimiento hasta tener la secuencia ζP ligada en un plásmido pBBR1 MCS-5. El plásmido pBBR1 MCS-5 / ζP se denominó pFMMCJG-ζ. A continuación, el plásmido pFMMCJG-ζ se transformó en células de *E. coli* DH5α competentes y se confirmó como se ha descrito anteriormente para los otros plásmidos. Confirmado el plásmido pFMMCJG-ζ, se transformó en células de la cepa *E. coli* S17- 1 competentes y se seleccionaron las clonas positivas como se ha mencionado anteriormente. La cepa *E. coli* S17- 1 / pFMMCJG-ζ, se conjugó con la cepa PdΔζ y se obtuvo una la cepa mutante complementada PdΔζ+ζ.

8.4 Confirmación de la cepa *P. denitrificans* Δζ (PdΔζ).

Confirmamos la obtención de la cepa PdWT, PdΔζ y PdΔζ+ζ mediante PCR y WB. Para confirmar las tres cepas mediante PCR, extrajimos el ADN total de las tres cepas y este ADN total junto con sus oligonucleótidos pertinentes (tabla 3) se utilizaron para amplificar mediante PCR el gen de la subunidad ζ o el cassette de resistencia a Km. Una vez que se llevaron a cabo los PCR de cada cepa, se separó el ADN mediante una electroforesis en gel de agarosa. El gen de la subunidad ζ se amplificó utilizando el ADN total de la cepa silvestre PdWT y PdΔζ+ζ (Figura 17 A). Sin embargo, en la cepa mutante PdΔζ como esperábamos no se amplificó el gen ζ (Figura 17 A). La secuencia de resistencia a Km se amplificó en las cepas mutante PdΔζ y mutante complementada PdΔζ+ζ (Figura 18), mientras que no se amplificó en la cepa silvestre PdWT (Figura 18). De la misma manera, confirmamos las tres cepas mediante WB. Primero obtuvimos lisados celulares de las tres cepas y estos lisados celulares se separaron mediante una electroforesis en gel de acrilamida en condiciones desnaturalizantes. Las proteínas del gel de acrilamida se transfirieron a una membrana y esta membrana se expuso a los anticuerpos anti-ζ y anti-β. Como se esperaba, el anticuerpo anti-ζ sólo reconoció la presencia de la subunidad ζ en los lisados celulares de las cepas PdWT y PdΔζ+ζ, e igualmente como esperábamos la subunidad ζ no fue reconocida por el anticuerpo anti-ζ en el lisado celular de la cepa mutante PdΔζ (Figura 17 B).

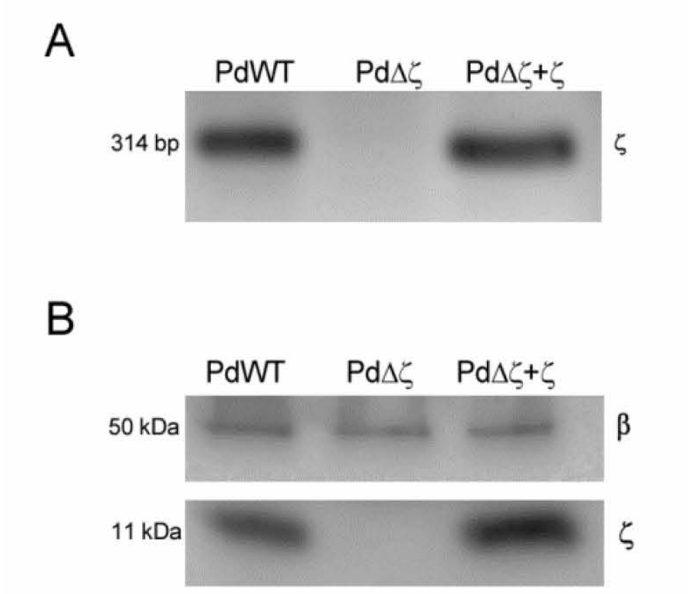

Figura 17. Confirmación de la cepa PdΔζ. A) El gen ζ (314 pb) se amplificó por PCR a partir de ADN genómico de tres cepas diferentes de *P. denitrificans*: la silvestre (PdWT), la mutante sin el gen ζ (PdΔζ) y la mutante complementada con el gen ζ (PdΔζ+ζ). Las amplificaciones de ADN se resolvieron mediante electroforesis en un gel de agarosa al 2%. B) Células de las cepas PdWT, PdΔζ y PdΔζ+ζ crecidas en medio LB durante 24 h y lisadas posteriormente por sonicación. Los lisados celulares se resolvieron mediante SDS-PAGE y mediante Western blot se identificaron las subunidades β y ζ.

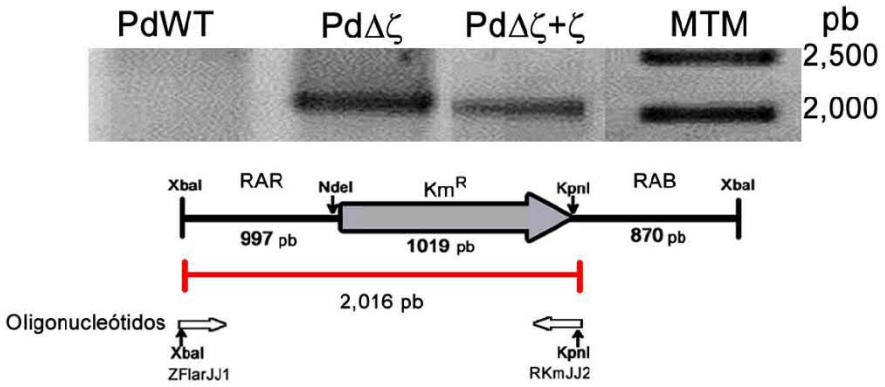

Figura 18. La cepa PdΔζ y PdΔζ+ζ amplifican la secuencia de resistencia a Kanamicina (RAR - Km^R). Se muestra una imagen de un gel de agarosa teñido con bromuro de etidio. La secuencia RAR - Km^R (2,016 pb) se amplificó por PCR a partir de ADN genómico de tres cepas diferentes de *P. denitrificans*: la silvestre (PdWT), la mutante sin el gen ζ (PdΔζ) y la mutante complementada con el gen

ζ (PdΔζ+ζ). Las amplificaciones de ADN se resolvieron mediante electroforesis en un gel de agarosa al 2%. En la parte inferior se muestra un esquema de la secuencia amplificada de 2,016 pb correspondiente a RAR – Km^R (línea roja). Los oligonucleótidos utilizados se muestran en la imagen y sus secuencias se especifican en la Tabla 3.

8.5 La subunidad ζ favorece la velocidad de crecimiento celular de *P. denitrificans.*

Dado que la actividad F_1F_O-ATPasa es adversa para la mayoría de los organismos, y que esta actividad en *P. denitrificans* es inhibida por la subunidad ζ, evaluamos el efecto de la ausencia ésta en la cepa de PdΔζ. Se utilizaron dos condiciones, la primera condición fue crecer células de las tres cepas en un medio de cultivo rico en nutrientes LB y la segunda fue crecer células de las tres cepas en un medio de cultivo cuya única fuente de carbono es el succinato. De las tres cepas PdWT, PdΔζ y PdΔζ+ζ se inocularon aproximadamente 4.8 x 10^8 células/ml en un matraz de 200 ml con 50 ml de medio de cultivo LB o succinato. Durante 48 h se incubaron los matraces inoculados con las tres cepas a 30 ºC a 200 rpm. Una alícuota se tomó cada dos horas y se midió su densidad óptica a 600 nm en un espectrofotómetro. Cuando las tres cepas se cultivaron en el medio rico en nutrientes LB no se encontraron diferencias en la velocidad de crecimiento celular (Figura 19 A). Pero, cuando se siguió el crecimiento celular en el medio mínimo succinato la cepa PdΔζ creció más lento que la cepa silvestre PdWT. En el medio succinato, la cepa mutante PdΔζ a las 24 h apenas comienza a crecer mientras que la cepa silvestre PdWT ya ha alcanzado su fase estacionaria (Figura 19 B). Además, la cepa PdΔζ+ζ recuperó la velocidad de crecimiento de la cepa PdWT descartando la posibilidad de que el crecimiento lento observado para la cepa PdΔζ se deba a otros cambios no específicos generados durante el proceso de eliminación del gen ζ en la cepa mutante PdΔζ.

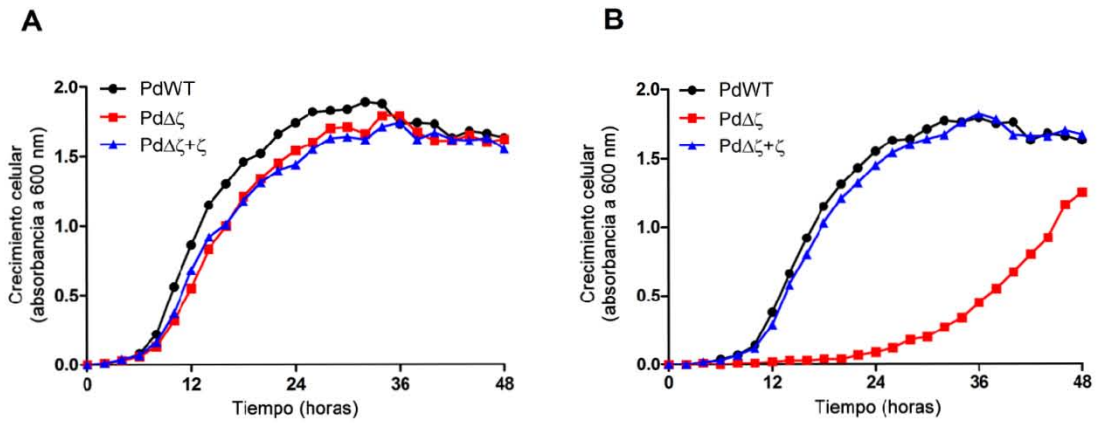

Figura 19. La subunidad ζ favorece la velocidad de crecimiento de *P. denitrificans.* Las células de cada cepa de *P. denitrificans:* PdWT (círculos negros), PdΔζ (cuadros rojos) y PdΔζ+ζ (triángulos azules), se cultivaron en medio LB hasta alcanzar 0.6 de absorbancia a 600 nm. De cada cepa en medio LB a 0.6 de absorbancia a 600nm se tomó 1 ml y se inocularon por separado en 50 ml de medio líquido LB (A) o succinato (B) dentro de matraces de 250 ml. Los matraces con medio LB o succinato inoculados con las cepas de *P. denitrificans* se incubaron a 30 °C durante 48 h a 200 rpm. De cada matraz con medio LB o succinato inoculado con las cepas de *P. denitrificans*, cada dos horas se tomó una alícuota de 0.2 ml y dicha alícuota se llevó hasta 1 ml con el medio en el que se encontraba cultivadas las células. De cada alícuota llevada a 1 ml, se le midió la absorbancia a 600 nm en un espectrofotómetro. A) muestra la curva de crecimiento en medio LB y B) muestra la curva de crecimiento en el medio succinato. Los datos son de uno de los tres experimentos diferentes que produjeron resultados similares.

8.6 La subunidad ζ de la F_1F_O-ATPasa de *P. denitrificans* es un inhibidor unidireccional.

Para probar si la subunidad ζ inhibe el giro del rotor de la F_1F_O-ATP sintasa en ambos sentidos (síntesis e hidrólisis de ATP), preparamos partículas sub-bacterianas (PSB) de las cepas PdWT y PdΔζ que fueron cultivadas en los medios de cultivo LB o succinato. Las PSB tienen toda la cadena respiratoria funcional y por lo tanto al añadirles sustratos específicos se puede activar la cadena respiratoria y generar un gradiente de protones que permite que la síntesis de ATP por la F_1F_O-ATP sintasa. De manera contraría, si a las PSB no se les añaden sustratos que alimenten la cadena transportadora de electrones, pero se añade ATP, ésto ocasionará que el rotor de la enzima rote en el sentido CCW e hidrolice al ATP. Las

PSB de las cepas PdWT y PdΔζ preparadas de ambos medios de cultivo tuvieron una actividad de síntesis de ATP muy similar (Figura 20 A), pero las PSB de la cepa PdDz en LB y en succinato tuvieron una mayor actividad de hidrólisis de ATP que las PSB de la cepa PdWT. Estos datos descartan que la subunidad ζ inhiba el giro del rotor de la enzima en el sentido de la síntesis de ATP y confirman que sólo inhibe el giro del rotor en el sentido de la hidrólsis de ATP.

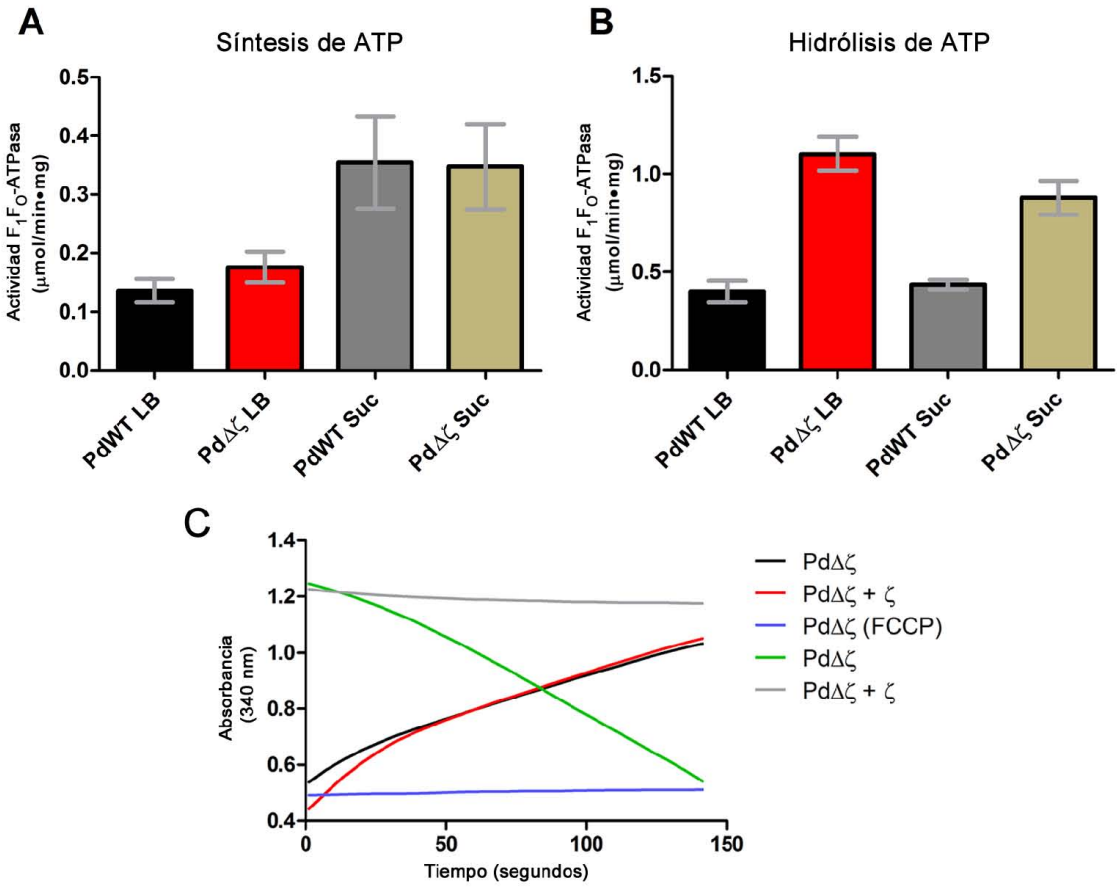

Figura 20. La subunidad ζ sólo inhibe el giro del rotor en el sentido de la hidrólisis de la F-ATPasa de *P. denitrificans*. Se prepararon PSB de las cepas PdWT y PdΔζ a partir de células que se cultivaron en medio LB o medio succinato (Suc). A) Actividad específica de síntesis de ATP (µmol/min*mg) y B) Actividad específica de hidrólisis de ATP (µmol/min*mg) de las PSB en presencia del activador LDAO. En A) y

B) las muestras de PSB PdWT LB (▪), PdΔζ LB (▪), PdWT Suc (▪), PdΔζ Suc (▪). Se muestra el promedio de tres experimentos y en las barras sus respectivas desviaciones estándar. C) A las PSB de la cepa PdΔζ se les midió la actividad de síntesis de ATP (línea negra y azul) y la actividad de hidrólisis de ATP (línea verde), adicionalmente a las PSB de la cepa PdΔζ se les reconstituyó con un exceso de subunidad ζ recombinante y se les midió la actividad de síntesis de ATP (línea roja) y la actividad de hidrólisis de ATP (línea gris). En línea azul, las PSB de la cepa PdΔζ se les incubó con el compuesto FCCP y se les midió la actividad de síntesis de ATP. El FCCP permite el paso de protones a través de la membrana e impide la generación de un gradiente de protones, por lo que se inhibe la capacidad de síntesis de ATP por la ATP sintasa. La actividad de síntesis de ATP y la actividad de hidrólisis de ATP se midió utilizando una disolución que mantiene constante la concentración de ADP para la actividad de síntesis o de ATP para la actividad de hidrólisis. Se grafica la absorbancia a 340 nm debido a que se sigue la aparición de NADPH para la actividad de síntesis de ATP y la desaparición de NADH para la actividad de hidrólisis de ATP. Para información detallada de las disoluciones utilizadas para llevar a cabo los experimentos revisar materiales y métodos.

8.7 Expresión de la F_1F_O-ATP sintasa y del complejo succinato deshidrogenasa de *P. denitrificans* en los medios de cultivo LB y succinato.

Dado que las cepas de *P. denitrificans* se cultivaron en dos condiciones diferentes, se evaluó la expresión de la F_1F_O-ATP sintasa en ambas condiciones. Adicionalmente, al observar que hubo un aumento en la actividad de síntesis de ATP en las PSB de las cepas PdWT y PdΔζ al ser cultivadas en la condición de cultivo LB respecto a la condición succinato, se evaluó la expresión del complejo succinato deshidrogenasa (SDH) en ambas condiciones. Para evaluar la expresión del complejo F_1F_O-ATP sintasa y SDH de *P. denitrificans* en los dos medios de cultivo LB y succinato, obtuvimos PSB de la cepa PdWT que fueron cultivadas en medio LB o medio succinato. Se realizó un WB de estas PSB utilizando los anticuerpos anti-subunidad A del complejo succinato deshidrogenasa (SDH) (70 kDa) y anti-subunidad β de la F_1F_O-ATP sintasa (50 kDa). En las PSB de PdWT se expresó la misma cantidad de subunidad β tanto en las células que se cultivaron en medio LB como en las células que se cultivaron en medio succinato (Figura 21 A y B). En el caso del complejo SDH, en las PSB de PdWT se expresó más la subunidad

A en las células que se cultivaron en medio succinato que en las células que se cultivaron en medio LB (Figura 21 A y B).

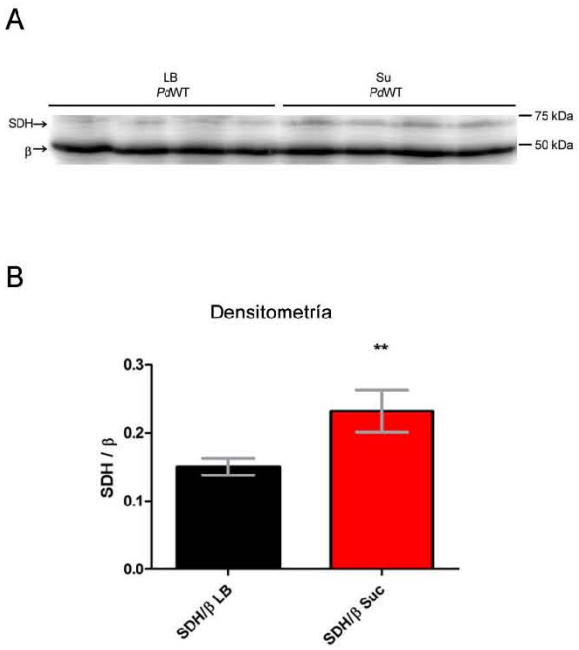

Figura 21. Western-blot de SBP de PdWT crecido en LB o medio de succinato contra complejo II (SDH) y complejo V (subunidad β). A) A cuatro PSB preparadas de lotes diferentes de células de la cepa PdWT, se les realizó un SDS-PAGE y posteriormente un WB. El WB se realizó utilizando el anticuerpo monoclonal producido contra la subunidad A del complejo II (SDH), la subunidad A tiene un peso molecular de SD70 kDa. El complejo II utilizado para generar el anticuerpo es de bovino. También se utilizó el anticuerpo monoclonal producido contra la subunidad β de la F_1-ATPasa, la subunidad b tiene un peso molecular de 50 kDa. El complejo F_1-ATPasa utilizado para generar el anticuerpo es de *E. coli*. En los primeros cuatro carriles, se cargaron 30 µg de cada uno de las cuatro PSB diferentes obtenidos de células cultivadas en LB. En los cuatro carriles de la derecha, se cargaron 30 µg de cada uno de los cuatro PSB diferentes obtenidos de células cultivadas en medio de succinato. La posición de los marcadores de peso molecular está indicada en el extremo derecho. B) Análisis de densitometría a partir de la intensidad de la banda perteneciente a la subunidad A del complejo SDH a partir de la imagen del WB. Se estimó la intensidad de la banda de 70 kDa (SDH) y el de la banda de 50 kDa (β) utilizando el programa GelQuant (DNR Bio-Imaging Systems Ltd., Jerusalem, Israel). El valor estimado de la intensidad de la banda de 70 kDa (SDH) se dividió entre el valor estimado de la intensidad de la banda de 50 kDa (β). Se realizó un análisis estadístico t de Student utilizando el programa GraphPad Prism 5 (California, USA). Los datos son promedio de cuatro repeticiones y en gris se muestra la desviación estándar. ** señala una diferencia estadísticamente significativa

($p = 0.0026$) en la expreción de SDH en medio succinato comparada con la expresión en medio LB.

8.8 La subunidad ζ inhibe el bombeo de protones por la F_1F_O-ATPasa.

Para probar el efecto de la subunidad ζ en el bombeo de protones de la F_1F_O-ATPasa, evaluamos la capacidad de bombeo de protones en PSB de las cepas PdWT y PdΔζ cultivadas en la condición LB o succinato. Las PSB acopladas tienen toda la cadena respiratoria funcional y por lo tanto se ensayó cualitativamente la formación de un gradiente de protones impulsado por succinato y ATP mediante la disminución de fluorescencia utilizando el fluoróforo ACMA. El fluoróforo ACMA responde al gradiente de protones (detalles en materiales y métodos). Se colocaron las PSB en la celda con la disolución que contenía al ACMA y posteriormente se tomaron las lecturas. Aproximadamente a los 60 s a la celda se le añadió succinato, los complejos respiratorios encontrados en las PSB bombearon protones al interior de la membrana y la fluorescencia emitida por el ACMA disminuyó (Figura 22 A y 22 B). La fluorescencia emitida por el ACMA en las PSB de las tres cepas cultivadas en medio succinato fue menor que la fluorescencia emitida por el ACMA en las PSB de las cepas cultivadas en medio LB (Figura 22 A y 22 B). A los 120 s a la celda se le añadió cianuro y el gradiente de protones se disipó, recuperándose la fluorescencia emitida por el ACMA (Figura 22 A y 22 B). A los 230 s se le añadió ATP, la F_1F_O-ATPasa bombeó protones al interior de las PSB y la fluorescencia emitida por el ACMA disminuyó (Figura 22 A y 22 B). La fluorescencia emitida por el ACMA fue menor en las PSB de la cepa PdΔζ que las PSB de la cepa PdWT. Mientras que la fluorescencia de las PSB de la cepa PdΔζ reconstituidas con un exceso de subunidad ζ recombinante, emitió la misma fluorescencia que las células de la cepa PdΔζ (Figura 22 A y 22 B). A los 350 s se añadió FCCP, desacoplándose las PSB y disipándose el gradiente de protones (Figura 22 A y 22 B). Estos resultados muestran la subunidad ζ inhibe el bombeo de protones debido que inhibe el giro del rotor de la F_1F_O-ATPasa.

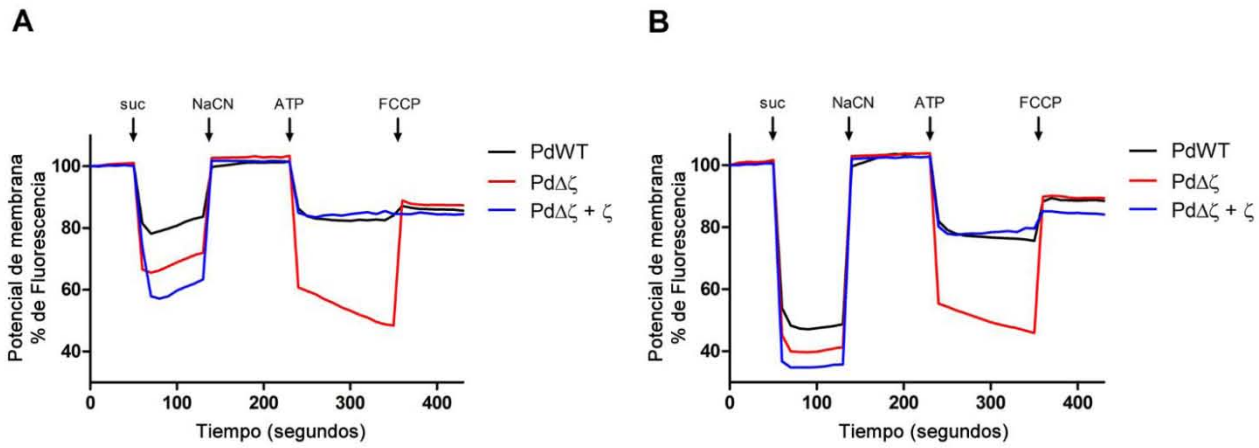

Figura 22. La subunidad ζ inhibe el potencial de membrana en PSB. Las PSB preparadas a partir de cepas silvestre PdWT o mutantes PdΔζ (300 µg de SBP) se diluyeron por separado en una celda de 3 ml que contenía la disolución de reacción (descrita en materiales y métodos). Después, las PSB preparadas de ambas cepas se les indujeron dos sucesos de bombeo de protones a través de la membrana, el primero se activó con succinato y se colapsó con cianuro (NaCN) y el segundo se activó con magnesio y ATP (Mg-ATP), colapsándose con el desacoplante de membrana FCCP. El bombeo de protones a través de la membrana de la cepa silvestre PdWT (líneas negras) y la de mutante que carece de la subunidad inhibidora ζ PdΔζ (líneas rojas). Se realizó un control negativo utilizando las PSB preparadas a partir de la cepa mutante PdΔζ a la cual se le añadió un exceso de subunidad ζ recombinante (120 µg) en 300 µg de PSB preparadas de la cepa mutante PdΔζ, esta fue diluida hasta 1 mg/ml en el amortiguador que contenía la sonda fluorescente ACMA con Mg-ATP 1 mM, en condiciones en las que la subunidad ζ inhibe esencialmente toda la capacidad de hidrolizar ATP por el complejo F_1F_0-ATPasa. Después de 20 minutos de incubación a temperatura ambiente las PSB reconstituidas con subunidad ζ recombinante se diluyeron en la celda y se siguió el bombeo de protones como se describió anteriormente (líneas azules). Los datos son un promedio de tres repeticiones de lotes diferentes de PSB.

8.9 La subunidad ζ inhibe el potencial de membrana en células vivas.

Para estimar el potencial de membrana en células vivas, se llevó a cabo citometría de flujo utilizando un sistema comercial de potencial de membrana BacLight. Las células se cultivaron en medio LB o succinato y se les incubó con el colorante $DiOC_2(3)$ durante 30 min. Una mayor acumulación del colorante $DiOC_2(3)$ dentro de las células implica un mayor potencial de membrana. Mediante citometría de flujo se estimó la relación de la fluorescencia emitida por el $DiOC_2(3)$. Las células PdWT, PdΔζ y PdΔζ+ζ cultivadas en medio LB tuvieron aproximadamente la misma relación

rojo/verde (Figura 23 A). De manera diferente, en las células de las tres cepas cultivadas en medio succinato hubo un valor mayor en la relación rojo/verde de las células de la cepa PdΔζ que en las células de las cepas PdWT y PdΔζ+ζ (Figura 23 B). Lo anterior implica que, en las células cultivadas en el medio succinato se formó un mayor potencial de membrana en las células PdΔζ respecto a las células de las cepas PdWT y PdΔζ+ζ (Figura 23 A).

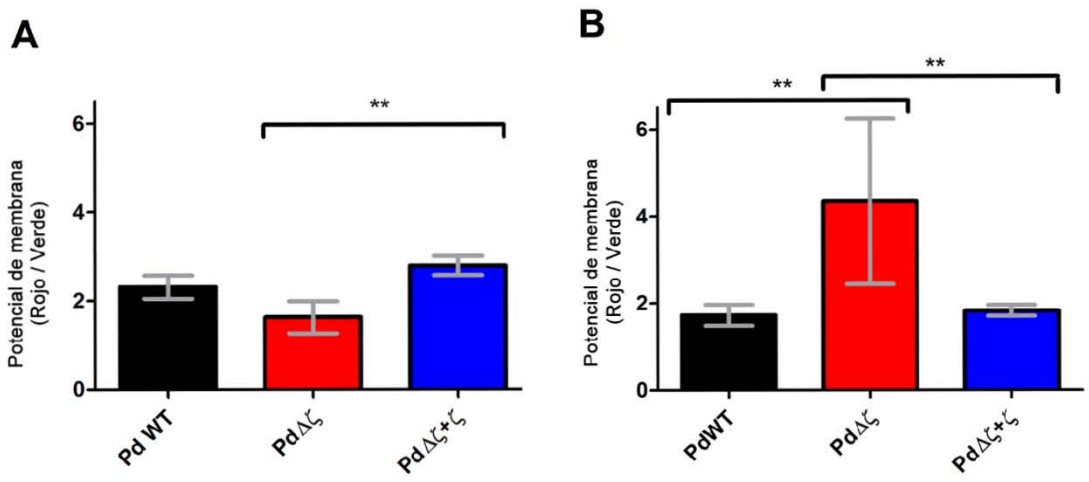

Figura 23. La subunidad ζ inhibe el potencial de membrana en células vivas. Se cultivaron células de las cepas PdWT, PdΔζ y PdΔζ+ζ en las condiciones de cultivo LB y succinato. A las células cultivadas en ambas condiciones se les estimó el potencial de membrana mediante citometría de flujo después de teñir con el colorante $DiOC_2(3)$. El potencial de membrana se estimó por el cambio en el cociente de la fluorescencia emitida en el espectro roja / la fluorescencia emitida en el espectro verde del compuesto $DiOC_2(3)$. Las células de las tres cepas se incubaron con $DiOC_2(3)$ 30 μM durante 30 minutos a temperatura ambiente antes de tomar las lecturas en el citómetro de flujo. Se detectaron las intensidades de fluorescencia promedio a 530 ± 15 nm (verde) y 690 ± 25 nm (rojo). Los valores de las intensidades de fluorescencia en rojo se dividieron entre los valores de las intensidades de fluorescencia en verde. Como control, a las células de cada cepa se les añadió el compuesto CCCP para desacoplar el potencial de membrana y después se incubaron con el colorante $DiOC_2(3)$. El valor obtenido del cociente de cada control se restó al valor obtenido del cociente de las muestras teñidas con el colorante $DiOC_2(3)$. A) Potencial de membrana de las células cultivadas en medio LB. B)

Potencial de membrana de las células cultivadas en medio succinato. Los datos son un promedio de 3-4 experimentos independientes y en las barras grises se muestran las desviaciones estándar. Se realizó un análisis estadístico ANOVA utilizando el programa GraphPad Prism 5. A) ** p=0.0074 y B) ** p=0.0042.

8.10 La subunidad ζ inhibe la hidrólisis de ATP de la fracción F_1-ATPasa.

Para evaluar el efecto de la ausencia de la subunidad ζ sobre la actividad de hidrólisis en la fracción F_1 de la F_1F_O-ATPasa, purificamos la fracción F_1 endógena de las cepas PdWT y PdΔζ, después confirmamos la ausencia de la subunidad ζ en la $F_1^{\Delta\zeta}$ mediante SDS-PAGE (Figura 24 A) y WB (Figura 24 B) y por último les medimos la actividad F_1-ATPasa en tres condiciones diferentes. La fracción de la F_1-ATPasa de las cepas PdWT (F_1^{WT}) y PdΔζ ($F_1^{\Delta\zeta}$) se purificó como se describe en materiales y métodos. Las subunidades de la F_1 purificada de ambas cepas se separaron en un SDS-PAGE teñido por coomassie. En la F_1 de la cepa PdΔζ se distinguen las subunidades α, β, γ, δ y ε; siendo notoria la ausencia de la subunidad ζ (Figura 24 A) y mientras que en la F_1 de la cepa PdWT sí se distingue la subunidad ζ debajo de las otras cinco subunidades (Figura 24 A). A la F_1 purificada de ambas cepas se les realizó un WB, se les expuso con el anticuerpo anti-β y anti-ζ y la subunidad ζ no pude ser detectada por el anticuerpo en la F_1 de la cepa PdΔζ, mientras que sí se puede detectar en la F_1 de la cepa PdWT (Figura 24 B). Además, se detecta por medio del anticuerpo anti-ζ la subunidad ζ en las PSB de la cepa PdWT provenientes de células cultivadas en medio LB y succinato. De manera contraria, la subunidad ζ no puede ser detectada por el anticuerpo anti-ζ en las PSB de la cepa PdΔζ provenientes de células cultivadas en medio LB y succinato (Figura 24 B). A la F_1-ATPasa purificada de ambas cepas se les midió la actividad de hidrólisis de ATP en un sistema regenerador de ATP. En la condición en la que no se utiliza ningún activador (Figura 24 C "---"), la F_1^{WT} alcanzó una actividad específica (μmol/min *mg de proteína) de 0.14 (DE 0.003) y la $F_1\Delta\zeta$ alcanzó una actividad específica (μmol/min *mg de proteína) de 0.87 (DE 0.12) (Figura 24 C). En la condición en la que se utilizó un activador LDAO 0.015%, la F_1^{WT} alcanzó una actividad específica (μmol/min *mg de proteína) de 2.38 (DE +/-0.23) y la $F_1\Delta\zeta$

alcanzó una actividad específica (μmol/min *mg de proteína) de 4.49 (DE +/-1.21) (Figura 24 C). En la tercera condición se utilizaron dos activadores LDAO 0.0015% y sulfito 1.5 mM, la F_1^{WT} alcanzó una actividad específica (μmol/min *mg de proteína) de 19.75 (DE +/-1.45) y la $F_1\Delta\zeta$ alcanzó una actividad específica (μmol/min *mg de proteína) de 30.07 (DE +/-1.2) (Figura 24 C). La $F_1^{\Delta\zeta}$ en las tres condiciones tuvo mayor actividad ATPasa que la F_1^{WT}. En la condición sin activadores la $F_1\Delta\zeta$ tuvo una actividad específica de ATPasa 6 veces mayor que la de la F_1^{WT}. En la condición el activador LDAO la $F_1^{\Delta\zeta}$ tuvo una actividad específica de ATPasa 2 veces mayor que la de la F_1^{WT}. En la condición con los dos activadores LDAO y sulfito la $F_1^{\Delta\zeta}$ tuvo una actividad específica de ATPasa 1.5 veces mayor que la de la F_1^{WT}. Los valores de mayor significancia son los obtenidos sin activador artificial (LDAO o sulfito) porque es en esa condición donde se observa el efecto que mimetiza la condición nativa de la remoción de ζ en la actividad de F_1-ATPasa, y es donde se observa una mayor activación de aproximadamente 6 veces en la actividad de F_1-ATPasa, corroborando así el papel inhibitorio de la subunidad ζ endógena en la enzima nativa.

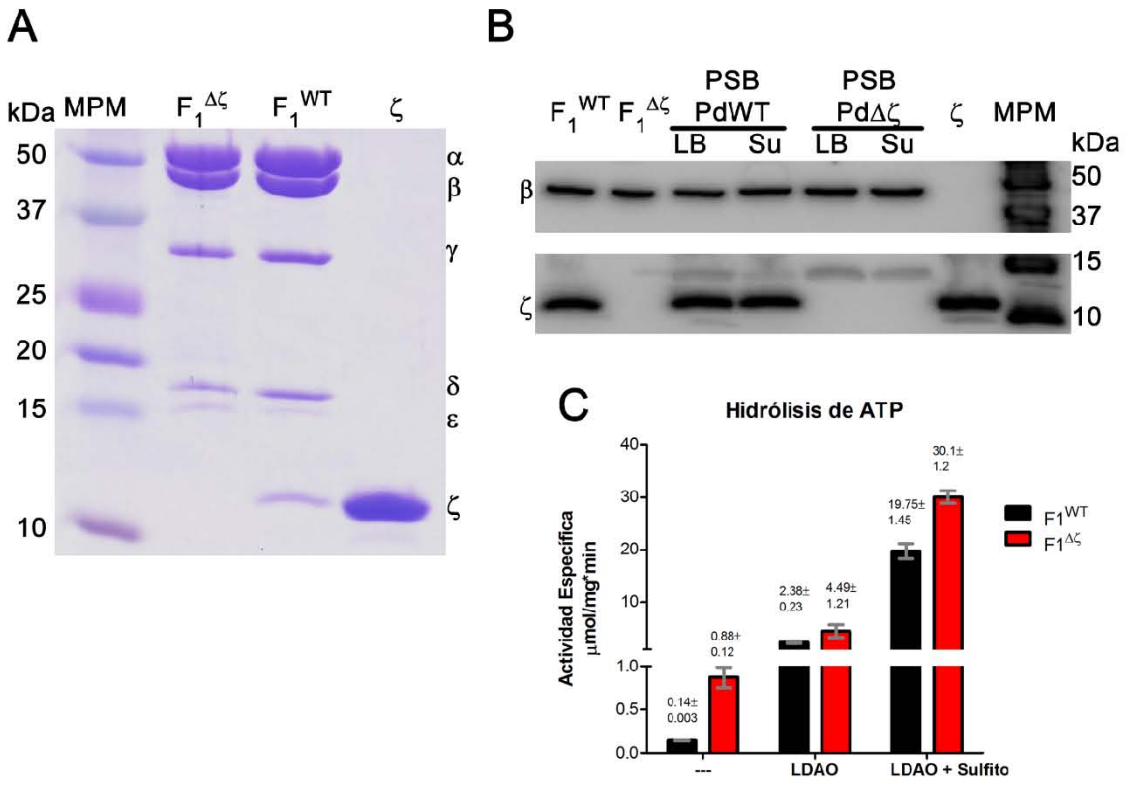

Figura 24. La subunidad ζ inhibe la actividad F_1-ATPasa. A) SDS-PAGE teñido con coomassie en el que se cargaron la fracción F_1 purificada de la cepa PdWT ($F1^{WT}$) y de la cepa PdΔζ ($F1^{\Delta\zeta}$), también se cargó la subunidad ζ recombinante purificada y el marcador de peso molecular (MPM). B) Western blot (WB) de la fracción F_1 purificada la cepa PdWT ($F1^{WT}$) y de la cepa PdΔζ ($F1^{\Delta\zeta}$), de las PSB de la cepa PdWT y de la cepa PdΔζ, la subunidad ζ recombinante purificada y el marcador de peso molecular (MPM). La línea que se encuentra debajo de las PSB indica que las PSB de esa cepa se corrieron en dos distintos carriles, una en la condición LB y la otra en la condición succinato (Su). En el WB se utilizaron los anticuerpo monoclonal anti-β y el anti-ζ policlonal. El MWM del WB se expuso al conjugado Strep-Tactin-HRP. C) Se grafica la actividad de hidrólisis de ATP de la fracción F_1 de ambas cepas (en barras negras la F_1WT y en barras rojas la $F_1\Delta\zeta$) se les midió la actividad de hidrólisis de ATP en tres condiciones. (---) indica la actividad sin ningún activador; (LDAO) indica la actividad con el detergente N-oxido de lauril dietil amina al 0.15% el cual activa la hidrólisis de ATP de la F_1; (LDAO+sulfito) indica la actividad con el detergente LDAO al 0.15% y sulfito a 2 mM, ambos compuestos son capaces de activar la hidrólisis de ATP de la F_1. Las barras son el promedio de tres experimentos y en barras de color gris se muestran las desviaciones estándar. Los datos son el promedio de tres experimentos.

8.11 La subunidad ζ recombinante inhibe más del 99% de la actividad F_1-ATPasa.

Para evaluar la capacidad de inhibición de la subunidad ζ recombinante de *P. denitrificans* sobre la actividad de hidrólisis de ATP de la F_1 purificada a partir de las cepas PdWT y PdΔζ, reconstituimos de manera homóloga a la F_1^{WT} y $F_1^{\Delta\zeta}$ con concentraciones crecientes de subunidad ζ recombinante. Se midió la actividad específica F_1-ATPasa de la F_1^{WT} y $F_1^{\Delta\zeta}$ con los dos activadores LDAO y sulfito. La F_1^{WT} alcanzó una actividad específica (μmol / min * mg de proteína) de 19.75 y la $F_1^{\Delta\zeta}$ alcanzó 30.1. La subunidad ζ recombinante a una concentración de 0.25 μM fue capaz de inhibir la actividad ATPasa en un 87.5 % de la F_1^{WT} y en un 91.7 % de la $F_1^{\Delta\zeta}$. Mientras que, la subunidad ζ recombinante a una concentración de 2.3 μM fue capaz de inhibir la actividad ATPasa en un 98.7 % de la F_1^{WT} y en un 99.1 % de la $F_1^{\Delta\zeta}$.

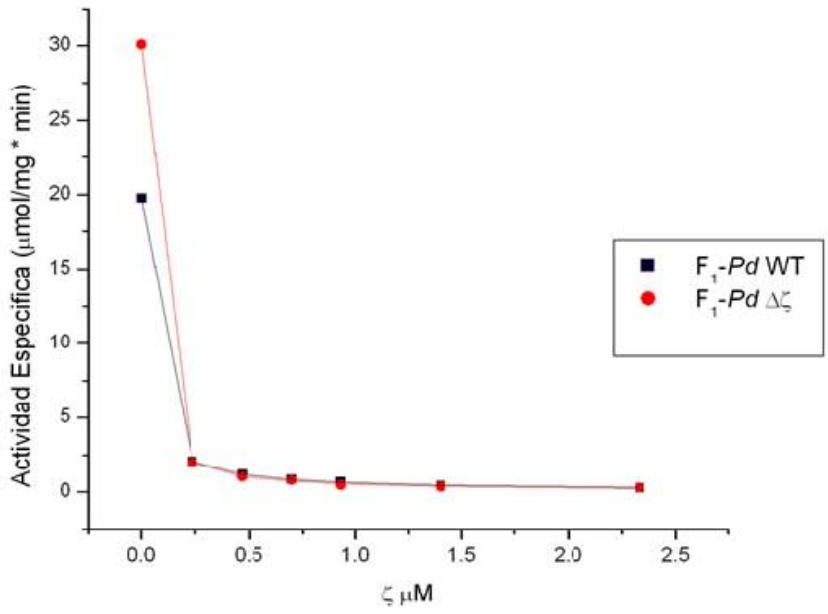

Figura 25. La subunidad ζ recombinante es capaz de inhibir casi al 100% la actividad F_1-ATPasa. Cinco microgramos de F_1^{WT} y $F_1^{\Delta\zeta}$ se reconstituyeron con una concentración creciente de la subunidad ζ recombinante de *P. denitrificans* (μM). La reconstitución se llevó a cabo durante 30 min a temperatura ambiente en presencia de 60 mM de sulfito. Se midió la actividad específica ATPasa (μmol/min * mg proteína) en una disolución regenerante de ATP en presencia de LDAO 0.15 % y de sulfito a 1.5 mM. En cuadros negros la actividad ATPasa de la F_1^{WT} y en cuadros rojos la de la $F_1^{\Delta\zeta}$. Los datos son un promedio de tres experimentos.

8.12 La subunidad inhibidora ζ de la F_1F_O-ATPasa mantiene la concentración de ATP intracelular en *P. denitrificans*.

Para determinar si la disminución en la velocidad de crecimiento de la cepa PdΔζ en el medio de cultivo succinato se debe a una disminución en la concentración de ATP intracelular debido al aumento en la actividad de hidrólisis de ATP por la F_1F_O-ATPasa, el ATP intracelular de las tres cepas se cuantificó. Se crecieron células de la cepa PdWT, PdΔζ y PdΔζ+ζ en medio de cultivo LB o succinato. Las células de las tres cepas se crecieron en los respectivos medios a 30 ºC a 200 rpm hasta alcanzar 1.0 de absorbancia. Se utilizaron 50 μl de células a una concentración aproximadamente $3.7x10^9$ y se diluyó en 500 μl de amortiguador de lisis. Los 500 μl se hirvieron durante 2 minutos y se removió la parte membranal mediante centrifugación. La parte soluble contenía el contenido intracelular de las células y a éste se le cuantificó el ATP intracelular utilizando el sistema comercial luciferina/luciferasa de sigma. Se estimó la concentración de ATP intracelular por peso seco celular (100). La concentración de ATP intracelular de las células cultivadas en el medio succinato fue menor en las de la cepa PdΔζ que en las de la cepa PdWT (Figura 26 B). Como se esperaba, la concentración de ATP intracelular de las células cultivadas en el medio succinato fue igual en las de la cepa PdΔζ+ζ que en las de la cepa PdWT (Figura 26 B). Y tal como se esperaba, la concentración de ATP intracelular fue igual en las células de las tres cepas cultivadas en medio LB (Figura 26 A). Este resultado implica que la remoción de ζ *in vivo* conduce a una disminución en el contenido de ATP celular en medio respiratorio.

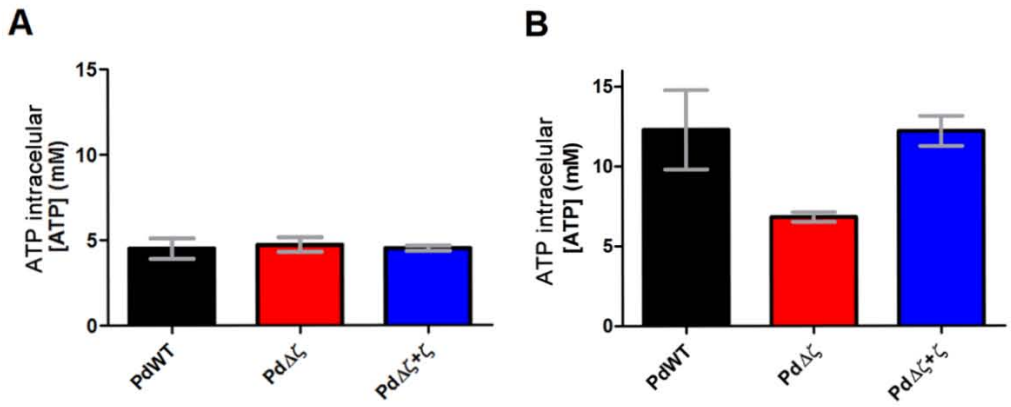

Figura 26. La subunidad ζ manteniendo la concentración de ATP intracelular en *P. denitrificans*. Las cepas PdWT (barras negras), PdΔζ (barras rojas) y la PdΔζ+ζ (barras azules) se cultivaron por separado en medio LB o medio succinato hasta alcanzar 1.0 de absorbancia (fase logarítmica). En dicho momento se cosecharon las células por medio de centrifugación. La pastilla que se formó al centrifugar las células de cada cepa se resuspendió hasta a una concentración de aproximadamente $3.7x10^9$ células/ml. Se tomaron 50 µl de células a $3.7x10^9$ células/ml y se llevó a 500 µl en una disolución de lisis y se colocaron en agua hirviendo durante 2 minutos. El contenido intracelular obtenido después de hervir las células se centrifugó para remover la parte membranal. Al contenido intracelular se le cuantificó la concentración de ATP y con dicho contenido de ATP se interpoló en una curva de concentración de ATP utilizando un ATP estándar. Para realizar las mediciones de ATP intracelular y la curva estándar de ATP se utilizó el sistema comercial de Sigma de luciferina/luciferasa. Se estimó la concentración de ATP intracelular por peso seco celular. A) ATP intracelular de las células de las tres cepas cultivadas en medio LB y B) ATP intracelular de las células de las tres cepas cultivadas en medio succinato. Se muestra el promedio de tres experimentos y en las barras grises sus respectivas desviaciones estándar.

8.13 Modelo del mecanismo de inhibición de la subunidad ζ.

Para poder entender el mecanismo de regulación por el cual la subunidad ζ es capaz de inhibir el giro del rotor de la F_1F_O-ATPasa sólo en el sentido de la hidrólisis y no en el sentido de la síntesis de ATP, se realizó un modelo del complejo F_1F_O-ATP sintasa de *P. denitrificans.* Se ensambló el C-terminal de la estructura de la subunidad ζ resuelta por resonancia magnética nuclear (RMN) (PDB ID 2LL0) (67) con el N-terminal de la estructura de la subunidad ζ resuelta por cristalografía de rayos X (PDB ID 5DN6) (69). Después se modeló esta subunidad ζ ensamblada sobre el sitio inhibitorio propuesto en la estructura cristalográfica de F_1F_O inhibido

por la subunidad ζ (69) (PDB ID 5DN6). El modelo de la F_1F_O-ATP sintasa de *P. denitrificans* se obtuvo por alineamiento estructural y minimización de energía en los programas de modelaje PyMol (31) y Chimera (32) similar al antes reportado en (68). Se muestra que en presencia de la subunidad ζ el rotor de la enzima sólo puede rotar en el sentido de la síntesis de ATP (Figura 27 A), pero en ausencia de la subunidad ζ, el rotor de la enzima puede girar tanto en el sentido de la síntesis como en el sentido de la hidrólisis de ATP (Figura 27 B).

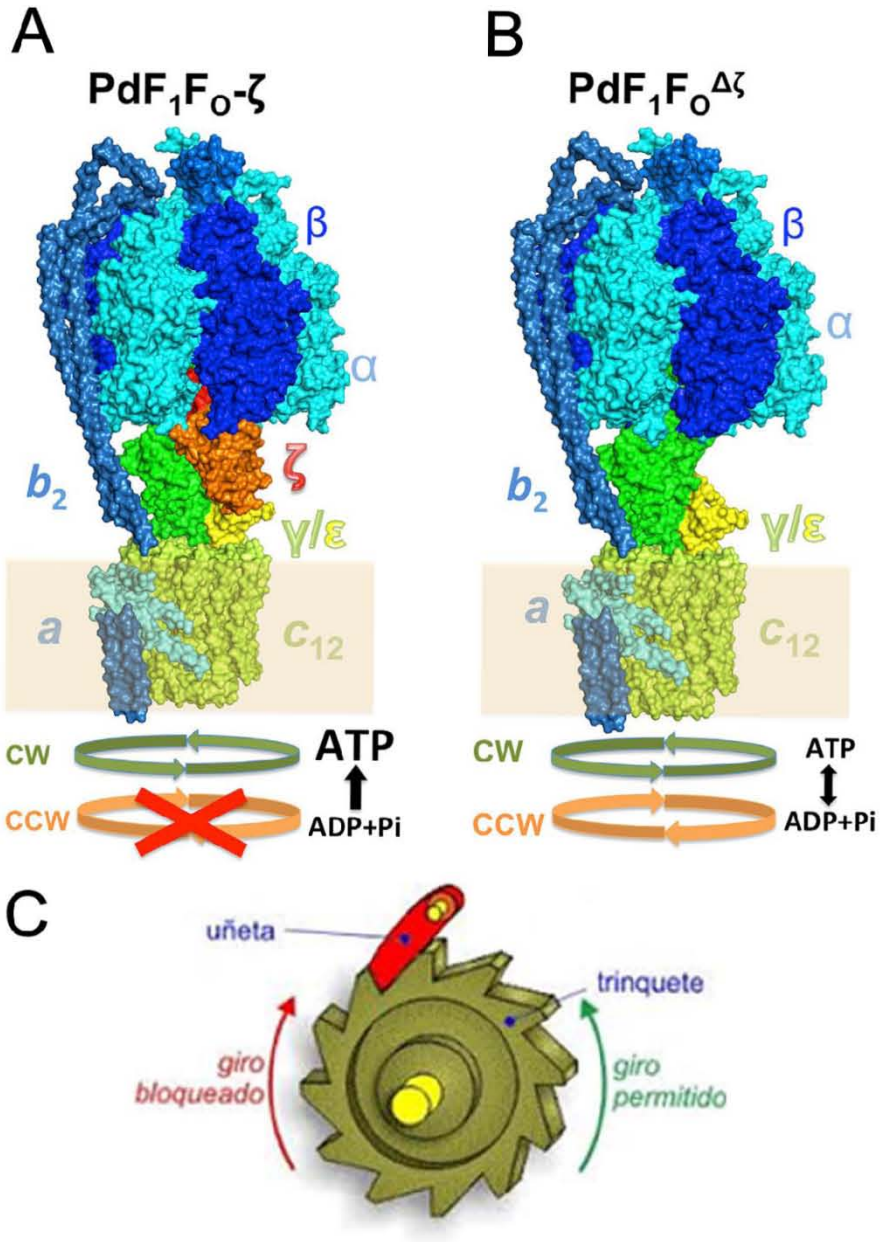

Figura 27. Modelo del mecanismo de inhibición de la subunidad ζ. A) y B) Modelos estructurales del mecanismo de inhibición de la subunidad ζ. A) F_1F_O inhibida con la subunidad ζ en la interfase α_{DP}/β_{DP}. En rojo el N-terminal de la subunidad ζ, en naranja el C-terminal de la subunidad ζ. B) F_1F_O sin subunidad ζ. C) Caricatura simulando a el mecanismo de la subunidad ζ funcionando como la uñeta de una matraca. Las estructuras fueron modeladas utilizando el programa PyMOL y UCSF Chimera.

9 Discusión

Dado que en la mayoría de los organismos la función de la F_1F_O-ATP sintasa es la síntesis de ATP y siendo la actividad de hidrólisis de ATP una función adversa de esta enzima, han surgido subunidades encargadas de inhibirla: ε, IF_1 y ζ. Las subunidades ε, IF_1 y ζ al inhibir la actividad F_1F_O-ATPasa, juegan un papel central en el metabolismo celular de los organismos. Por ello, en esta tesis evaluamos el rol fisiológico de la subunidad inhibidora ζ de la F_1F_O-ATPasa en el organismo *P. denitrificans*. Eliminamos el gen que codifica para la subunidad inhibidora ζ del organismo *P. denitrificans* y evaluamos diferentes parámetros en la cepa silvestre PdWT y en la cepa mutante PdΔζ. Los parámetros evaluados en ambas cepas son: crecimiento celular, actividad de síntesis e hidrólisis de ATP, potencial de membrana y concentración de ATP intracelular.

La subunidad ζ ayuda a la velocidad de crecimiento celular de *P. denitrificans*. La cepa PdΔζ tuvo una menor velocidad de crecimiento que las cepas PdWT y PdΔζ+ζ al ser cultivadas en el medio de succinato (Figura 19 B). Este medio está compuesto de sales y tiene como única fuente de carbono al succinato (ver materiales y métodos). El succinato es sustrato del complejo II (succinato deshidrogenasa) de la cadena transportadora de electrones (CTE). Cuando el complejo II de la CTE cataliza la reducción del succinato a fumarato pasa dos electrones ($2e^-$) y dos protones (H^+) del succinato a la ubiquinona (Q), reduciendo a la ubiquinona en ubiquinol (QH_2) (101,102). Los electrones del ubiquinol se transportan al complejo III de la CTE (citocromo c reductasa) y posteriormente llegan hasta el aceptor final de electrones (en este caso es el oxígeno). Dicho flujo de electrones da lugar al bombeo de protones generando un gradiente electroquímico, y entonces el ATP sintetizado será por la fosforilación oxidativa. Si todo el ATP de la bacteria es sintetizado por la ATP sintasa y en *P. denitrificans* WT se sabe que sólo el 50% de la enzima tiene subunidad ζ (datos no publicados, Chávez C., y García-Trejo, J. J.), esto implica que 50% funciona como ATP sintasa y el otro 50% esta dividido en dos poblaciónes, las que puede funcionar como ATP sintasa hay tiene gradiente electroquímico y como ATPasa si no hay gradiente electroquímico

(103). Por ello en la cepa PdWT la población de ATPasas será menor que la población de ATP sintasas, por lo que la concentración de ATP intracelular será abundante. De manera opuesta, en la cepa PdΔζ al no haber subunidad ζ todas las enzimas pueden funcionar como ATPasas cuando el gradiente electroquímico decaiga. Por ello, la población de ATPasas será mayor que la de ATP sintasa, existiento una disminución en el ATP intracelular y esto se ve reflejado en una menor velocidad de crecimiento de la cepa PdΔζ que en la silvestre en el medio succinato (Figura 19 B). En la cepa PdΔζ cultivada en el medio succinato, la disminución velocidad de crecimiento respecto al de la cepa PdWT podría deberse a otros cambios aleatorios sufridos durante el proceso de eliminación del gen ζ. Sin embargo, descartamos dicha posibilidad ya que la cepa complementada PdΔζ+ζ revirtió del fenotipo (Figura 19 B). Lo anterior demuestra que el fenotipo observado en la cepa PdΔζ se debe únicamente a la ausencia de la subunidad ζ.

En el medio de cultivo LB, las cepas PdWT, PdΔζ y PdΔζ+ζ tuvieron la misma velocidad de crecimiento (Figura 19 A). Esto se puede deber a que el medio LB es rico en nutrientes ya que conteniene una cantidad abundante de aminoácidos. Los aminoácidos se pueden catabolizar en el ciclo de Krebs (Figura 28) donde ocurre una reacción de fosforilación a nivel sustrato (Figura 28 A), adicionalmente, existen otras reacciones a nivel sustrato que se pueden aprovechar (Figura 28 B, C y D). Adicionalmente, las bacterias no necesitarían estar sintetizando los aminoácidos ya que, al estar presentes en el medio de cultivo, las bacterias se ahorrarían el gasto implicado en tener que sintetizarlos. Por ello, la cepa mutante PdΔζ, compensaría el gasto adicional de ATP por la mayor población de ATPasas al sintetizarlo mediante fosforilaciones a nivel sustrato y no gastando ATP para sintetizar a.a. Por ello, las cepas PdWT, PdΔζ y PdΔζ+ζ tienen la misma velocidad de crecimiento en el medio de cultivo LB (Figura 19 A).

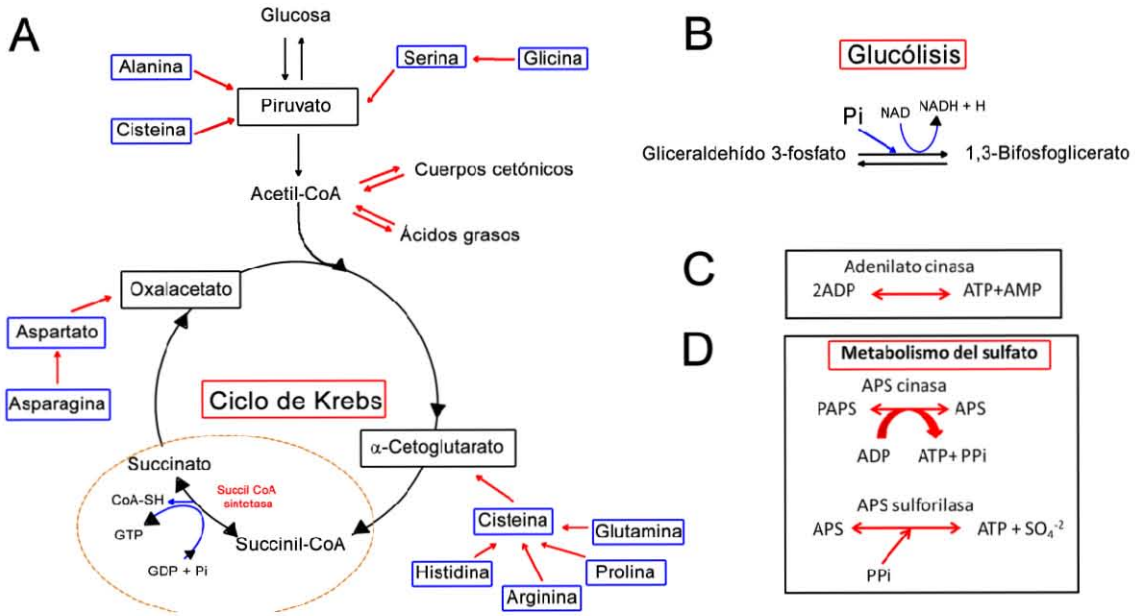

Figura 28. *P. denitrificans* puede obtener ATP por diferentes fosforilaciones a nivel sustrato. A) Esquema del ciclo de Krebs en donde se muestra 1 fosforilación a nivel sustrato (dentro del círculo marrón). Además, en el esquema del ciclo de Krebs se muestran los diferentes aminoácidos (dentro de cuadros azules) y en que sustratos del ciclo de Krebs se pueden catabolizar (dentro de cuadros negros). B) En la vía de la glucólisis, se muestra la reacción en la cual ocurre una fosforilación a nivel sustrato. C) Se muestra la reacción de la adenilato cinasa en donde ocurre una fosforilación a nivel sustrato. D) En el metabolismo del sulfato hay dos reacciones en las que ocurren fosforilaciones a nivel sustrato.

La subunidad ζ sólo inhibe el giro del rotor de la F_1F_o-ATP sintasa de *P. denitrificans*. Se sabe que la subunidad ζ inhibe el giro del rotor de la enzima mediante su N-terminal, el cual atraviesa la interfase α/β e interactúa con γ (28,69). Sin embargo, existe la posibilidad que la subunidad ζ también impida el giro del rotor de la enzima en el sentido de la síntesis de ATP. En este trabajo demostramos que la subunidad ζ sólo inhibe el giro del rotor en el sentido de la hidrólsis de ATP (Figura 20 B, 24 C y 25). Para que la subunidad ζ sólo inhiba el giro del rotor en el senitdo CCW existen dos posibles mecanismos: el primero, la subunidad atraviesa la interfase α/β/γ, venciendo la fuerza de rotación ejercida por los cambios conformacionales de β al unir e hidrólisar al ATP. En cambio, la fuerza del giro del rotor de la enzima en el sentido CW que es impulsado por el paso de protones y por

la unión de ADP+Pi, condensación y liberación del ATP, vencerá a la fuerza de la interacción de la subunidad ζ con la interfase α/β/γ. Por ello, la subunidad ζ puede liberar el sitio inhibitorio o sufrir cambios conformacionales tales que permitan el giro del rotor sin que sea necesario que ζ salga del sitio de interacción funcionando como el trinquete de una matraca.

Expresión de la F_1F_O-ATP sintasa y del complejo succinato deshidrogenasa de *P. denitrificans* en los medios de cultivo LB y succinato. Al utilizar dos condiciones de cultivo de las células de *P. denitrificans* fue necesario evaluar la expresión de la F_1F_O-ATP sintasa y del complejo succinato deshidrogenasa (SDH). Esperabamos ambos complejos se expresarán más en el medio succinato que en el medio LB, esto debido a que el medio LB tiene diversos nutrientes que permiten la obtención de ATP por rutas metabólicas alternas a la fosforilación oxidativa. Mientras que en el medio succinato la única fuente de carbono succinato y estaría alimentando directamente la fosforilación oxidativa, requiriendo de mayor cantidad de complejo SDH y de F_1F_O-ATP sintasa. Como se esperaba, el complejo SDH sí aumentó su expresión en el medio succinato respecto al LB (Figura 21) y concuerda con lo reportado anteriormente (104). Implicando que su expresión se encuentra determinada por la presencia del succinato. Sin embargo, nosotros esperábamos un aumento en la expresión de la F_1F_O-ATP sintasa en el medio succinato, pero la enzima se expresó igual en ambas condiciones (Figura 21 y 24 B). Esto se puede deber a que la enzima puede disminuir o aumentar su actividad de síntesis de ATP cuando el gradiente electroquímico disminuye o aumenta, lo cual concuerda con nuestro resultado (Figura 20 A y B), la otra posibilidad es que la expresión de los genes de la enzima podría ser constitutiva en en *P. denitrificans.* Se requerirán experimentos adicionales para determinar si la expresión de la ATP sintasa es constitutiva en *P. denitrificans*.

La subunidad ζ inhibe totalmente el bombeo de protones por la F_1F_O-ATPasa. Al evaluar la actividad de bombeo de protones generada por la actividad F_1F_O-ATPasa en las PSB de la cepa PdΔζ y en las PSB de la cepa PdWT esperábamos que la actividad fuese mayor en las PSB de la cepa PdΔζ. Esperábamos dicho

aumento debido a que las PSB de la cepa PdΔζ tenían una mayor actividad de hidrólisis de ATP por la F_1F_O-ATP que las PSB de la cepa PdWT (Figura 20 B). Como esperábamos, la actividad de bombeo de protones generada por la actividad F_1F_O-ATPasa en las PSB de la cepa PdΔζ fue mayor que en las PSB de la cepa PdWT (Figura 22 A y B). El aumento en la actividad de bombeo de protones en las PSB de la cepa PdΔζ confirma que al aumentar la actividad de hidrólisis de ATP por la F_1F_O-ATPasa, esta enzima bombea más protones a través de la membrana. En resumen, la subunidad ζ al inhibir la actividad F_1F_O-ATPasa inhibe el bombeo de protones generado por la enzima.

La subunidad ζ inhibe el potencial de membrana en las células. Dado que la subunidad ζ inhibe el bombeo de protones en las PSB, se decidió evaluar el potencial de membrana las células mediante citometría de flujo esperando que el potencial aumentara en las células PdΔζ respecto a las silvestres. Esperábamos dicho aumento debido a que las PSB de la cepa PdΔζ tenían una mayor actividad de hidrólisis de ATP y bombeaban más protones por la F_1F_O-ATP que las de la cepa PdWT (Figura 20 B y Figura 22 A y B). Como esperábamos, el potencial de membrana en las células de la cepa PdΔζ fue mayor que el potencial de membrana en las células de la cepa PdWT y PdΔζ+ζ en el medio succinato(Figura 23 B). Sin embargo, en las células de PdΔζ en el medio LB el potencial de membrana fue igual que el de las cepas PdWT y PdΔζ+ζ (Figura 23 A). Lo anterior se puede deber a que en el medio LB no se requiere tanto potencial de membrana debido a que en el medio se cuenta con una cantidad considerable de aminoácidos que se aprovechan para la síntesis de proteínas y además para la obtención de ATP mediante el catabolismo de éstos.

La subunidad ζ endógena inhibe más del 84% de la actividad F_1-ATPasa. Dado que la subunidad ζ inhibe la actividad F_1-ATPasa, analizamos que tan inhibida se encuentra la F_1^{WT} por su subunidad ζ endógena. Sin activador la $F_1^{\Delta\zeta}$ alcanzó 0.88 μmol/mg*min y la de la F_1^{WT} fue de 0.14 μmol/mg*min, esto implica que la enzima silvestre está inhibida de manera endógena en un 84.1% (Figura 24 C). Además, la

actividad F_1-ATPasa reportadas en esta tesis sin activador, con un activador o con dos activadores de la cepa PdWT y de la Pd$\Delta\zeta$ son las más altas reportadas en la literatura (Figura 24 C). En los ensayos de reconstitución homóloga en donde se añadió ζ recombinante a la F_1 endógena, una concentración de 0.25 μM de la subunidad ζ inhibió la actividad ATPasa en un 87.5 % de la F_1^{WT} y en un 91.7 % de la $F_1^{\Delta\zeta}$. Mientras que, la subunidad ζ recombinante a 2.3 μM inhibió la actividad ATPasa en un 99.3 % de la F_1^{WT} y en un 99.7 % de la $F_1^{\Delta\zeta}$ (Figura 25), por lo que podemos corroborar que la subunidad ζ es un inhibidor total.

La subunidad ζ inhibe la actividad F_1F_O-ATPasa manteniendo la concentración de ATP intracelular en *P. denitrificans*. La concentración de ATP intracelular de las células cultivadas en medio succinato fue menor en las de la cepa Pd$\Delta\zeta$ que en las de la cepa PdWT (Figura 26 B). La disminución en la concentración del ATP intracelular es una consecuencia directa del aumento en la actividad F_1F_O-ATPasa de la cepa Pd$\Delta\zeta$. Se puede descartar que la disminución del ATP intracelular se deba a otros motivos ajenos a la ausencia de la subunidad ζ, debido a que en la cepa Pd$\Delta\zeta$+ζ la concentración de ATP intracelular es aproximadamente igual al de la cepa silvestre PdWT (Figura 26 B). Por el contrario, se esperaba que la concentración de ATP en las células de las cepas PdWT, Pd$\Delta\zeta$ y Pd$\Delta\zeta$+ζ cultivadas en medio LB tuvieran la misma concentración de ATP intracelular debido a que tuvieron el mismo potencial de membrana en células vivas (Figura 22 A) y velocidades de crecimiento celulares similares (Figura 26 A). En la condición de cultivo LB, el cual es un medio de cultivo rico, las células cultivadas tienen los aminoácidos necesarios para sintetizar las proteínas que requieran, además no necesitan consumir ATP para sintetizar aminoácidos y finalmente, también pueden catabolizar los aminoácidos para la síntesis de ATP a nivel sustrato.

Modelo del mecanismo de inhibición de la subunidad ζ. La subunidad ζ inhibe la actividad F_1F_O-ATPasa (Figura 20 B). El mecanismo de inhibición ha sido dilucidado realizando reconstituciones homólogas de ζ recombinante sobre F_1 endógena purificada de *P. denitrificans* (27,28). Además, se han realizado análisis

de las subunidades que interactúan del complejo F_1 con la subunidad ζ. Estos análisis de interacción se llevaron a cabo al reconstituir ζ recombinante con F_1 endógena purificada y se añadió el compuesto DSP que interactúa y enlaza de manera covalente con proteínas/subunidades que se encuentren a distancias de 14 Å o menos. Posteriormente, se llevan a cabo geles de 2 dimensiones para identificar las subunidades que se entrecruzaron y por ende son capaces de interactuar. Con estos entrecruzamientos se dilucidó que la subunidad ζ interactúa con α, β y γ (28). Además, se obtuvo una subunidad ζ recombinante que carece de los primeros 14 residuos de aminoácidos del N-terminal ($\zeta^{\Delta NT}$) y se observó que es capaz de interactuar con la fracción F_1, pero incapaz de inhibir la actividad de hidrólisis de ATP por la F_1-ATPasa. La $\zeta^{\Delta NT}$ confirmó funcionalmente que el N-terminal es el dominio encargado de la inhibición de la actividad F_1-ATPasa (28). Adicionalmente, se ha resuelto la estructura de la F_1F_O-ATPasa inhibida por la subunidad ζ mediante cristalografía de rayos X (69) (PDB ID 5DN6), sin embargo, esta estructura no contiene a toda la subunidad ζ resuelta, ya que sólo cuenta con los 32 de los primeros 33 residuos del N-terminal y 22 residuos del C-terminal. Para tratar de conocer todos los residuos de interacción de la subunidad ζ sobre la estructura del complejo F_1F_O, nosotros ensamblamos los residuos restantes de la subunidad ζ de la estructura resulta por RNM (PDB ID 2LL0) sobre la estructura de la subunidad ζ resuelta por cristalografía de rayos X (PDB ID 5DN6) (Figura 27 A). Con el modelo de la estructura de la F_1F_O-ATPasa inhibida con la subunidad ζ completa, anudado con nuestros datos funcionales de síntesis e hidrólisis de ATP en las PSB (Figura 20 A y B), proponemos que la subunidad ζ se mantiene en su sitio de interacción en la interfase α/β. Adicionalmente, proponemos que la subunidad ζ funciona como la uñeta de una matraca, permitiendo el giro del rotor de la enzima en el sentido CW, e inhibiendo a éste en el sentido CCW (Figura 27 A, B y C). Sin embargo, de momento queda como incógnita si el N-terminal de la subunidad ζ se mantiene totalmente en el sitio de interacción con las subunidades α, β y γ o si hay una liberación parcial del sitio de interacción del N-terminal de la subunidad ζ con las subunidades α, β y γ cuando el rotor de la enzima está girando en el sentido CW.

Además, también queda como incógnita la estructura secundaria del N-terminal de la subunidad ζ cuando la enzima está girando en el sentido de la síntesis de ATP. La estructura del N-terminal de la subunidad ζ cuando se encuentra en el sitio inhibitorio del complejo F_1F_O se encuentra estructurado en α-hélice (PDB ID 5DN6), pero el N-terminal de la subunidad ζ se encuentra intrínsecamente desordenado cuando la subunidad ζ se encuentra en solución (PDB ID 2LL0). En resumen, proponemos que la subunidad ζ funciona como la uñeta de una matraca en la F_1F_O-ATPasa deteniendo el giro de la enzima en el sentido de la hidrólisis de ATP y permitiendo el giro de la enzima en el sentido de la síntesis de ATP.

***Paracoccus denitrificans* como modelo de estudio para dilucidar el rol de las subunidades reguladoras de la F_1F_O-ATPasa.** Proponemos a la bacteria *Paracoccus denitrificans* como un mejor modelo de estudio para los trabajos que involucren la eliminación de la subunidad inhibidora de la F_1F_O-ATP sintasa. Ésto debido a que su subunidad inhibidora ζ no es una subunidad estructural como la subunidad ε para la enzima de *E. coli*. En *E. coli* se removió la subunidad inhibidora ε (42) y encontraron que la fracción F_1 se disocia de la fracción F_O, dejando la F_1F_O-ATPsintasa de sintetizar ATP y además dejando libre a la F_1 para hidrolizar el ATP intracelular de la bacteria *E. coli*. Por otra parte, en la levadura *S. cerevisiae* removieron la subunidad inhibidora IF_1 y dos proteínas homólogas a IF_1: los factores de estabilización stf1 y stf2 (84). En la levadura *S. cerevisiae* sin las tres proteínas (IF_1, stf1 y stf2) se observó un aumento en la hidrólisis de ATP por la F_1F_O-ATPsintasa en preparaciones de partículas sub-mitocondriales (PSM) que son preparaciones similares a las partículas sub-bacterianas (PSB). Sin embargo, en la cepa de *S. cerevisiae* carente de las tres proteínas (IF_1, stf1 y stf2) no encontraron cambios en el crecimiento celular con respecto a la cepa de *S. cerevisiae* silvestre, aun cuando las levaduras se cultivaron en un medio nutritivo y en otro respiratorio. Por último, en ratones se removió la subunidad inhibidora IF_1 (88) y no se observó ningún cambio en el crecimiento con respecto al de los ratones silvestres. En ratones habría sido importante remover también las proteínas homólogas a la IF_1

para descartar la posibilidad de que las proteínas homólogas suplieran el papel de la proteína inhibidora IF_1. Debido a que la proteína inhibidora ζ no es una proteína estructural para la F_1F_O-ATPsintasa y además no tiene proteínas homólogas dentro del genoma de *P. denitrificans*, proponemos a *P. denitrificans* como un mejor modelo de estudio para los trabajos que involucren la eliminación de la subunidad inhibidora de la F_1F_O-ATP sintasa.

La subunidad ζ como un posible blanco terapéutico para el tratamiento de enfermedades ocasionadas por α-proteobacterias patógenas. En la clase de las α-proteobacterias hay géneros de bacterias patógenas causantes de enfermedades en humanos, vacas y plantas como *Brucella* que causa Brucelosis, *Bartonella* que causa Bartonelosis, *Ochrobactrum* que causa endocarditis y *Agrobacterium* que causa tumores en plantas (105). Dado que la F_1F_O-ATP sintasa de otras bacterias patógenas como *Mycobacterium tuberculosis* se ha aprovechado como blanco terapéutico (106-108), nosotros proponemos que la ATP sintasa y en particular la subunidad inhibidora ζ puede ser un buen blanco terapéutico para el desarrollo de nuevos fármacos con el fin de tratar los padecimientos ocasionados por bacterias patógenas pertenecientes a la clase de las α-proteobacterias como las Rickettsias, Brucellas, Bartonellas, etc.

10 Conclusión

Este estudio demuestra que la subunidad inhibidora ζ es esencial para mantener la velocidad de crecimiento celular de la bacteria *P. denitrificans* en el medio respiratorio succinato debido a que inhibe la actividad F_1F_O-ATPasa. Siendo que la subunidad ζ no es una proteína estructural de la enzima y que no tiene genes homólogos dentro del genoma de *P. denitrificans,* esta bacteria es un modelo ideal para trabajos que involucren la eliminación de la subunidad inhibidora de la F_1F_O-ATP sintasa. Además, puesto que la subunidad inhibidora ζ no se encuentra codificada en el genoma de los humanos, esta subunidad puede ser un buen blanco terapéutico para el desarrollo de nuevos fármacos con el fin de tratar los padecimientos ocasionados por bacterias patógenas pertenecientes a la clase de las α-protoebacterias como las Rickettsias, Brucellas, Bartonellas, etc.

11 Perspectivas

- Añadir glucosa o aminoácidos al medio succinato y cultivar a la cepa Pd$\Delta\zeta$ para observar si se revierte el fenotipo al observado en la condición LB.
- Cultivar las células de las tres cepas en condiciones anaeróbicas (con nitrato como aceptor final de electrones) y observar si la ausencia del gen ζ tiene algún efecto.
- Analizar la expresión de genes encargados de codificar enzimas de fosforilaciones a nivel sustrato en las condiciones LB y succinato, para analizar si hay un cambio en la expresión de estas.
- Obtener una cepa mutante complementada Pd$\Delta\zeta$+ζ con un plásmido al que se le pueda modular la expresión del gen ζ para poder observar si la expresión diferencial tiene efectos diferentes al de la complementada actual al ser cultivada en el medio succinato.
- Hacer otras mutantes nulas de ζ en otras α-proteobacterias para evaluar el papel biológico de esta subunidad en otras especies.

12 Proyecto paralelo

12.1 “Pérdida de la función reguladora de la subunidad ζ en algunas α-proteobacterias simbióticas y desaparición del gen-ζ en orden de las Rickettsiales”

El gen que codifica para la subunidad ζ (gen-ζ), estudiado anteriormente en *P. denitrificans* (léase la primera parte de esta tesis), también se encuentra presente en el genoma de la gran mayoría de las bacterias pertenecientes a la clase de las α-proteobacterias (Figura 29) (27). Además, la secuencia de aminoácidos del gen-ζ se encuentra conservada en las α-proteobacterias (Figura 29 D) (28).

A

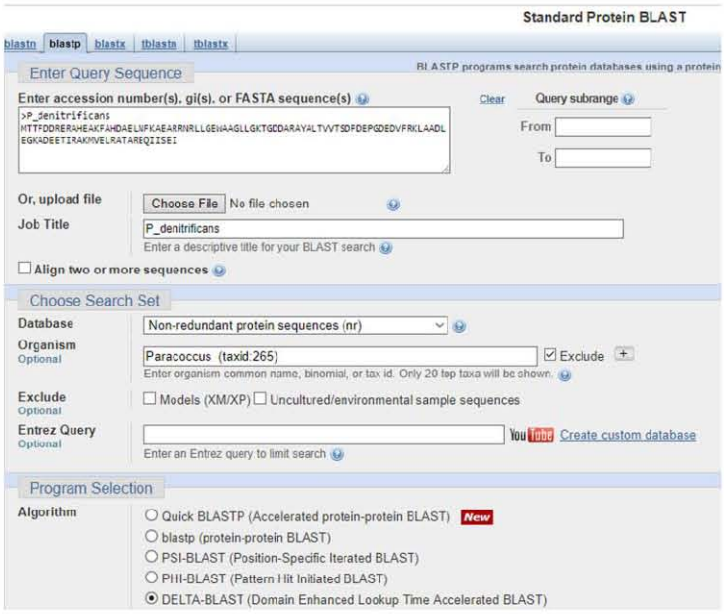
Standard Protein BLAST
blastn
blastp
blastx
tblastn
tblastx
Enter Query Sequence
Enter accession number(s), gi(s), or FASTA sequence(s)
Clear
Query subrange
From
To
Or, upload file
Choose File
No file chosen
Job Title
P_denitrificans
Enter a descriptive title for your BLAST search
Align two or more sequences
Choose Search Set
Database
Non-redundant protein sequences (nr)
Organism
Optional
Paracoccus (taxid:265)
Exclude
Enter organism common name, binomial, or tax id. Only 20 top taxa will be shown.
Exclude
Optional
Models (XM/XP)
Uncultured/environmental sample sequences
Entrez Query
Optional
Create custom database
Enter an Entrez query to limit search
Program Selection
Algorithm
Quick BLASTP (Accelerated protein-protein BLAST)
New
blastp (protein-protein BLAST)
PSI-BLAST (Position-Specific Iterated BLAST)
PHI-BLAST (Pattern Hit Initiated BLAST)
DELTA-BLAST (Domain Enhanced Lookup Time Accelerated BLAST)

B

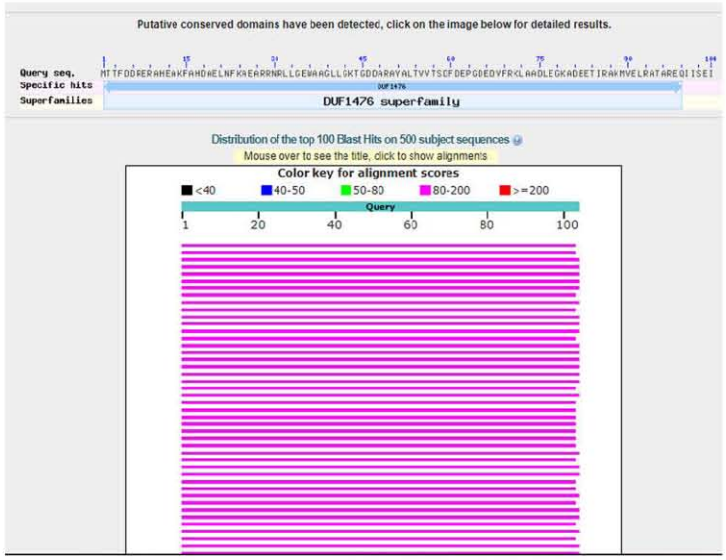
Putative conserved domains have been detected, click on the image below for detailed results.
Query seq.
Specific hits
Superfamilies
DUF1476 superfamily
Distribution of the top 100 Blast Hits on 500 subject sequences
Mouse over to see the title, click to show alignments
Color key for alignment scores
<40
40-50
50-80
80-200
>=200
Query
1
20
40
60
80
100

C

	Description	Max score	Total score	Query cover	E value	Ident	Accession	for PSI blast	to build PSSM
☐	DUF1476 domain-containing protein [Kocuria rhizophila]	134	134	99%	6e-39	80%	PZP19529.1	☑	
☐	DUF1476 domain-containing protein [Methylarcula marina]	129	129	99%	6e-37	77%	WP_106690870.1	☑	
☐	DUF1476 domain-containing protein [Thioclava indica]	122	122	99%	4e-34	70%	WP_038129815.1	☑	
☐	DUF1476 domain-containing protein [Yoonia vestfoldensis]	120	120	100%	2e-33	70%	WP_087206840.1	☑	
☐	hypothetical protein perhaps implicated in de Novo purine biosynthesis	120	120	100%	3e-33	70%	EYD70730.1	☑	
☐	DUF1476 domain-containing protein [Yoonia vestfoldensis]	119	119	100%	9e-33	68%	WP_019955121.1	☑	
☐	DUF1476 domain-containing protein [Sulfitobacter pseudonitzschiae]	119	119	100%	1e-32	68%	WP_089422194.1	☑	
☐	DUF1476 domain-containing protein [Sulfitobacter sp. 20_GPM-1509m]	119	119	100%	1e-32	68%	WP_028956441.1	☑	
☐	MULTISPECIES: DUF1476 domain-containing protein [Thioclava]	118	118	99%	2e-32	66%	WP_075774539.1	☑	
☐	DUF1476 domain-containing protein [Sulfitobacter pseudonitzschiae]	117	117	100%	3e-32	67%	WP_037920637.1	☑	
☐	MULTISPECIES: DUF1476 domain-containing protein [Thioclava]	117	117	99%	3e-32	70%	WP_078527966.1	☑	
☐	DUF1476 domain-containing protein [Amylibacter ulonae]	117	117	100%	6e-32	67%	WP_101656951.1	☑	

D

```
Paracoccus denitrificans        MTTFDDREHAHSAKFAHDAELNFKAEARRNKLLGEWAAGLLGKTGDJAKAYALTVVTSDF 60
Rhodobacter capsulatus          MTTFDDREHAYSAKFAHDADLRFKAEARSVKILAQWAAGLLGKTEAALDAYVGEVLAADF 60
Rhodobacter sphaeroides         MTTFDDRERAFSSKFAHDAEMQFRAEVRRNKLVGLWAAELLGKTGESAQVYARAVIQADL 60
Jannaschia sp.                  MSTFDDRENAFSNKFAHDAEMQFKAEARRNKLMGLWVAEVLGKSGDSANAYAAEVVKADF 60
Oceaniglobus indicus            MSTFDDRKNAFSNKFSHDAEMQFKAEARRNKLLGLWAAELMGKSGDSAEAYAREVIKSDF 60
Gemmobacter megaterium          MTTFDDRQRAFSSKFAHDAEMQFRATARRNKLLGLWAAGLLGKTGADADAYAVEVVKSDF 60
Lentibacter algarum             MSTFDDRENAFSNKFAHDEEVKFKAEARTNKLLGLWAAELLGKSGDSAAAYAAEVVKADF 60
Pelagicola litorisediminis      MTTFDDRESAFSNKFAHDEEMNFRAEARRNKLLGLWAAELMGKTGESADAYAKEVVKSDF 60
Actibacterium mucosum           MTTFDDRENAFSNKFAHDAEMQFKAQARANKLLGLWAAELLGKSGDSAEAYATEVVKSDF 60
Loktanella vestfoldensis        MSTFDDRQQAFSAKFAHDAEMQFKAEARRNKLLGLWAAELMGKTGDSAAAYAIAVVKSDF 60
                                *:***** *.* **:** ::.*:* .*  :::. *.* ::**:     .*.  *: :*:

Paracoccus denitrificans        DEPGDEDVFRKLAADLEGKADEETIRAKMVELRATAREQIISEI-- 104
Rhodobacter capsulatus          EEAGKDDVVRKLVADLAGKADEATIRAELQKSMAEAMKQLASAG-- 104
Rhodobacter sphaeroides         HEPGFEDVVRKVSADLGDRASADMVRGKMLELLPVAKAQLMTETQA 106
Jannaschia sp.                  EEAGHEDVMRKVLGDLDGKRPEAEVRAKYEGLMAVAKAQLMDEL-- 104
Oceaniglobus indicus            EEAGDEDVVRKVSGDLGDKADEATTRAKMSDLLVEAKAQLMTELRD 106
Gemmobacter megaterium          EEAGDDDVLRKVAADLSGKATPEDIRAKMDALLAEAKAQLASDI-- 104
Lentibacter algarum             EEAGHEDVVRKVAADLGEMADTDTIRAKRAELSVLAKTQVMTEVG- 105
Pelagicola litorisediminis      EEAGIEDVVRKVAGDLGDIADADTIRKKMAELLIVAKGQILNEV-- 104
Actibacterium mucosum           EEAGHEDVFRKVSGDLGDKADEETIRNKMAEVLAEAKDQLLNEG-- 104
Loktanella vestfoldensis        EEAGDEDVYRKVAGDLEGRADEATIRAKMVSLMAEAKAQLMTEL-- 104
                                .* * :** **: .**        :* :       *  *:
```

Figura 29. El gen-ζ se encuentra distribuido y conservado en el genoma de las α-proteobacterias. Utilizando la secuencia de aminoácidos de la subunidad ζ de *P. denitrificans* cepa 1222 se buscó en el genoma de otras α-proteobacterias la presencia de del gen-ζ. Para detectar el gen-ζ en el genoma de otras α-proteobacterias se realizó un DELTA-BLAST utilizando el servidor NCBI. A) Captura de pantalla donde se muestra la secuencia de la subunidad ζ de *P. denitrificans* como secuencia problema utilizada (query sequence) y los parámetros utilizados para la búsqueda del DELTA-BLAST. B) Captura de pantalla mostrando el resumen gráfico de los resultados de la búsqueda (hits). En este resumen gráfico hubo más de 500 secuencias encontradas (hits) que pueden ser ortólogos de la subunidad ζ de *P. denitrificans*. El color rosa en las secuencias encontradas implica que la cobertura de la secuencia encontradas es mayor de 80 aminoácidos y menor de 200 aminoácidos respecto a la secuencia de la subunidad ζ de *P. denitrificans*. C) Captura de pantalla de las secuencias que tienen mayor identidad con la secuencia de la subunidad ζ de *P. denitrificans*, donde se muestra el valor de E y los datos

de acceso a cada una de estas secuencias. D) Alineamiento de la secuencia de aminoácidos de la subunidad ζ de *P. denitrificans* con otras 9 secuencias de aminoácidos tomadas al azar de los resultados obtenidos del DELTA-BLAST. El alineamiento se realizó utilizando CLUSTAL OMEGA. En el alineamiento, el * (Asterisco) indica posiciones en las cuales se contiene un residuo totalmente conservado (idéntico). : (Dos puntos) indica posiciones en las cuales se contiene un residuo con propiedades fuertemente similares. . (Punto) indica posiciones en las cuales se contiene un residuo con propiedades débilmente similares.

Sin embargo, en el laboratorio del Dr. García Trejo no se había podido detectar la expresión del gen-ζ en todas las α-proteobacterias fotosintéticas mediante WB. Sí se logró detectar la expresión en *Rhodobacter sphaeroides* (Rsp) (Figura 30A) (datos no publicados). Pero no se había podido detectar la expresión en *Rhodospirillum marinarum* (Rm), *Rhodopseudomonas palustris* (Rp), *Rhodovibrio salinarum* (Rsa), *Rhodospirillum rubrum* (Rr), *Rhodobacter capsulatus* (Rc) y *Phaeospirillum fulvum* (Pf) (Figura 30 A) (datos no publicados). Posteriormente, durante mi proyecto de maestría sí logramos detectar la expresión del gen-ζ en las α-proteobacterias fotosintéticas (Figura 30 B).

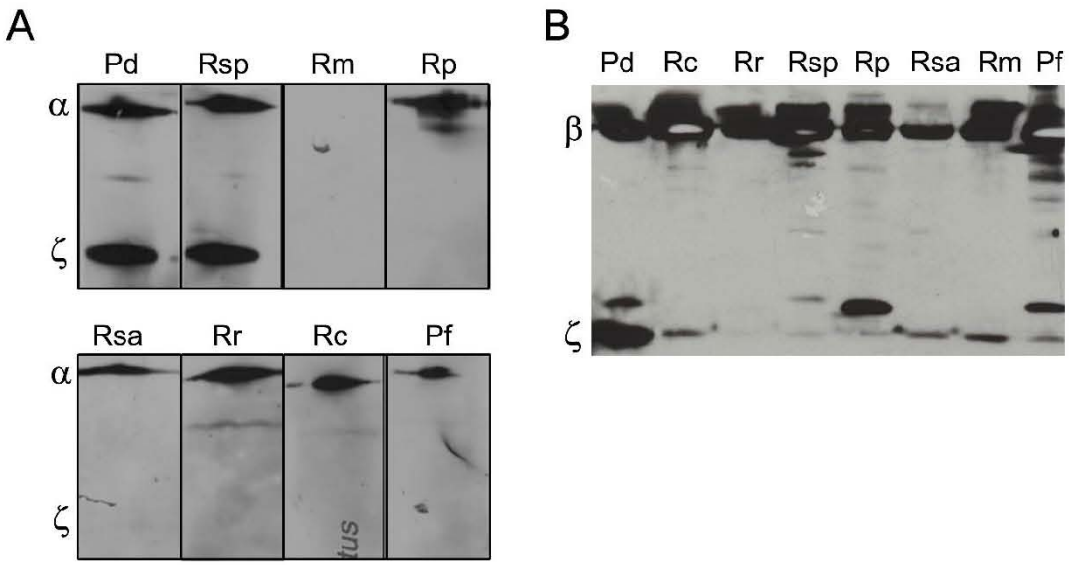

Figura 30. Expresión del gen-ζ en diferentes α-proteobacterias fotosintéticas. A) WB de solubilizados de F_1F_O corridos en un gel nativo y posteriormente corridos en una segunda dimensión desnaturalizante para

asegurar que la subunidad ζ se encuentra asociada al complejo F_1F_O de diferentes α-proteobacterias fotosintéticas: *Rhodobacter sphaeroides* (Rsp), *Rhodospirillum marinarum* (Rm), *Rhodopseudomonas palustris* (Rp), *Rhodovibrio salinarum* (Rsa), *Rhodospirillum rubrum* (Rr), *Rhodobacter capsulatus* (Rc) y *Phaeospirillum fulvum* (Pf). Se utilizó el anticuerpo policlonal anti-ζ obtenido en contra de la subunidad ζ de *P. denitrificans* (Pd) y el anticuerpo monoclonal anti-α de Bos taurus. Este WB es un dato no publicado del laboratorio del Dr. García-Trejo. B) WB de la F_1 enriquecida de esas mismas α-proteobacterias fotosintéticas utilizando el mismo anticuerpo anti-ζ y el anticuerpo monoclonal anti-β de Bos taurus. La F_1 se enriqueció al extraerla con cloroformo a partir de los cromatóforos de cada una de esas α-proteobacterias. La F_1 extraída se corrió en un gel desnaturalizante y posteriormente se realizó el WB.

Adicionalmente, dado que el gen-ζ se encuentra conservado (Figura 29 D) nuestro objetivo fue confirmar que el gen-ζ mantuviera su función inhibidora de la actividad F_1F_O-ATPasa en otras α-proteobacterias. La función inhibidora del gen-ζ en otras α-proteobacterias ya se había confirmado parcialmente de manera heteróloga. La confirmación heteróloga se llevó a cabo al obtener la ζ recombinante de *Jannaschia sp.* y realizar ensayos de inhibición sobre la F_1-ATPasa endógena de *P. denitrificans* (Figura 31) (28). La subunidad ζ recombinante de *Jannaschia sp.* fue capaz de inhibir la actividad F_1-ATPasa de *P. denitrificans* (Figura 31). Pero era necesario confirmar que el gen-ζ conserva su función de manera homóloga. Debido a que no podíamos cultivar en nuestro laboratorio a *Jannaschia sp*., decidimos trabajar con la bacteria *R. capsulatus*.

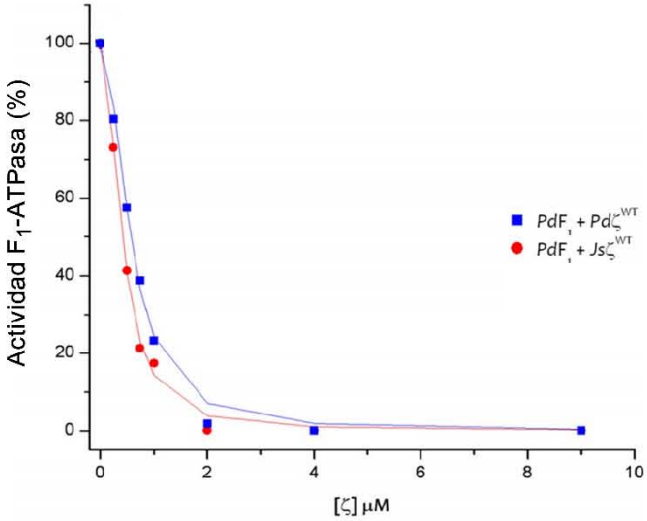

Figura 31. La subunidad ζ de *P. denitrificans* y de *Jannaschia sp.* son capaces de inhibir la hidrólisis de ATP por la F_1-ATPasa de *P. denitrificans.* La fracción F_1 de *P. denitrificans* (PdF_1) fue incubada en presencia de una concentración creciente de la subunidad ζ recombinante de *P. denitrificans* ($Pd\zeta^{WT}$, cuadros azules) o de la subunidad ζ recombinante de *Jannaschia sp.* ($Js\zeta^{WT}$, círculos rojos). Posteriormente a la incubación con la subunidad ζ, a la fracción F_1 se le midió la actividad de hidrólisis de ATP. Modificado de (28).

Nos propusimos purificar la F_1 endógena de *R. capsulatus* y a la cual ya le habíamos detectado la expresión del gen-ζ mediante WB (Figura 30 B). Elegimos a la α-proteobacteria fotosintética *R. capsulatus*, primero debido a que la secuencia de a.a. de su subunidad ζ tiene más identidad con la secuencia de a.a. de la subunidad ζ de *P. denitrificans* de todas las que probamos. Y segundo, debido a que el Dr. Helidoro Celis del Instituto de Fisiología Celular (UNAM) nos podía apoyar cultivándola y donándonos una gran cantidad de células de esta. Una vez que nos obsequiaron una gran cantidad de células de *R. capsulatus*, purificamos la fracción F_1 endógena de dicha bacteria (Figura 32 A). Adicionalmente, confirmamos la expresión del gen-ζ en la F_1 purificada de *R. capsulatus* (Figura 32 B).

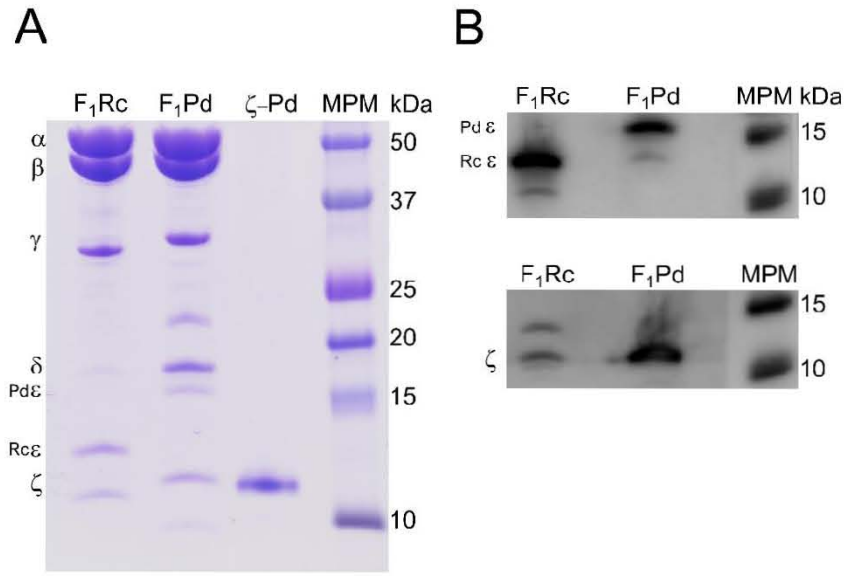

Figura 32. Purificación de la fracción F_1-ATPasa de *R. capsulatus*. A) SDS-PAGE teñido con coomassie de la purificación de la F_1 de *R. capsulatus* (Rc). Se aprecian todas las subunidades de la fracción F_1 de Rc: α, β, γ, δ, ε y ζ. La subunidad ε de Rc tiene un peso molecular de 13 kDa el cual es menor que el de la misma subunidad de *P. denitrificans* (Pd) el cual es 15.8 kDa. B) Detección de la subunidad ε y ζ de Rc mediante WB. La membrana superior e inferior son la misma, se reveló primero la de abajo (anti-ζ) y posteriormente se removieron los anticuerpos (stripping) y se expuso al anticuerpo anti-ε y se reveló nuevamente.

De *R. capsulatus* no logramos obtener la subunidad ζ recombinante *de R. capsulatus* (datos no mostrados). Y al no contar con la subunidad ζ recombinante de *R. capsulatus*, decidimos llevar a cabo ensayos de inhibición heteróloga utilizando la subunidad ζ recombinante de *P. denitrificans* y de *Jannaschia sp*. para evaluar si ambas eran capaces de inhibir la actividad F_1F_O-ATPasa de *R. capsulatus* (Figura 33).

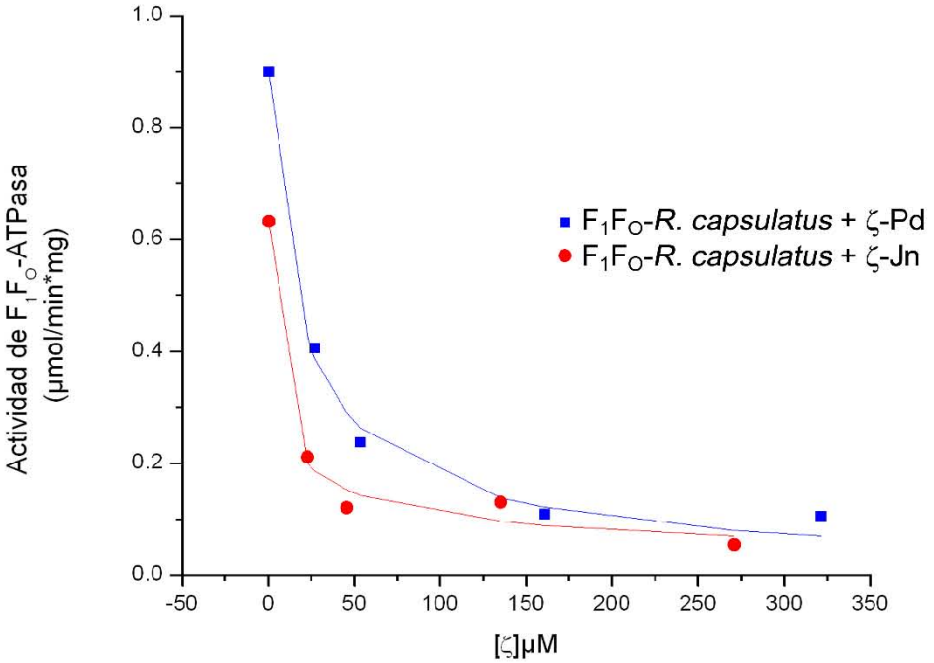

Figura 33. La subunidad ζ recombinante de *P. denitrificans* y de *Jannaschia sp.* son capaces de inhibir la hidrólisis de ATP por la F_1F_O-ATPasa de *R. capsulatus*. Se solubilizó el complejo F_1F_O de *R. capsulatus* (F_1F_O-*R. capsulatus*) a partir de cromatóforos. Este complejo F_1F_O fue incubado en presencia de una concentración creciente de la subunidad ζ recombinante de *P. denitrificans* (ζ-Pd, cuadros azules) o de la subunidad ζ recombinante de *Jannaschia sp.* (ζ-Jn, círculos rojos). Posteriormente a la incubación con la subunidad ζ, al complejo F_1F_O se le midió la actividad de hidrólisis de ATP.

En el tiempo que transcurrió durante los experimentos fallidos para la obtención de la subunidad ζ recombinante de *R. capsulatus*, el Dr. Miguel Ángel Cevallos del Centro de Ciencias Genómicas (UNAM) nos proporcionó cepas de las α-proteobacterias Rhizobiales. Entre las cepas que nos proporcionó se encontraban las bacterias fijadoras de nitrógeno: *Rhizobium etli* (*R. etli*), *Sinorhizobium meliloti* (*S. meliloti*) y *Methylobacterium nodulans* (*M. nodulans*). Inmediatamente purificamos la fracción F_1 endógena de *R. etli*, *S. meliloti* y semi-purificamos la F_1 de *M. nodulans* (Figura 34 A y B). Para nuestra sorpresa, la subunidad ζ no se detectó mediante SDS-PAGE teñidos por coomassie de las purificaciones de la

fracción F_1 de las tres Rhizobiales, por ello les realizamos un WB y confirmamos que la subunidad ζ si se encuentra asociada al complejo F_1 de ellas.

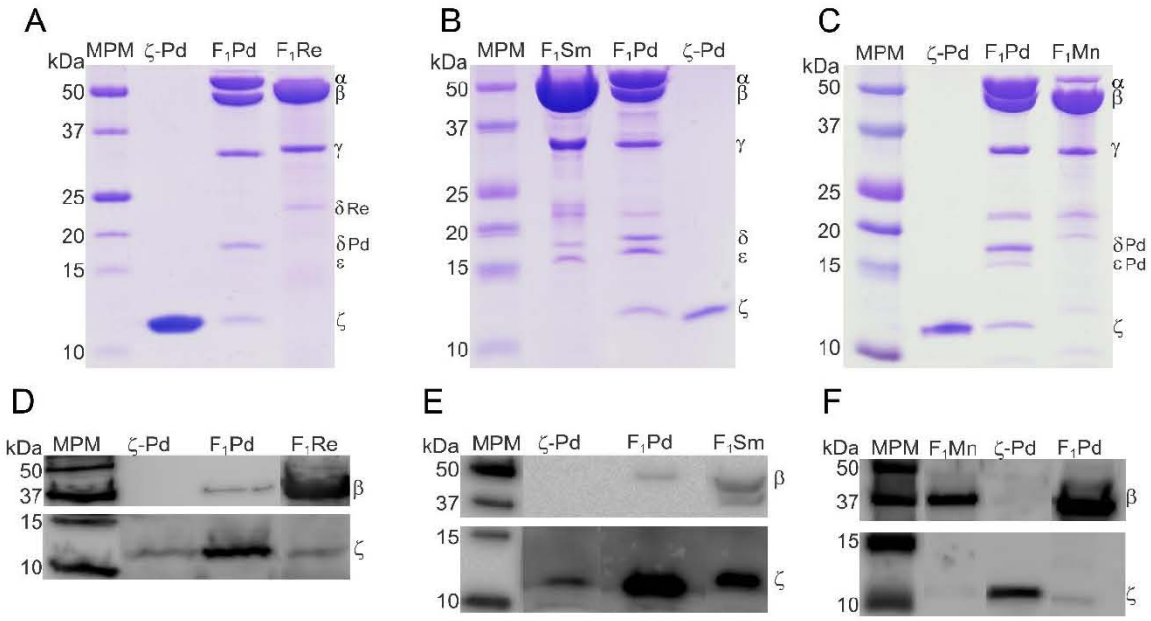

Figura 34. El gen-ζ se expresa y se asocia al complejo F_1 de *R. etli, S. meliloti* y *M. nodulans*. A), B) y C) SDS-PAGE teñido con coomassie de la purificación de F_1 de *R. etli* (Re), *S. meliloti* (Sm) y semi-purificación de la F_1 de M*. nodulas* (Mn), respectivamente. D), E) y F) WB anti-ζ del complejo F_1 de Re, Sm y Mn, respectivamente.

La subunidad ζ de *P. denitrificans* no es capaz de inhibir la actividad F_1-ATPasa de *R. etli* y de *S. meliloti*. Dado que nos interesaba conocer si la subunidad ζ de las bacterias Rhizobiales se disoció durante los pasos de purificación, tiene poca afinidad por el complejo F_1 o se expresa menos en estas tres bacterias, primero decidimos realizar ensayos de inhibición heterólogos utilizando la subunidad ζ de *P. denitrificans* en la F_1 de *R. etli* o de *S. meliloti*. Ésto último para probar la capacidad de asociación de la subunidad ζ recombinante sobre la F_1 de las dos bacterias Rhizobiales y adicionalmente debido a que tenemos el antecedente que la subunidad ζ de *P. denitrificans* es capaz de inhibir homólogamente su propia F_1 (Figura 31), así como heterólogamente en la F_1F_O de

R. capsulatus (Figura 33). Una vez llevado a cabo el ensayo de inhibición de las F_1 con la subunidad ζ de *P. denitrificans* reconstituida, encontramos que la subunidad ζ de *P. denitrificans* no fue capaz de inhibir la actividad de F_1-ATPasa de *R. etli* y de *S. meliloti* (Figura 35 A). El motivo por el cual la ζ de *P. denitrificans* es incapaz de inhibir la actividad de hidrólisis de ATP de las F_1 de *R. etli* y *S. meliloti* puede deberse a cambios en las secuencias de a.a. de las subunidades ζ de *R. etli* y de *S. meliloti* (Figura 35 B y C). Para probar esta teoría, decidimos obtener la subunidad ζ recombinante de *R. etli* y de *S. meliloti* para llevar a cabo los ensayos de reconstitución homóloga de ζ de *R. etli* en la F_1 de *R. etli* y la ζ de *S. meliloti* en la F_1 de *S. meliloti*. Adicionalmente, seguimos sin responder si la subunidad ζ de las bacterias Rhizobiales se disocia de la fracción F_1 durante los pasos de purificación, tiene poca afinidad por el complejo F_1 o se expresa menos en estas tres bacterias Rhizobiales. Por ello, proponemos obtener la subunidad ζ recombinante de ellas y realizar ensayos de reconstitución sobre el complejo F_1.

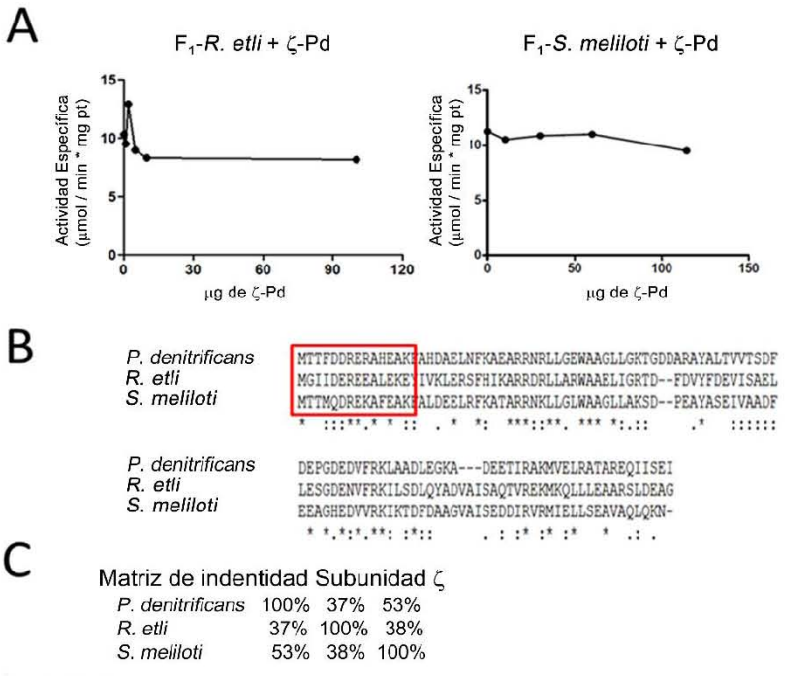

Figura 35. La subunidad ζ de *P. denitrificans* no es capaz de inhibir la actividad de hidrólisis de ATP de la F_1-ATPasa de *R. etli* y de *S. meliloti*. A) Ensayo de actividad de hidrólisis de ATP por la F_1-ATPasa F_1 de *R. etli* (panel izquierdo) y en F_1 de *S. meliloti* (panel derecho) reconstituidas con la subunidad ζ

de *P. denitrificans*. La subunidad ζ de *P. denitrificans* a una cantidad mayor de 100 μg no fue capaz de inhibir la actividad de hidrólisis de ATP por las F_1-ATPasas de *R. etli* y de *S. meliloti*. B) Alineamiento de secuencia de aminoácidos de las subunidades ζ de *P. denitrificans*, *R. etli* y *S. meliloti*. Los primeros 14 aminoácidos del N-terminal de *P. denitrificans* son esenciales para la función inhibitoria y se muestran en el recuadro rojo (28). C) Matriz de identidades de las secuencias de aminoácidos de *P. denitrificans, R. etli* y *S. meliloti*. El alineamiento y la matriz de identidades se realizaron utilizando Clustal Omega.

La subunidad ζ recombinante de *S. meliloti* no inhibe la actividad de hidrólisis de ATP por la F_1 de *S. meliloti*. Dado que nos interesaba conocer si la subunidad ζ de las bacterias Rhizobiales se disocia del complejo F_1 durante los pasos de purificación, tiene poca afinidad por el complejo F_1 o se expresa menos en estas tres bacterias Rhizobiales, clonamos el gen que codifica para la subunidad ζ de *R. etli*, *S. meliloti* y *M. nodulans* (datos no mostrados). Después, purificamos las subunidades recombinantes de *R. etli* y *S. meliloti* (Figura 36 A y B). Una vez purificada la ζ de *R. etli* y *S. meliloti* confirmamos que la ζ recombinante de *S. meliloti* tiene un plegamiento secundario similar al de la subunidad ζ de *P. denitrificans* (Figura 36 C). Debido a que la ζ de *P. denitrificans* y la ζ de *S. meliloti* tienen el mismo patrón en el dicroísmo circular, podemos pensar que el plegamiento de la subunidad ζ de *S. meliloti* es el nativo (Figura 36 C).

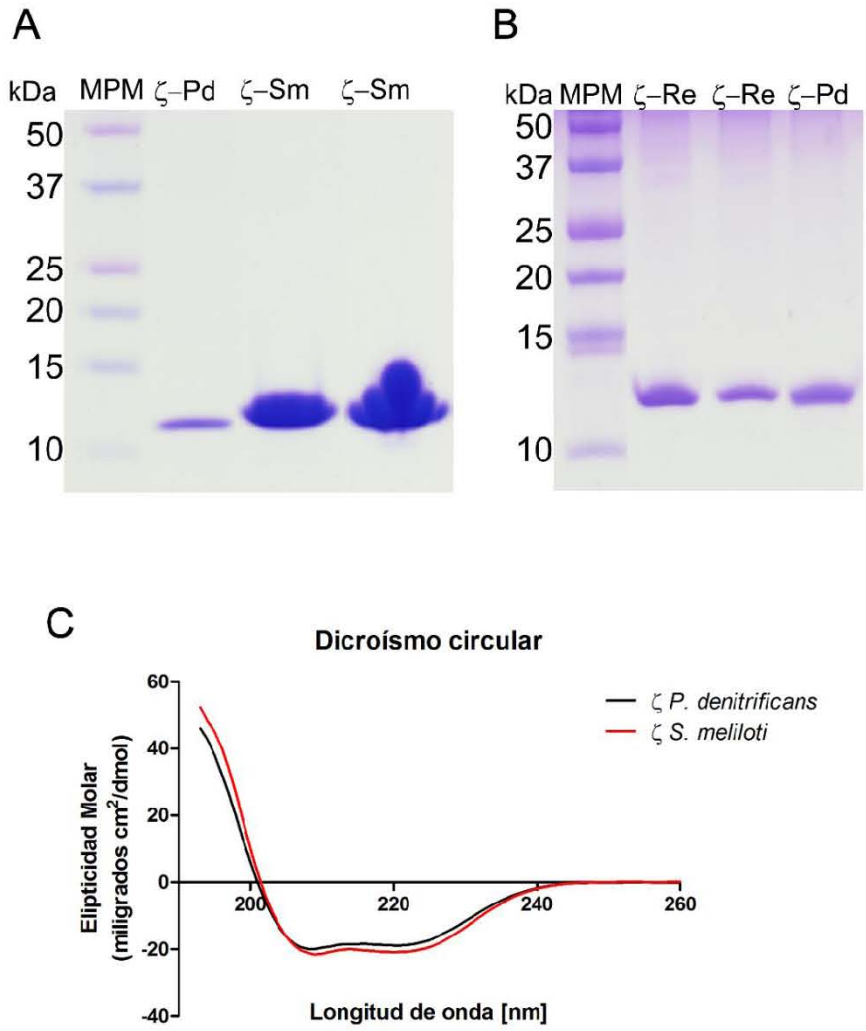

Figura 36. Purificación de la subunidad ζ recombinante de *R. etli y de S. meliloti*. A y B) SDS-PAGE teñidos con coomassie de la subunidad ζ de *S. meliloti* (Sm) y de *R. etli* (Re), respectivamente C) Dicroísmo circular de las subunidades ζ recombinantes de *S. meliloti* (líneas rojas) y de *P. denitrificans* (líneas negras).

Una vez purificada la subunidad ζ de *S. meliloti*, llevamos a cabo ensayos de inhibición de la ζ de *S. meliloti* en la F_1 endógena de *S. meliloti* (Figura 37 A). La F_1 de *S. meliloti* con el activador sulfito (2mM) alcanzó una actividad específica de hidrólisis de ATP aproximada de 6 μmol/min*mg. Cuando le añadimos 15 μg de ζ de *S. meliloti* la actividad específica de hidrólisis de ATP siguió siendo aproximada

a 6 μmol/min*mg. Realizando una comparación, en la F_1 de *P. denitrificans* cuando se le mide la actividad de hidrólisis de ATP en presencia de los activadores LDAO (0.015%) y sulfito (2mM) se logra una actividad específica de 20 μmol/min*mg. Al añadir a la F_1 de *P. denitrificans* una cantidad de 5 μg de ζ de *P. denitrificans* la actividad de 20 μg/min*mg se inhibe hasta alcanzar 2.1 μg/min*mg, esto es una inactivación del 89.7%. Los datos muestran que aun cuando añadimos una cantidad considerable de ζ de *S. meliloti*, la actividad de hidrólisis de ATP por la F_1 de *S. meliloti* no se ve afectada. Por ende, la ζ recombinante de *S. meliloti* no inhibe a su propia F_1-ATPasa. De momento nos hace falta repetir el experimento varias veces para confirmar el dato preliminar y realizar lo mismo con la ζ de *R. etli* sobre la F_1 de *R. etli*. Siguiendo la misma línea de pensamiento, realizamos un ensayo de inhibición de ζ de *S. meliloti* sobre la F_1 de *P. denitrificans* (Figura 37 B). A diferencia de lo ocurrido al añadir ζ de *P. denitrificans* sobre la F_1 de *S. meliloti*, no se inhibió la actividad de hidrólisis de ATP (Figura 35 A), hay una clara inhibición de la actividad de hidrólisis de ATP por la ζ de *S. meliloti* en la F_1 de *P. denitrificans*. De momento es necesario repetir los experimentos para poder llegar a una conclusión, sin embargo, los datos preliminares muestran que la ζ de *S. meliloti* no inhibe la actividad de hidrólisis de ATP de su propia F_1, pero parece que sí inhibe dicha actividad en la F_1 ajena de *P. denitrificans*, mientras que la ζ de *P. denitrificans* no es capaz de inhibir dicha actividad en la F_1 ajena de *S. meliloti*.

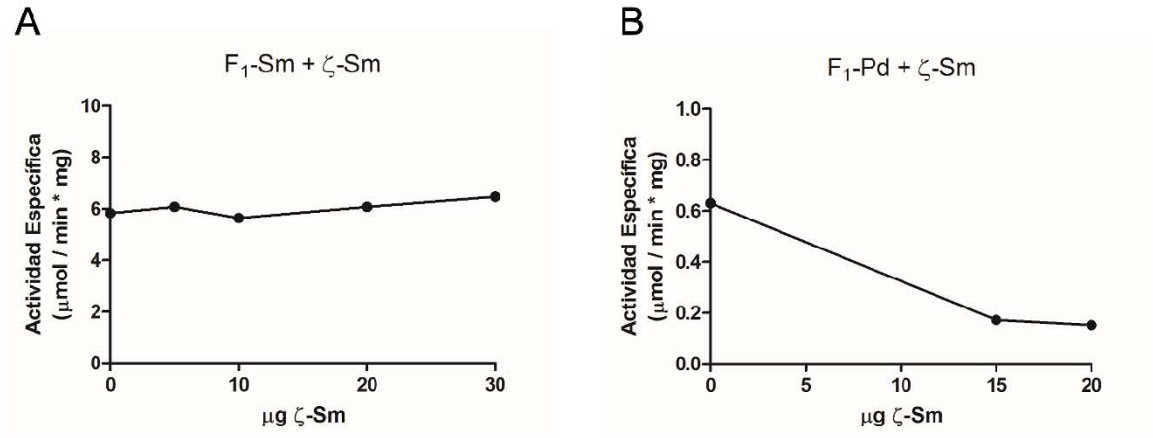

Figura 37. La subunidad ζ recombinante de *S. meliloti* no inhibe la actividad de hidrólisis de ATP de la F_1 de *S. meliloti*. La fracción F_1 de *S. meliloti* (A) o de *P. denitrificans* (B) fueron reconstituidas de manera homóloga o heteróloga con una cantidad creciente de subunidad ζ recombinante de *S. meliloti*. Posterior a la reconstitución a la F_1 se le midió la actividad de hidrólisis de ATP.

Los residuos del sitio inhibitorio de la subunidad ζ con la F_1-ATPasa de *S. meliloti* se encuentran conservados. Debido a que la capacidad inhibidora de la subunidad ζ de *S. meliloti* en la F_1-ATPasa de *S. meliloti* se perdió (Figura 37 A), pero que a la vez se conservó la capacidad inhibidora de la subunidad ζ de *S. meliloti* en la F_1-ATPasa de *P. denitrificans* (Figura 37 B), sospechamos que la pérdida de la inhibición en la actividad de F_1-ATPasa de *S. meliloti* se debe a que han ocurrido cambios en las subunidades α, β y γ de la F_1 de *S. meliloti*. Por ello, nos basamos en los sitios de interacción de la subunidad ζ con las subunidades α, β y γ identificados en la estructura resuelta por cristalografía (Figura 38 A) (69). Realizamos alineamientos de las secuencias α, β, γ y ζ de *S. meliloti* con las mismas secuencias de las subunidades de *P. denitrificans* e identificamos los sitios de interacción de la subunidad ζ con las subunidades α, β y γ (Figura 38 B, C, D y E). Los sitios de interacción de la subunidad ζ con las subunidades α, β y γ de *P. denitrificans* en los alineamientos realizados con las subunidades de *S. meliloti* se encuentran totalmente conservados (Figura 38 B, C y D). Por ello, intentamos detectar cambios en residuos aledaños a los residuos de interacción en los alineamientos realizados. Sin embargo, sólo hay pocos cambios y éstos son conservados (Figura 38 B, C y D).

A

ζ	γ	α_{DP}	β_{DP}
T1	S13		D382
T2	R10, S13, V14		
R6		F407	I386
E7			Q381, I384, A385
A9		A403, A404	
H10		F407	I384, A385, G388
E11			Y377, I384, Q381, R404
K13		A404, S409, L411	
F14			M389, D390
A15			R404, E450
H16		D412, T415	
E19			D451
L20		D412	
F22			H447, P449

B

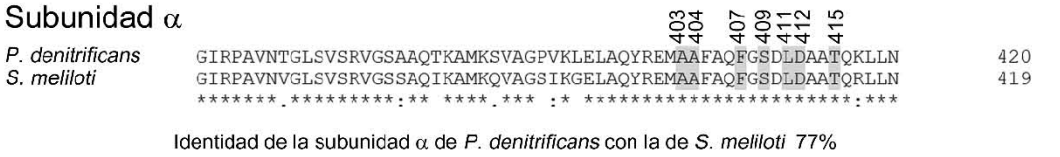

Identidad de la subunidad α de *P. denitrificans* con la de *S. meliloti* 77%

C

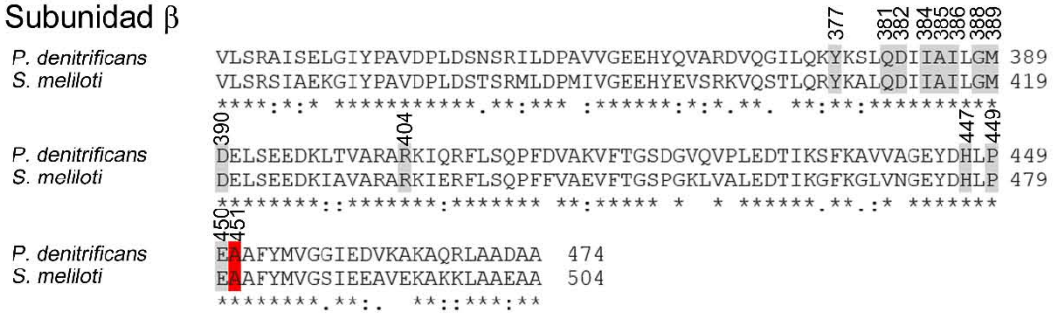

Identidad de la subunidad β de *P. denitrificans* con la de *S. meliloti* 80%

D

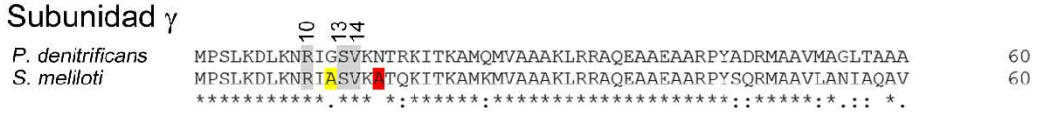

Identidad de la subunidad γ de *P. denitrificans* con la de *S. meliloti* 63%

E

Identidad de la subunidad ζ de *P. denitrificans* con la de *S. meliloti* 53%

Figura 38. Interacciones de la subunidad ζ con las subunidades α, β y γ. A) Tabla de residuos de interacción entre la subunidad ζ y las subunidades α, β y γ de *P. denitrificans* Modificado de material suplemenario de (69). B) Alineamiento de la

secuencia de aminoácidos de la subunidad α de *P. denitrificans* con la misma subunidad de *S. meliloti*. C) Alineamiento de la secuencia de aminoácidos de la subunidad β de *P. denitrificans* con la misma subunidad de *S. meliloti*. D) Alineamiento de la secuencia de aminoácidos de la subunidad γ de *P. denitrificans* con la misma subunidad de *S. meliloti*. E) Alineamiento de la secuencia de aminoácidos de la subunidad ζ de *P. denitrificans* con la misma subunidad de *S. meliloti*. En los alineamientos, los residuos sombreados son los residuos identificados en la tabla de interacciones. Los residuos sombreados se encuentran identificados en la parte superior con el número que los identifica en la tabla de interacciones. El color gris implica residuos que se son idénticos, en color amarillo o azul los residuos que han sufrido cambios conservados. En color rojo los residuos que han sufrido cambios no conservados. Debajo de las secuencias alineadas, el punto indica que el residuo es idéntico, los dos puntos indican que el residuo se encuentra conservado, el punto indica que el resiudo esta poco conservado y cuando no hay símbolo implica que el residuo no se encuentra conservado.

Modelo de la F_1-ATPasa de *Sinorhizobium meliloti*. Para tratar de entender por qué la subunidad ζ de *S. meliloti* no es capaz de inhibir la actividad F_1-ATPasa de *S. meliloti* (Figura 37 A) pero si es capaz de inhibir la actividad F_1-ATPasa de *P. denitrificans* (Figura 37 B), y dado que en los alineamientos realizados de las subunidades α, β y γ de *P. denitrificans* con las mismas subunidades de *S. meliloti* no hubo cambios en los residuos de interacción con la subunidad ζ, además de que no hubieron cambios en los residuos aledaños a los residuos de interacción de la subunidad ζ con las subunidades α, β y γ. Decidimos diseñar un modelo de la fracción F_1 de *S. meliloti* asociada a su subunidad ζ. El modelo nos permitirá analizar los cambios de residuos que en la secuencia podrían estar alejados de los residuos de interacción entre la subunidad ζ con α, β y γ, pero que en la estructura podrían estar cercanos a las interfases entre α, β y γ con la subunidad ζ. Si existen cambios en los residuos cercanos a las interfases entre α, β y γ con ζ, éstos al estar cercanos a las interfases entre las subunidades podrían estar modificando las interacciones entre las subunidades. Si la interfase es modificada, las interacciones entre las subunidades podrían ser debilitadas. Por ende, identificarlas podría aportar información al porque la subunidad ζ de *S. meliloti* no puede inhibir la actividad de hidrólisis de ATP de la F_1-ATPasa de *S. meliloti*, pero si la inhibe en la F_1-ATPasa de *P. denitrificans*. El modelo se diseñó utilizando el programa de modelaje Swiss Model Prot (44). Cada una de las subunidades de la F_1 de *S. meliloti*

se diseñó por separado tomando como base del modelo la estructura resuelta por cristalografía de la F_1F_O de *P. denitrificans* (PDB ID 5DN6) (69). Una vez que se modelaron cada una de las subunidades de la fracción F_1 de *S. meliloti*, se alinearon sobre la estructura de la F_1 de *P. denitrificans* (PDB ID 5DN6) utilizando el programa PyMol (31). Las subunidades α, β, γ y ζ se muestran en el modelo de superficie y las cadenas laterales de los residuos de aminoácidos se colorearon utilizando el script YRB (109). En la estructura de superficie el color **rojo** implica carga negativa, el color **azul** implica carga positiva, el **amarillo** implica hidrofobicidad y el **blanco** implica polaridad (Figuras 39, 40, 41, 42 y 43).

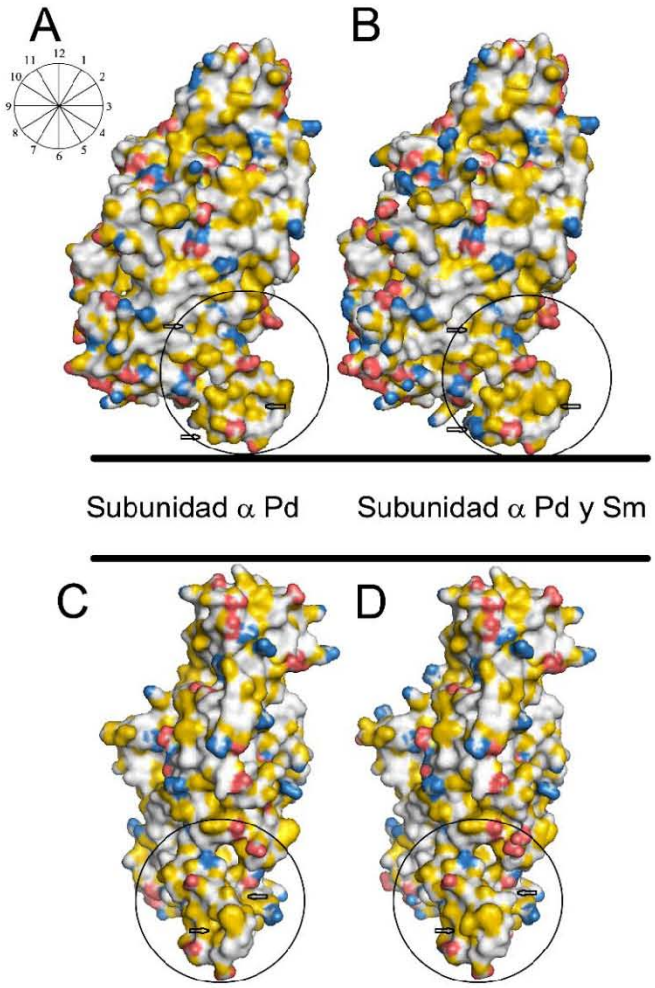

Figura 39. Modelo de la subunidad α de la F_1-ATPasa de *Sinorhizobium meliloti*. La subunidad α_{DP} de *S. meliloti* se modeló con el programa de modelaje

Swiss Model Prot utilizando la subunidad α_{DP} de *P. denitrificans* como molde (44). Las subunidades se muestran en el modelo de superficie y las cadenas laterales de los residuos de aminoácidos se colorearon utilizando el script YRB (109). En la estructura de superficie el color **rojo** implica carga negativa, el color **azul** implica carga positiva, el **amarillo** implica hidrofobicidad y el **blanco** implica polaridad. A) y C) Se muestra la subunidad α de *P. denitrificans*. B) y D) Muestran la subunidad α de *P. denitrificans* superpuesta con la subunidad α de *S. meliloti*. A) y B) Vista lateral de las subunidades. C) y D) Vista frontal de las subunidades. En el círculo se delimita la zona de interacción con la subunidad ζ. Las flechas indican lugares donde hay cambios en las estructuras. El círculo dividido en 12 partes sirve para identificar las zonas en las que imaginariamente se divide el círculo de la zona de la interfase con la subunidad ζ. Las imágenes se tomaron utilizando el programa PyMol (31).

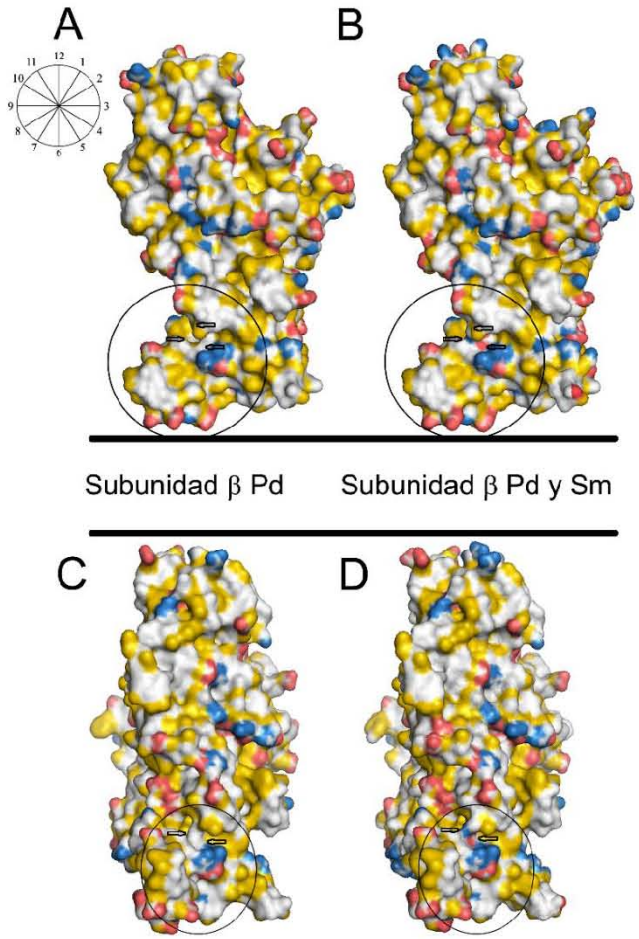

Figura 40. Modelo de la subunidad β de la F_1-ATPasa de *Sinorhizobium meliloti*. La subunidad β_{DP} de *S. meliloti* se modeló con el programa de modelaje Swiss Model Prot utilizando la subunidad β_{DP} de *P. denitrificans* como molde (44).

Las subunidades se muestran en el modelo de superficie y las cadenas laterales de los residuos de aminoácidos se colorearon utilizando el script YRB (109). En la estructura de superficie el color **rojo** implica carga negativa, el color **azul** implica carga positiva, el **amarillo** implica hidrofobicidad y el **blanco** implica polaridad. A) y C) Se muestra la subunidad β de *P. denitrificans*. B) y D) Muestran la subunidad β de *P. denitrificans* superpuesta con la subunidad β de *S. meliloti*. A) y B) Vista lateral de las subunidades. C) y D) Vista frontal de las subunidades. En el círculo se delimita la zona de interacción con la subunidad ζ. Las flechas indican lugares donde hay cambios en las estructuras. El círculo dividido en 12 partes sirve para identificar las zonas en las que imaginariamente se divide el círculo de la zona de la interfase con la subunidad ζ. Las imágenes se tomaron utilizando el programa PyMol (31).

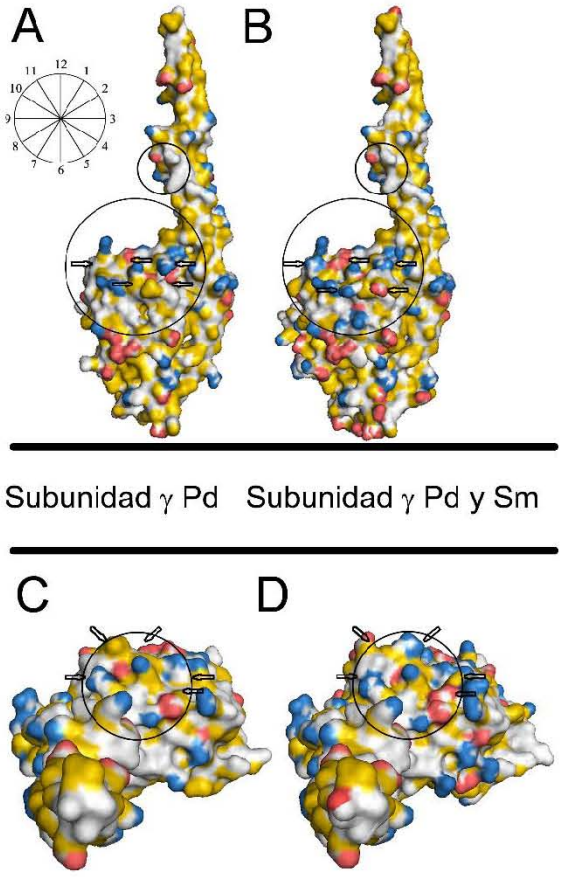

Figura 41. Modelo de la subunidad γ de la F_1-ATPasa de *Sinorhizobium meliloti*. La subunidad γ de *S. meliloti* se modeló con el programa de modelaje Swiss Model Prot utilizando la subunidad γ de *P. denitrificans* como molde (44). Las subunidades se muestran en el modelo de superficie y las cadenas laterales de los residuos de aminoácidos se colorearon utilizando el script YRB (109). En la

estructura de superficie el color **rojo** implica carga negativa, el color **azul** implica carga positiva, el **amarillo** implica hidrofobicidad y el **blanco** implica polaridad. A) y C) Se muestra la subunidad γ de *P. denitrificans*. B) y D) Muestran la subunidad γ de *P. denitrificans* superpuesta con la subunidad γ de *S. meliloti*. A) y B) Vista lateral de las subunidades. C) y D) Vista superior de las subunidades. En el círculo superior se delimita la zona de interacción con la subunidad ζ y en el círculo inferior se delimita la zona de interacción de la subunidad γ con la subunidad α_{DP} Las flechas indican lugares donde hay cambios en las estructuras. El círculo dividido en 12 partes sirve para identificar las zonas en las que imaginariamente se divide el círculo de la zona de la interfase con la subunidad ζ o con α_{DP}. Las imágenes se tomaron utilizando el programa PyMol (31).

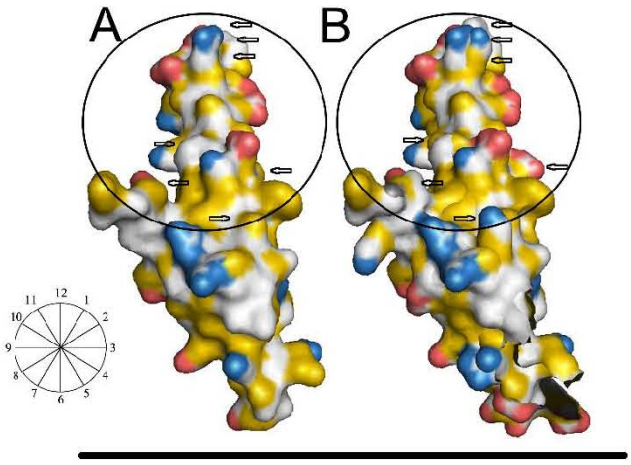

Figura 42. Modelo de la subunidad ζ de la F_1-ATPasa de *Sinorhizobium meliloti.* La subunidad ζ de *S. meliloti* se modeló con el programa de modelaje Swiss Model Prot utilizando la subunidad ζ de *P. denitrificans* como molde (44). Las subunidades se muestran en el modelo de superficie y las cadenas laterales de los residuos de aminoácidos se colorearon utilizando el script YRB (109). En la estructura de superficie el color **rojo** implica carga negativa, el color **azul** implica carga positiva, el **amarillo** implica hidrofobicidad y el **blanco** implica polaridad. A) Muestra la subunidad ζ de *P. denitrificans*. B) Muestra la subunidad ζ de *P. denitrificans* superpuesta con la subunidad ζ de *S. meliloti*. En el círculo se delimita la zona de interacción con las subunidades α_{DP} y β_{DP}. Las flechas indican lugares donde hay cambios en las estructuras. El círculo dividido en 12 partes sirve para identificar las zonas en las que imaginariamente se divide el círculo de la zona de la interfase con la subunidad ζ. Las imágenes se tomaron utilizando el programa PyMol (31).

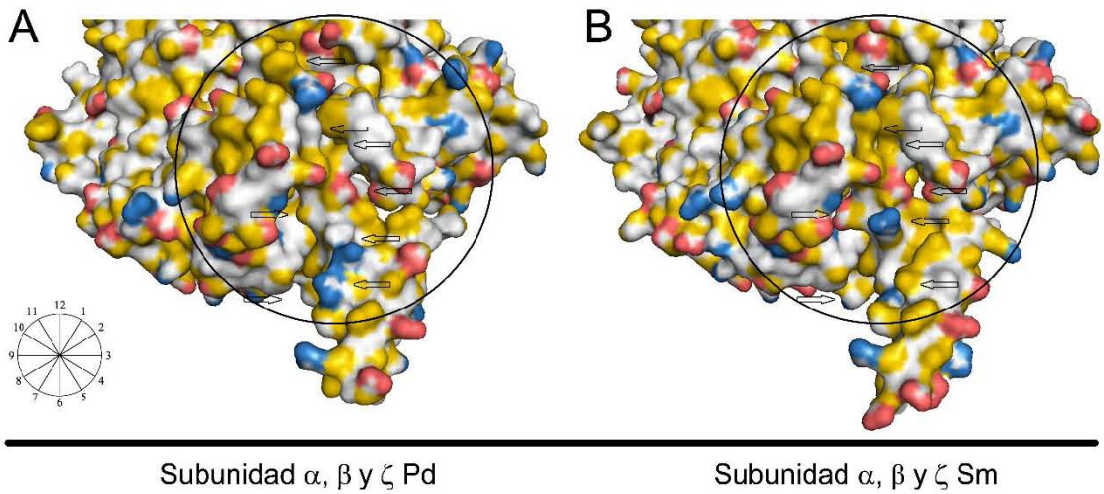

Figura 43. Modelo del sitio de interacción de la subunidad ζ en la interfase α_{DP} y β_{DP} de *S. meliloti*. El sitio de interacción de la subunidad ζ en la interase α_{DP} y β_{DP} de *S. meliloti* se modeló con el programa de modelaje Swiss Model Prot utilizando las subunidades de *P. denitrificans* por separado como molde (44). Una vez modeladas las subunidades de manera individual se alinearon las estructuras una por una con la estructura de la F_1 de *P. denitrificans* (PDB ID 5DN6). Las subunidades se muestran en el modelo de superficie y las cadenas laterales de los residuos de aminoácidos se colorearon utilizando el script YRB (109). En la estructura de superficie el color **rojo** implica carga negativa, el color **azul** implica carga positiva, el **amarillo** implica hidrofobicidad y el **blanco** implica polaridad. A) Muestra las subunidades α_{DP}, β_{DP} y ζ de *P. denitrificans*. B) Muestra las subunidades α_{DP}, β_{DP} y ζ de *S. meliloti*. En el círculo se delimita la zona de interacción con las subunidades α_{DP} y β_{DP}. Las flechas indican lugares donde hay cambios en las estructuras. El círculo dividido en 12 partes sirve para identificar las zonas en las que imaginariamente se divide el círculo de la zona de la interfase con la subunidad ζ. Las imágenes se tomaron utilizando el programa PyMol (31).

Cambios en las estructuras de las subunidades α, β, γ y ζ de *S. meliloti*. Al comparar las estructuras de las subunidades α, β, γ y ζ de *P. denitrificans* (resueltas por cristalografía) con las de *S. meliloti* (modeladas) es notorio que existen bastantes cambios tridimensionales en cada una de las subunidades, así como en las interfases de contacto entre ellas. Se compara la subunidad α de *P. denitrificans* (Figura 39 A y C) con la subunidad de *S. meliloti* (Figura 39 B y D) y se coloca un

círculo para delimitar el área de la subunidad α que interactúa con la subunidad ζ. Para poder discutir los cambios señalados dentro del círculo, de manera imaginaria se divide el circulo en 12 partes, similar a lo que uno observa en un reloj de manecillas y el cual se encuentra dividido de la 1' a las 12'. Esto último se ejemplifica en el círculo dividido en 12 partes que se encuentra en el panel A. **En la subunidad α de *S. meliloti*** (Figura 39 B) en la zona delimitada por el círculo (interfase con la subunidad ζ) se señalan tres cambios cada uno con una flecha diferente. El cambio señalado a las 10' muestra la pérdida de una protuberancia hidrofóbica. El cambio señalado a las 7' muestra la aparición de una protuberancia con carga positiva. El cambio señalado a las 5' muestra desaparición de un orificio (Figura 39 A) y la aparición de una protuberancia hidrofóbica (Figura 39 B). Éste último cambio se vuelve a mostrar en la Figura 39 C y D (desde la perspectiva de la subunidad α girada 90 grados) y ahora se encuentra a las 7'. Adicionalmente, a las 3' se observa un cambio adicional. El cambio adicional (3') muestra la aparición de una protuberancia polar (Figura 39D). **En la subunidad β de *S. meliloti*** (Figura 40 B) en la zona delimitada por el círculo (interfase con la subunidad ζ) se muestran tres cambios señalados cada uno por una flecha. El cambio a la 1' muestra la aparición de una protuberancia polar. El cambio a entre las 2' y las 3' muestra la aparición de una carga negativa. El cambio entre las 11' y 12' muestra la desaparición de un orificio hidrofóbico y la aparición de una carga positiva (Figura 40 B). La Figura 40 C y D muestran la subunidad β girada 90 grados respecto a la subunidad β de la Figura A y C. En la Figura 40 D se muestran dos cambios en la zona delimitada por el círculo. El cambio a la 1' muestra la aparición de una carga negativa (Figura 40 D) en una zona que era polar (Figura 40 C). El cambio a las 11' muestra la aparición de una carga positiva (Figura 40 D) en una zona que era polar (Figura 40 C). **En la subunidad γ de *S. meliloti*** (Figura 41 B) la zona delimitada por el círculo superior muestra la zona de la interfase con el N-terminal de la subunidad ζ. La zona delimitada por el círculo inferior muestra la zona de la interfase con la subunidad α_{DP} y con el C-terminal de la subunidad ζ. En el círculo superior no se muestran cambios debido a que en la interfase de γ con ζ no hay cambios estructurales observables. En el círculo inferior, se muestran cinco cambios señalados cada uno

por una flecha (Figura 41 B). El cambio en el centro del círculo inferior muestra la aparición de una protuberancia con carga negativa (Figura 41 B) donde antes había una pequeña zona hidrofóbica (Figura 41 A). El cambio a las 3' muestra la desaparición de una protuberancia positiva. El cambio a las 4' muestra la aparición de una protuberancia con carga negativa. El cambio a las 8' muestra la aparición de una protuberancia con carga positiva. El cambio a las 9' muestra la aparición de una carga positiva. En la Figura 41 C y D se muestra la subunidad γ vista desde arriba y se señalan 5 cambios. El cambio a 1' muestra la aparición de una protuberancia con carga positiva. El cambio a las 3' muestra la aparición de una protuberancia hidrofóbica. El cambio a las 4' muestra la aparición de una carga negativa donde había una carga hidrofóbica. El cambio a las 9' muestra la aparición de una protuberancia con carga positiva donde no había una protuberancia tan marcada. El cambio a las 11' muestra el desplazamiento de una cadena lateral, en donde se pierde hidrofobicidad y se gana una carga negativa. **En la subunidad ζ de *S. meliloti*** (Figura 42 B) en la zona delimitada por el círculo (interfase con las subunidades α y β) se muestran siete cambios señalados cada uno por una flecha. Los tres cambios a la 1' muestran la aparición de una protuberancia polar, el segundo cambio muestra el desplazamiento de una cadena lateral con carga positiva y el tercer cambio muestra de esa misma cadena lateral desplazada como contiene una zona hidrofóbica (Figura 42 B) mientras que anteriormente había una cadena lateral polar con dos cargas positivas (Figura 42 A). El cambio a las 4' muestra la aparición de una protuberancia con carga negativa. El cambio a las 6' muestra la aparición de una protuberancia con carga positiva. El cambio 7' muestra la aparición de una zona polar donde antes había una zona hidrofóbica. El cambio a las 9' muestra la aparición de una pequeña protuberancia hidrofóbica. En la Figura 43 A y B se muestra a la subunidad ζ en la interfase entre las subunidades α y β, *P. denitrificans* en A y *S. meliloti* en B. En el círculo se muestra la subunidad ζ entre las subunidades α y β. Adicionalmente, en la interfase de ζ con α y β de *S. meliloti* (Figura 43B) en el círculo se muestran 8 cambios señalados cada uno con una flecha. El cambio a las 12' muestra la desaparición de una protuberancia hidrofóbica. Los dos cambios en el centro del círculo muestran dos zonas

hidrofóbicas donde antes había una zona polar y un pequeño orificio. El cambio a las 4' muestra la desaparición de una zona polar y la aparición de un pequeño hueco. El cambio a las 5' muestra la aparición de una protuberancia con carga positiva. El cambio entre las 5' y las 6' muestra la desaparición de una carga positiva y la aparición de una zona hidrofóbica. El cambio a las 7' muestra la aparición de una protuberancia polar. El cambio a las 8' muestra la aparición de una protuberancia con dos cargas negativas. En resumen, en la estructura modelada de las subunidades de la F_1-ATPasa de *S. meliloti* (α, β, γ y ζ) hay varios cambios que son notorios respecto a la estructura resuelta por cristalografía de las subunidades de la F_1-ATPasa de *P. denitrificans* (Figura 39-43). Los cambios estructurales nos muestran sitios en los que hubo modificaciones en diferentes residuos de la secuencia de las subunidades de *S. meliloti* y que pueden estar relacionados con la incapacidad de la subunidad ζ de *S. meliloti* para inhibir su F_1-ATPasa (Figura 37 A). Anteriormente habíamos realizado alineamientos para tratar de detectar los cambios en la secuencia que podrían estar relacionados en la incapacidad de la subunidad ζ de *S. meliloti* para inhibir su F_1-ATPasa, sin embargo, no había cambios notorios cerca de los residuos de interacción entre ζ, α, β y γ, lo que implicaba que los cambios tendrían que ser en partes de la secuencia que no eran cercanas a los residuos de interacción. En los alineamientos de las secuencias de las diferentes subunidades es notorio que existen muchos cambios, por ejemplo, en las subunidades α de *P. denitrificans* y *S. meliloti* hay una identidad del 77%. Una identidad del 77% implica que existe un 33% de residuos que están poco o nada conservados. Poder identificar entre el 33% de los residuos que están poco o nada conservados cuáles eran los residuos que podrían estar relacionados en la incapacidad de la subunidad ζ de *S. meliloti* para inhibir su F_1-ATPasa era una tarea demasiado complicada. El modelo nos ha permitido delimitar los cambios, los cuales han sido identificados en las secuencias de las diferentes subunidades para posteriormente mediante mutaciones puntuales y ensayos funcionales mostrar si son el motivo por el cual la subunidad ζ de *S. meliloti* no es capaz de inhibir la actividad de la F_1-ATPasa de *S. meliloti* (Figura 37 A) pero si mantiene su función inhibidora en la F_1-ATPasa de *P. denitrificans* (Figura 37 B).

13 La subunidad ζ no se encuentra en todas las α-proteobacterias y tampoco es exclusiva de las α-proteobacterias.

Ausencia del gen-ζ en el orden de las α-proteobacterias Rickettsiales. A la par de estudiar la función de la subunidad ζ en las bacterias Rhizobiales, decidimos estudiar si el gen-ζ se encontraba presente en todas las bacterias pertenecientes a la clase de las α-proteobacterias. Después de realizar diversas búsquedas utilizando el algoritmo DELTA-BLAST de la plataforma NCBI, encontramos que el gen-ζ se encuentra ausente en todo el orden Rickettsiales (Figura 44). Aunque hay dos hits en el DELTA-BLAST realizado con la secuencia de la subunidad ζ de *P. denitrificans* sobre el orden de las Rickettsiales, uno con identificador OUX40697.1 pertenece a una proteína hipotética CBE29_01460 de 212 a.a. Además, el hit con el identificador OUX40697.1 tiene un valor de E de 4.2 (Figura 44 C). Este valor de E positivo indica que la probabilidad de que el resultado sea debido al azar es alta, por ello se descarta la posibilidad de que dicha proteína tenga homología con la subunidad ζ. El hit con el identificador WP_044577965.1 que tiene un valor de E de $1e^{-10}$ proviene de una bacteria denominada *Rickettsiales bacterium* Ac37b, la cual existe la posibilidad de que se encuentre clasificada en el orden de las Rickettsiales de manera inadecuada (Figura 44 C).

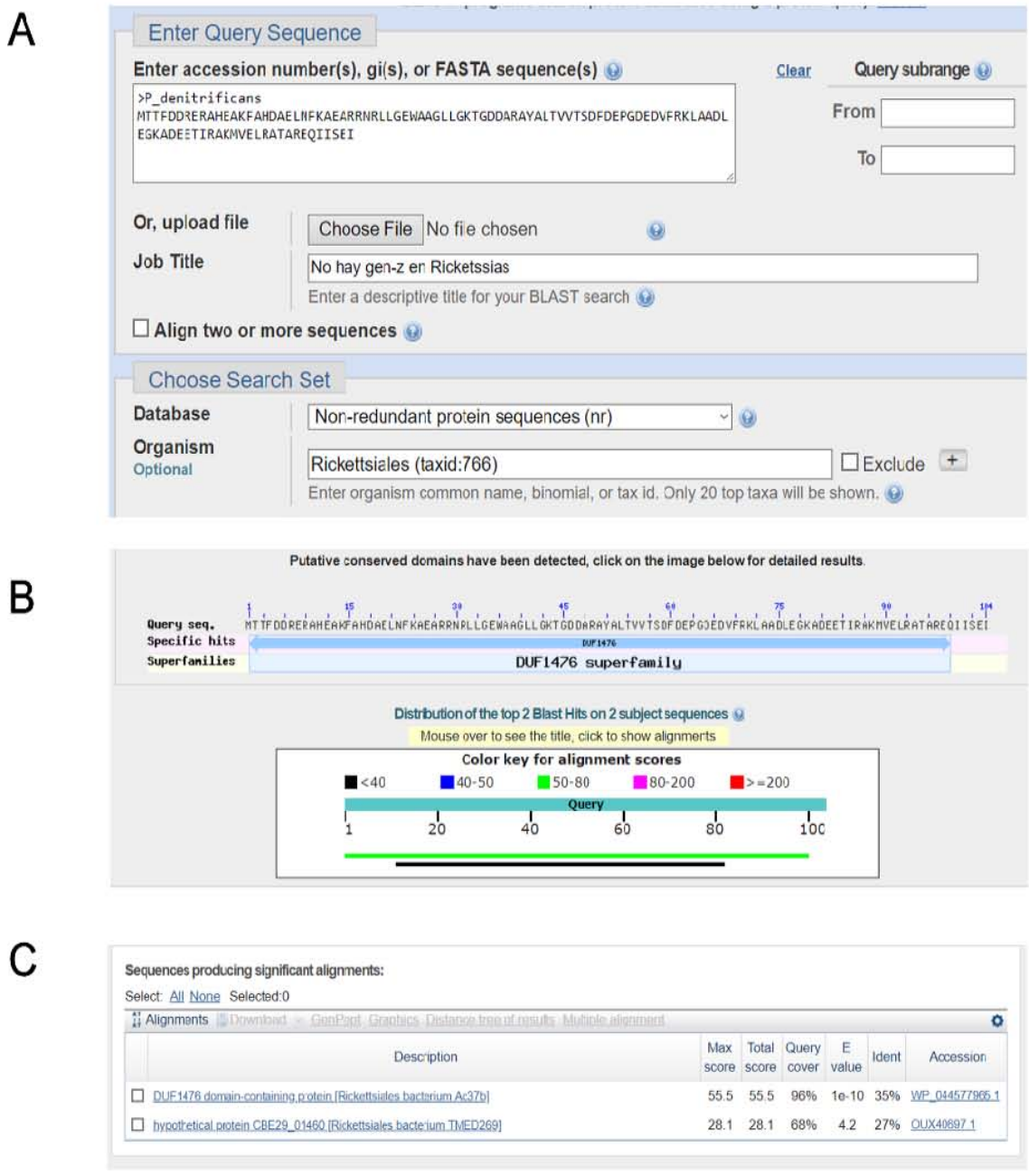

Figura 44. Ausencia del gen-ζ en el genoma del orden de las Rickettsiales de las α-proteobacterias. Utilizando la secuencia de aminoácidos de la subunidad ζ de *P. denitrificans* cepa 1222 se buscó en el genoma del orden de las Rickettsiales la presencia de del gen-ζ. Para detectar el gen-ζ en el genoma de las Rickettsiales se realizó un DELTA-BLAST utilizando el servidor NCBI. A) Captura de pantalla donde se muestra la secuencia de la subunidad ζ de *P. denitrificans*

como secuencia problema utilizada (query sequence) y los parámetros utilizados para la búsqueda del DELTA-BLAST. B) Captura de pantalla mostrando el resumen gráfico de los resultados de la búsqueda. En este resumen gráfico hubo 2 secuencias encontradas (hits) que debido a la cobertura probablemente no son secuencias homólogas de la subunidad ζ de *P. denitrificans*. C) Captura de pantalla de las dos secuencias identificadas (hits), donde se muestra el valor de E y los datos de acceso a cada una de estas secuencias.

El gen-ζ no es exclusivo de la clase de las α-proteobacterias. Anteriormente no se había detectado el gen-ζ en otras bacterias no pertenecientes a la clase de las α-proteobacterias. Sin embargo, recientemente identificamos que el gen si se encuentra en otras bacterias no pertenecientes a esta clase de bacterias (Figura 45). Detectamos mediante el algoritmo DELTA-BLAST utilizando la secuencia de a.a. de la subunidad ζ de *P. denitrificans* la presencia de 45 secuencias del gen-ζ en organismos no pertenecientes a la clase de las α-proteobacterias. Los 45 hits obtenidos de la búsqueda incluyen a *Kocuria rhizophila*, *Pseudomonas stutzeri*, *Pseudomonas bauzanensis*, *Arthrobacter sp*. TPD3018, *Acinetobacter baumanii*, entre otros (Figura 45 B), éstos 45 hits son menos que los >500 hits obtenidos del DELTA-BLAST utilizando la secuencia de a.a. de la subunidad ζ de *P. denitrificans* en organismos pertenecientes a la clase de las α-proteobacterias (Figura 29 B). Las bacterias *Kouria rhizophila* y *Arthrobacter* sp., pertenecen a la división Actinobacteria y dicha división en cuestiones de genómica se encuentra poco estudiada, en cambio los genomas de *Pseudomonas* y *Acinetobacter baumanii* si han sido extensamente estudiados y se ha encontrado que llevan a cabo transferencia horizontal de material genético con otras bacterias, por ello y debido a que los resultados obtenidos del DELTA-BLAST indican que el gen-ζ se encuentra con mayor frecuencia en las α-proteobacterias, ésto es un claro indicio de que el gen-ζ se originó en alguna bacteria ancestral perteneciente a las α-proteobacterias y bacterias las bacterias agenas a dicha clase pudieron haber obtenido el gen-ζ a partir de transferencia horizontal.

A

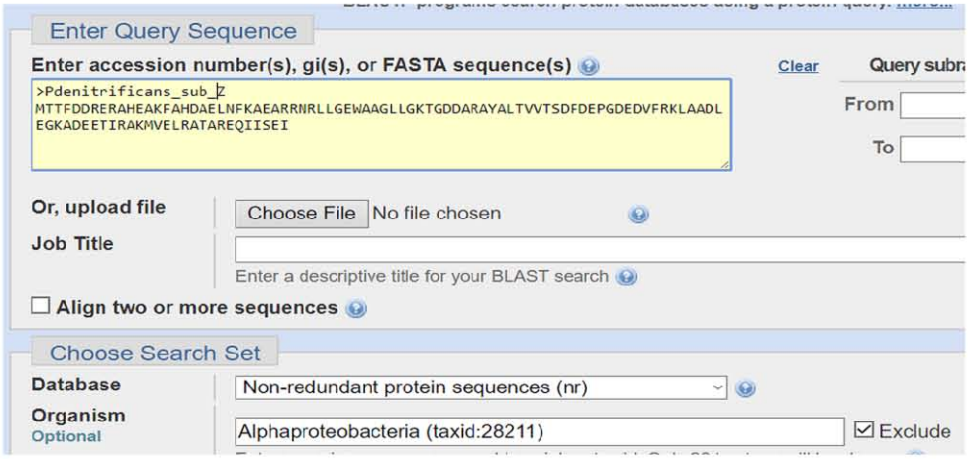

B

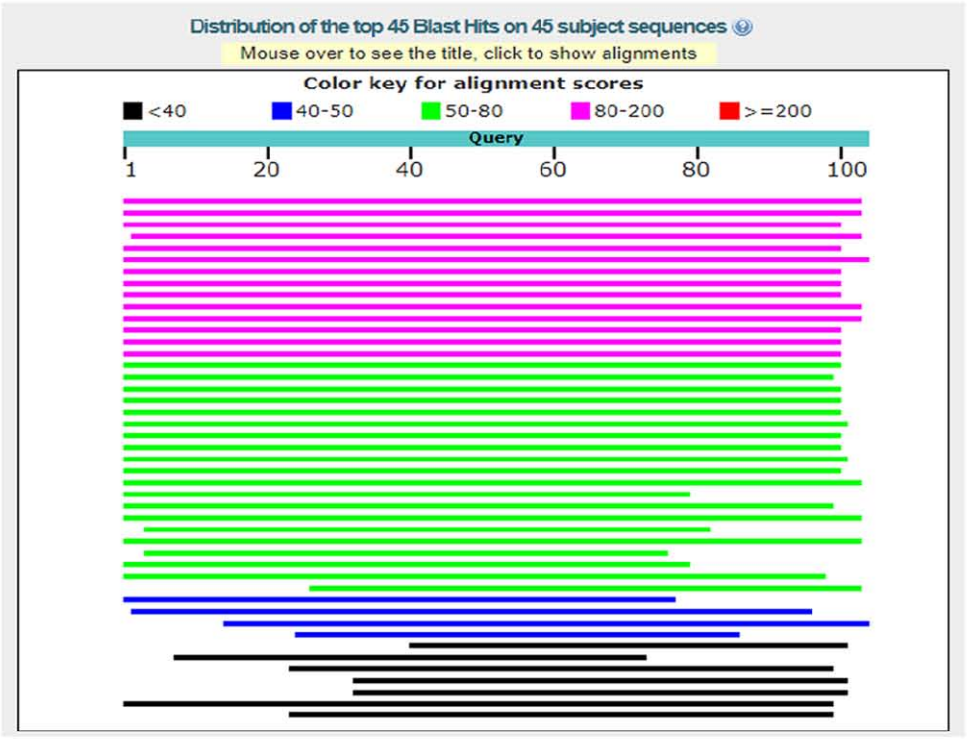

C

Description	Max score	Total score	Query cover	E value	Ident	Accession
DUF1476 domain-containing protein [Kocuria rhizophila]	134	134	99%	5e-39	80%	PZP19529.1
hypothetical protein ACD_54C00369G0002 [uncultured bacterium]	107	107	99%	5e-28	53%	EKD61138.1
hypothetical protein A4S14_10620 [Proteobacteria bacterium SG_bin9]	96.3	96.3	96%	1e-23	56%	OQW56214.1
aldolase [Proteobacteria bacterium]	94.7	94.7	98%	4e-23	56%	PIE18350.1
DUF1476 domain-containing protein [Proteobacteria bacterium]	90.1	90.1	96%	2e-21	55%	PZN86407.1
DUF1476 domain-containing protein [Nostoc sp. 2335mG]	89.0	89.0	100%	9e-21	51%	WP_110156870.1
hypothetical protein A4S15_14410 [Proteobacteria bacterium SG_bin8]	87.0	87.0	96%	5e-20	54%	OQW54296.1
DUF1476 domain-containing protein [Proteobacteria bacterium]	85.9	85.9	96%	1e-19	56%	PZN42048.1
hypothetical protein BVN31_10030 [Proteobacteria bacterium ST_bin15]	85.9	85.9	96%	1e-19	53%	OQW81822.1
B328 [uncultured bacterium]	84.7	84.7	99%	3e-19	52%	ART35876.1
hypothetical protein BMS3Bbin10_80524 [bacterium BMS3Bbin10]	84.7	84.7	99%	4e-19	54%	GBE42463.1
DUF1476 domain-containing protein [bacterium YEK0313]	84.0	84.0	96%	6e-19	57%	WP_038305964.1
DUF1476 domain-containing protein [Pseudomonas stutzeri]	83.6	83.6	96%	9e-19	55%	PZR91927.1
DUF1476 domain-containing protein [Proteobacteria bacterium]	82.0	82.0	96%	4e-18	53%	PZN14037.1
hypothetical protein CF98_11050 [Pseudomonas bauzanensis]	79.7	79.7	90%	3e-17	54%	EZQ15354.1
hypothetical protein CBD66_06120 [Flavobacteriaceae bacterium TMED206]	77.8	77.8	95%	1e-16	47%	OUW62829.1
aldolase [Proteobacteria bacterium ST_bin13]	76.6	76.6	96%	6e-16	48%	OQW73492.1
hypothetical protein A4S17_12270 [Proteobacteria bacterium HN_bin10]	76.3	76.3	96%	7e-16	50%	OQW58032.1
conserved hypothetical protein [Homo sapiens]	76.3	76.3	96%	8e-16	51%	SJM31072.1
DUF1476 domain-containing protein [Arthrobacter sp. TPD3018]	75.9	75.9	97%	9e-16	47%	PVE61830.1

Figura 45. El gen-ζ no es exclusivo de la clase de las α-proteobacterias. Utilizando la secuencia de aminoácidos de la subunidad ζ de *P. denitrificans* cepa 1222 se buscó la presencia de del gen-ζ en el genoma de bacterias no pertenecientes a la clase de las α-proteobacterias. Para detectar el gen-ζ en el genoma de bacterias no pertenecientes a la clase de las α-proteobacterias se realizó un DELTA-BLAST utilizando el servidor NCBI. A) Captura de pantalla donde se muestra la secuencia de la subunidad ζ de *P. denitrificans* como secuencia problema utilizada (query sequence) y los parámetros utilizados para la búsqueda del DELTA-BLAST. B) Captura de pantalla mostrando el resumen gráfico de los resultados de la búsqueda. En este resumen gráfico hubo 45 secuencias encontradas (hits). C) Captura de pantalla de las dos secuencias identificadas (hits), donde se muestra el valor de E y los datos de acceso a cada una de estas secuencias.

14 Comparación de la actividad específica de hidrólisis de ATP por la F_1-ATPasa de diferentes α-proteobacterias.

Purificación de la fracción F_1 de *Wolbachia pipientis* perteneciente al orden de las Rickettsiales. Una vez que identificamos que el gen-ζ no se encuentra en el orden de las Rickettsiales, aprovechamos una colaboración con el Dr. Salvador Uribe del Instituto de Fisiología Celular, quien amablemente nos proporcionó células de una α-proteobacteria perteneciente al orden de las Rickettsiales: *Wolbachia pipientis* (*W. pipientis*). Las células de *W. pipientis* se cultivaron de manera intracelular en eritrocitos de carnero, aunque ahora cultivan las bacterias dentro de levaduras (110). Logramos purificar la fracción F_1 (Figura 46 A). Adicionalmente, hicimos un WB y confirmandos la ausencia del gen-ζ en la F_1 de *W. pipientis*, (Figura 46 A, B y 44).

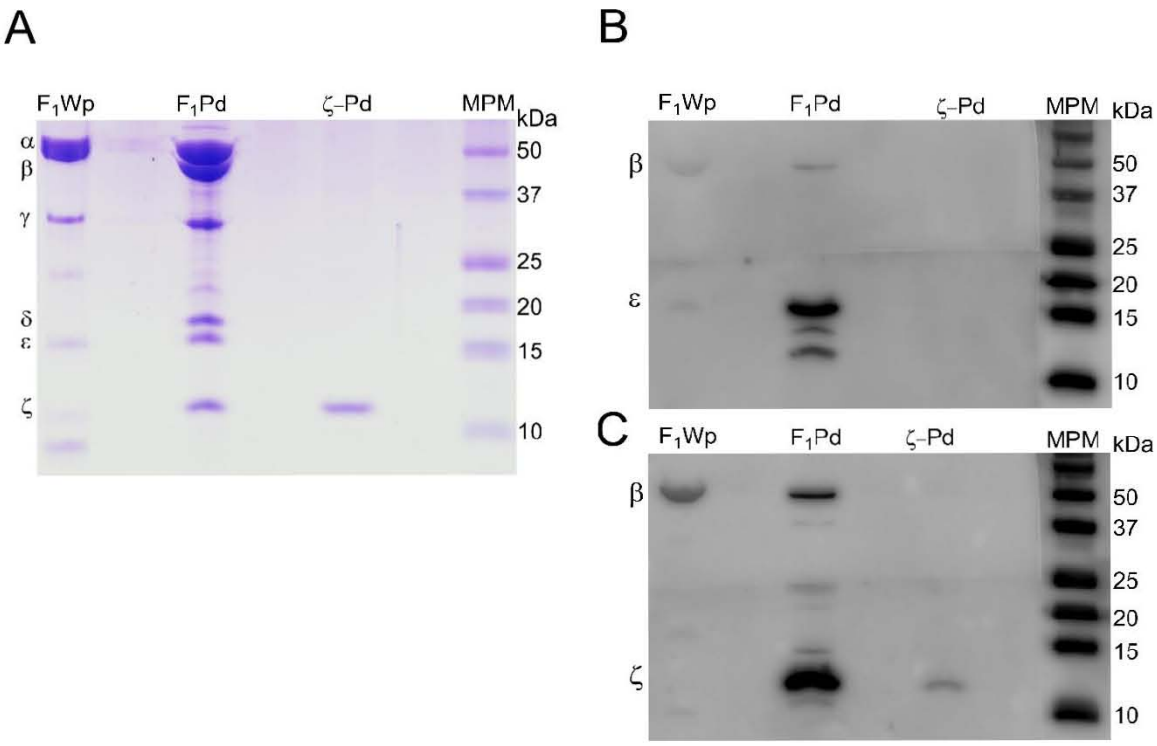

Figura 46. Confirmación de la ausencia de la subunidad ζ en la F_1 de *W. pipientis*. Purificamos la fracción F_1 de *Wolbachia pipientis* la cual perteneciente al orden de las Rickettsiales. A) SDS-PAGE teñido con coomassie de la purificación de F_1 de W. pipientis (F_1Wp). B) WB anti-ε del complejo F_1 de Wp. C) WB anti-ζ del complejo F_1 de Wp. La membrana del WB anti-ζ se reveló primero y después se le removieron los anticuerpos (stripping) y se le expuso con el anticuerpo anti-ε y se volvió a revelar.

Comparación de la actividad específica de hidrólisis de ATP por la F_1-ATPasa de todas las α-proteobacterias que purificamos. Durante este trabajo logramos purificar la fracción F_1 de varias α-proteobacterias. Entre ellas purificamos la F_1 de 3 bacterias del orden de las Rhodobacterales, las cuales tienen un crecimiento en estado de vida libre: *P. denitrificans* WT (Figura 24), *P. denitrificans* Δζ (Figura 24) y *R. capsulatus* (Figura 32). También purificamos la fracción F_1 de 2 bacterias del orden de las Rhizobiales, las cuales tienen un crecimiento en estado de vida libre y en estado de vida intracelular simbiótico: *R. etli* (Figura 34) y *S. meliloti* (Figura 34). De la misma manera, semi-purificamos la fracción F_1 otra bacteria perteneciente al orden de las Rhizobiales de *M. nodulans* (Figura 34). Por último, purificamos la fracción F_1 de una bacteria perteneciente al orden de las Rickettsiales, las cuales

tienen un crecimiento en estado de vida intracelular parásita: *W. pipientis* (Figura 46 A). Inmediatamente después de purificar o semi-purificar la F_1 de cada una de estas α-proteobacterias les medimos la actividad específica de hidrólisis de ATP (Figura 47). Las actividades específicas de F_1-ATPasa obtenidas no tuvieron una clara tendencia entre los tres grupos de bacterias: vida libre, intracelulares facultativas (simbióticas) e intracelulares obligadas (intracelulares parásitas) (Figura 47 B). Nosotros esperábamos que al tener asociada una menor cantidad de subunidad ζ en la F_1 purificada de las Rhizobiales y posteriormente al darnos cuenta de que su subunidad ζ no tiene capacidad inhibidora, estas tendrían una mayor actividad de hidrólisis de ATP que las de vida libre. De la misma manera, esperábamos que la F_1 de *W. pipientis* intracelular obligada que no tiene el gen-ζ en su genoma que tuviera una mayor actividad de hidrólisis de ATP que todas las demás bacterias. Un motivo por el cual no observamos el patrón esperado en las actividades de F_1-ATPasa se debe a que, en el caso de la F_1 de *M. nodulans* no se encontraba totalmente purificada y esperamos que una vez purificada totalmente su actividad sea similar al de las otras dos Rhizobiales. En el caso de la F_1 de *W. pipientis*, sólo logramos purificar su F_1 una vez y nuestros datos preliminares muestran que la enzima es inestable, debido a que se podría estar disociando y por ello tener una actividad F_1-ATPasa tan baja. En el caso de la F_1 de *R. capsulatus*, la alta actividad que alcanzó la enzima se debe a que se purificó de manera continua sin interrupciones entre las cromatografías y se le determinó la actividad inmediatemente antes de congelarla o almacenarla, por ello consideramos que es necesario purificar más F_1 ATPasas de otras α-proteobacterias tanto fotosintéticas como de otras de vida libre y de más Rhizobiales para poder realizar un estudio detallado y determinar los patrones de actividad en las α-proteobactrias de vida libre, intracelulares facultativas (simbióticas) y en las intracelulares obligadas (Rickettsiales).

A

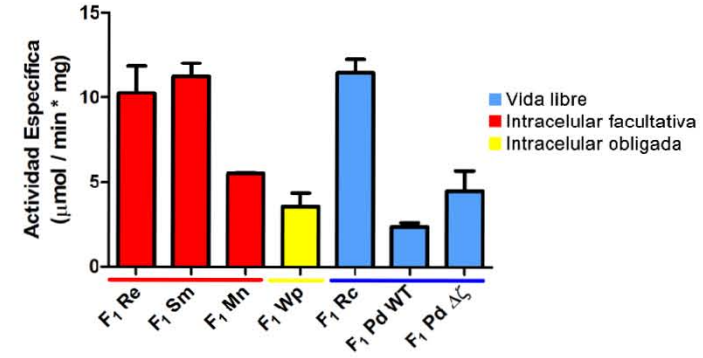

B

α-proteobacteria	Actividad F1-ATPasa AE*	DE**
R. etli (Re)	10.3	1.57
S. meliloti (Sm)	11.24	0.79
M. nodulans (Mn)	5.53	0.03
W. pipientis (Wp)	3.58	0.78
R. capsulatus (Rc)	11.47	0.82
P. denitrificans WT (PdWT)	2.37	0.23
P. denitrificans Δζ (PdΔζ)	4.48	1.21

*AE = Actividad Específica (μmol/min*mg pt)
**DE = Desviación Estándar (μmol/min*mg pt)

Figura 47. Comparación de la actividad específica de hidrólisis de ATP por la F_1-ATPasa de diferentes α-proteobacterias. A) Gráfica comparativa de las actividades específicas (μmol/min*mg pt) de diferentes α-proteobacterias. En las barras se muestra el promedio de la actividad específica (AE) y en las barras se muestra la desviación estándar (DE). B) Tabla comparativa de las actividades específicas (μmol/min*mg pt) de diferentes α-proteobacterias. Las actividades de hidrólisis de ATP (F1-ATPasa) se midieron en presencia del activador LDAO al 0.15%.

En resumen, en este se gundo proyecto se confirmó la presencia de ζ en Rhizobiales y α-proteobacterias fotosintéticas, y la función inhibitoria de ζ se conserva en las segundas, pero se pierde en las primeras. Además, se confirmó la ausencia de ζ en Rikettsiales como Wolbachia, por medios bioinformáticos y por Western-Blot. Esto nos lleva a proponer que en bacterias de vida libre la subunidad ζ mantiene una fuerte función inhibitoria, mientras que en simbióticas la función inhibitoria se ha perdido parcial o totalmente y en las bacterias parásitas obligadas se ha perdido el gen y la proteína ζ dado que en éstas por ser parásitas no necesitan ζ para favorecer la síntesis del ATP dado que lo obtienen preferentemente del hospedero.

15 Referencias

1. Knowles, J. R. (1980) Enzyme-catalyzed phosphoryl transfer reactions. *Annu. Rev. Biochem.* **1980**, 877-919
2. Hanson, R. W. (1989) The Role of ATP in Metabolism. *Biochemical Education* **17**, 86-92
3. Kamerlin, S. C. L., Sharma, P. K., Prasad, R. B., and Warshel, A. (2013) Why nature really chose phosphate. *Q Rev Biophys.* **46**, 1-132
4. Cori, C. F. (1983) Embden and the glycolytic pathway. *Trends Biochem Sci.* **8**, 257-259
5. Fothergill-Gilmore, L. A., and Michels, P. A. (1993) Evolution of glycolysis. *Prog Biophys Mol Biol.* **59**, 105-235
6. Bonora, M., Patergnani, S., Rimessi, A., De Marchi, E., Suski, J. M., Bononi, A., Giorgi, C., Marchi, S., Missiroli, S., Poletti, F., Wieckowski, M. R., and Pinton, P. (2012) ATP synthesis and storage. . *Purinergic Signal.* **8**, 343-357
7. Entner, N., and Doudoroff, M. (1952) Glucose and gluconic acid oxidation of Pseudomonas saccharophila. *J Biol Chem.* **196**, 853-862
8. Conway, T. (1992) The Entner-Doudoroff pathway: history, physiology and molecular biology. *FEMS Microbiol Rev.* **103**, 1-27
9. Krebs, H. A., and Johnson, W. A. (1980) The role of citric acid in intermediate metabolism in animal tissues. *FEBS Lett.* **117**, K2-K10
10. Akram, M. (2014) Citric Acid Cycle and Role of its Intermediates in Metabolism. *Cell Biochem Biophys.* **68**, 475-478
11. Boyer, P. D., Chance, B., Ernster, L., Mitchell, P., Racker, E., and Slater, E. C. (1977) Oxidative Phosphorylation and Photophosphorylation. *Annu Rev Biochem.* **46**, 955-1026
12. Boyer, P. D. (1997) The ATP synthase--a splendid molecular machine. *Annu Rev Biochem.* **66**, 717-749
13. Noji, H., and Yoshida, M. (2001) The Rotary Machine in the Cell, ATP Synthase. *J Biol Chem.* **276**, 1665-1668
14. von Ballmoos, C., Wiedenmann, A., and Dimroth, P. (2009) Essentials for ATP synthesis by F1F0 ATP synthases. *Annu Rev Biochem.* **78**, 649-672
15. Walker, J. E. (2013) The ATP synthase: the understood, the uncertain and the unknown. *Biochem Soc Trans.* **41**, 1-16
16. Mitchell, P. (1961) Coupling of Phosphorylation to Electron and Hydrogen Transfer by a Chemi-Osmotic type of Mechanism. *Nature.* **191**, 144-148
17. Fillingame, R. H., and Steed, P. R. (2014) Half channels mediating H+ transport and the mechanism of gating in the Fo sector of Escherichia coli F1Fo ATP synthase. *Biochim Biophys Acta.* **1837**, 1063-1068
18. Muench, S. P., Trinick, J., and Harrison, M. A. (2011) Structural divergence of the rotary ATPases. *Q Rev Biophys.* **44**, 311-356
19. Müller, V., and Grüber, G. (2003) ATP synthases: structure, function and evolution of unique energy converters. *Cell Mol Life Sci.* **60**, 474-494

20. Koumandow, V. L., and Kossida, S. (2014) Evolution of the F0F1 ATP Synthase Complex in Light of the Patchy Distribution of Different Bioenergetic Pathways across Prokaryotes. *PLoS Comput Biol.* **10**, e1003821
21. Mulkidjanian, A., Makarova, K., Galperin, M., and Koonin, E. (2007) Inventing the dynamo machine: the evolution of the F-type and V-type ATPases. *Nature reviews. Microbiology* **5**, 892-899
22. Abrahams, J. P., Leslie, A. G. W., Lutter, R., and Walker, J. E. (1994) Structure at 2.8 Â resolution of F1-ATPase from bovine heart mitochondria. *Nature.* **370**, 621-628
23. García-Trejo, J. J., and Morales-Ríos, E. (2008) Regulation of the F1F0-ATP Synthase Rotary Nanomotor in its Monomeric-Bacterial and Dimeric-Mitochondrial Forms. *J Biol Phys.* **34**, 197-212
24. Sobti, M., Smits, C., Wong, A. S. W., Ishmukhametov, R., Stock, D., Sandin, S., and Stewart, A. G. (2016) Cryo-EM structures of the autoinhibited *E. coli* ATP synthase in three rotational states. *Elife.* **5**, e21598
25. Groth, G., and Pohl, E. (2001) The Structure of the Chloroplast F1-ATPase at 3.2 Å Resolution. *J Biol Chem.* **276**, 1345-1352
26. Shirakihara, Y., Shiratori, A., Tanikawa, H., Nakasako, M., Yoshida, M., and Suzuki, T. (2015) Structure of a thermophilic F1-ATPase inhibited by an ε-subunit: deeper insight into the ε-inhibition mechanism. *FEBS J.* **282**, 2895-2913
27. Morales-Rios, E., de la Rosa-Morales, F., Mendoza-Hernandez, G., Rodriguez-Zavala, J. S., Celis, H., Zarco-Zavala, M., and Garcia-Trejo, J. J. (2010) A novel 11-kDa inhibitory subunit in the F_1F_0 ATP synthase of Paracoccus denitrificans and related α-proteobacteria. *FASEB journal : official publication of the Federation of American Societies for Experimental Biology* **24**, 599-608
28. Zarco-Zavala, M., Morales-Ríos, E., Mendoza-Hernández, G., Ramírez-Silva, L., Pérez-Hernández, G., and J., G.-T. J. (2014) The ζ subunit of the F1FO-ATP synthase of α-proteobacteria controls rotation of the nanomotor with a different structure. *FASEB journal : official publication of the Federation of American Societies for Experimental Biology* **28**, 2146-2157
29. Sánchez-Vásquez, L., and González-Halphen, D. (2017) Topología y función de las subunidades intrínsecas de la membrana de las F1FO-ATP sintasa mitocondriales. *TIP Revista Especializada en Ciencias Químico-Biológicas* **20**, 29-47
30. Mendoza-Hoffmann, F., Pérez-Oseguera, Á., Cevallos, M. Á., Zarco-Zavala, M., Ortega, R., Peña-Segura, C., Espinoza-Simon, E., Uribe-Carvajal, S., and García-Trejo, J. J. (2018) The Biological Role of the ζ Subunit as Unidirectional Inhibitor of the F1FO-ATPase of Paracoccus denitrificans. *Cell Reports* **22**, 1067-1078
31. DeLano, W. L. (2002) Pymol: An open-source molecular graphics tool. CCP4 Newsletter On Protein Crystallography. *CCP4 Newsletter On Protein Crystallography* **40**, 82-92
32. Pettersen, E. F., Goddard, T. D., Huang, C. C., Couch, G. S., Greenblatt, D. M., Meng, E. C., and Ferrin, T. E. (2004) UCSF Chimera—A visualization system for

exploratory research and analysis. *Journal of Computational Chemistry* **25**, 1605-1612
33. Nicholls, D., and Ferguson, S. J. (1992) Bioenergetics 2. 255
34. Elston, T., Wang, H., and Oster, G. (1998) Energy transduction in ATP synthase. *Nature.* **391**, 510-513
35. Fillingame, R. H., Peters, L. K., White, L. K., Mosher, M. E., and Paule, C. R. (1984) Mutations altering aspartyl-61 of the omega subunit (uncE protein) of Escherichia coli H+ -ATPase differ in effect on coupled ATP hydrolysis. *J Bacteriol.* **158**, 1078-1083
36. Symersky, J., Pagadala, V., Osowski, D., Krah, A., Meier, T., Faraldo-Gómez, J. D., and Mueller, D. M. (2012) Structure of the c(10) ring of the yeast mitochondrial ATP synthase in the open conformation. *Nat Struct Mol Biol.* **19**, 485-491
37. Lightowlers, R. N., Howitt, S. M., Hatch, L., Gibson, F., and Cox, G. B. (1987) The proton pore in the Escherichia coli F0F1-ATPase: a requirement for arginine at position 210 of the a-subunit. *Biochim Biophys Acta.* **894**, 399-406
38. Cain, B. D., and Simoni, R. D. (1989) Proton translocation by the F1F0ATPase of Escherichia coli. Mutagenic analysis of the a subunit. *J Biol Chem.* **264**, 3292-3300
39. Pogoryelov, D., Krah, A., Langer, J. D., Yildiz, Ö., Faraldo-Gómez, J. D., and Meier, T. (2010) Microscopic rotary mechanism of ion translocation in the Fo complex of ATP synthases. *Nat Chem Biol.* **6**, 891-899
40. Stock, D., Leslie, A. G. W., and Walker, J. E. (1999) Molecular Architecture of the Rotary Motor in ATP synthase. *Science.* **286**, 1700-1705
41. Rondelez, Y., Tresset, G., Nakashima, T., Kato-Yamada, Y., Fujita, H., Takeuchi, S., and Noji, H. (2005) Highly coupled ATP synthesis by F1-ATPase single molecules. *Nature.* **433**, 773-777
42. Klionsky, D. J., Brusilow, W. S. A., and Simoni, R. D. (1984) In vivo evidence for the role of the epsilon subunit as an inhibitor of the proton-translocating ATPase of Escherichia coli. *J Bacteriol.* **160**, 1055-1060
43. Richter, M. L., Patrie, W. J., and McCarty, R. E. (1984) Preparation of the epsilon subunit and epsilon subunit-deficient chloroplast coupling factor 1 in reconstitutively active forms. *The Journal of biological chemistry* **259**, 7371-7373
44. Waterhouse, A., Bertoni, M., Bienert, S., Studer, G., Tauriello, G., Gumienny, R., Heer, F. T., de Beer, T. A. P., Rempfer, C., Bordoli, L., Lepore, R., and Schwede, T. (2018) SWISS-MODEL: homology modelling of protein structures and complexes. *Nucleic Acids Res.* **Epub ahead of print**
45. Cross, R. L. (1981) The mechanism and regulation of ATP synthesis by F1-ATPases. *Annu Rev Biochem.* **50**, 681-714
46. Stewart, A. G., Sobti, M., Harvey, R. P., and Stock, D. (2013) Models, machine elements and technical specifications. *Bioarchitecture.* **3**, 2-12
47. Boyer, P. D. (2002) Catalytic site occupancy during ATP synthase catalysis. *FEBS Lett.* **512**, 29-32
48. Oster, G., and Wang, H. (2000) Reverse engineering a protein: the mechanochemistry of ATP synthase. *Biochim Biophys Acta.* **1458**, 482-510

49. Walker, J. E., and Dickson, V. K. (2006) The peripheral stalk of the mitochondrial ATP synthase. *Biochim Biophys Acta.* **1757**, 286-296
50. Junge, W., Sielaff, H., and Engelbrecht, S. (2009) Torque generation and elastic power transmission in the rotary FOF1-ATPase. *Nature.* **459**, 364-370
51. Chandel, N. S., and Schumacker, P. T. (1999) Cells depleted of mitochondrial DNA (rho0) yield insight into physiological mechanisms. *FEBS Lett.* **454**, 173-176
52. García-Trejo, J. J., Zarco-Zavala, M., and Morales-Ríos, E. (2012) Estructura y Mecanismo de la nueva subunidad inhibitoria ζ del nanomotor F1F0 ATP sintasa de las α-proteobacterias en Paracoccus denitrificans. *Mensaje Bioquímico* **XXXVI**, 106-126
53. Smith, J. B., and Sternweis, P. C. (1977) Purification of membrane attachment and inhibitory subunits of the proton translocating adenosine triphosphatase from *Escherichia coli*. *Biochemistry* **16**, 306-311
54. Cingolani, G., and Duncan, T. D. (2011) Structure of the ATP synthase catalytic complex F(1) from Escherichia coli in an autoinhibited conformation. *Nat Struct Mol Biol.* **18**, 701-707
55. Tsunoda, S. P., Rodgers, A. J. W., Aggeler, R., Wilce, M. C. J., Yoshida, M., and Capaldi, R. A. (2001) Large conformational changes of the ε subunit in the bacterial F1F0 ATP synthase provide a ratchet action to regulate this rotary motor enzyme. *Proc Natl Acad Sci U S A.* **98**, 6560-6564
56. Dautant, A., Velours, J., and Giraud, M.-F. (2010) Crystal Structure of the Mg·ADP-inhibited State of the Yeast F1c10-ATP Synthase. *J Biol Chem.* **285**, 29502-29510
57. Pullman, M. E., and Monroy, G. C. (1963) A Naturally Ocurring Inhibitor of Mitochondrial Adenosine Triphosphatase. *J Biol Chem.* **238**, 3762-3769
58. García, J., Morales-Ríos, E., Cortés-Hernandez, P., and Rodríguez-Zavala, J. (2006) The inhibitor protein (IF1) promotes dimerization of the mitochondrial F1F0-ATP synthase. *Biochemistry* **45**, 12695-12703
59. Paumard, P., Vaillier, J., Coulary, B., Schaeffer, J., Soubannier, V., Mueller, D. M., Brèthes, D., di Rago, J.-P., and Velours, J. (2002) The ATP synthase is involved in generating mitochondrial cristae morphology. *EMBO J.* **21**, 221-230
60. Minauro-Sanmiguel, F., Wilkens, S., and García, J. J. (2005) Structure of dimeric mitochondrial ATP synthase: Novel F₀ bridging features and the structural basis of mitochondrial cristae biogenesis. *Proceedings of the National Academy of Sciences of the United States of America* **102**, 12356
61. Faccenda, D., and Campanella, M. (2012) Molecular Regulation of the Mitochondrial F(1)F(o)-ATPsynthase: Physiological and Pathological Significance of the Inhibitory Factor 1 (IF(1)). *Int J Cell Biol.* **2012**, 367934
62. Bason, J. V., Montgomery, M. G., Leslie, A. G., and Walker, J. E. (2014) Pathway of binding of the intrinsically disordered mitochondrial inhibitor protein to F1-ATPase. *Proc Natl Acad Sci U S A.* **111**, 11305-11310
63. Minauro, F., Bravo, C., and García-Trejo, J. J. (2002) Cross-Linking of the Endogenous Inhibitor Protein (IF 1) with Rotor (γ,ε) and Stator (α) Subunits of

the Mitochondrial ATP Synthase. *Journal of Bioenergetics and Biomembranes* **34**, 433-443
64. Cabezon, E., Runswick, M., Leslie, A. G. W., and Walker, J. (2001) The stucture of bovine IF1, the regulatory subunit of mitochondrial F-ATPase. *EMBO J.* **20**, 6990-6996
65. Bason, J. V., Montgomery, M. G., Leslie, A. G. W., and Walker, J. E. (2014) Pathway of binding of the intrinsically disordered mitochondrial inhibitor protein to F1-ATPase. *Proc Natl Acad Sci U S A.* **111**, 11305-11310
66. Zarco-Zavala, M., morales-Ríos, E., Serrano-Navarro, P., Wüthrich, K., Mendoza-Hernández, G., Ramírez-Silva, L., and García-Trejo, J. J. (2012) The ζ subunit of the α-proteobacterial F1FO-ATP synthase in Paracoccus denitrificans: A novel control mechanism of the central rotor. *Biochim Biophys Acta.* **1817**, S27-S28
67. Serrano, P., Geralt, M., Mohanty, B., and Wüthrich, K. (2014) NMR Structures of α-Proteobacterial ATPase-Regulating ζ-Subunits. *Journal of molecular biology* **426**, 2547-2553
68. García-Trejo, J. J., Zarco-Zavala, M., Mendoza-Hoffmann, F., Hernández-Luna, E., Ortega, R., and Mendoza-Hernández, G. (2016) The Inhibitory Mechanism of the ζ Subunit of the F1FO-ATPase Nanomotor of Paracoccus denitrificans and Related α-Proteobacteria. *J Biol Chem.* **291**, 538-546
69. Morales-Rios, E., Montgomery, M. G., Leslie, A. G. W., and Walker, J. E. (2015) Structure of ATP synthase from Paracoccus denitrificans determined by X-ray crystallography at 4.0 Å resolution. *Proc Natl Acad Sci U S A.* **112**, 13231-13236
70. Zarco-Zavala, M., Mendoza-Hoffmann, F., and García-Trejo, J. J. (2018) Unidirectional regulation of the F1FO-ATP synthase nanomotor by the ζ pawl-ratchet inhibitor protein of Paracoccus denitrificans and related α-proteobacteria. *Biochimica et Biophysica Acta (BBA) - Bioenergetics* **1859**, 762-774
71. Mendoza-Hoffmann, F., Zarco-Zavala, M., Ortega, R., and García-Trejo, J. J. (2018) Control of rotation of the F1FO-ATP synthase nanomotor by an inhibitory α-helix from unfolded ε or intrinsically disordered ζ and IF1 proteins. *J Bioenerg Biomembr.* **[Epub ahead of print]**
72. Gahura, O., Panicucci, B., Váchová, H., Walker, J. E., and Zíková, A. (2018) Inhibition of F1-ATPase from Trypanosoma brucei by its regulatory protein inhibitor TbIF1. *FEBS J.* **[Epub ahead of print]**
73. Taniguchi, N., Suzuki, T., Berney, M., Yoshida, M., and Cook, G. M. (2011) The regulatory C-terminal domain of subunit ε of F_0F_1 ATP synthase is dispensable for growth and survival of Escherichia coli. *Journa of Bacteriology* **193**, 2046-2052
74. Shah, N. B., and Duncan, T. M. (2015) Aerobic Growth of Escherichia coli Is Reduced, and ATP Synthesis Is Selectively Inhibited when Five C-terminal Residues Are Deleted from the ϵ Subunit of ATP Synthase. *J Biol Chem.* **290**, 21032-21041
75. Federation, W. H. (2017) The World's most common cause of death. . *Cardiovascular Diseases Global Facts and Figures*
76. Maierean, S., Serban, M.-C., Rizzo, M., Lippi, G., Sahebkar, A., and Banach, M. (2017) The potential role of mitochondrial ATP synthase inhibitory factor 1

(IF1) in coronary heart disease: a literature review. *Lipids in Health and Disease* **16**, 1-7
77. Vuorinen, K., Ylitalo, K., K., P., Raatikainen, P., Ala-Rami, A., and Hassinen, I. E. (1995) Mechanisms of ischemic preconditioning in rat myocardium. Roles of adenosine, cellular energy state, and mitochondrial F1F0-ATPase. . *Circulation* **91**, 2810-2818
78. Rouslin, W., and Broge, C. W. (1996) IF1 function in situ in uncoupler-challenged ischemic rabbit, rat, and pigeon hearts. *Journal of Biological Chemistry* **271**, 23638-23641
79. Hassinen, I. E., Vuorinen, K. H., Ylitalo, K., and Ala-Rami, A. (1998) Role of cellular energetics in ischemia-reperfusion and ischemic preconditioning of myocardium. *Bioenergetics of the Cell: Quantitative Aspects* **184**, 393-400
80. Yang, K., Long, Q., Saja, K., Huang, F., Pogwizd, S. M., Zhou, L., Yoshida, M., and Yang, Q. (2017) Knockout of the ATPase inhibitory factor 1 protects the heart from pressure overload-induced cardiac hypertrophy. *Sci Rep.* **7**, 10501
81. Campanella, M., Casswell, E., Chong, S., Farah, Z., Wieckowski, M. R., Abramov, A. Y., Tinker, A., and Duchen, M. R. (2008) Regulation of mitochondrial structure and function by the F1Fo-ATPase inhibitor protein, IF1. *Cell Metabolism* **8**, 13-25
82. Faccenda, D., Tan, C., Seraphim, A., Duchen, M., and Campanella, M. (2013) IF1 limits the apoptotic-signalling cascade by preventing mitochondrial remodelling. *Cell death and differentiation* **20**, 686-697
83. Campanella, M., Seraphim, A., Abeti, R., Casswell, E., Echave, P., and Duchen, M. (2009) IF1, the endogenous regulator of the F(1)F(o)-ATPsynthase, defines mitochondrial volume fraction in HeLa cells by regulating autophagy. *Biochimica et biophysica acta* **1787**, 393-401
84. Lu, Y.-m., Miyazawa, K., Yamaguchi, K., Nowaki, K., Iwatruki, H., Wakamatru, Y., Ichikawa, N., and Hashimoto, T. (2001) Deletion of Mitochondrial ATPase Inhibitor in the Yeast Saccharomyces cerevisiae Decreased Cellular and Mitochondrial ATP Levels under Non-Nutritional Conditions and Induced a Respiration-Deficient Cell-Type. *The Journal of Biochemistry* **130**, 873-878
85. Ichikawa, N., Yoshida, Y., Hashimoto, T., Ogasawara, N., Yoshikawa, H., Imamoto, F., and Tagawa, K. (1990) Activation of ATP hydrolysis by an uncoupler in mutant mitochondria lacking an intrinsic ATPase inhibitor in yeast. *The Journal of biological chemistry* **265**, 6274-6278
86. Fernández-Cárdenas, L. P., Villanueva-Chimal, E., Salinas, L. S., José-Nuñez, C., Tuena de Gómez-Puyou, M., and Navarro, R. E. (2017) Caenorhabditis elegans ATPase inhibitor factor 1 (IF1) MAI-2 preserves the mitochondrial membrane potential (Δψm) and is important to induce germ cell apoptosis. *Plos One* **12**, e0181984
87. Faccenda, D., Nakamura, J., Gorini, G., Dhoot, G. K., Piacentini, M., Yoshida, M., and Campanella, M. (2017) Control of Mitochondrial Remodeling by the ATPase Inhibitory Factor 1 Unveils a Pro-survival Relay via OPA1. *Cell Rep.* **18**, 1869-1883

88. Nakamura, J., Fujikawa, M., and Yoshida, M. (2013) IF1, a natural inhibitor of mitochondrial ATP synthase, is not essential for the normal growth and breeding of mice. *Biosci Rep* **33**
89. Ludwig, B. (1986) Cytochrome c oxidase from Paracoccus denitrificans. *Methods in Enzymology* **126**, 153-159
90. Simon, R., Priefer, U., and Pühler, A. (1983) A Broad Host Range Mobilization System for In Vivo Genetic Engineering: Transposon Mutagenesis in Gram Negative Bacteria. *Nature biotechnology*, 784-791
91. Quandt, J., and Hynes, M. F. (1993) Versatile suicide vectors which allow direct selection for gene replacement in Gram-negative bacteria. *Gene* **127**, 15-21
92. Kovach, M. E., Elzer, P. H., Hill, D. S., Robertson, G. T., Farris, M. A., Roop II, R. M., and Peterson, K. M. (1995) Four new derivatives of the broad-host-range cloning vector pBBR1MCS, carrying different antibiotic-resistance cassettes. *Gene* **166**, 175-176
93. Lowry, O. H., Rosebrough, N. J., Farr, A. L., and Randall, R. J. (1951) Protein Measurement with the Folin Phenol Reagent. *Journal of Biological Chemistry* **193**, 265-275
94. Peterson, G. L. (1977) A Simplification of the Protein Assay Method of Lowry et al. Which is More Generally Applicable. *Analytical Biochemistry* **83**, 346-356
95. Schägger, H., and von Jagow, G. (1987) Tricine-sodium dodecyl sulfate-polyacrylamide gel electrophoresis for the separation of proteins in the range from 1 to 100 kDa. *Anal Biochem.* **166**, 368-379
96. Towbin, H., Staehelin, T., and Gordon, J. (1979) Electrophoretic transfer of proteins from plyacrylamide gels to nitrocellulose sheets Procedure and applications. *Proc Natl Acad Sci U S A.* **76**, 4350-4354
97. Ogilvie, I., Aggeler, R., and Capaldi, R. A. (1997) Cross-linking of the delta subunit to one of the three alpha subunits has no effect on functioning, as expected if delta is a part of the stator that links the F1 and F0 parts of the Escherichia coli ATP synthase. *J Biol Chem* **272**, 16652-16656
98. Novo, D., Perlmutter, N. G., and Shapiro, H. K. (1999) Accurate flow cytometric membrane potential measurement in bacteria using diethyloxacarbocyanine and a ratiometric technique. *Cytometry* **35**, 55-63
99. Shapiro, H. M. (2004) Estimation of membrane potential by flow cytometry. *Current Protocols in Cytometry.* **Chapter 9**
100. Erecinska, M., Davis, J. S., and Wilson, D. F. (1979) Regulation of respiration in Paracoccus denitrificans: The dependence on redox state of cytochrome c and [ATP]/[ADP][Pi]. *Archives of Biochemistry and Biophysics* **197**, 463-469
101. Waltmough, N. J., and Frerman, F. E. (2010) The electron transfer flavoprotein: Ubiquinone oxidoreductases. *Biochimica et Biophysica Acta - Bioenergetics* **1797**, 1910-1916
102. Kregiel, D. (2012) Succinate Dehydrogenase of Saccharomyces cerevisiae – The Unique Enzyme of TCA Cycle – Current Knowledge and New Perspectives. *IntechOpen* **Dehydrogenases Rosa Angela Canuto**, 212-234
103. Zharova, T. V., and Vinogradov, A. D. (2017) Functional heterogeneity of Fo·F1H+-ATPase/synthase in coupled Paracoccus denitrificans plasma membranes. *Biochimica et Biophysica Acta - Bioenergetics* **1858**, 939-944

104. Hederstedt, L. (2002) Succinate:quinone oxidoreductase in the bacteria Paracoccus denitrificans and Bacillus subtilis. *Biochimica et Biophysica Acta - Bioenergetics* **1553**, 74-83
105. Kersters, K., De Vos, P., Gillis, M., Swings, J., VanDamme, P., and Stackebrandt, E. (2006) Introduction to the Proteobacteria *Prokaryotes* **5**, 3-37
106. Joon, S., Ragunathan, P., Sundararaman, L., Nartey, W., Kundu, S., Manimekalai, M. S. S., Bogdavonic, N., Dick, T., and Grüber, G. (2018) The NMR solution structure of Mycobacterium tuberculosis F-ATP synthase subunit ε provides new insight into energy coupling inside the rotary engine. *The FEBS Journal* **285**, 1111-1128
107. Kundu, S., Biukovic, G., Grüber, G., and Dick, T. (2016) Bedaquiline Targets the ε Subunit of Mycobacterial F-ATP Synthase. *Antimicrobial Agents and Chemotherapy* **60**, 6977-6979
108. Lakshmanan, M., and Xavier, A. S. (2013) Bedaquiline – The first ATP synthase inhibitor against multi drug resistant tuberculosis. *Journal of Young Pharmacists* **5**, 112-115
109. Hagemans, D., van Belzen, I. A. E. M., Luengo, T. M., and Rüdiger, S. G. D. (2015) A script to highlight hydrophobicity and charge on protein surfaces. *Front Mol Biosci.* **2**
110. Uribe-Alvarez, C., Chiquete, N., Morales-García, L., Bohorquez, A., Laura Delgado-Buenrostro, N., Vaca, L., Peña, A., and Uribe-Carvajal, S. (2018) Wolbachia pipientis grows in Saccharomyces cerevisiae evoking early death of the host and deregulation of mitochondrial metabolism. *Microbiologyopen.* **[Epub ahead of print]**, e00675

16 Artículos publicados

Article

Cell Reports

The Biological Role of the ζ Subunit as Unidirectional Inhibitor of the F_1F_O-ATPase of *Paracoccus denitrificans*

Graphical Abstract

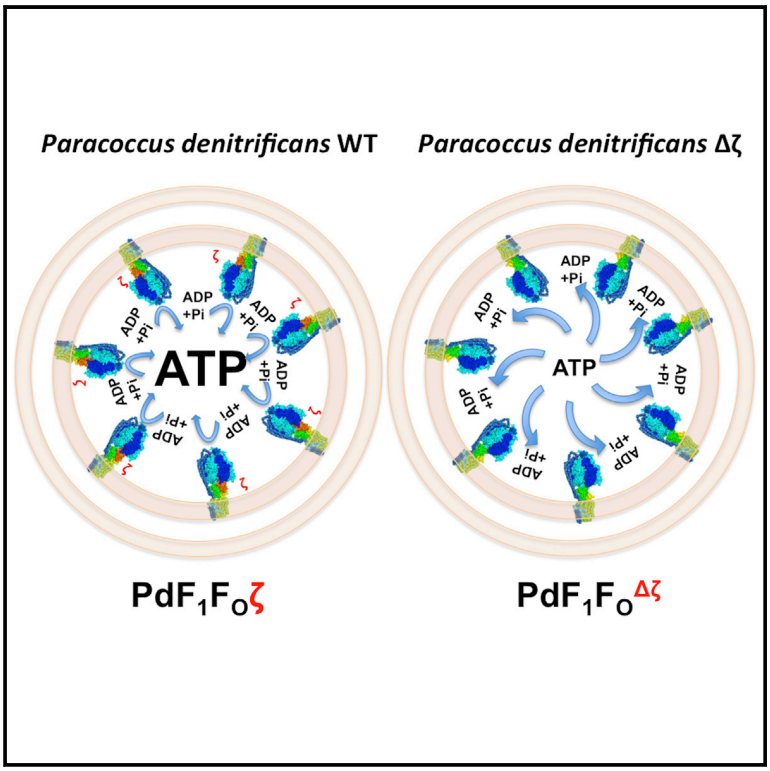

Authors

Francisco Mendoza-Hoffmann, Ángeles Pérez-Oseguera, Miguel Ángel Cevallos, ..., Emilio Espinoza-Simón, Salvador Uribe-Carvajal, José J. García-Trejo

Correspondence

jjgartre@unam.mx

In Brief

The ATP synthase nanomotor provides most of the chemical energy for life in the form of ATP. Mendoza-Hoffmann et al. resolve the role and mechanism of a natural bacterial ζ inhibitor protein working as a unidirectional pawl-ratchet to block wasteful ATP cleavage by this nanomotor, thus favoring energy preservation for life.

Highlights

- We obtained a knockout of an F_1F_O-ATPase inhibitor Δζ with a clear phenotype
- The *Paracoccus denitrificans* Δζ mutant grows more slowly than the WT in respiratory media
- ζ is a unidirectional F_1F_O-ATPase inhibitor, not affecting the ATP synthase turnover
- ζ works as a pawl-ratchet favoring clockwise ATP synthase rotation and cell division

Mendoza-Hoffmann et al., 2018, Cell Reports *22*, 1067–1078
January 23, 2018
https://doi.org/10.1016/j.celrep.2017.12.106

CellPress

Cell Reports
Article

The Biological Role of the ζ Subunit as Unidirectional Inhibitor of the F_1F_O-ATPase of *Paracoccus denitrificans*

Francisco Mendoza-Hoffmann,[1] Ángeles Pérez-Oseguera,[2] Miguel Ángel Cevallos,[2] Mariel Zarco-Zavala,[3] Raquel Ortega,[1] Claudia Peña-Segura,[4] Emilio Espinoza-Simón,[4] Salvador Uribe-Carvajal,[4] and José J. García-Trejo[1,5,*]
[1]Departamento de Biología, Facultad de Química, Ciudad Universitaria, Universidad Nacional Autónoma de México (U.N.A.M.), Delegación Coyoacán, Ciudad de México (CDMX) 04510, México
[2]Programa de Genómica Evolutiva, Centro de Ciencias Genómicas, U.N.A.M., Cuernavaca, Morelos, México
[3]University of Tokyo, Hongo, Bunkyo-ku, Tokyo, Japan
[4]Instituto de Fisiología Celular, U.N.A.M., Ciudad de México (CDMX), México
[5]Lead Contact
*Correspondence: jjgartre@unam.mx
https://doi.org/10.1016/j.celrep.2017.12.106

SUMMARY

The biological roles of the three natural F_1F_O-ATPase inhibitors, ε, ζ, and IF_1, on cell physiology remain controversial. The ζ subunit is a useful model for deletion studies since it mimics mitochondrial IF_1, but in the F_1F_O-ATPase of *Paracoccus denitrificans* (PdF_1F_O), it is a monogenic and supernumerary subunit. Here, we constructed a *P. denitrificans* 1222 derivative (PdΔζ) with a deleted ζ gene to determine its role in cell growth and bioenergetics. The results show that the lack of ζ *in vivo* strongly restricts respiratory *P. denitrificans* growth, and this is restored by complementation in *trans* with an exogenous ζ gene. Removal of ζ increased the coupled PdF_1F_O-ATPase activity without affecting the PdF_1F_O-ATP synthase turnover, and the latter was not affected at all by ζ reconstitution *in vitro*. Therefore, ζ works as a unidirectional pawl-ratchet inhibitor of the PdF_1F_O-ATPase nanomotor favoring the ATP synthase turnover to improve respiratory cell growth and bioenergetics.

INTRODUCTION

ATP synthases are the cornerstone of cellular bioenergetics in bacteria, mitochondria, and chloroplasts; these F_1F_O-ATP synthases synthesize more than 90% of the ATP required by most organisms to live. The F_1F_O complex harnesses the energy stored in electrochemical gradients ($\Delta\mu_{H+}$) generated by electron transport chains (Mitchell, 1961) by coupling the proton flow through the F_O channel to drive ATP synthesis from ADP and Pi at the F_1 water-soluble portion. The F_1 part has five essential subunits—namely, α, β, γ, δ, and ε—and can be isolated as a water-soluble F_1-ATPase (Boyer, 1997). In α-proteobacteria such as *Paracoccus denitrificans*, the F_1 portion also contains a sixth supernumerary subunit named ζ (de la Rosa-Morales, 2005; Morales-Ríos et al., 2010). The F_O proton channel is composed of three essential subunits, *a*, *b*, and *c*. In eukaryotes, the mitochondrial enzyme includes the mitochondrial inhibitor (IF_1), which is a regulatory (Pullman and Monroy, 1963) and stabilizing factor of dimeric and oligomeric forms of the mitochondrial ATP synthase (García et al., 2006).

The F_1F_O-ATP synthase is a rotary reversible nanomotor (Duncan et al., 1995; Noji et al., 1997; Sabbert et al., 1996); i.e., the central rotor gyrates in a clockwise (CW) direction (viewed from F_O to F_1) to synthesize ATP (Rondelez et al., 2005) and in a counterclockwise (CCW) sense to hydrolyze it (Noji et al., 1997). In the absence of oxygen or of a final electron acceptor, or during uncoupling (i.e., without a proton gradient), the F_1F_O nanomotor becomes thermodynamically prone to rotate in the reverse CCW ATP hydrolysis turnover, consuming the cellular ATP. Therefore, the CCW F_1F_O-ATPase turnover has to be somehow controlled to favor the F_1F_O-ATP synthase activity and prevent the wasteful F_1F_O-ATPase from functioning. In mitochondria, the protein in charge of blocking the F_1F_O-ATPase activity is the inhibitor protein of the F_1-ATPase, or IF_1 (Pullman and Monroy, 1963), whereas in bacteria such as *Escherichia coli*, it is the rotor subunit ε with the inhibitory function (Sternweis and Smith, 1980). Both inhibitor proteins (IF_1 and ε) insert an α-helix at the $\alpha_{DP}/\beta_{DP}/\gamma$ interface of their respective F_1-ATPases to block γ rotation (Cingolani and Duncan, 2011; Shirakihara et al., 2015).

In α-proteobacteria, which are closely related to the mitochondrial protoendosymbiont (John and Whatley, 1975; Ku et al., 2015; Margulis and Chapman, 1998), the ε subunit does not have an inhibitory function; instead, this has been transferred to a natural inhibitor that we discovered in *Paracoccus denitrificans* and related α-proteobacteria and named as the ζ subunit (de la Rosa-Morales, 2005; Morales-Ríos et al., 2010). We found the open reading frame (ORF) of ζ (DUF1476) conserved along the α-proteobacteria class and identified the inhibitory domain at the N terminus of ζ. The latter preserves some similarity with the inhibitory domain of IF_1 (Zarco-Zavala et al., 2014), notwithstanding that the full ζ structure (PDB: 2LL0) is different from those of mitochondrial IF_1 and bacterial ε (Serrano et al., 2014; Zarco-Zavala et al., 2012, 2014). Cross-linking studies showed that the ζ N terminus blocks rotation of the γ subunit of

the F_1-ATPase of *P. denitrificans*, similarly to IF_1 (Minauro-Sanmiguel et al., 2002). Crystals of the native PdF_1-ζ complex lacked the γ, δ, ε, and ζ subunits (Morales-Ríos et al., 2015a); thus, further structural alignment of the ζ N terminus with the inhibitory domain of IF_1, together with functional studies, showed that ζ also binds into the $\alpha_{DP}/\beta_{DP}/\gamma$ interface-blocking γ rotation, very similarly to mitochondrial IF_1 (García-Trejo et al., 2016). In other words, the ζ subunit blocks the intrinsic rotation of the *P. denitrificans* nanomotor by mimicking IF_1. This binding site of ζ at the $\alpha_{DP}/\beta_{DP}/\gamma$ interface was found before the release of the crystallographic PdF_1F_O structure of *P. denitrificans* (PDB: 5DN6), which confirmed that ζ binds to the $\alpha_{DP}/\beta_{DP}/\gamma$ interface (Morales-Rios et al., 2015b). Taken together, the ζ nuclear magnetic resonance (NMR) structure (Serrano et al., 2014; Zarco-Zavala et al., 2012, 2014), the functional and modeling studies (García-Trejo et al., 2016), and the crystallographic data (Morales-Rios et al., 2015b) show that the ζ N terminus shifts from an intrinsically disordered region (IDR) to an inhibitory α-helix that can be superimposed with the inhibitory IF_1 N terminus bound to the mitochondrial F_1 (Cabezón et al., 2003). In summary, ζ is an α-proteobacterial inhibitor protein that blocks the activity of the F_1F_O-ATPase complex of *P. denitrificans* with an IF_1-like N-terminal structure and mechanism; therefore, it can be used as a model to study the structure, function, and mechanism of these F_1-ATPase inhibitors. These data also support the endosymbiotic origin of mitochondria as derived from α-proteobacteria (John and Whatley, 1975; Ku et al., 2015; Margulis and Chapman, 1998), as shown by the close similarity of the primary and tertiary structures of the F_1 subunits from *P. denitrificans* and bovine heart mitochondria (García-Trejo et al., 2016).

The physiological role of the ATP synthase's natural inhibitor proteins has been a subject of a number of studies. For instance, IF_1 knockouts in yeast (*Saccharomyces cerevisiae*) and mice have shown that IF_1 is non-essential, and its absence did not exert a major effect in yeast growth or in mouse development and bioenergetics, respectively (Lu et al., 2001; Nakamura et al., 2013). Furthermore, mitochondrial IF_1 is encoded by 2–3 different genes, depending on the species; besides, there are two IF_1 homologous stabilizing factors of 9 kDa (Stf1) and 15 kDa (Stf2) in mitochondria (Hashimoto et al., 1983, 1984, 1987, 1990a), with Stf1 also working as an F_1-ATPase inhibitor (Hashimoto et al., 1987, 1990b). Furthermore, the three simultaneous yeast knockouts of the IF_1 (INH1), 9-kDa (STF1), and 15-kDa (STF2) genes showed no significant effects on cell growth, mitochondrial bioenergetics, and/or ATP synthase dimerization (Dienhart et al., 2002), unless the cells are exposed to severe starvation (Lu et al., 2001). Similar results have been observed with the homologous protein of IF_1 (MAI-2) in *Caenorhabditis elegans* (Fernández-Cárdenas et al., 2017). On the other hand, bacterial ε is an important structural subunit, forming a key connection between the rotary γ and *c*-ring subunits of the enzyme (see, for instance, Figure 7); thus, bacterial ε cannot be deleted without disassembling F_1 from F_O (Klionsky et al., 1984). Then again, the ζ subunit is encoded by a single supernumerary gene in α-proteobacteria (Morales-Ríos et al., 2010; Zarco-Zavala et al., 2014). Taken together, these precedents indicate that, since ζ mimics IF_1, it is a suitable model to assess the biological role of the natural ATP synthase inhibitors, especially because *P. denitrificans* can grow in a respiratory medium where it relies exclusively on its mitochondrial-like electron transport chain (Berry and Trumpower, 1985; Iwata et al., 1995; Kleinschroth et al., 2011; Ludwig and Schatz, 1980; Pennoyer et al., 1988; Yagi, 1986).

Once it was predicted that the ζ subunit would be a suitable model to study the role of the natural F_1-ATPase inhibitors, we analyzed the effect of the deletion of the ζ subunit of the F_1F_O-ATPase from *Paracoccus denitrificans* 1222 (Pd1222) on bacterial growth and cell bioenergetics, and the results are here presented. This was carried out by construction of a stable *P. denitrificans* Δζ mutant strain (PdΔζ), as well as a complemented strain (PdΔζ +ζ). The comparison of their growth curves in rich lysogeny broth (LB) medium and succinate respiratory minimal medium show clearly that removal of a natural inhibitor of the ATP synthase has strong and deleterious effects on the bacterial respiratory growth and bioenergetics. The ATP synthesis and hydrolysis of inside-out membrane vesicles of Pd1222 (PdWT) and PdΔζ mutant strains, and the PdF_1-ATPase activity of the enzyme purified from both strains, were also analyzed; these activities correlate well with the phenotype observed in the mutant PdΔζ. Finally the kinetic effects of the ζ deletion and reconstitution on the F_1F_O-ATPase and F_1F_O-ATP synthase turnovers strongly support that the ζ subunit works unidirectionally as the previously proposed pawl-ratchet (García-Trejo et al., 2016) to block selectively the CCW rotation of the PdF_1F_O central rotor and, thus, favoring ATP synthesis over its hydrolysis to improve bacterial respiratory growth.

RESULTS AND DISCUSSION

Construction of a Mutant Lacking the ζ Gene and Complementation of the Knockout Strain

A suicidal plasmid, pFMMCJG-Δζ (see Table S1), replaced the entire ζ gene with the kanamycin resistance cassette by homologous recombination. To confirm that the observed effects of the mutant strain are derived exclusively from the deletion of the ζ subunit (Δζ), the best control is to complement the PdΔζ strain with an expression plasmid containing the recombinant ζ gene. Therefore, a pBBR derivative ζ construction (pFMMCJG-Δζ+ζ) was obtained using a multi-host plasmid, pBBR1 MCS-5 (Kovach et al., 1995) (Table S1). The PdΔζ+ζ strain was subsequently obtained by conjugation of S17/pFMMCJG+ζ into the PdΔζ strain, as explained in Experimental Procedures.

Our PdΔζ knockout mutant was confirmed by PCR and western blotting. In the PCR, the ζ gene was amplified correctly from the chromosomal DNA of the Pd1222 (PdWT), but, as expected, it could not be amplified at all from the PdΔζ strain (Figure 1A). Furthermore, the wild-type (WT) ζ gene can be also amplified from the complemented PdΔζ+ζ strain. We also confirmed that the kanamycin resistance (Km^R) was amplified only from the PdΔζ and PdΔζ+ζ strains, but not from the Pd1222 (PdWT) (data not shown). On the other hand, anti-ζ western blot analyses of cell extracts from the three strains confirmed that the ζ protein is totally absent in the PdΔζ strain and that ζ reappeared in the PdΔζ+ζ strain, as shown in Figure 1B.

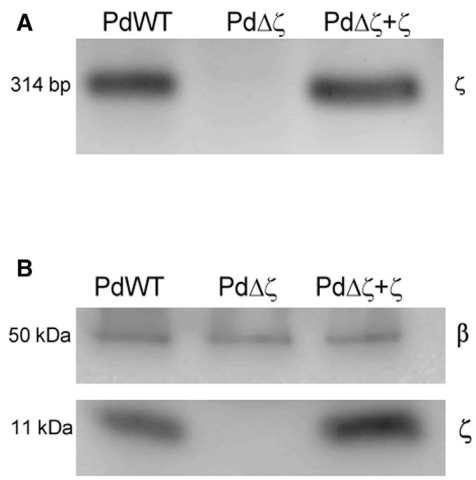

Figure 1. Confirmation of the Inhibitory ζ Subunit Depletion in PdΔζ
(A) The ζ gene (314 bp) was PCR-amplified from the genomic DNA of three different *P. denitrificans* strains: the wild-type PdWT, the mutant lacking the ζ gene PdΔζ, and the mutant PdΔζ complemented with the ζ gene PdΔζ+ζ. DNA amplifications were resolved by 2% agarose gel electrophoresis.
(B) PdWT, PdΔζ, and PdΔζ+ζ were grown for 24 hr on LB medium. Cell lysates were resolved by SDS-PAGE and western blotted for β and ζ proteins. Data are representative of three separate experiments.

Cell Growth

Cells from Pd1222 (PdWT), PdΔζ, and PdΔζ+ζ strains were grown separately in either rich LB medium or respiratory succinate minimal medium at 30°C for 48 hr. It was observed that, in LB-rich medium, there are no significant differences in the growth rate of all three strains other than a slight delay in the lag phase of the PdΔζ mutant (Figure 2A). In marked contrast, when the bacterial growth was followed in the minimal succinate medium, we clearly observed a phenotype in the PdΔζ strain in that it grows much more slowly than the Pd1222 (PdWT). In the first 24 hr, the mutant (PdΔζ) barely starts to grow in this respiratory medium, whereas the WT (Pd1222) has already reached saturation (Figure 2B). In addition, the complemented mutant (PdΔζ+ζ) reverted to the WT phenotype, thus discarding the possibility that the slow growth observed for the PdΔζ strain could result from other non-specific changes in the mutant strain. The complemented PdΔζ+ζ phenotype reached a similar growth rate compared to that of the Pd1222 (PdWT) strain (Figure 2B). In summary, these results show that the ζ gene is not essential for bacterial growth and not very important physiologically in rich LB medium. However, when *P. denitrificans* is forced to respire with oxygen and to obtain ATP exclusively from oxidative phosphorylation (Ox-Phos), the mutant has serious difficulties growing in the absence of ζ, which then becomes a key ATP synthase regulatory subunit (Figure 2).

The Effect of ζ Deletion on ATP Synthesis and ATP Hydrolysis of SBPs

We prepared sub-bacterial particles (SBPs) from the PdWT and mutant PdΔζ strains grown in both the LB-rich medium and the minimal respiratory succinate medium. The SBPs were used to measure their ATP synthesis rates as described in Experimental Procedures. We found no significant differences in the F_1F_O-ATP synthase rates of the WT (Pd1222) and the mutant (PdΔζ) (Figure 3A). However, both preparations are more active in their synthetic activities when grown in succinate compared to LB medium. The higher ATP synthesis rates obtained in succinate are in concordance with an increased expression of the respiratory chain in oxidative media in *P. denitrificans* (Cox et al., 1978; Hederstedt, 2002; Scholes and Smith, 1968) and with a higher succinate-driven proton-pumping activity obtained in succinate than in LB media (Figure 4). In concordance, the succinate dehydrogenase (SDH) activity of complex II increases slightly when *P. denitrificans* is grown in the presence of succinate versus in its absence, together with a several-fold

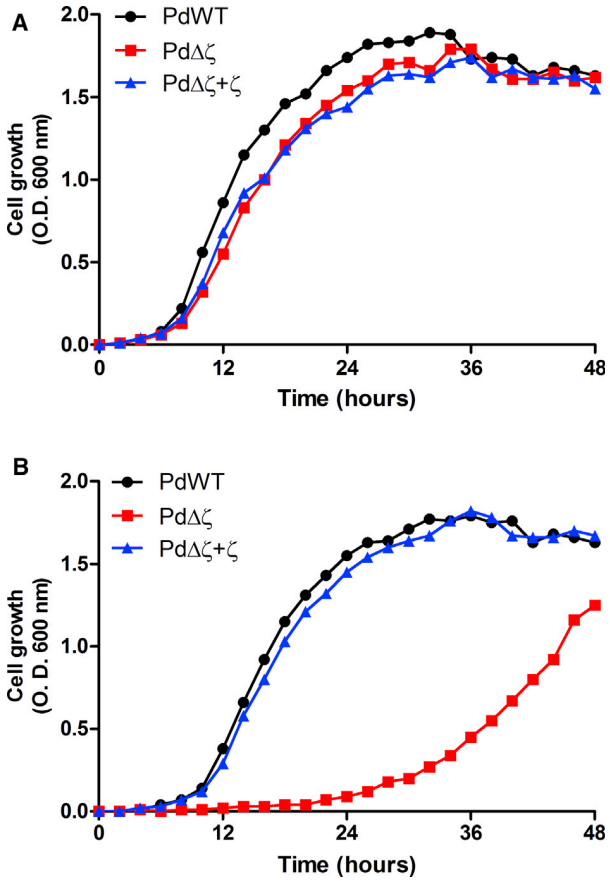

Figure 2. Effect of ζ Deletion on the Growth of *P. denitrificans*
Approximately 4.8 × 10^8 cells per milliliter of each strain of *P. denitrificans*: the wild-type PdWT (black circles), the mutant lacking the ζ gene PdΔζ (red squares), or the mutant PdΔζ complemented with the ζ gene PdΔζ+ζ (blue triangles) were inoculated separately into 60 mL of LB or succinate liquid medium and incubated at 30°C for 48 hr at 200 rpm. Aliquots were taken every 2 hr, and the optical density (O.D.) was read spectrophotometrically at 600 nm.
(A) The growth curve in LB medium.
(B) The growth curve in succinate medium.
Data are representative from at least three experiments. SD is not shown for clarity but is ≤15%.

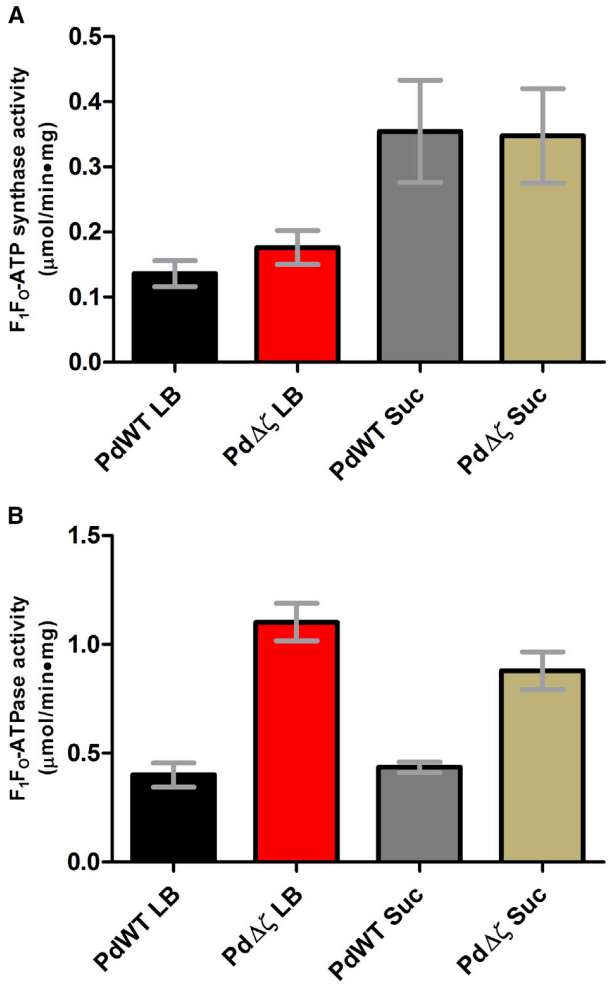

Figure 3. The ζ Subunit Inhibits the F_1F_O-ATPase Activity, but Not the F_1F_O-ATP Synthase Activity, in SBPs

The wild-type PdWT and the mutant PdΔζ strains were grown in LB or succinate (Suc) medium, cells were harvested, and coupled sub-bacterial particles (SBPs) were prepared.

(A) The F_1F_O-ATP-synthase-specific activity (micromolar/minute • milligrams) of the wild-type PdWT grown in LB (black), the PdΔζ strain grown in LB (red), the PdWT grown in succinate medium (gray), and the mutant PdΔζ strain grown in succinate medium (green).

(B) The PdF_1F_O-ATPase-specific activity (micromolar/minute • milligrams). Activities were measured in the presence of LDAO (0.15%) as an activator. From left to right: the wild-type PdWT grown in LB (black); the mutant strain PdΔζ grown in LB medium (red); the wild-type PdWT grown in succinate (gray); and the mutant strain PdΔζ grown in succinate (green).

The average of three experiments is shown with SD.

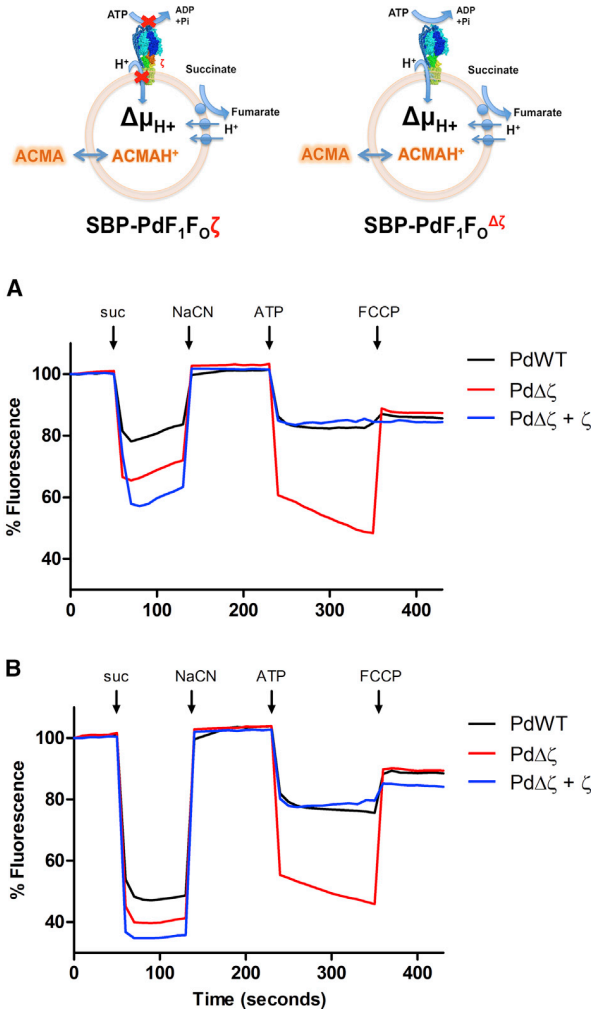

Figure 4. Effect of the ζ Deletion on Membrane Energization of SBPs from *Paracoccus denitrificans*

Upper diagram: the ACMA quenching fluorescence assay. Proton pumping is coupled either to succinate oxidation by the respiratory chain or to ATP hydrolysis carried out by the PdF_1F_O complex (see Supplemental Experimental Procedures for details).

(A and B) SBPs were prepared from wild-type PdWT and the PdΔζ strains grown in (A) LB medium or (B) succinate medium (suc). Two subsequent events of membrane energization and collapse were induced, with succinate/NaCN and Mg-ATP/FCCP as described in Experimental Procedures. 300 µg of each SBP were diluted in 3 mL ACMA medium directly in the fluorescence cell. Black and red indicate membrane energization of PdWT and PdΔζ, respectively. As a control, shown in blue, 120 µg of exogenous recombinant ζ was added to 300 µg of SBPs from PdΔζ (PdΔζ + ζ) in conditions where ζ inhibits essentially all of the PdF_1F_O-ATPase activity (see Figure 5D). ACMA fluorescence data shown are the average of three different experiments.

increase in the mRNA of the *sdh* operon (Hederstedt, 2002). To confirm this, we carried out anti-SD70 western-blot analyses of SBPs isolated from PdWT and PdΔζ strains grown in LB or succinate media and confirmed that there is actually a modest but significant increase in the amount of succinate dehydrogenase in both PdWT and PdΔζ strains (Figure S2). Thus, the higher ATP synthase and proton-pumping activities in succinate media for SBPs isolated from PdWT and PdΔζ cells could be, at some extent, the result of a higher expression of the succinate-oxidizing respiratory chain. Nevertheless, and more importantly, aside from the differences in Ox-Phos and $\Delta\mu_{H+}$ observed in LB and succinate media used to grow *P. denitrificans*, it was clearly observed that the ATP synthesis

rates of both the control Pd1222 (PdWT) and the PdΔζ strains are essentially the same (Figure 3A). We also corroborated that the ATP synthase was expressed in similar amounts in PdWT and PdΔζ strains and in both LB and succinate media (Figures S2 and S4), indicating that the Δζ deletion or the shift from LB to succinate does not alter the amounts of ATP synthase, thus confirming that the observed changes in activities or proton pumping described later are not due to changes in the number of ATP synthase enzymes. In brief, the complete removal of the ζ subunit does not have any significant effect on the full oxidative phosphorylation of *P. denitrificans*, as supported by succinate oxidation. At this point, it seems worth mentioning that, in contrast to the *E. coli* ATP synthase, which has a low (0.1) control coefficient of the full Ox-Phos *in vivo* (Jensen et al., 1993), the PdF_1F_O-ATP synthase has a control coefficient of 1.0 of the full Ox-Phos in the SBPs of *P. denitrificans* (Pérez and Ferguson, 1990); this means that the major rate-limiting step of the full Ox-Phos of the SBPs is the ATP synthase of this bacterium; therefore, the effect of an inhibitor of the PdF_1F_OATP synthase on the full Ox-Phos reaction can be correlated directly with its rotary kinetic mechanism. In summary, this indicates that ζ does not have any effect at all on the rate of the synthetic CW intrinsic rotation of the PdF_1F_O ATP synthase coupled to ATP synthesis.

We had previously shown the inhibitory function of the ζ subunit on the PdF_1-ATPase and PdF_1F_O-ATPase activities by homologous reconstitution of the recombinant ζ subunit (Morales-Ríos et al., 2010; Zarco-Zavala et al., 2014) and by the observation that partial removal of the ζ subunit increased the PdF_1-ATPase activity. Now, thanks to this ζ deletion study, we are in optimal conditions to confirm whether there is a higher increase in PdF_1-ATPase and PdF_1F_O-ATPase activities associated with full ζ removal, as expected from the inhibitory function of ζ. The effect of ζ deletion on ATP hydrolysis was measured in SBPs prepared from the Pd1222 (PdWT) and PdΔζ strains grown in LB or succinate media (Figure 3B). It was clearly observed that the removal of ζ produced a higher hydrolytic activity of the PdΔζ samples grown in LB or in succinate media, compared to the WT (Pd1222) samples. The PdΔζ preparations reached about 200% of the activities of the Pd1222 (PdWT) SBPs, regardless of the media used (275.5% for LB and 202.1% for succinate). Since ζ works as a total PdF_1-ATPase inhibitor (Zarco-Zavala et al., 2014), if all PdF_1F_O-ATPases were inhibited by ζ, there should not be residual PdF_1F_O-ATPase activity in the PdWT strain; therefore, the ≈50% residual PdF_1F_O-ATPase (Figure 3B) and PdF_1-ATPase (Figure 5C, LDAO [lauryl dimethylamine oxide]) activities observed for the PdWT in the presence of LDAO, as compared to the Δζ mutant, are likely due to a fraction of enzymes lacking ζ that are susceptible to inhibition by exogenous recombinant ζ *in vitro*, as we showed previously (Morales-Ríos et al., 2010; Zarco-Zavala et al., 2014). In summary, the PdF_1-ATPase and PdF_1F_O-ATPase activations induced by the total ζ removal, together with the null effect of the ζ deletion on ATP synthesis, strongly suggest that ζ does not affect ATP synthesis, but it strongly inhibits the F-ATPase activity. Therefore, it works as unidirectional inhibitor of the PdF_1F_O-ATPase.

Effect of ζ Deletion on the Proton-Pumping Activity of the PdF_1F_O-ATPase

As in other bacterial systems, the reverse PdF_1F_O-ATPase activity should work physiologically as a primary proton pump, energizing the membrane at the expense of ATP hydrolysis. However, since this reversal PdF_1F_O-ATPase activity is strongly inhibited and latent in *P. denitrificans* (Pacheco-Moisés et al., 2000; Pérez and Ferguson, 1990), the proton-pumping activity should be relatively low in the Pd1222 (PdWT) strain, as compared with that of the PdΔζ strain, if the increased $PdF_1F_O{}^{\Delta\zeta}$-ATPase activity (Figure 3B) is catalyzed by a coupled $PdF_1F_O{}^{\Delta\zeta}$ complex pumping protons properly. The low proton-pumping PdF_1F_O-ATPase activity of the WT strain has been evidenced previously by a very low ATP ⇔ $[^{32}P]P_i$ exchange reaction observed in *P. denitrificans* SBPs, which relies on the formation of the ATP-driven membrane potential (Pacheco-Moisés et al., 2000; Pérez and Ferguson, 1990). To test the effect of ζ removal on the proton pumping of the PdF_1F_O-ATPase, we prepared SBPs from Pd1222 (PdWT) and PdΔζ strains grown in both LB and succinate media. Coupled SBPs have the entire respiratory chain; therefore, we assayed qualitatively the formation of succinate-driven and ATP-driven proton gradients by fluorescence quenching of the membrane potential probe ACMA. The first control around the first 100 s of proton pumping with succinate indicates that the SBPs are properly coupled (Figure 4). When SBPs were prepared from cells grown in succinate, formation of the proton gradient was higher than when grown in LB media (compare first 100 s in Figures 4A and 4B). After the addition of cyanide, respiratory formation of the proton gradient is collapsed (as shown by fluorescence recovery); thus, the subsequent proton gradient was formed by the coupled PdF_1F_O-ATPase. Regardless of the media used to grow *P. denitrificans* (LB or succinate medium), it was clear that the ATP-driven proton gradient was much higher when the ζ subunit was deleted (Figures 4A and 4B, red traces) than in control SBPs isolated from the Pd1222 (PdWT) strain (Figures 4A and 4B, black traces). To confirm that the increase in proton pumping is derived from the removal of ζ in the PdΔζ mutant, control experiments were carried out by pre-incubating the SBPs of the PdΔζ mutant with a molar excess of recombinant ζ in conditions that block completely the PdF_1 and PdF_1F_O-ATPase activity (Zarco-Zavala et al., 2014). As expected from an inactive reconstituted PdF_1F_O-ζ complex unable to pump protons, the ATP-driven ACMA fluorescence quenching returned to very low levels, similar to those observed with the Pd1222 (PdWT) strain expressing the endogenous ζ (Figures 4A and 4B, blue traces); thus, the increase in proton pumping of the mutant was completely abolished by the PdF_1F_O-ATPase inhibition by exogenous ζ. In summary, these results show, on one hand, that the deletion of the ζ subunit does not affect the functional coupling between the F_1 and F_O sectors of the PdF_1F_O complex, as expected from a non-essential regulatory subunit, and that, on the other hand, removal of the ζ subunit from *P. denitrificans* increases the coupled proton-pumping $PdF_1F_O{}^{\Delta\zeta}$-ATPase activity, leading to a higher membrane energization than with the control PdF_1F_O-ζ complex in the Pd1222 (PdWT) strain. It is worthwhile to mention that a similar enhancement in ATP-driven H^+ pumping has been described previously when the mitochondrial IF_1 and

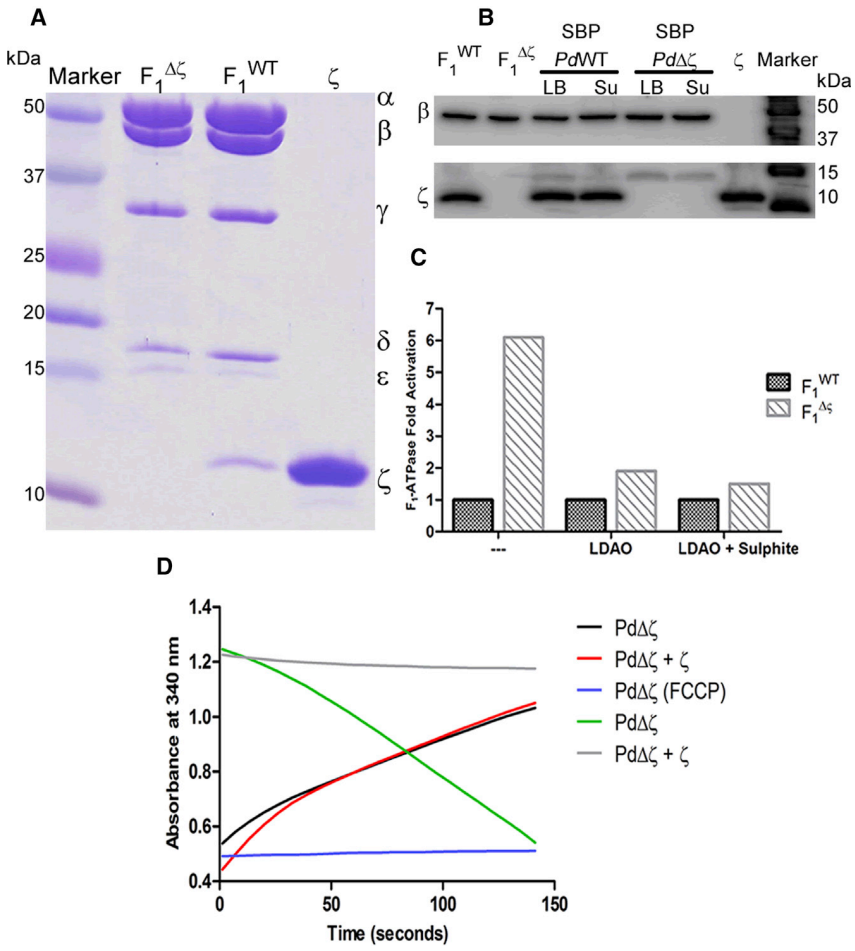

Figure 5. Activation of the Isolated PdF_1-ATPase by the ζ Deletion

(A) SDS-PAGE (from left to right) of the purified mutant $PdF_1^{\Delta\zeta}$, the wild-type PdF_1, and pure recombinant Pdζ; size markers are shown in the first lane.

(B) Western blot (from left to right) of the PdF_1^{WT}, the $PdF_1^{\Delta\zeta}$ mutant, SBPs of the wild-type grown in LB or succinate medium (Su), SBPs of the mutant grown in LB or succinate (Su), and the purified Pdζ; size markers are in the last lane. The polyvinylidene fluoride (PVDF) membrane was cut in three pieces; the upper part was exposed to the anti-β antibody, the lower part was exposed to the anti-Pdζ antibody, and the molecular weight markers (MWM) lane was exposed to the Strep-Tactin-HRP conjugate.

(C) The normalized ATPase activities of the wild-type (PdF_1^{WT}-ATPase; dark gray) and the mutant ($PdF_1^{\Delta\zeta}$; light gray) are shown as activation-fold relative to the PdF_1^{WT} activity. Specific activities are shown in the Supplemental Experimental Procedures. Data are the average of three experiments.

(D) Effect of the reconstitution of the ζ subunit on the PdF_1F_O-ATPase and PdF_1F_O-ATP synthase activities of SBPs from $Pd^{\Delta\zeta}$. The $PdF_1F_O^{\Delta\zeta}$-ATPase (absorbance decay in green and gray) and the $PdF_1F_O^{\Delta\zeta}$-ATP synthase (absorbance increase in black, red, and blue) activities were followed spectrophotometrically by coupled assays in real time. In red and gray traces, 100 μg SBPs from PdΔζ were pre-incubated during 20 min at room temperature with 110 μg exogenous recombinant ζ. The ATP synthesis blank shown in blue was made in the presence of uncoupler FCCP (4 μM) and venturicidin (4 μg), which completely block ATP synthesis. Turnover rates were obtained from the linear slopes and were obtained from at least three experiments.

its two stabilizing factors (Stf1 and Stf2) were deleted simultaneously in yeast mitochondria (Lu et al., 2001), indicating further similarities between α-proteobacterial ζ and mitochondrial IF_1 functioning *in vivo*. In a further effort to confirm the effect of ζ deletion on the membrane potential *in vivo*, we took advantage of the fluorescent probe $DiOC_2(3)$, which is instrumental to evidence bacterial membrane energization by its increase in red/green fluorescence ratio in flow cytometry experiments (Novo et al., 1999). Thus, the WT (PdWT), mutant (PdΔζ), and complemented (PdΔζ+ζ) *P. denitrificans* cells were incubated with this probe for 30 min before the determination of the red/green fluorescence ratio by flow cytometry. It was observed that the membrane potential (as evidenced by the CCCP-sensitive change in red/green fluorescence ratio) increased in response to the Δζ mutation, particularly when the cells were grown in succinate media, and that this increase was reverted by the complementation of the mutant with the exogenous recombinant ζ gene (Figure S3), i.e., similar to the membrane energization of SBPs followed with ACMA (Figure 4). These data confirm that, not only *in vitro* in SBPs but also *in vivo* in whole bacterial cells, and particularly in succinate media, the removal of the ζ subunit activates the H^+-PdF_1F_O-ATPase working as a primary pump, thus increasing the proton motive force across the bacterial cell membrane in comparison with the PdWT strain, which is inhibited in the proton-pumping H^+-PdF_1F_O-ATPase activity by its endogenous ζ subunit.

Purification of the PdF_1-ATPase from Pd1222 and PdΔζ

The F_1-ATPases from the PdWT and PdΔζ strains were purified as described previously (Zarco-Zavala et al., 2014) and are detailed in Experimental Procedures. The absence of the ζ subunit in the pure PdF_1 of the PdΔζ mutant was confirmed by anti-ζ and anti-β western blot analyses carried out with both PdF_1 samples and also with SBPs prepared from both strains grown either on LB or succinate medium (Figure 5B). The specific F_1-ATPase activity (SF_1A; units = μmol/min × mg of protein) was measured as described in the Experimental Procedures. The WT PdF_1-ATPase exhibited an SF_1A of 0.140 ± 0.003 U without activators, while the $PdF_1^{\Delta\zeta}$ reached 0.87 ± 0.12 U of SF_1A; i.e., removal of ζ exerted a 6.2-fold increase in PdF_1-ATPase turnover. The same PdF_1^{WT}-ATPase sample in the presence of LDAO showed an SF_1A of 2.38 ± 0.23 U, and the mutant reached 4.49 ± 1.20 U, 1.9-fold of the WT. The SF_1A in the presence of 0.15% of LDAO and residual 1.5 mM sulfite for the WT was

19.75 ± 1.45 U, and for the mutant, it reached 30.07 ± 1.2, a 1.5-fold increase relative to the WT (Figure 5C). This activity of the $PdF_1^{\Delta\zeta}$ mutant is the highest reported so far through the studies of the PdF_1-ATPase (Zarco-Zavala et al., 2014), likely due to the full removal of the ζ subunit. In all cases, the mutant achieved an increase ≥1.5-fold of the hydrolytic activity of the WT. In order to assess the productive binding of the recombinant ζ to the isolated $PdF_1^{\Delta\zeta}$-ATPase, the latter was subjected to an homologous reconstitution by preincubation with increasing concentrations of the recombinant Pd-ζ in the presence of 60 mM sulfite, 1 mM ATP and $MgCl_2$, as described in Experimental Procedures. This preincubation improves the binding of ζ, which requires some partial MgATP hydrolysis turnovers to effectively inhibit the PdF_1^{WT}-ATPase (Zarco-Zavala et al., 2014). Under these conditions, we observed a total $PdF_1^{\Delta\zeta}$-ATPase inhibition with a concentration of inhibitor that decreases the enzyme activity to 50% (IC_{50}) of 0.015 μM, which is in the nanomolar range, similar to that previously observed with PdF_1^{WT}-ATPase (Zarco-Zavala et al., 2014). Taken together, the activation of the $PdF_1^{\Delta\zeta}$-ATPase (Figure 5C) and that of the $PdF_1F_O^{\Delta\zeta}$-ATPase of SBPs (Figure 3B) confirm that removal of the ζ subunit exerts a 1.5- to 6-fold activation in the PdF_1-ATPase or PdF_1F_O-ATPase activities, with the latter coupled to enhanced transmembrane proton translocation in *P. denitrificans* (Figures 3B and 5C).

Effect of the ζ Subunit on the PdF_1F_O-ATP Synthase and PdF_1F_O-ATPase Activities

Although several reports show either unidirectional or bidirectional effects of IF_1 and ε on ATP synthesis and hydrolysis (Gómez-Puyou et al., 1979; Iino et al., 2009; Lippe et al., 1988; Masaike et al., 2006; Schwerzmann and Pedersen, 1986; Tsunoda et al., 2001), our results with the ζ subunit of *P. denitrificans* (Figure 3) suggest that these regulators block exclusively the CCW rotation in the F_1-ATPase direction but not the synthetic CW direction. To determine whether ζ works as a unidirectional ζ PdF_1F_O-ATPase inhibitor, we carried out the reconstitution of ζ into the ATP synthase of SBPs prepared from the PdΔζ mutant, taking advantage of the total lack of ζ subunit of this preparation. The reconstitution of the ζ subunit was carried out in the same conditions used for the PdF_1-ATPase assay, in the presence of low concentrations of MgATP, which promote the productive binding and lock of the ζ subunit into the $\alpha_{DP}/\beta_{DP}/\gamma$ interface to block completely the PdF_1 or PdF_1F_O-ATPase activity (Zarco-Zavala et al., 2014). Once the ζ subunit was reconstituted into the SBPs, approximately 100 μg of the latter were added to reaction cells pre-equilibrated at 37°C to measure the rates of ATP synthesis or ATP hydrolysis by real-time coupled assays as described in Experimental Procedures. The rate of ATP hydrolysis is followed by the negative linear decay of NADH disappearance (Figure 5D, green and gray traces), whereas the rate of ATP synthesis is measured by the positive slope of NADPH production (Figure 5D, blue, black, and red traces). As can be seen, the control $PdF_1F_O^{\Delta\zeta}$-ATPase activity (Figure 5D, green) was almost completely blocked (95% inhibition) by reconstitution with a molar excess of ζ subunit (Figure 5D, gray), consistent with the described function of ζ as total inhibitor of the PdF_1-ATPase (Zarco-Zavala et al., 2014). In marked contrast, the control PdF_1F_O-ATP synthase activity (Figure 5D, black trace) was not affected at all by the same molar excess of ζ (Figure 5D, red trace) that halted almost completely the $PdF_1F_O^{\Delta\zeta}$-ATPase activity (Figure 5D, gray trace). Indeed, the ATP synthase rates were essentially superimposed with or without previous reconstitution of the ζ subunit (Figure 5D, black and red traces). As an important blank control, the basal NADPH production in the presence of uncoupler (4 μM FCCP) and venturicidin (4 μg/mL) is indicated in blue in Figure 5D; this basal rate was subtracted from the black and red traces to obtain the net ATP synthesis rates. The experiments in Figure 5D show representative traces that were repeated at least three times, confirming clearly that the ζ subunit works as a unidirectional inhibitor of the PdF_1F_O-ATPase activity, because it does not inhibit the PdF_1F_O-ATP synthase activity at all.

Effect of the Δζ Mutation on the Intracellular ATP Concentration of *Paracoccus denitrificans*

In order to determine whether the unidirectional PdF_1F_O-ATPase inhibition exerted by ζ reflects on the cellular ATP concentrations, the PdWT, PdΔζ, and PdΔζ+ζ strains were grown in LB or succinate media to an absorbance of approximately 1.0 during the log phase, and the steady-state concentration of ATP was determined by the luciferin-luciferase assay (see Experimental Procedures). The results showed that, in LB, the concentration of intracellular ATP was about 4.5 mM, and it was very similar for all strains (PdWT, PdΔζ, and PdΔζ+ζ), with no significant differences between them (Figure 6A). In contrast, when the concentration of [ATP] was determined in cells grown in succinate, it was nearly 3-fold higher than in LB (Figure 6B), i.e., around 13.0 mM in the WT strain (PdWT), and this dropped significantly in the PdΔζ strain to about half (6.8 mM). Furthermore, this drop in [ATP] was restored to about 12 mM in the PdΔζ+ζ strain (Figure 6B). In summary, the key result here was that, in succinate, the PdΔζ mutant decreased its cellular [ATP] to about half that of the PdWT (Figure 6B), and this is accompanied by a slower growth rate for this mutant in succinate medium (Figure 2B). In addition, this lower [ATP] of the mutant was recovered in the PdΔζ+ζ complemented strain (Figure 6B), together with the restored growth in succinate, as compared with the PdWT strain (Figure 2B). Furthermore, the similar intracellular [ATP] in LB media found for all strains (Figure 6A) reflects the similar growth of PdWT, PdΔζ, and PdΔζ+ζ strains in LB (Figure 2A). In summary, regardless of the differences in net [ATP] concentrations in WT strains in LB or in succinate, it is clear that the growth curves (Figure 2), ATP synthesis, and ATP hydrolysis assays (Figures 3 and 5C), as well as the intracellular [ATP] determinations (Figure 6), support each other and confirm the role of the ζ subunit as unidirectional PdF_1F_O-ATPase inhibitor to favor ATP synthesis and cell growth in succinate respiratory media.

One may also wonder why the growth rate and the intracellular [ATP] are affected by the ζ deletion only in succinate media and not in LB (Figures 2B and 6B), if ATP comes mostly from the PdF_1F_O-ATP synthase in either medium. As indicated in the Supplemental Experimental Procedures, the Δζ knockout is non-deleterious in LB, probably because the $H^+PdF_1F_O^{\Delta\zeta}$-ATPase may be less activated than in succinate and/or because the cellular ATP pools could be restored in LB by alternative substrate-level phosphorylation pathways besides the Ox-Phos. In

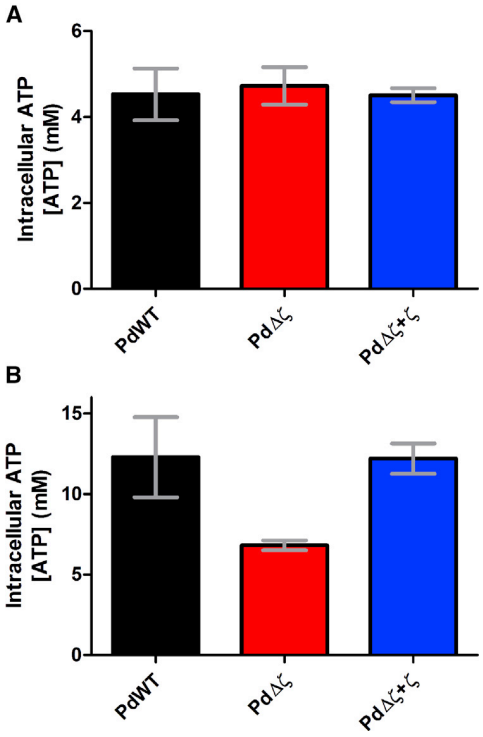

Figure 6. Determination of Intracellular ATP Concentration in PdWT, PdΔζ, and PdΔζ+ζ Strains

(A and B) The wild-type PdWT, the mutant lacking the ζ gene PdΔζ, and the complemented PdΔζ+ζ strains were separately grown to the log phase (OD of 1 at 600 nm) in LB or succinate medium at 30°C. At this point, cells were harvested by centrifugation (6,414 RCF), resuspended in 350 μL at a concentration of approximately 3.7×10^9 cells/mL, and diluted 1:10 in lysis buffer to be processed as described in the Experimental Procedures. ATP concentration was estimated by interpolation of sample data into a standard curve of ATP with a luciferin/luciferase kit. The figure shows the estimated intracellular ATP concentration in millimolar; (A) Bacterial strains grown in LB medium and (B) bacterial strains grown in succinate medium. The average of three experiments is shown with SD.

contrast, in succinate minimal medium, ATP seems to be synthesized exclusively by the PdF_1F_O-ATP synthase; therefore, here, the Δζ deletion has a stronger phenotypic effect because it transforms the essentially unidirectional forward-CW-rotating $H^+PdF_1F_O{}^{\zeta}$-ATP synthase into a bidirectional $H^+PdF_1F_O{}^{\Delta\zeta}$-ATPase, thus reverting the rotation of the nanomotor from the CW-ATP synthase to the CCW-ATPase turnover, which is the only source of cellular ATP in succinate media.

Model of the PdF_1F_O-ζ Complex with the ζ Subunit Working as the Pawl of a Ratchet to Selectively Block the CCW Rotor Gyration to Favor ATP Synthesis

In its final inhibitory position, the ζ subunit inserts its N-terminal α-helix (Figure 7, left panel, red) into the $\alpha_{DP}/\beta_{DP}/\gamma$ iterface and contacts the γ subunit thus blocking its rotation, but apparently in both senses, i.e., in the CW-ATP synthase and in the CCW-ATPase directions; however, according to the unidirectional effects of the ζ subunit, the PdF_1F_O-ζ complex is able to gyrate its central rotor in the CW-ATP synthesis direction, but not in the CCW direction of the PdF_1F_O-ATPase turnover (Figure 7, left panel). This implies that ζ works either *mechanically* or *conformationally* as the pawl of a ratchet blocking unidirectionally γ rotation, as previously proposed (García-Trejo et al., 2016). This ζ pawl favors the "forward" ATP synthesis turnover and the overall bacterial bioenergetics to improve oxidative cell growth (Figure 2B). On the other hand, the $PdF_1F_O{}^{\Delta\zeta}$ mutant lacking ζ rotates in both directions (CW and CCW) to carry out both coupled ATP synthesis and hydrolysis (Figure 7, right panel). In the model of Figure 7, the N terminus of ζ (red) interacts directly with the γ subunit (green), thus blocking γ rotation; however, in order to allow rotation in the CW-ATP synthase direction, this ζ N terminus can either be partially or completely separated from the $\alpha_{DP}/\beta_{DP}/\gamma$ interface as induced by the $\Delta\mu_{H+}$, thus working as a conformational pawl; alternatively, it can be kept in place allowing CW rotation but not CCW rotation without its release, thus working as a mechanical pawl-ratchet. Previous studies, including ours, had shown that the $\Delta\mu_{H+}$ induces an active F_1F_O-ATPase state (Fischer et al., 2000; Gómez-Puyou et al., 1979; Lippe et al., 1988; Pacheco-Moisés et al., 2000; Zharova and Vinogradov, 2004); therefore, the driving force of the $\Delta\mu_{H+}$ must be added to the ADP and P_i binding energies to drive CW rotation (Garcia, 2000; García et al., 1997; Okazaki and Hummer, 2013; Souid and Penefsky, 1995; Watanabe and Noji, 2014); therefore, $\Delta\mu_{H+}$ and ADP/P_i binding energies can be used either to separate the N terminus of ζ from the $\alpha_{DP}/\beta_{DP}/\gamma$ interface or to overcome the torque resistance of the $\gamma/\varepsilon/c_{12}$ rotor gyration imposed by the ζ N terminus kept in the $\alpha_{DP}/\beta_{DP}/\gamma$ interface. On the contrary and reverse CCW PdF_1F_O-ATPase turnover, the smaller rotational driving force induced only by ATP binding energy and hydrolysis, working uphill against the proton gradient will probably not be enough to drive $\gamma/\varepsilon/c_{12}$ CCW rotation with the ζ N terminus bound to its inhibitory place ($\gamma/\alpha_{DP}/\beta_{DP}$ interface; Figure 7A). This would be in concordance with a relatively high rotation torque resistance of the PdF_1F_O-$\gamma/\varepsilon/c_{12}$ central rotor (Figure 7), which will require both the ADP/P_i binding energies and the $\Delta\mu_{H+}$-driven proton flow to keep the PdF_1F_O-ATP synthase rotating in the CW direction, particularly in the presence of ζ. This could be similar, for instance, to the high torque of the unidirectional TA2.A1 ATP synthase (McMillan et al., 2016). At the moment, there is not enough experimental evidence to discern whether the ζ subunit works as a mechanical or conformational pawl. Our previous studies with *P. denitrificans* SBPs (Pacheco-Moisés et al., 2000) and other studies with submitochondrial particles (Dreyfus et al., 1981) have shown a partial exposure of endogenous ζ or IF_1 upon membrane energization, respectively, thus supporting the $\Delta\mu_{H+}$-induced conformational pawl-ratchet ζ mechanism. However, further work is necessary to resolve these details of the ζ pawl-ratchet mechanism.

Given the similarity between the ζ N terminus and the inhibitory domain of IF_1 mimicking IF_1 (García-Trejo et al., 2016; Zarco-Zavala et al., 2014), it is suitable to propose that at least mitochondrial IF_1 should also work as a unidirectional F_1F_O-ATPase inhibitor, although this pawl-ratchet mechanism may also extend to the bacterial ε subunit. Indeed, the unidirectional mechanism of IF_1 has been proposed before (Pullman and Monroy, 1963; Schwerzmann and Pedersen, 1986). However, this is

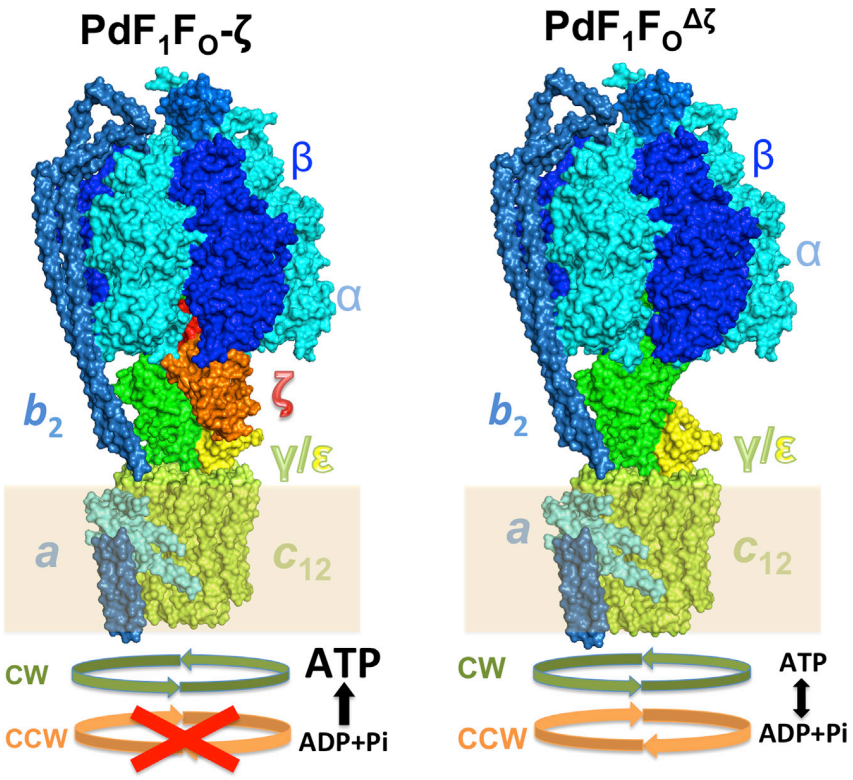

Figure 7. Structural Models of the PdF_1F_O-ζ and $PdF_1F_O^{\Delta\zeta}$ Complexes Showing the Inhibitory Binding Site and Unidirectional Pawl-Ratchet Mechanism of the ζ Subunit

The model constructed as indicated in the Supplemental Experimental Procedures shows the position of the N-terminal inhibitory domain of ζ (Zarco-Zavala et al., 2014) in red and the globular and C-terminal domain of ζ (in orange) bound into the $\alpha_{DP}/\beta_{DP}/\gamma$ interface in the left panel. The F_1-stator complex ($\alpha_3/\beta_3/\delta/b_2/a$) is shown in shades of blue. The $\gamma/\varepsilon/c_{12}$ rotor (in green and yellow) is unable to rotate in the counterclockwise (CCW) direction driving ATP hydrolysis but is able to rotate in the clockwise (CW) direction of ATP synthesis; the latter rotation is driven by the proton flow and gradient with or without partial release of the inhibitory ζ-N terminus; in either case, ζ works as a pawl-ratchet, blocking rotation of the $\gamma/\varepsilon/c_{12}$ rotor only in the CCW direction. In the right panel, the $PdF_1F_O^{\Delta\zeta}$ structure is shown after removal of the ζ subunit *in silico*. In the $PdF_1F_O^{\Delta\zeta}$ complex, the $\gamma/\varepsilon/c_{12}$ rotor is able to rotate in both CW and CCW directions; therefore, it can carry out both ATP synthesis and ATP hydrolysis according to the load of substrates and proton gradients. In summary, the ζ subunit favors ATP synthesis and, therefore, oxidative bacterial growth by working as a pawl-ratchet or unidirectional PdF_1F_O-ATPase inhibitor, thus making the PdF_1F_O-ζ complex a unidirectional ATP synthase.

controversial, since several studies point to bidirectional effects of IF_1 and ε, whereas other studies suggest that IF_1 and ε work as unidirectional inhibitors (García-Bermúdez et al., 2015; Gómez-Puyou et al., 1979; Iino et al., 2009; Masaike et al., 2006; Schwerzmann and Pedersen, 1986; Tsunoda et al., 2001). Moreover, a ratchet mechanism was first proposed for the *E. coli* ε subunit (Tsunoda et al., 2001), and similar to our present results with Pd-ζ, a recent short C-terminal deletion study of the *E. coli* ε inhibitory C terminus also showed detrimental effects on bacterial oxidative growth (Shah and Duncan, 2015). These studies suggest that all natural ATP synthase inhibitors (ε, ζ, and IF_1) may work through a similar unidirectional mechanism, since they bind to the same $\gamma/\alpha_{DP}/\beta_{DP}$ interface, named the "inhibition-general core region" (Shirakihara et al., 2015); however, further work will be required to ascertain whether ε, ζ, and IF_1 work with the same unidirectional mechanics. Meanwhile, the present work demonstrates that at least the ζ subunit of *P. denitrificans* and related α-proteobacteria works as a unidirectional pawl of a mechanical or conformational ratchet, blocking exclusively the PdF_1F_O-ATPase activity and, thus, favoring the PdF_1F_O-ATP synthase turnover, the overall cell bioenergetics, and bacterial oxidative growth.

Finally, this work establishes the biological function of a natural ATP synthase inhibitor; therefore, *P. denitrificans* and its natural PdF_1F_O-ATPase inhibitor ζ seem suitable models to shed light on these studies. Previously, the F_1F_O-ATPase inhibitory role of ζ has been demonstrated only *in vitro* (Morales-Ríos et al., 2010; Zarco-Zavala et al., 2014). Since the F_1F_O-ATPase is kinetically regulated by a number of natural intrinsic and extrinsic factors—for instance, inhibitory MgADP or activating oxyanions (Pacheco-Moisés et al., 2000, 2002; Zharova and Vinogradov, 2003, 2006a, 2006b)—it remained unclear whether these natural inhibitory proteins had a physiological F_1F_O-ATPase regulatory role *in vivo* or whether the ATP synthase was controlled more effectively by the other factors. This work demonstrates that the ζ subunit controls the inherent rotation of the α-proteobaterial ATP synthase nanomotor to improve the overall cell bioenergetics and oxidative growth. This result is important, because the fact that bacterial growth is affected by the direct control of the ζ subunit (Figure 2) adds support for taking advantage of the bacterial ATP synthase as a target for antimicrobial drug design. Moreover, the key role of ζ as a regulatory subunit demonstrated here explains the control mechanism of this ATP synthase and why this is an essentially undirectional ATP synthase and a poor or latent ATPase (Pacheco-Moisés et al., 2002; Pérez and Ferguson, 1990; Zharova and Vinogradov, 2003). Indeed, the ATP synthase of *P. denitrificans* has the highest ratio of ATP synthase/ATPase rates described so far (Pacheco-Moisés et al., 2002; Pérez and Ferguson, 1990; Zharova and Vinogradov, 2003). In this context, this work shows that the ζ subunit has a key role as a pawl-ratchet inhibitor to make of this enzyme from *P. denitrificans* a unidirectional ATP synthase. Further oncoming work will confirm whether mitochondrial IF_1 and inhibitory bacterial ε subunits have similar unidirectional pawl mechanisms and *in vivo* roles in nature as the ζ subunit does in α-proteobacteria.

EXPERIMENTAL PROCEDURES

Plasmids, Bacterial Strains, and Growth Conditions

The bacterial strains and plasmids used in this study are listed in Table S1. *Escherichia coli* strains DH5α, (Hanahan, 1983) and S17-1 (Simon et al., 1983) were grown at 37°C in LB medium. *P. denitrificans* strains Pd1222 (PdWT) [de Vries et al., 1989], PdΔζ, and PdΔζ+ζ were grown at 30°C in LB or succinate medium (Ludwig, 1986). Antibiotics, when used, were added at the following concentrations (in micrograms per milliliter): rifampicin (Rf), 50; kanamycin (Km), 50; gentamicin (Gm), 30; and ampicillin (Ap), 100.

Knockout Mutagenesis and DNA Isolation and Manipulation

To delete the ζ gene from the Pd1222 bacterial strain, we used homologous recombination to replace the ζ gene with a kanamycin-resistance marker (Figure S1). A suicide plasmid, pJQ200SK (Gm^R) (Pelicic et al., 1996), was instrumental to build the construct pFMMCJG-Δζ. *E. coli* S17-1 (see Table S1) was transformed, and the plasmid construct was transferred to the Pd1222 strain by conjugation. Details of DNA manipulation, the construct, and complementation of the mutant *P. denitrificans* Δζ (PdΔζ) are indicated in the Supplemental Experimental Procedures.

Growth Curves, Cell Lysate Preparations, Protein Quantification, SDS-PAGE, and Western Blotting

Standard methods for growth curves, protein quantification, SDS-PAGE, cell extracts, and western blotting were carried out as described previously (Zarco-Zavala et al., 2014) and/or detailed in the Supplemental Experimental Procedures.

PdF_1F_O-ATP Synthase Assays

The steady-state rates of ATP synthesis activity were determined with a coupled hexokinase/glucose-6-phosphate dehydrogenase (G6PDH) assay, as described previously (Cortés-Hernández et al., 2007). Details provided in the Supplemental Experimental Procedures.

Determination of Intracellular ATP Concentration

Intracellular ATP was measured using the ATP Bioluminescent Assay Kit (Sigma-Aldrich, St. Louis, MO, USA). Details are provided in the Supplemental Experimental Procedures.

Membrane Potential Estimated by Flow Cytometry

Membrane potential was determined by flow cytometry using a BacLight Bacterial Membrane Potential Kit (Molecular Probes/Thermo Fisher Scientific, Waltham, MA, USA). Details are explained in the Supplemental Experimental Procedures.

PdF_1F_O-ATPase Assays

The steady-state rates of ATP hydrolysis activity were determined with a coupled pyruvate kinase (PK)/lactate dehydrogenase (LDH) assay as described previously (Cortés-Hernández et al., 2007). Details are described in the Supplemental Experimental Procedures.

Purification of PdF_1

Purifications of the PdF_1 fraction from Pd1222 (PdWT) and PdΔζ were obtained using chloroform extraction from inside-out vesicles of each strain as described previously (Zarco-Zavala et al., 2014), with modifications described in the Supplemental Experimental Procedures.

Inhibition Assays PdF_1 and PdF_1F_O with Reconstituted ζ Subunit

Reconstitution of the recombinant ζ subunit in PdF_1 and PdF_1F_O-ATPase complexes were carried out as described previously (Zarco-Zavala et al., 2014) and detailed in the Supplemental Experimental Procedures.

Membrane Energization of *P. denitrificans* Inverted Membranes Evidenced by ACMA Fluorescence Quenching

Succinate-driven or ATP-driven membrane energization of SBP was evidenced by the fluorescence quenching of 9-amino-6-chloro-2-methoxyacridine (ACMA), as described previously (Ogilvie et al., 1997), with details explained in the Supplemental Experimental Procedures.

SUPPLEMENTAL INFORMATION

Supplemental Information includes Supplemental Experimental Procedures, four figures, and two tables and can be found with this article online at https://doi.org/10.1016/j.celrep.2017.12.106.

ACKNOWLEDGMENTS

This work was supported by grants from México (CONACyT) (CB-2011-01-167622) and U.N.A.M. (DGAPA) (PAPIIT- IN221216) (both to J.J.G.-T.) and partially funded by grants CONACyT 239487 and UNAM-DGAPA-PAPIIT IN204015 (both to S.U.-C.). We acknowledge Professors Alejandro Fernández-Velasco and Georgina Garza-Ramos for kindly making their fluorometer available to us. We acknowledge Héctor Adan Martínez-Torres for buffers and media preparation. This work is part of the PhD thesis of F.M.-H. at the "Programa de Maestría y Doctorado en Ciencias Bioquímicas de la Universidad Nacional Autónoma de México (U.N.A.M.), with J.J.G.-T. as PhD advisor. F.M.-H. was supported by CONACYT PhD Fellowship no. 277245, and M.Z.-Z. was supported by CONACyT Fund I0010 Fellowship no. 277592. We thank the LABNALCIT-UNAM for the technical support, acquisition, and processing of flow cytometry data, particularly Dr. Gloria Soldevila; Dr. Andrea Bedoya; Carlos Castellanos-Barba, MSc; Roxana Olguín-Alor, MSc; and Erick Espindola, MSc. Monoclonals anti-β and anti-SD70 were kind gifts of Prof. Roderick A. Capaldi. $DiOC_2(3)$ was kindly provided by Prof. Teresita Padilla-Benavides. We acknowledge Leslie Olmedo-Nieva for her kind help on the design of figures and tables. The logistic support of Héctor Mendoza and Concepción García-Ramírez are also acknowledged. The editor and reviewers are also deeply acknowledged; their excellent work improved the final version of this paper.

This work is dedicated to the memory of Prof. Armando Gómez-Puyou for his major contributions to Bioenergetics, ATP synthase, and the structure and function of proteins and for being one of the most outstanding scientists from U.N.A.M. and México.

AUTHOR CONTRIBUTIONS

F.M.-H. designed the primers; carried out the molecular biology experiments of the Δζ construction, the growth curves of all *P. denitrificans* strains, the ACMA and $DiOC_2(3)$ membrane potential assays by fluorometry and flow cytometry, and the [ATP] determinations; purified the PdF_1^{WT} and $PdF_1^{\Delta\zeta}$ ATPases; and wrote the first preliminary draft. A.P.-O. assisted in the construction of the PdΔζ mutant. M.A.C. designed the PdΔζ construction strategy, provided the plasmids, and advised on the molecular biology experiments. M.Z.-Z. purified the recombinant ζ subunit. R.O. and C.P.-S. assisted on the microbiology and preparation of growth media. E.E.-S. and S.U.-C. assisted with and carried out the ATP determinations by luciferin-luciferase ATP assay. J.J.G.-T. designed the research, helped with the PdΔζ design and construction, carried out the PdF_1F_O-ATP synthesis and PdF_1F_O-ATP hydrolysis assays, made the experiments of membrane energization by ACMA fluorescence quenching, helped in the determination and calculations of intracellular [ATP], constructed the PdF_1F_O-ζ structural model, advised the PhD thesis of F.M.-H., and wrote the paper.

DECLARATION OF INTERESTS

The authors declare no conflict of interests. J.J.G.-T., M.A.C., and F.M.-H. are waiting for a pending patent: MX/a/2017/016448.

Received: June 8, 2017
Revised: September 9, 2017
Accepted: December 28, 2017
Published: January 23, 2018

REFERENCES

Berry, E.A., and Trumpower, B.L. (1985). Isolation of ubiquinol oxidase from *Paracoccus denitrificans* and resolution into cytochrome bc_1 and cytochrome c-aa_3 complexes. J. Biol. Chem. *260*, 2458–2467.

Boyer, P.D. (1997). The ATP synthase–a splendid molecular machine. Annu. Rev. Biochem. *66*, 717–749.

Cabezón, E., Montgomery, M.G., Leslie, A.G., and Walker, J.E. (2003). The structure of bovine F1-ATPase in complex with its regulatory protein IF1. Nat. Struct. Biol. *10*, 744–750.

Cingolani, G., and Duncan, T.M. (2011). Structure of the ATP synthase catalytic complex (F(1)) from *Escherichia coli* in an autoinhibited conformation. Nat. Struct. Mol. Biol. *18*, 701–707.

Cortés-Hernández, P., Vázquez-Memije, M.E., and García, J.J. (2007). *ATP6* homoplasmic mutations inhibit and destabilize the human F_1F_0-ATP synthase without preventing enzyme assembly and oligomerization. J. Biol. Chem. *282*, 1051–1058.

Cox, J.C., Ingledew, W.J., Haddock, B.A., and Lawford, H.G. (1978). The variable cytochrome content of *Paracoccus denitrificans* grown aerobically under different conditions. FEBS Lett. *93*, 261–265.

de la Rosa-Morales, F. (2005). Composición de Subunidades y Mecanismo de Regulación de la F1FoATP Sintasa de *Paracoccus denitrificans* [Composition of subunits and mechanism of regulation of the F_1F_o-ATP synthase of *Paracoccus denitrificans*]. Masters thesis. Posgrado en Ciencias Biólogicas (Biología Experimental), Facultad de Ciencias [Postgraduate Program in Biological Sciences (Experimental Biology), Faculty of Sciences] (Direccion General de Bibliotecas: Universidad Nacional Autónoma de Mexico [U.N.A.M.]). http://132.248.9.195/ptd2005/00377/0346694/Index.html.

de Vries, G.E., Harms, N., Hoogendijk, J., and Stouthamer, A.H. (1989). Isolation and characterization of *Paracoccus denitrificans* mutants with increased conjugation frequencies and pleiotropic loss of a (nGATCn) DNA-modifying property. Arch. Microbiol. *152*, 52–57.

Dienhart, M., Pfeiffer, K., Schagger, H., and Stuart, R.A. (2002). Formation of the yeast F_1F_0-ATP synthase dimeric complex does not require the ATPase inhibitor protein, Inh1. J. Biol. Chem. *277*, 39289–39295.

Dreyfus, G., Gómez-Puyou, A., and Iuena de Gómez-Puyou, M. (1981). Electrochemical gradient induced displacement of the natural ATPase inhibitor protein from mitochondrial ATPase as directed by antibodies against the inhibitor protein. Biochem. Biophys. Res. Commun. *100*, 400–406.

Duncan, T.M., Bulygin, V.V., Zhou, Y., Hutcheon, M.L., and Cross, R.L. (1995). Rotation of subunits during catalysis by *Escherichia coli* F_1-ATPase. Proc. Natl. Acad. Sci. USA *92*, 10964–10968.

Fernández-Cárdenas, L.P., Villanueva-Chimal, E., Salinas, L.S., José-Nuñez, C., Tuena de Gómez Puyou, M., and Navarro, R.E. (2017). *Caenorhabditis elegans* ATPase inhibitor factor 1 (IF_1) MAI-2 preserves the mitochondrial membrane potential ($\Delta\psi m$) and is important to induce germ cell apoptosis. PLoS ONE *12*, e0181984.

Fischer, S., Graber, P., and Turina, P. (2000). The activity of the ATP synthase from *Escherichia coli* is regulated by the transmembrane proton motive force. J. Biol. Chem. *275*, 30157–30162.

Garcia, J.J. (2000). In The F_0F_1-ATP Synthase: Binding Energy, Coupling and Rotational Catalysis, First Edition (Trivandrum: Transworld Research Network).

García, J.J., Gómez-Puyou, A., Maldonado, E., and Tuena De Gómez-Puyou, M. (1997). Acceleration of unisite catalysis of mitochondrial F1-adenosinetriphosphatase by ATP, ADP and pyrophosphate–hydrolysis and release of the previously bound [gamma-32P]ATP. Eur. J. Biochem. *249*, 622–629.

García, J.J., Morales-Ríos, E., Cortés-Hernandez, P., and Rodríguez-Zavala, J.S. (2006). The inhibitor protein (IF1) promotes dimerization of the mitochondrial F1F0-ATP synthase. Biochemistry *45*, 12695–12703.

García-Bermúdez, J., Sánchez-Aragó, M., Soldevilla, B., Del Arco, A., Nuevo-Tapioles, C., and Cuezva, J.M. (2015). PKA phosphorylates the ATPase inhibitory factor 1 and inactivates its capacity to bind and inhibit the mitochondrial H(+)-ATP synthase. Cell Rep. *12*, 2143–2155.

García-Trejo, J.J., Zarco-Zavala, M., Mendoza-Hoffmann, F., Hernández-Luna, E., Ortega, R., and Mendoza-Hernández, G. (2016). The inhibitory mechanism of the ζ subunit of the F1FO-ATPase nanomotor of *Paracoccus denitrificans* and related α-proteobacteria. J. Biol. Chem. *291*, 538–546.

Gómez-Puyou, A., de Gómez-Puyou, M.T., and Ernster, L. (1979). Inactive to active transitions of the mitochondrial ATPase complex as controlled by the ATPase inhibitor. Biochim. Biophys. Acta *547*, 252–257.

Hanahan, D. (1983). Studies on transformation of *Escherichia coli* with plasmids. J. Mol. Biol. *166*, 557–580.

Hashimoto, T., Yoshida, Y., and Tagawa, K. (1983). Binding properties of an intrinsic ATPase inhibitor and occurrence in yeast mitochondria of a protein factor which stabilizes and facilitates the binding of the inhibitor to F_1F_0-ATPase. J. Biochem. *94*, 715–720.

Hashimoto, T., Yoshida, Y., and Tagawa, K. (1984). Purification and properties of factors in yeast mitochondria stabilizing the F_1F_0-ATPase-inhibitor complex. J. Biochem. *95*, 131–136.

Hashimoto, T., Yoshida, Y., and Tagawa, K. (1987). Binding properties of 9K protein to F1-ATPase: a counterpart ligand to the ATPase inhibitor. J. Biochem. *102*, 685–692.

Hashimoto, T., Yoshida, Y., and Tagawa, K. (1990a). Regulatory proteins of F1F0-ATPase: role of ATPase inhibitor. J. Bioenerg. Biomembr. *22*, 27–38.

Hashimoto, T., Yoshida, Y., and Tagawa, K. (1990b). Simultaneous bindings of ATPase inhibitor and 9K protein to F_1F_0-ATPase in the presence of 15K protein in yeast mitochondria. J. Biochem. *108*, 17–20.

Hederstedt, L. (2002). Succinate:quinone oxidoreductase in the bacteria *Paracoccus denitrificans* and *Bacillus subtilis*. Biochim. Biophys. Acta *1553*, 74–83.

Iino, R., Hasegawa, R., Tabata, K.V., and Noji, H. (2009). Mechanism of inhibition by C-terminal alpha-helices of the epsilon subunit of *Escherichia coli* F_oF_1-ATP synthase. J. Biol. Chem. *284*, 17457–17464.

Iwata, S., Ostermeier, C., Ludwig, B., and Michel, H. (1995). Structure at 2.8 A resolution of cytochrome *c* oxidase from *Paracoccus denitrificans*. Nature *376*, 660–669.

Jensen, P.R., Michelsen, O., and Westerhoff, H.V. (1993). Control analysis of the dependence of *Escherichia coli* physiology on the H^+-ATPase. Proc. Natl. Acad. Sci. USA *90*, 8068–8072.

John, P., and Whatley, F.R. (1975). *Paracoccus denitrificans* and the evolutionary origin of the mitochondrion. Nature *254*, 495–498.

Kleinschroth, T., Castellani, M., Trinh, C.H., Morgner, N., Brutschy, B., Ludwig, B., and Hunte, C. (2011). X-ray structure of the dimeric cytochrome bc(1) complex from the soil bacterium *Paracoccus denitrificans* at 2.7-Å resolution. Biochim. Biophys. Acta *1807*, 1606–1615.

Klionsky, D.J., Brusilow, W.S., and Simoni, R.D. (1984). In vivo evidence for the role of the epsilon subunit as an inhibitor of the proton-translocating ATPase of *Escherichia coli*. J. Bacteriol. *160*, 1055–1060.

Kovach, M.E., Elzer, P.H., Hill, D.S., Robertson, G.T., Farris, M.A., Roop, R.M., 2nd, and Peterson, K.M. (1995). Four new derivatives of the broad-host-range cloning vector pBBR1MCS, carrying different antibiotic-resistance cassettes. Gene *166*, 175–176.

Ku, C., Nelson-Sathi, S., Roettger, M., Sousa, F.L., Lockhart, P.J., Bryant, D., Hazkani-Covo, E., McInerney, J.O., Landan, G., and Martin, W.F. (2015). Endosymbiotic origin and differential loss of eukaryotic genes. Nature *524*, 427–432.

Lippe, G., Sorgato, M.C., and Harris, D.A. (1988). Kinetics of the release of the mitochondrial inhibitor protein. Correlation with synthesis and hydrolysis of ATP. Biochim. Biophys. Acta *933*, 1–11.

Lu, Y.M., Miyazawa, K., Yamaguchi, K., Nowaki, K., Iwatsuki, H., Wakamatsu, Y., Ichikawa, N., and Hashimoto, T. (2001). Deletion of mitochondrial ATPase inhibitor in the yeast *Saccharomyces cerevisiae* decreased cellular and mitochondrial ATP levels under non-nutritional conditions and induced a respiration-deficient cell-type. J. Biochem. *130*, 873–878.

Ludwig, B. (1986). Cytochrome *c* oxidase from *Paracoccus denitrificans*. Methods Enzymol. *126*, 153–159.

Ludwig, B., and Schatz, G. (1980). A two-subunit cytochrome *c* oxidase (cytochrome aa3) from *Paracoccus dentrificans*. Proc. Natl. Acad. Sci. USA *77*, 196–200.

Margulis, L., and Chapman, M.J. (1998). Endosymbioses: cyclical and permanent in evolution. Trends Microbiol. *6*, 342–345, discussion 345–346.

Masaike, T., Suzuki, T., Tsunoda, S.P., Konno, H., and Yoshida, M. (2006). Probing conformations of the beta subunit of F0F1-ATP synthase in catalysis. Biochem. Biophys. Res. Commun. *342*, 800–807.

McMillan, D.G., Watanabe, R., Ueno, H., Cook, G.M., and Noji, H. (2016). Biophysical characterization of a thermoalkaliphilic molecular motor with a high stepping torque gives insight into evolutionary ATP synthase adaptation. J. Biol. Chem. *291*, 23965–23977.

Minauro-Sanmiguel, F., Bravo, C., and García, J.J. (2002). Cross-linking of the endogenous inhibitor protein (IF1) with rotor (gamma, epsilon) and stator (alpha) subunits of the mitochondrial ATP synthase. J. Bioenerg. Biomembr. *34*, 433–443.

Mitchell, P. (1961). Coupling of phosphorylation to electron and hydrogen transfer by a chemi-osmotic type of mechanism. Nature *191*, 144–148.

Morales-Ríos, E., de la Rosa-Morales, F., Mendoza-Hernández, G., Rodríguez-Zavala, J.S., Celis, H., Zarco-Zavala, M., and García-Trejo, J.J. (2010). A novel 11-kDa inhibitory subunit in the F_1F_O ATP synthase of *Paracoccus denitrificans* and related alpha-proteobacteria. FASEB J. *24*, 599–608.

Morales-Ríos, E., Montgomery, M.G., Leslie, A.G., García-Trejo, J.J., and Walker, J.E. (2015a). Structure of a catalytic dimer of the α- and β-subunits of the F-ATPase from *Paracoccus denitrificans* at 2.3 Å resolution. Acta Crystallogr. F Struct. Biol. Commun. *71*, 1309–1317.

Morales-Rios, E., Montgomery, M.G., Leslie, A.G., and Walker, J.E. (2015b). Structure of ATP synthase from *Paracoccus denitrificans* determined by X-ray crystallography at 4.0 Å resolution. Proc. Natl. Acad. Sci. USA *112*, 13231–13236.

Nakamura, J., Fujikawa, M., and Yoshida, M. (2013). IF1, a natural inhibitor of mitochondrial ATP synthase, is not essential for the normal growth and breeding of mice. Biosci. Rep. *33*, e00067.

Noji, H., Yasuda, R., Yoshida, M., and Kinosita, K., Jr. (1997). Direct observation of the rotation of F1-ATPase. Nature *386*, 299–302.

Novo, D., Perlmutter, N.G., Hunt, R.H., and Shapiro, H.M. (1999). Accurate flow cytometric membrane potential measurement in bacteria using diethyloxacarbocyanine and a ratiometric technique. Cytometry *35*, 55–63.

Ogilvie, I., Aggeler, R., and Capaldi, R.A. (1997). Cross-linking of the delta subunit to one of the three alpha subunits has no effect on functioning, as expected if delta is a part of the stator that links the F_1 and F_0 parts of the *Escherichia coli* ATP synthase. J. Biol. Chem. *272*, 16652–16656.

Okazaki, K., and Hummer, G. (2013). Phosphate release coupled to rotary motion of F1-ATPase. Proc. Natl. Acad. Sci. USA *110*, 16468–16473.

Pacheco-Moisés, F., García, J.J., Rodríguez-Zavala, J.S., and Moreno-Sánchez, R. (2000). Sulfite and membrane energization induce two different active states of the *Paracoccus denitrificans* F_0F_1-ATPase. Eur. J. Biochem. *267*, 993–1000.

Pacheco-Moisés, F., Minauro-Sanmiguel, F., Bravo, C., and García, J.J. (2002). Sulfite inhibits the F1F0-ATP synthase and activates the F1F0-ATPase of *Paracoccus denitrificans*. J. Bioenerg. Biomembr. *34*, 269–278.

Pelicic, V., Reyrat, J.M., and Gicquel, B. (1996). Expression of the *Bacillus subtilis sacB* gene confers sucrose sensitivity on mycobacteria. J. Bacteriol. *178*, 1197–1199.

Pennoyer, J.D., Ohnishi, T., and Trumpower, B.L. (1988). Purification and properties of succinate-ubiquinone oxidoreductase complex from *Paracoccus denitrificans*. Biochim. Biophys. Acta *935*, 195–207.

Pérez, J.A., and Ferguson, S.J. (1990). Kinetics of oxidative phosphorylation in Paracoccus denitrificans. 1. Mechanism of ATP synthesis at the active site(s) of F0F1-ATPase. Biochemistry *29*, 10503–10518.

Pullman, M.E., and Monroy, G.C. (1963). A naturally occurring inhibitor of mitochondrial adenosine triphosphatase. J. Biol. Chem. *238*, 3762–3769.

Rondelez, Y., Tresset, G., Nakashima, T., Kato-Yamada, Y., Fujita, H., Takeuchi, S., and Noji, H. (2005). Highly coupled ATP synthesis by F1-ATPase single molecules. Nature *433*, 773–777.

Sabbert, D., Engelbrecht, S., and Junge, W. (1996). Intersubunit rotation in active F-ATPase. Nature *381*, 623–625.

Scholes, P.B., and Smith, L. (1968). Composition and properties of the membrane-bound respiratory chain system of *Micrococcus denitrificans*. Biochim. Biophys. Acta *153*, 363–375.

Schwerzmann, K., and Pedersen, P.L. (1986). Regulation of the mitochondrial ATP synthase/ATPase complex. Arch. Biochem. Biophys. *250*, 1–18.

Serrano, P., Geralt, M., Mohanty, B., and Wüthrich, K. (2014). NMR structures of α-proteobacterial ATPase-regulating ζ-subunits. J. Mol. Biol. *426*, 2547–2553.

Shah, N.B., and Duncan, T.M. (2015). Aerobic growth of *Escherichia coli* is reduced, and ATP synthesis is selectively inhibited when five C-terminal residues are deleted from the E subunit of ATP synthase. J. Biol. Chem. *290*, 21032–21041.

Shirakihara, Y., Shiratori, A., Tanikawa, H., Nakasako, M., Yoshida, M., and Suzuki, T. (2015). Structure of a thermophilic F1-ATPase inhibited by an ε-subunit: deeper insight into the ε-inhibition mechanism. FEBS J. *282*, 2895–2913.

Simon, R., Priefer, U., and Pühler, A. (1983). A broad host range mobilization system for *in vivo* genetic engineering: transposon mutagenesis in Gram negative bacteria. Nat. Biotechnol. *1*, 784–791.

Souid, A.K., and Penefsky, H.S. (1995). Energetics of ATP dissociation from the mitochondrial ATPase during oxidative phosphorylation. J. Biol. Chem. *270*, 9074–9082.

Sternweis, P.C., and Smith, J.B. (1980). Characterization of the inhibitory (epsilon) subunit of the proton-translocating adenosine triphosphatase from *Escherichia coli*. Biochemistry *19*, 526–531.

Tsunoda, S.P., Rodgers, A.J., Aggeler, R., Wilce, M.C., Yoshida, M., and Capaldi, R.A. (2001). Large conformational changes of the epsilon subunit in the bacterial F1F0 ATP synthase provide a ratchet action to regulate this rotary motor enzyme. Proc. Natl. Acad. Sci. USA *98*, 6560–6564.

Watanabe, R., and Noji, H. (2014). Timing of inorganic phosphate release modulates the catalytic activity of ATP-driven rotary motor protein. Nat. Commun. *5*, 3486.

Yagi, T. (1986). Purification and characterization of NADH dehydrogenase complex from *Paracoccus denitrificans*. Arch. Biochem. Biophys. *250*, 302–311.

Zarco-Zavala, M., Morales-Ríos, E., Serrano-Navarro, P., Wüthrich, K., Mendoza-Hernández, G., Ramírez-Silva, L., and García-Trejo, J.J. (2012). Corrigendum to "The ζ subunit of the α-proteobacterial F1FO-ATP synthase in Paracoccus denitrificans: A novel control mechanism of the central rotor.". Biochim. Biophys. Acta *1827*, 60.

Zarco-Zavala, M., Morales-Ríos, E., Mendoza-Hernández, G., Ramírez-Silva, L., Pérez-Hernández, G., and García-Trejo, J.J. (2014). The ζ subunit of the F1FO-ATP synthase of α-proteobacteria controls rotation of the nanomotor with a different structure. FASEB J. *28*, 2146–2157.

Zharova, T.V., and Vinogradov, A.D. (2003). Proton-translocating ATP-synthase of *Paracoccus denitrificans*: ATP-hydrolytic activity. Biochemistry (Mosc.) *68*, 1101–1108.

Zharova, T.V., and Vinogradov, A.D. (2004). Energy-dependent transformation of F_o•F_1-ATPase in *Paracoccus denitrificans* plasma membranes. J. Biol. Chem. *279*, 12319–12324.

Zharova, T.V., and Vinogradov, A.D. (2006a). Energy-linked binding of P_i is required for continuous steady-state proton-translocating ATP hydrolysis catalyzed by F_o•F_1 ATP synthase. Biochemistry *45*, 14552–14558.

Zharova, T.V., and Vinogradov, A.D. (2006b). Requirement of medium ADP for the steady-state hydrolysis of ATP by the proton-translocating *Paracoccus denitrificans* F_o•F_1-ATP synthase. Biochim. Biophys. Acta *1757*, 304–310.

Journal of Bioenergetics and Biomembranes
https://doi.org/10.1007/s10863-018-9773-9

MINI-REVIEW

Control of rotation of the F_1F_O-ATP synthase nanomotor by an inhibitory α-helix from unfolded ε or intrinsically disordered ζ and IF_1 proteins

Francisco Mendoza-Hoffmann[1] · Mariel Zarco-Zavala[2] · Raquel Ortega[1] · José J. García-Trejo[1]

Received: 8 May 2018 / Accepted: 13 September 2018

Abstract

The ATP synthase is a ubiquitous nanomotor that fuels life by the synthesis of the chemical energy of ATP. In order to synthesize ATP, this enzyme is capable of rotating its central rotor in a reversible manner. In the clockwise (CW) direction, it functions as ATP synthase, while in counter clockwise (CCW) sense it functions as an proton pumping ATPase. In bacteria and mitochondria, there are two known canonical natural inhibitor proteins, namely the ε and IF_1 subunits. These proteins regulate the CCW F_1F_O-ATPase activity by blocking γ subunit rotation at the $\alpha_{DP}/\beta_{DP}/\gamma$ subunit interface in the F_1 domain. Recently, we discovered a unique natural F_1-ATPase inhibitor in *Paracoccus denitrificans* and related α-proteobacteria denoted the ζ subunit. Here, we compare the functional and structural mechanisms of ε, IF_1, and ζ, and using the current data in the field, it is evident that all three regulatory proteins interact with the $\alpha_{DP}/\beta_{DP}/\gamma$ interface of the F_1-ATPase. In order to exert inhibition, IF_1 and ζ contain an intrinsically disordered N-terminal protein region (IDPr) that folds into an α-helix when inserted in the $\alpha_{DP}/\beta_{DP}/\gamma$ interface. In this context, we revised here the mechanism and role of the ζ subunit as a unidirectional F-ATPase inhibitor blocking exclusively the CCW F_1F_O-ATPase rotation, without affecting the CW-F_1F_O-ATP synthase turnover. In summary, the ζ subunit has a mode of action similar to mitochondrial IF_1, but in α-proteobacteria. The structural and functional implications of these intrinsically disordered ζ and IF_1 inhibitors are discussed to shed light on the control mechanisms of the ATP synthase nanomotor from an evolutionary perspective.

Keywords ATP synthase · Natural inhibitor · ζ subunit · *Paracoccus denitrificans* · Pawl · Ratchet · Instrisically disordered

Introduction

Adenosine triphosphate (ATP) is the main biological energy currency used by all organisms to carry out biological processes (Hanson 1989; Kamerlin et al. 2013; Knowles 1980). To synthesize ATP, organisms need to condense adenosine diphosphate (ADP) with inorganic phosphate (Pi). There are several metabolic pathways that synthesize ATP such as glycolysis (Embden-Myerhof-Parnas pathway) (Bonora et al. 2012; Cori 1983; Fothergill-Gilmore and Michels 1993), the Entner-Doudoroff pathway (Conway 1992; Entner and Doudoroff 1952) and the Tricarboxylic acid cycle (Krebs cycle) (Akram 2014; Bonora et al. 2012; Krebs and Johnson 1980) among others. Nevertheless, none of these metabolic pathways produce ATP as efficiently as oxidative phosphorylation and photophosphorylation (Boyer et al. 1977). Oxidative phosphorylation and photophosphorylation have one thing in common, they use the same enzyme to synthesize ATP: the ATP synthase (Boyer 1997; Noji and Yoshida 2001; von Ballmoos et al. 2009; Walker 2013). The F_O part of the ATP synthase is embedded in a membrane, for the ATP synthase to function optimally there needs to be a higher concentration of protons (H^+) (in some cases sodium Na^+) on one side of the membrane than on the other side of the membrane. This higher concentration of protons or sodium on one side of the membrane is known as an electrochemical gradient and it is conceived as a proton or sodium motive force ($\Delta\tilde{\mu}^+$) as it is explained in the chemiosmotic theory (Mitchell 1961). The electrochemical gradient is generated by the electron transport chain complexes as they pump protons/sodium ions across the membrane while they are transferring electrons from an electron donor to the final electron acceptor (Mitchell 1961). Once

✉ José J. García-Trejo
jjgartre@unam.mx

[1] Departamento de Biología, Facultad de Química, Ciudad Universitaria, Universidad Nacional Autónoma de México (U.N.A.M.), Circuito Escolar s/n. Laboratorio 203, Edificio "F"., Delegación Coyoacán, 04510 Mexico City, CP, Mexico

[2] Department of Applied Chemistry, Graduate School of Engineering, The University of Tokyo, Tokyo 113-8656, Japan

Published online: 28 September 2018

the electrochemical gradient is generated, then protons/sodium ions can flow across two hemicanals of the ATP synthase formed by the interface between the *a* subunit and *c*-subunit proteolipid ring in the F_O domain in F-type ATP synthases (Fillingame and Steed 2014). This, in turn produces a mechanical motion in the enzyme that culminates in the synthesis of ATP (Boyer 1997; Noji and Yoshida 2001; von Ballmoos et al. 2009; Walker 2013).

Types of ATP synthases

There are two types of ATP synthases, the F-type and the A-type (McMillan et al. 2011; Muench et al. 2011). The F-type ATP synthases are present in two domains of life: Eukarya (mitochondria and chloroplast) and Bacteria. While the A-type ATP synthases are present mostly in the third domain of life: Archaea. Although, in some rare cases, the A-type ATP synthases are also present in bacteria. This is the case of some bacterial species belonging to the following lineages: clostridia, chlamydiae, deinococci, fibrobacteres, spirochaetaceae, synergistetes and mollicutes (Koumandow and Kossida 2014; Müller and Grüber 2003). Although the F-type and the A-type ATP synthases have the same function and a similar overall rotor/stator archicture, they have differences in their detailed structure. The A-Type ATP synthases, for instance, have two peripheral stalks (Nakanishi et al. 2018), whereas the F-type ATP synthases have only one. These A-Type ATP synthases are evolutively closer to the eukaryotic V-Type ATPases than to the F-Type ATP synthases. The V-Type ATPases, in contrast, lack the ability to synthesize ATP, and function only as ATP-driven primary proton pumps (Harrison and Muench 2018; Lau and Rubinstein 2012; Muench et al. 2011). In this review we will only focus on the F-Type ATP synthases (F_1F_O-ATP synthases).

Composition of the F-type ATP synthases

F_1F_O-ATP synthases as their name implies, are composed of two sectors, the F_1 and F_O. The F_1 sector is a water soluble portion and it is the catalytic entity of the enzyme (Kagawa and Racker 1966). The F_1 portion is exposed to the aqueous phase of the cell cytoplasm, the mitochondrial matrix, or the stroma in bacteria, mitochondria, and chloroplasts respectively. The F_O domain is hydrophobic and it is embedded into the cytoplasmic membrane, the internal mitochondrial membrane, or the thylakoid membrane in bacteria, mitochondria, and chloroplasts respectively (Fillingame and Steed 2014). The basic structure of the F_1F_O-ATP synthase discovered to date is common to all of the ATP synthases and composed of 8 canonical subunits (Table 1 and Fig. 1a) (García-Trejo and Morales-Ríos 2008). The simplest F_1F_O-ATP synthase's structures are the ones present in bacteria (García-Trejo and Morales-Ríos 2008; Sobti et al. 2016) and chloroplast (Groth and Pohl 2001), and are composed of only 8 subunits (Table 1 and Fig. 1a). In these complexes, the core F_1 fraction is composed of 5 subunits: α, β, γ, δ and ε, whereas the F_O sector is composed of 3 essential subunits: *a*, *b*, and *c* (Table 1 and Fig. 1a). The F_1F_O-ATP synthases of most bacteria like *E. coli* (Sobti et al. 2016) and *Bacillus* PS3 (Shirakihara et al. 2015b) are conformed of only these 8 canonical subunits However, at the moment there is an exemption in α-proteobacteria, here their F_1 portion has an additional subunit called ζ (Table 1 and Fig. 1b) (de la Rosa-Morales 2005; Morales-Rios et al. 2010; Zarco-Zavala et al. 2014). The mitochondrial F-type ATP synthases are structurally more complex as they are composed of not only the 8 canonical subunits but they have 8 or more additional supernumerary subunits distributed between the F_1 and F_O sectors (Table 1). The supernumerary subunits of the mitochondrial enzyme such as the b, i/j, k, e, and IF_1 (described below) help in the dimerization and oligomerization of the F_1F_O-ATP synthase that shape the mitochondrial cristae (Allen 1995; Arnold et al. 1998; Arselin et al. 2003; Arselin et al. 2004; García et al. 2006; García-Trejo and Morales-Ríos 2008; Guo et al. 2017; Paumard et al. 2002).

Synthesis of ATP by the F_1F_O-ATP synthases

The F_O nanomotor

As described above, the F_1F_O-ATP synthase uses an electrochemical gradient in order to synthesize ATP (Boyer et al. 1977; Mitchell 1961). Through two hemicanals in the F_O portion of the ATP synthase, protons (H^+) or sodium (Na^+) ions are conducted from the side of the membrane that has a higher concentration of H^+ or Na^+ (known as the P side) to the other side of the membrane that has a lower ion concentration (H^+ or Na^+, known as the N side) (Elston et al. 1998; Fillingame and Steed 2014). These hemicanals are in the interface of the *c* subunit ring and the *a* subunit (Fig. 2). One hemicanal is in the bottom of the interface and the other is in the upper part of the interface (looking from the bottom of the F_1F_O).

This ion transport process is best described in H^+ coupled F_1F_O ATP synthases and here we describe the proposed mechanism of H^+ transfer for ATP synthesis. At the mouth of the interface on the P-side of the membrane in the *a* subunit there is a histidine in *E. coli* (aH^{245}) or lysine in alkaliphiles (aK^{180}), which have been shown to have a role in proton capture. After proton capture, H^+ are able to pass into the junction between the 2 *a*/*c* hemicanals. At the interface of the *c* ring and the *a* subunit there is an interaction of a negative charge and a positive charge (Elston et al. 1998; Fillingame and Steed 2014). The negative charge comes from a highly conserved carboxylate of an aspartate or glutamate of 1 *c*

Table 1 Bacterial, Chloroplast, and α-proteobacterial enzymes have 8 subunits, but the mitochondrial enzyme has 16 or more subunits

Subunit composition of the F_1F_O-ATP synthase from different organisms.				
	Bacteria	Chloroplast	α-proteobacteria	Mitochondria
F_1	α_3	α_3	α_3	α_3
	β_3	β_3	β_3	β_3
	γ	γ	γ	γ
	δ	δ	δ	OSCP
	*ε	*ε	ε	δ
				ε
			*ζ	*IF_1
F_O	a	IV	a	a or Sub. 6
	b_2	I,II	b_2	b
	c_{9-12}	III_{9-12}	c_{12}	C_{8-12}
				A6L, d, e, f, g, i/j, F6, 8.

Subunits are accommodated according to their corresponding homologs in the other enzymes. Mitochondrial OSCP is the homologue of δ in the other enzymes, and mitochondrial δ is the homologue of ε in the other enzymes. Mitochondrial ε has no homologue in the other enzymes. The inhibitory subunits are marked with an asterisk. The stoichiometry of the subunits is indicated in the subscript number, and if the subunit has no number then its stoichiometry is one. Color coding from the subunits of Table 1 matches the color coding of the structures from Fig. 1

subunit (Fillingame et al. 1984; Symersky et al. 2012). And the positive charge comes from a highly conserved arginine of the *a* subunit (Cain and Simoni 1989; Lightowlers et al. 1987). The prevailing notion at this point is that when the H^+ meets the carboxylate residue on the *c* subunit exposed to the aqueous phase, the carboxylate of the subunit *c* becomes

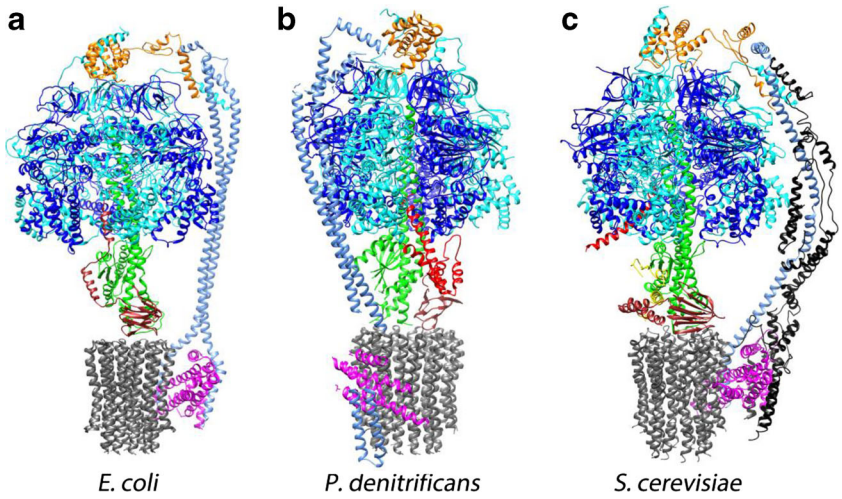

Fig. 1 Structures of the F_1F_O-ATPsynthase from *E. coli*, *P. denitrificans*, and *S. cerevisiae*. **a** The bacterial F_1F_O-ATPsynthase is represented by the enzyme of *E. coli* (PDB ID 5T4O). The enzyme from *E. coli* is inhibited by its ε subunit (brown). **b** The α-proteobacterial F_1F_O is represented by the enzyme of *P. denitrificans* (Model from Mendoza-Hoffmann et al. 2018). The enzyme from *P. denitrificans* is inhibited by its ζ subunit (red). **c** The mitochondrial F_1F_O-ATPsynthase is represented by the enzyme of *S. cerevisiae* (PDB ID 6CP6, and the IF_1 from the *S. cerevisiae* enzyme was superimposed from the PDB ID 3ZIA). The enzyme from *S. cerevisiae* is inhibited by the IF_1 subunit (red). The F_1-IF_1 structure from *S. cerevisiae* (PDB ID 3ZIA) was aligned with the F_1F_O structure of *S. cerevisiae.* Then the F_1 from *S. cerevisiae* 3ZIA was removed and the IF_1 was left superimposed on the F_1F_O structure from *S. cerevisiae*. The alignment was done using PyMol. The images of the structures from the three enzymes were taken using UCSF Chimera. Color coding of the subunits from the structures matches the color coding of the subunits from Table 1

protonated (Elston et al. 1998; Fillingame and Steed 2014). The protonation of the carboxylate nulifies the negative charge of this residue, inciting a conformation change in the side chain of this residue (Pogoryelov et al. 2010). This results in a loss of the previous interaction with the positive charge of the guanidinium from the conserved arginine of the *a* subunit. Due to this repulsion effect, the protonated *c* subunit rotates clockwise away from the positive charge of the arginine residue of the *a* subunit and a new deprotonated *c* subunit interacts with the positive charge of the arginine side chain of the *a* subunit (Elston et al. 1998; Fillingame and Steed 2014). Once all *c* subunits are protonated, the *c* ring will have rotated a full 360° in the clock wise direction (CW) when viewed from the transmembranous proton conducting F_O sector to the water-soluble catalytic F_1 part (Fig. 2). Once the *c* ring has rotated almost 360°, the proton from the first *c* subunit is passed to the other side of the membrane through the upper hemicanal (Fig. 2). The newly deprotonated *c* subunit recovers its negative charge on its carboxylate side chain and is once again able to interact with the positive charge of the conserved arginine in the *a* subunit. The cycle then repeats and the process will keep repeating itself as long as there is an electrochemical gradient being generated by the electron transfer chain. The flow of protons through the hemicanal system is favored by the electrochemical gradient, and will keep the *c* subunit ring rotating in the CW direction.

The net result of the *c* ring rotation because it is physically attached to the central γ subunit through the ε subunit, is a conduction of mechanical CW rotary motion to the γ subunit of the F_1 portion. This is because the ε subunit increases the contact surface between the *c* ring of the F_O sector with the γ subunit of the F_1 portion (Fig. 1) (Stock et al. 1999; von Ballmoos et al. 2009). Thus, the ε subunit structural role is to stabilize and create an effective interface area between the γ subunit and the c ring, because this is the area where the mechanical torque is applied (Fig. 1) (Rondelez et al. 2005). Evidence supporting this structural role of the ε subunit is that without the ε subunit, the F_1 portion dissociates from the F_O sector eliminating the F_1F_O coupling of the ATP synthase (Klionsky et al. 1984). Once the γ subunit starts rotating in the CW direction, the asymmetry of the γ subunit causes the mechanical energy generated by the rotation of the *c* ring to be transferred to the catalytic hexameric α and β subunits on the F_1 sector (Figs. 2 and 3) (Noji and Yoshida 2001).

The F_1 nanomotor

The γ subunit is structurally asymmetrical, this is because the N-terminal α-helix is smaller in length than the C-terminal α-helix, and also at the base of γ there is a globular domain that connects the N-terminal and C-terminal α-helixes (Abrahams et al. 1994). Thus, depending on the position of the N-terminal and globular domain of the γ subunit, it interacts differently with the α and β subunits. Therefore, the physical position of the γ subunit determines the conformational states of α and β (Figs. 2 and 3) (Abrahams et al. 1994). The α and β subunits are assembled in the shape of an hexamer ring that alternates α and β, this α_3/β_3 hexamer

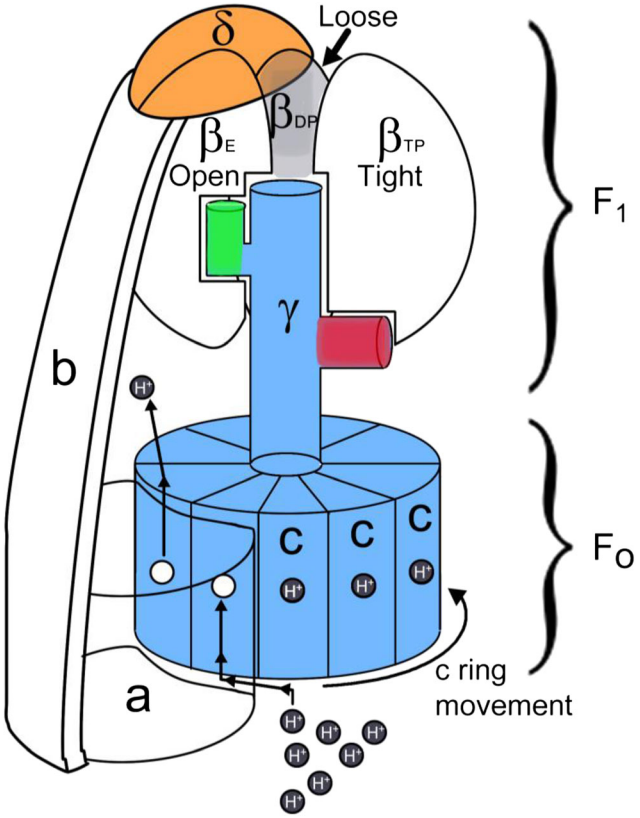

Fig. 2 Representation of the F_1F_O-ATPsynthase from bacteria. Protons (H^+) pass through the bottom hemicanal of the interface between a subunit and the c ring (blue). Then a subunit c becomes protonated and moves away from the subunit a. Once all of the c subunits are protonated, the c subunit that has gone a full 360° becomes deprotonated. The released proton from the newly deprotonated c subunit then passes through the upper hemicanal. The rotation of the c ring will be passed on to the γ subunit (blue) which will give way to the conformational states of the β subunits. The asymmetry of γ subunit is depicted by its N-terminal (green) and its globular domain (red). Its N-terminal will be closest to the Open state, and the globular domain will be closest to the Tight state. Rotor subunits are depicted in blue. β subunit in the Loose state is depicted in grey. α and ε subunits where not included in this representation. The figure is adapted from (Elston et al. 1998)

ring is part of the stator of the F_1F_O nanomotor. The γ subunit is the axis of this α_3/β_3 hexamer ring, and the interactions of the N-terminal α-helix and the globular domain of the γ subunit with the α_3/β_3 hexamer ring will render different conformational states for the α and β subunits (Figs. 2 and 3) (Abrahams et al. 1994). The α and β subunits have three different conformational states: Open (β_E), Loose (β_{DP}) and Tight (β_{TP}) (Figs. 2 and 3) (Abrahams et al. 1994; Boyer 2002; Cross 1981; Stewart et al. 2013; von Ballmoos et al. 2009). Here we will focus on the conformational states of the β subunit. When the β subunit conformational state is Open, its nucleotide binding site is empty because an ATPMg has been released from the site and this Open site can now bind new substrates (ADPMg+Pi). When the β subunit conformational state is Loose, its nucleotide binding site now has bound ADPMg+Pi. And, when the β subunit conformational state is Tight, its nucleotide binding site has condensed the ADP + Pi into ATP, so this Tight site now has an ATPMg bound (Fig. 3) (Stewart et al. 2013). Since the conformational states depend on the interactions with the asymmetrical γ subunit, when the N-terminal of the γ subunit is interacting with the nearest β subunit the conformational state of this β subunit will be the Open state. Simultaneously the globular domain of γ will be interacting with a different β subunit, and this interaction will render the conformational state of this β subunit into the Tight state. And, at the same time, the C-terminal α-helix of γ will be interacting with the third β subunit rendering the conformational state of this β subunit as the Loose state (Figs. 2 and 3) (Oster and Wang 2000). Therefore, when the γ subunitis in one specific position there will be 3 different conformational states for the each one of the three β subunits: one β will be in the Open state, the second β will be in the Tight state and the third β will be in the Loose state (Fig. 3) (Boyer 1997). Hence, each 360° turn of the *c* subunit ring will produce a 360° rotation of the γ subunit, and this in turn means that each β subunit will have gone through the three different conformational states associated to the three 120° partial γ subunit movements (Senior 2012). In consequence, each β subunit condenses one ATP from ADP + Pi per each 120° rotation of γ. Some intermediate states of the β subunit related to partial rotation sub-steps of angles <120° have also been described (Bilyard et al. 2013; McMillan et al. 2016; Suzuki et al. 2014; Yasuda et al. 2001) and will be here briefly reviewed (Figs. 4 and 5). This means that one 360° turn of γ will render 3 newly synthesized ATP molecules.

The peripheral stalk

The peripheral stalk is composed of subunits *a*, *b* and δ. The *a* subunit is membrane-bound and acts as a collar around the *c*-ring as previously described. However the other function of the *a* subunit is structural, anchoring the b_2 homodimer into the membrane phase. The b_2 dimer then extends as a peripheral entity adjacent to the central γ subunit stalk, reaching over the α_3/β_3 hexamer ring to contact the δ subunit at the distal end of α_3/β_3 hexamer ring. The peripheral stalk keeps the α/β hexamer as part of the stator and prevents it from following the rotation drag of the γ subunit. The peripheral stalk structure may be composed of more than these essential subunits depending on its bacterial, chloroplastidic, or mitochondrial origin of the F_1F_O namomotor (Walker and Dickson 2006). However, in bacteria the peripheral stalk is composed of the subunits *a*, *b* and δ (Fig. 1a).

Hydrolysis of ATP by the F_1F_O-ATP synthases

The F_1F_O-ATP synthase nanomothor is both, kinetically and thermodynamically reversible and therefore its central rotor can also rotate in the direction of ATP hydrolysis which is

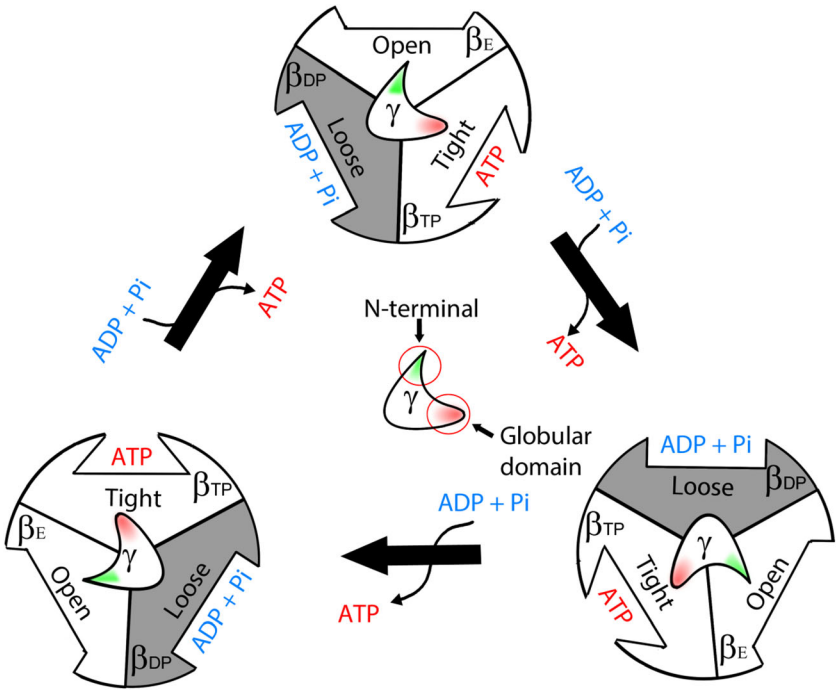

Fig. 3 Model of the ATP synthesis binding change mechanism. The three different conformational states of the β subunit are depicted: Open, Loose, and Tight. The Open conformational state of β that has liberated an ATP can now bind a new ADP + Pi (blue). The Loose conformational state of β (grey) has an ADP + Pi bound. The Tight conformational state of β has condensed the ADP + Pi into an ATP (red). The γ subunit is depicted in the middle of the β subunits, and its asymmetry is represented by its N-terminal (green) and its globular domain (red). When the γ subunit starts rotating its N-terminal and globular domain will give way to the conformational states of the β subunits. Its N-terminal will be closest to the Open state, and the globular domain will be closest to the Tight state. The Open state is also known as β_E, the Loose state is also known as β_{DP}, and the Tight state is also known as β_{TP} (Abrahams et al. 1994). The figure is adapted from (Cross 1981) and from (Boyer 2002)

Counter-Clock-Wise (CCW) (viewed from F_O to F_1) (Noji and Yoshida 2001). The CCW rotation is driven by ATP binding and hydrolysis, because of this the F_1F_O-ATP synthase is referred to as the F_1F_O-ATPase when it is hydrolyzing ATP (Abrahams et al. 1994; Junge et al. 2009). In nature, conditions commonly occur where the electrochemical proton gradient ($\Delta\tilde{\mu}_{H+}$) is partially or totally collapsed. For instance, in the absence of a final electron acceptor of the electron transfer chain in bacteria and during anoxia in mitochondria. In the case of photosynthetic bacteria and chloroplasts this occurs in the dark phase. In these conditions where the $\Delta\tilde{\mu}_{H+}$ diminishes, the enzyme is driven thermodynamically into the ATP-driven CCW rotation of the central rotor, i.e. in the F_1F_O-ATPase turnover since it cannot harness the proton-motive force to drive the CW F_1F_O-ATP synthase rotation. This hydrolytic mechanism follows the same three 120° steps of the γ subunit seen in the synthetic mechanism (Fig. 3); however, recent single molecule experiments have refined the mechanism of ATP hydrolysis by the F_1-ATPase. In *Bacillus* PS3 the 120° steps occur in two substeps. First, the binding of ATP renders a 80° substep. Second, the release of Pi toghether with the hydrolysis of ATP renders a 40° substep (Fig. 4) (Noji et al. 2017; Watanabe et al. 2010). In the case of the human F_1-ATPase, the 120° steps occur in three substeps. First, ATP binding renders a 65° substep. Second, Pi release renders a 25° substep. Third, ATP hydrolysis renders a 30° substep (Fig. 5) (Suzuki et al. 2014). In *E. coli* the 120° step is divided into 90° and 30° substeps (Bilyard et al. 2013), and in *Caldalkalibacillus thermarum* these are 70° and 50° substeps (McMillan et al. 2016).

In general, the F_1F_O-ATPase activity is detrimental for living cells unless there is a strict requirement for ATP-driven proton pumping when an electron transfer chain is unable to form the proton-motive force ($\Delta\tilde{\mu}_{H+}$) or to prevent cytoplasmic acidification. For instance, in the absence of a final electron acceptor in some bacteria or in reverse functioning of Rho^0 mitochondria (Chandel and Schumacker 1999). Therefore, under most organisms physiological conditions, the CCW rotation of the F_1F_O-ATPase is preferably inhibited to avoid energy dissipation by futile consumption of intracellular ATP pools. This is because, cells are urged to maintain a high ATP/ADP ratio in order to drive most of the vital functions described above. Therefore, in order to prevent wasteful ATP hydrolysis by the F_1F_O-ATPase nanomotor, nature has specially designed several natural inhibitory proteins which hinder the F_1F_O-ATPase activity, thus favoring the rotation in the CW direction of the F_1F_O-ATP synthase. Since these natural inhibitors target the extramembranous catalytic part of the enzyme, the F_1 fraction, these inhibitory proteins will be described as F_1-ATPase inhibitor proteins.

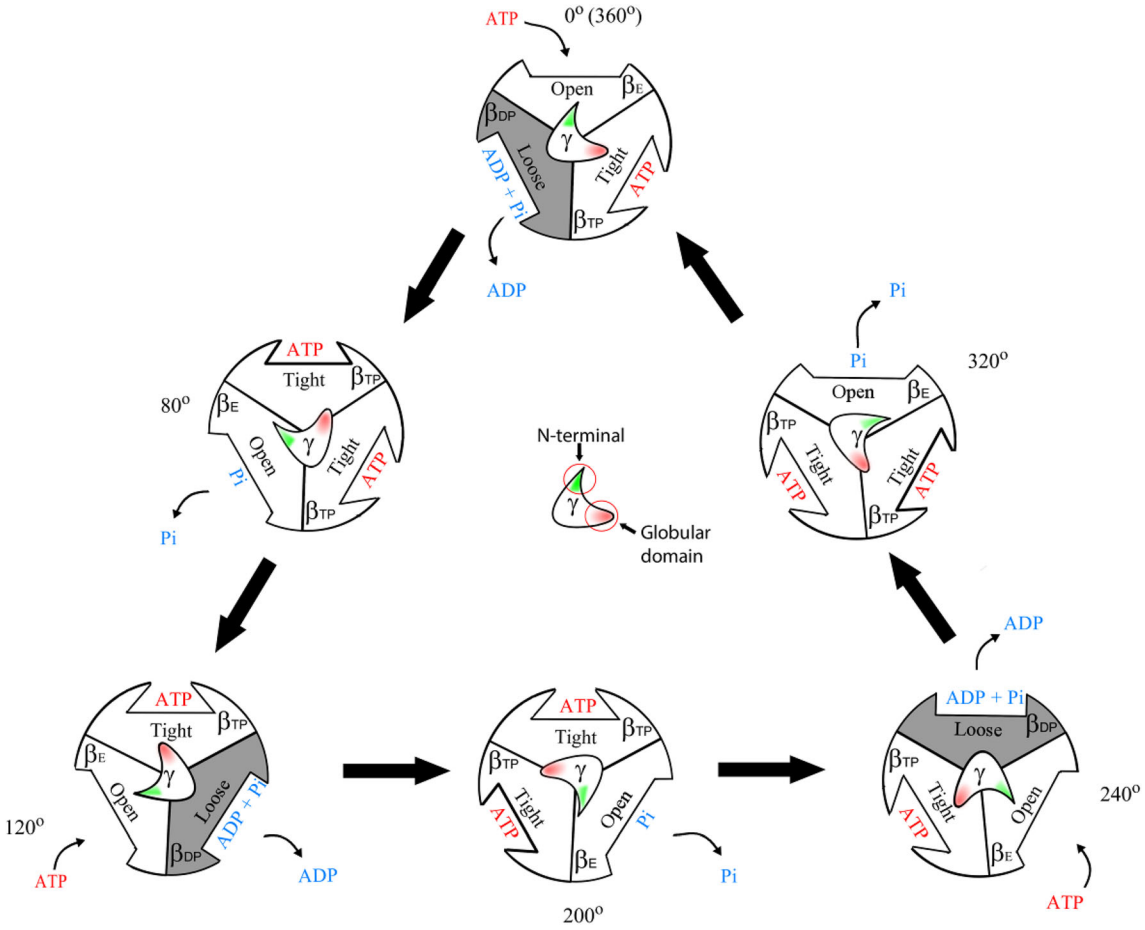

Fig. 4 Model of the ATP hydrolysis binding change mechanism for the bacterial F_1-ATPase. In the ATP hydrolysis mechanism the CCW rotation of γ subunit is driven by the hydrolysis of ATP by the β subunits. The three different conformational states of the β subunit are depicted: Open, Loose, and Tight. In order for the γ subunit to accomplish a 120° step, this 120° step is divided by two substeps. The first substep of 80° is rendered by the binding of ATP by the Open state β subunit. The second substep of 40° is rendered by the release of Pi by the Open state β subunit and the hydrolysis of an a ATP molecule by the Tight state β subunit. The figure is adapted from (Martin et al. 2018; Noji et al. 2017)

The bacterial ε subunit

An excellent review of the bacterial ε subunit has appeared recently (Krah et al. 2018) thus we will revisit this subunit briefly regarding its inhitiory properties. The primary role of the ε subunit is to couple the F_1 fraction to the F_O fraction of the enzyme. The ε subunit couples F_1 to F_O by establishing a bigger contact surface of the central stalk of F_1 or "foot" of F_1 to the rotating c ring. Thus, making of the $\gamma/\varepsilon/c_{12-15}$ domain a central part that rotates all together as the central rotor relative to the stator formed by the catalytic F_1 subunits (α_3, β_3), and the peripheral stalk proteins (δ, b_2, a). Evidence of the structural role of ε subunit was first observed from cross-linking experiments, where the enzyme's rotation in general was unaffected by γ-ε or ε-c crosslinkages. Whereas, the γ-β, γ-α, ε-β, and ε-α adducts inhibited the rotary turnover of the enzyme, reviewed in (Capaldi et al. 2000). Further unimolecular rotary experiments confirmed this, when the primary fluorescent actin filament used to demonstrate the real-time rotation of the γ subunit (Noji et al. 1997) was then attached to the c ring of the central $\gamma/\varepsilon/c_{10-15}$ rotor (Tsunoda et al. 2000).

Besides its central role as a coupling protein between F_1 and F_O, the ε subunit was also found to play a role as a partial inhibitor of the bacterial F_1-ATPase activity, initially in the *Escherichia coli* enzyme (EcF_1). The ε subunit was found to dissociate from the EcF_1-ATPase with a concomitant activation of the enzyme (Smith and Sternweis 1977). Eventually, the structure of the ε subunit was solved for the *E. coli* model, and it was found to form a globular β-sheet N-terminal part, and a C-terminal hairpin domain formed by two antiparallel α-helixes (Figs. 6 and 7b) (Uhlin et al. 1997; Wilkens and Capaldi 1998). Further limited proteolysis and site directed mutagenesis showed that the 2 C-terminal α-helixes (CαH) form the inhibitory domain of the protein (Fig. 1a) (Capaldi and Schulenberg 2000). More recently, a large conformational change of these two α-helixes has been observed, both by cross-linking experiments (Capaldi et al. 1994; Capaldi and Schulenberg 2000) and by further crystallographic studies

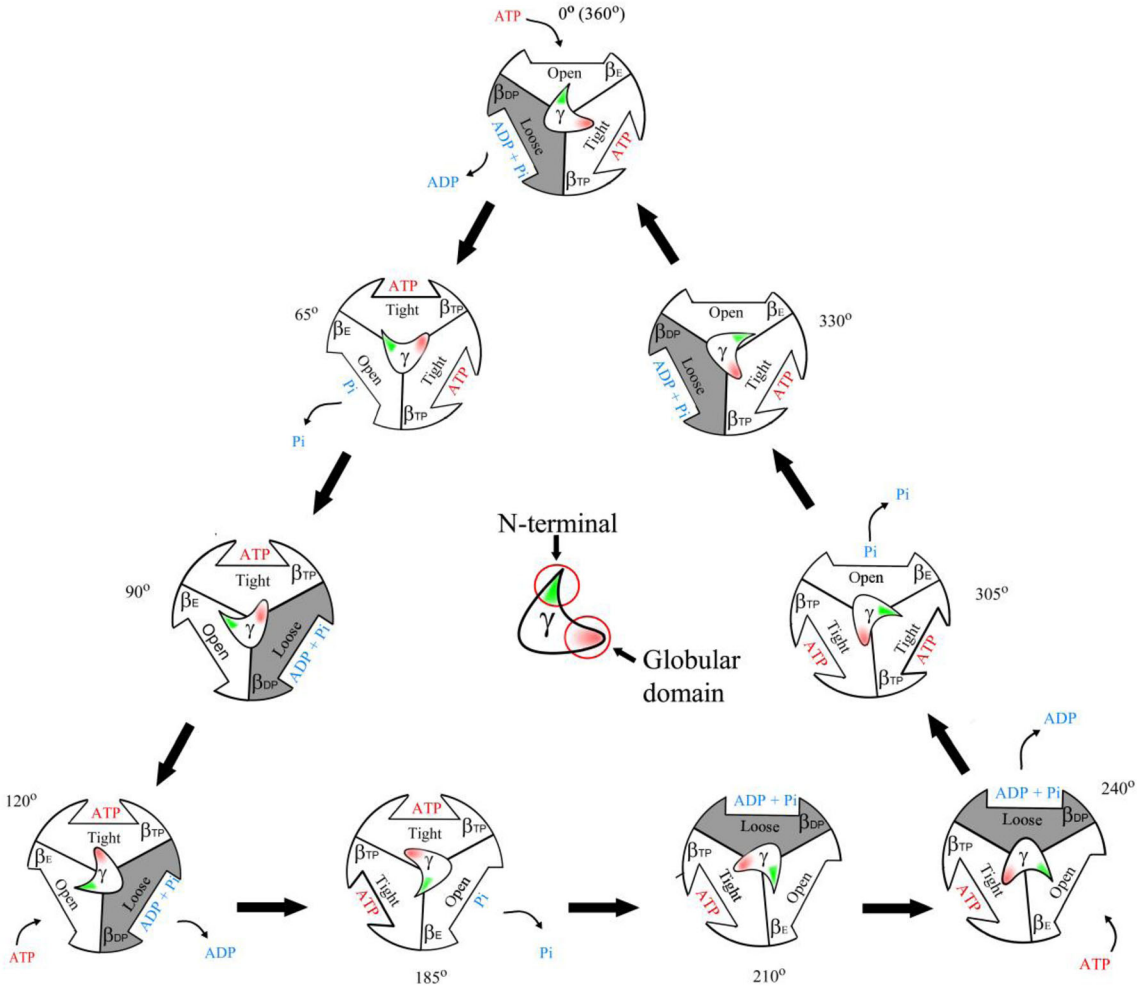

Fig. 5 Model of the ATP hydrolysis binding change mechanism for the human F_1-ATPase. In the ATP hydrolysis mechanism the CCW rotation of γ subunit is driven by the hydrolysis of ATP by the β subunits. The three different conformational states of the β subunit are depicted: Open, Loose, and Tight. In order for the γ subunit to accomplish a 120° step, this 120° step is divided by three substeps. The first substep of 65° is rendered by the binding of an ATP molecule by the Open state β subunit. The second substep of 25° is rendered by the release of Pi by the Open state β subunit. The third substep of 30° is rendered by the hydrolysis of ATP by the Tight state β subunit, this β subunit may have an ATP bound and hydrolyzes it after it changes into the Loose conformational state. The figure is adapted from (Martin et al. 2018; Suzuki et al. 2014)

(Hausrath et al. 1999). A first partial extension of the α-helixes was observed by crystallization of a reconstituted γ/ε subcomplex, which explained the formation of previously observed ε-α and ε-β adducts (Rodgers and Wilce 2000; Tsunoda et al. 2001). The ε-α and ε-β cross-linkages could not be formed if the ε subunit observed in solution which is in a compact conformation (Fig. 6a) was the only one present in the central rotor γ/ε domain of the EcF_1-ATPase. In sum, it was concluded that the CαH domain of ε exerts a large conformational change from the compact globular form observed by NMR in solution (Fig. 6a) to an extended inhibitory form where the CαH interacts with α, β and γ subunits (Figs. 1a and 6c). The extended inhibitory form of the ε subunit works as a ratchet and therefore blocks the CCW rotation of the central stalk selectively, i.e., blocking rotation during the CCW F_1-ATPase turnover, but not during the CW rotation of the ATP synthase activity (Tsunoda et al. 2001) (Figs. 1a and 6c). More recently, the extended inhibitory conformation of ε has been solved in the F_1-ATPase from *E. coli* and also for the F_1-ATPase of the thermophilic *Geobacillus stearothermophilus* (*Bacillus* PS3). In both cases, it was found that the CαH of the ε subunit extends further than initially observed (Cingolani and Duncan 2011; Shirakihara et al. 2015b). The ε subunit CαH wraps the γ subunit and also interacts with the α_{DP} and β_{DP} subunits. Therefore, these interactions block the rotation of the central stalk. There is some controversy on the ratchet mechanism of the ε subunit, since some groups showed that ε inhibits preferably the F_1-ATPase activity without significant effect on the F_1F_O-ATP synthase turnover, even during cross-linking of CαH of ε with γ (Suzuki et al. 2003; Tsunoda et al. 2001). Whereas, other laboratories showed that ε actually inhibits the ATP synthase turnover (Iino et al. 2009). Further studies are required to resolve if the ε

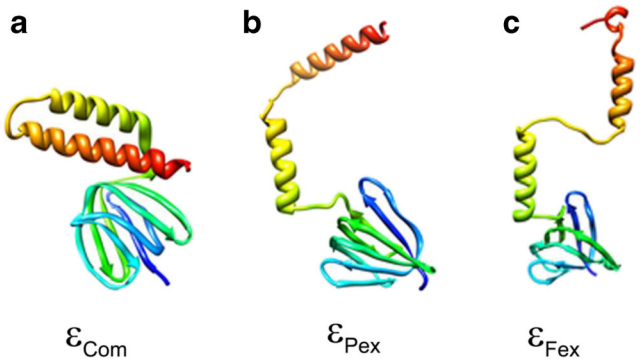

Fig. 6 Conformational changes of the bacterial ε subunit during active to inactive F_1-ATPase transitions. Structural transitions of the *E. coli* ε subunit that allow ATP hydrolysis or inhibit ATP hydrolysis by the F_1-ATPase. In red and yellow the C-terminal α-helix domain (CαH domain), and the globular β-sheet domain in blue, cyan and green. **a** The CαH domain is in the compact globular form (ε_{Com}) (PDB ID 1AQT). This ε_{Com} conformation allows the F_1-ATPase to rotate in the CCW direction. **b** The CαH domain is in the partially extended conformation (ε_{Pex}) (PDB ID 1FS0). **c** The CαH domain is in the fully extended conformation (ε_{Fex}) (PDB ID 3OAA). This ε_{Fex} form inhibits the CCW rotation of the F_1-ATPase. The images of the structures were taken using UCSF Chimera. Image is adapted from (Cingolani and Duncan 2011)

subunit inhibits both CCW and CW rotation. The ε subunit is not a total inhibitor, it works as a partial inhibitor because it consistently leaves some residual F_1-ATPase activity. Because of this, the ε subunit cannot be regardad as a total inhibitor protein but as a subunit that modulates the rate of rotary motion of the central rotor (Capaldi and Schulenberg 2000; Feniouk et al. 2006). Finally, a significant feature of the ε subunit, is that it possesses an ATP binding site which is of low affinity in *E. coli* (Kd ≈ 22 mM) (Yagi et al. 2007) and of higher affinity in *Bacillus* PS3 (Kd ≈ 200 μM) (Kato et al. 2007). This ATP binding stabilizes the compact structure of ε, thus the ε subunit also works as a cellular ATP sensor. When there is a relatively high concentration of intracellular ATP, the ε subunit will bind an ATP molecule and it will contract its CαH domain into the compact conformation allowing the CCW rotation of the F_1-ATPase (Figs. 6a and 7b). When there is a relatively low intracellular concentration of ATP, the ε subunit will not be able to bind an ATP molecule and it will extend its CαH domain and wrap the γ subunit, thus controlling the CCW rotation of the F_1-ATPase (Figs. 1a and 6c) (Kadoya et al. 2011). The ATP binding site of the ε subunit is conformed by 7 residues (Ferguson et al. 2016). In the case of the bacteria belonging to the bacilli class of the phylum firmicutes: *Caldalkalibacillus thermarum (C. thermarum)*, *Geobacillus stearothermophilus* (*Bacillus* PS3, *Bacillus subtilis (B. subtilis)* and *Bacillus anthracis (B. anthracis)* the sequence of the ATP binding site from their ε subunit has all the 7 residues totally conserved. All of the 7 residues from the binding site from the bacilli bacteria described before are identical (Fig. 7a magenta) (Ferguson et al. 2016). In the sequence of the ε subunit belonging to the γ-proteobacteria from the phylum proteobacteria: *Escherichia coli* (*E. coli*), *Klebsiella pneumoniae* (*K. pneumoniae*) and *Salmonella enterica* (*S. enterica*) the ATP binding site is also conserved, but from the seven residues that form the ATP binding site, 2 are identical (Fig. 7a magenta), 4 are conserved (Fig. 7a yellow), and one is not conserved (Fig. 7a grey). In the sequence of ε subunit belonging to the α-proteobacteria: *P. denitrificans*, *Rhodobacter capsulatus* (*R. capsulatus*) and *Rhodobacter sphaeroides* (*R. sphaeroides*) the ATP binding site is absent. From the seven residues that conform the ATP binding site, 1 is conserved (Fig. 7a yellow) and the other six are not conserved (Fig. 7a grey). But, in *P. denitrificans* there is a second residue that is identical to the ATP binding site, making it the only sequence of the three α-proteobacteria shown that has 1 identical residue, 1 conserved and 5 not conserved. Similar alignments had been recently shown for other bacteria, examining differences in ATP binding affinities (Krah et al. 2018). Therefore, from a sequence viewpoint, the ATP binding pocket of the ε subunit in the α-proteobacteria is essentialy absent, and therefore the ε subunit from α-proteobacteria should not bind ATP, however its CαH domain seems to be in the compact conformation as indicated by the lack of α-ε and β-ε crosslinking interactions on the PdF_1-ATPase of *P. denitrificans* vs that of *E. coli* which forms α-ε and β-ε crosslinking adducts in relatively high yield (Garcia-Trejo et al. 2016). As another example of a bacterial ε subunit unable to bind ATP but resolved in the compact conformation, we can cite a mutant of *C. thermarum* (Ferguson et al. 2016). This support the non-inhibitory compact conformation of the ε subunit of *P. denitrificans*, and the latter is in concordance with the structure observed for the non-inhibitory δ subunit of mitochondria (mitochondrial δ subunit is a homologe to the ε subunit of bacteria) which lacks the ATP binding site and its CαH domain is in the compact conformation in the structure of the F_1-ATPase (Fig. 1c) (Dautant et al. 2010; Zhou et al. 2015). As mentioned, the CαH domain of the ε subunit of *P. denitrificans* does not interact with the α and β subunits (García-Trejo et al. 2016) and it does not inhibit the CCW rotation of the F_1-ATPase activity (Zarco-Zavala et al. 2014). Therefore, taking together these data with the absence of the ATP binding site in the sequence of the ε subunit of *P. denitrificans*, all together strongly suggests that the CαH domain of the ε subunit from *P. denitrificans* is in the compact conformation. Recently a different sequence for the ATP binding pocket of the bacterial ε subunit has been proposed (Krah et al. 2017), thus further work is needed in order to determine the role of ε subunit as partial inhibitor of the different bacterial F_1-ATPases and its ATP binding properties.

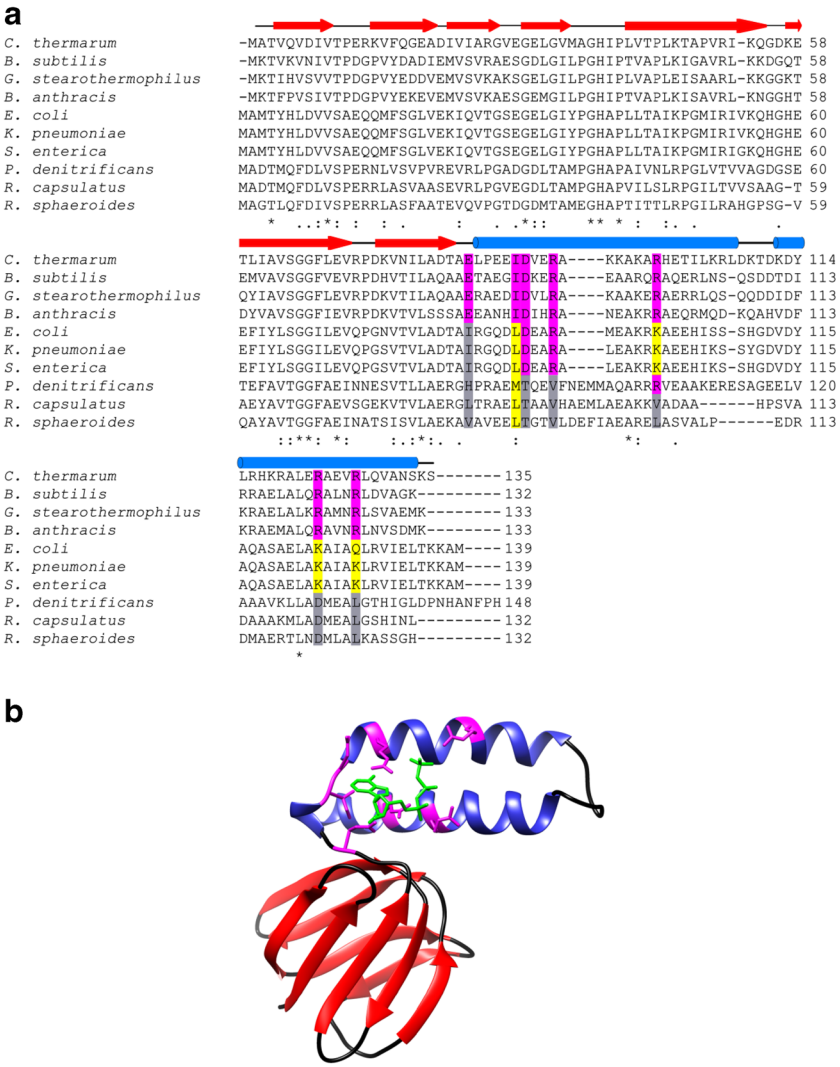

Fig. 7 Loss of ATP binding site of the ε subunit from bacteria belonging to the α-proteobacteria class. The ATP binding site considered here is the one from the ε subunit from *Caldalkalibacillus thermarum* (PDB ID 5IK2). **a** Alignment of the amino acid sequence of the ε subunit from diferent bacteria; from the bacilli class: *C. thermarum*, *B. subtilis*, *G. stearothermophilus*, *B. anthracis*. From the γ-proteobacteria class: *E. coli, K. pneumoniae, S. enterica*. From the α-proteobacteria class: *P. denitrificans, R. capsulatus, R. sphaeroides*. The residues that interact the ATP molecule (shown in green) are highlighted. In magenta the residues that are identical, in yellow the residues that are conserved, and in grey the residues that are not conserved. The red arrow indicates the N-terminal part of the sequence which is β-sheet. The blue cilinder indicates the C-terminal part of the sequence which is structured as α-helix, also named the CαH domain. The black lines indicate the loops. The asterisk (*) indicates positions in the alignment that have an identical residue, the colon (:) indicates positions in the alignment that are conserved (similar), the period (.) indicates positions in the sequences that are weakly conserved (weakly similar), and no symbol indicates positions in the sequences that are not conserved at all. Alignment was made using CLUSTAL-Omega. **b** Structure of the ε subunit from *C. thermarum.* In red the N-terminal (β-sheet), in blue the C-terminal (α-helix), in magenta the side chains that interact with the ATP molecule, and in green the ATP molecule. The image of the structure was obtained using UCSF Chimera

In summary, the large conformational change of ε can be described as partial unfolding since it involves the detachment of the CαH domain from the globular β-sheet domain, and a large stretching of both C-terminal α-helixes (Fig. 6a and c). To achieve this, the loop connecting both domains works as a hinge allowing the CαH domain of ε to extend as much as possible to wrap the γ subunit (Fig. 1a). Therefore, there are three conformational changes of the ε subunit: the compact globular form where the CαH domain cannot interact with α and β subunits (ε_{Com}) consequently allowing F_1-ATPase activity (Fig. 6a); the partially extended form (ε_{Pex}) which is probably an intermediate conformation between the ε_{Com} and ε_{Fex} conformations (Fig. 6b); and the fully extended form (ε_{Fex}) where the CαH domain wraps the γ subunit and interacts with the α and β subunits and it inhibits the F_1-ATPase hydrolytic activity (Fig. 6c) (Cingolani and Duncan 2011; Shirakihara et al. 2015b; Sobti et al. 2016).

The inhibitor protein of the mitochondrial F_1-ATPase, IF_1

In the early sixties, shortly after the first purifications of a functional F_1-ATPase from mitochondria, a natural inhibitor peptide of ≈10 kDa was found to control the F_1-ATPase activity (Pullman and Monroy 1963b). This protein became a target of a large number of studies characterizing the properties of this natural inhibitor, called IF_1 or "inhibitor of the F_1-ATPase". The protein was shown to possess a pH sensitive region that renders it as a strong inhibitor at relatively acidic pH (6.0–6.8), and a weak inhibitor at alkaline pH (8–9), this is due to a couple of histidine pairs flanking the inhibitory region of the protein, which lies at the N-terminal side of the protein (Cabezon et al. 2000). The stoichiometry of IF_1 is 1 per F_1-ATPase, and the binding affinity is about 200 μM (Hashimoto et al. 1981; Klein et al. 1980) with a binding/lock mechanism that relies on some catalytic F_1-ATPase turnovers in order to lock IF_1 in its final inhibitory position, which coincides with the F_1:ADPMg inhibited form of the enzyme (Tuena de Gomez-Puyou et al. 1983). The inhibitory domain of the protein is on the average a segment of positions 10–40 of the protein (van Raaij et al. 1996), and the C-terminal domain seems to work for dimerization and oligomerization of IF_1 (Cabezon et al. 2000; Faccenda and Campanella 2012; García-Trejo and Morales-Ríos 2008). The protein is highly expressed in tissues of high demand of mitochondrial ATP such as cardiac and skeletal muscle, brain, kidney, the retina, etc., and its expression seems to be lower in tissues that use more of a glycolytic metabolism such as the liver. The function of the protein is to prevent the backward F_1F_O-ATPase activity during collapse of the mitochondrial proton gradient during ischemia or uncoupling, and it also promotes the dimerization of the F_1F_O-ATP synthase (García et al. 2006). The dimerization of the ATP synthase by the IF_1 protein favours the formation of mitochondrial cristae (Faccenda et al. 2017; Faccenda et al. 2013; García et al. 2006). The IF_1 protein has an elongated α-helical structure, but the far N-terminal extreme residues 1–10, are intrinsically disordered and unresolved either by NMR or crystallography (Fig. 8) (Cabezon et al. 2001; Gordon-Smith et al. 2001). These intrinsically disordered residues from the N-terminal sequence of the IF_1 subunit have not been resolved because their high movility and disordered character. But when the IF_1 subunit is binding to the F_1 complex in the interface between the α and β subunits, the N-terminal of the IF_1 subunit is found structured in an α-helix. This means that the N-terminal of the IF_1 subunit undergoes a transition from a disordered to an ordered structure. These kind of transitions from disordered to ordered structures are not uncommon in biology (Oldfield and Dunker 2014; Sotomayor-Pérez et al. 2015; Uversky 2016). This Entrance-Rotation-Alpha-Helix-Lock mechanism of IF_1 has been recently abbreviated as ERAHL to simplify its description given the complexity o the process (Zarco-Zavala et al. 2018). The IF_1 subunit works by blocking rotation of the γ subunit and by interacting with the α and β subunits (Gledhill et al. 2007) since it makes contacts with γ, α, and β subunits at the same α_{DP}/β_{DP} interphase where the bacterial ε CαH domain binds. Therefore, IF_1 is likely to also work as a pawl-ratchet, thus inhibiting preferably the CCW rotation of the F_1F_O-ATPase turnover, without hindering the CW rotation of the ATP synthase turnover. However, it has been observed that IF_1 may slow down the F_1F_O-ATP synthase turnover during the initial pre-steady state kinetics and also during continuous ATP synthesis in mitochondria (Gómez-Puyou et al. 1979). Interestingly, we also observed that the IF_1 subunit is over-expressed in animal cancer cells such as rat hepatoma (Bravo et al. 2004), and this IF_1 upregulation was later confirmed in human cancerous cell lines (Sánchez-Cenizo et al. 2010; Yin et al. 2015). In the latter, the authors claim that upregulation of the IF_1 subunit leads to the inhibition of ATP synthesis and this in turn leads the cancer cells to shift from oxidative phosphorylation to glycolytic metabolism (Esparza-Moltó and Cuezva 2018; García-Bermúdez and Cuezva 2016) also known as the Warburg effect (Hammad et al. 2016; Koukourakis and Giatromanolaki 2018; Lu et al. 2014). The oberverved inhibition of the "forward" ATP synthase turnover by IF_1 in the latter studies is, however, contrary to the unidirectional effect of IF_1 inhibiting only the "reverse" F-ATPase activity but not the "forward" ATP synthase rate, as observed since the very first isolation and characterization of mitochondrial IF_1 (Pullman and Monroy 1963a). It seems therefore that this controversy will require further detailed studies to discern on the actual unidirectional or bidirectional effects of IF_1 on the mitochondrial F_1F_O-ATP synthase/ATPase in whole cells.

Structurally, IF_1 is an elongated α-helix and forms some dimeric and tetrameric aggregates by antiparallel coiled-coil interactions of the C-terminal domain in vitro (Fig. 8a). Mechanistically, in order to inhibit the intrinsic rotation of the mitochondrial F_1-ATPase, the N-terminal side of IF_1 enters through the open catalytic α_E/β_E interface, and a first 120° rotation of γ/ε is coupled to a deeper insertion of IF_1 and to the extension of the α-helical domain towards the far N-terminal side of IF_1 which was intrinsically disordered (Figs. 1c, 8a, and c). Finally, a second 120° rotation of γ/ε inserts IF_1 even deeper and now IF_1 contacts with the γ subunit. And at the very far end of the N-terminus of IF_1, its inhibitory domain acquires a further α-helical structure interacting directly with the γ subunit, thus stalling γ rotation (Fig. 8b and c) (Bason et al. 2014). Interestingly, this far N-terminal inhibitory domain was intrinsically disordered in solution (Gordon-Smith et al. 2001) and becomes more and more ordered into a long α-helix as it becomes deeply inserted into one α/β interface to finally become locked into the $\alpha_{DP}/\beta_{DP}/\gamma$ interface (Fig. 8b and c) (Bason et al. 2014). Thus γ/ε rotation is coupled to

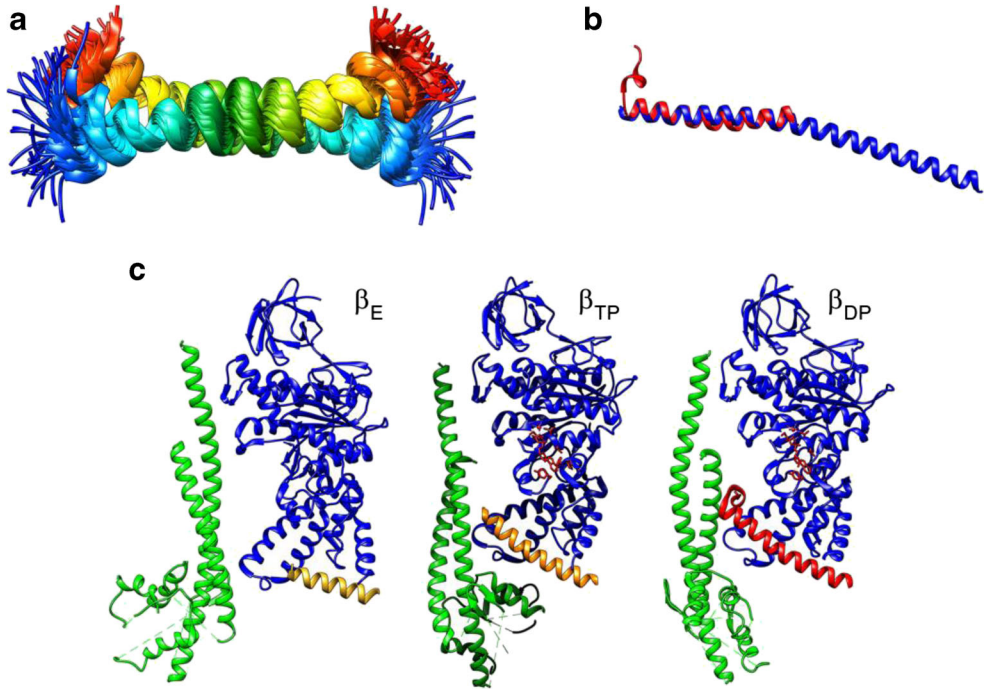

Fig. 8 Conformational change of the mitochondrial IF_1 from short N-terminal α-helix to extended N-terminal inhibitory α-helix. **a** Bovine mitochondrial IF_1 from dimeric state in solution by NMR (PDB ID 1HF9, the inhibitory C-terminal domain is shown in red and the N-terminal domain in blue). **b** The bound state of IF_1 from bovine F_1-IF_1 complex by X-ray diffraction (PDB ID 4TT3), all F_1-IF_1 subunits were removed and only chain H is shown, chain H is shown in red. The unbound IF_1 resolved by X-ray diffraction (PDB ID 1GMJ), chain A is shown in blue. The structure of chain H from PDB ID 4TT3 is aligned with the structure of PDB ID 1GMJ chain A. **c** Visualization of the F_1-ATPase inhibited by the IF_1 subunit. Sideview of the F_1; only subunits β (blue), γ (green) and IF_1 (gold, orange and red) are shown. When IF_1 is entering the α/β empy interfase (β_E), the IF_1 subunit (gold) has its N-terminal in an intrinsically disordered secondary structure. When IF_1 is in the α/β tight interfase (β_{TP}), the IF_1 subunit (orange) has its N-terminal begining to structure itself into an α-helix. When IF_1 is in the α/β loose interfase (β_{DP}), the IF_1 subunit (red) has its N-terminal in a fully structured α-helix conformation. Modified from (Bason et al. 2014). The alignment was done using PyMol and the structures were imaged with UCSF Chimera

insertion and folding of this N-terminus of IF_1, and to the two ATP hydrolysis reactions until rotation halts completely according to the ERAHL mechanism (Zarco-Zavala et al. 2018). This takes place when the mitochondrial membrane potential is partially or totally collapsed, to prevent wasteful ATP hydrolysis, and it is reverted when the membrane potential is re-established.

A novel natural inhibitor protein in the F_1F_O-ATP synthase of α-proteobacteria: The ζ subunit

The ATP synthase of α-proteobacteria had been studied mostly in photosynthetic bacteria carrying out photophosphorylation, including bacteria of the rhodobacteraceae family such as *R. sphaeroides*, *R. capsulatus*, *Rhodospirillum rubrum*, etc. These enzymes had the conserved structure as the other bacterial F-ATPases and some unique kinetic properties such a proton slip (Feniouk et al. 2005) or a high F_1-ATPase activity in the presence of Ca^{2+} (Maldonado et al. 1998); however, no other different characteristics had been observed. For instance, they have a normal H^+/ATP stoichiometry and common activation parameters of ATP hydrolysis and synthesis (Turina et al. 2004; Turina et al. 1992). Furthermore, a highly purified preparation of the full F_1F_O-ATPase from *R. capsulatus* showed only the well-known F_1F_O subunits α, β, γ, δ and ε from F_1, and *a*, *b* and *c* from F_O (Gabellini et al. 1988). In the case of the ATP synthase from *P. denitrificans*, it has some unique properties such as a very high ATP synthase rate and a very low F_1- or F_1F_O-ATPase turnover, with an ATP synthase/ATPase ratio of 20–120, thus more than 100 times higher than those of other bacteria such as *E. coli* (ratio 0.25) or the mitochondrial ATP synthase (ratio 0.2). Thus, the F_1F_O complex from *P. denitrificans* is practically an unidirectional F_1F_O-ATP synthase (Perez and Ferguson 1990; Zharova and Vinogradov 2003). In addition, it shows a kinetic control by ADP and Pi, and a significant F_1F_O-ATPase activation by proton motive force and by organic oxyanions such as phosphate or sulphite (Pacheco-Moisés et al. 2000). Because of its resemblance to mitochondria, *P. denitrificans* was considered the "free living mitochondrion" (John 1987) and in consequence for several years it was described as the α-proteobacterium closest to mitochondria (John and Whatley 1975). This is because it has a very similar aerobic respiratory chain including the four mitochondrial respiratory complexes. Besides, the respiration of

P. denitrificans exhibits the classical respiratory control (acceleration of respiration by ADP) just like mitochondria. To our knowledge, no other bacteria has been described experimentally with so many similarities with mitochondria. Therefore, it turned out interesting to resolve how the ATP synthase of this α-proteobacterium could be controlled in order to have such a high and almost unidirectional ATP synthase turnover. It was also interesting solving how this control evolved in α-proteobacteria as compared with the bacterial ε subunit and the mitochondrial IF_1, before the endosymbiotic origin of mitochondria (Margulis and Chapman 1998; Sagan 1967).

A previous isolation of the F_1-ATPase from *P. denitrificans* (PdF_1) showed a very low ATPase activity (Harris et al. 1977), in accordance with the latent ATPase activity reported for this enzyme by others (Perez and Ferguson 1990; Zharova and Vinogradov 2003). The subunit composition of this PdF_1 preparation contained only the five canonical F_1 subunits, namely α, β, γ, δ and ε (Harris et al. 1977). Afterwards, a Blue Native PAGE (BN-PAGE) of inverted membranes from *P. denitrificans* showed that the ATP synthase was monomeric and not dimeric as the mitochondrial enzyme is (Schägger and Pfeiffer 2000). However, this BN-PAGE was not further analysed by 2D SDS-PAGE to resolve the individual PdF_1F_O subunits (Stroh et al. 2004). Another group reported on the proteomic examination of membrane protein expression in *P. denitrificans* by 2D SDS-PAGE, but they were unable to identify the ζ subunit due to cutting off the gel at 20 kDa (Bouchal and Kučera 2003). To our knowledge, no further PdF_1 or PdF_1F_O isolations were carried out before we isolated both the PdF_1-ATPase and the PdF_1F_O-ATP synthase complexes from *P. denitrificans* (de la Rosa-Morales 2005; Morales-Rios et al. 2010). This might be related to the latent PdF_1-ATPase activity which we enhanced by sulphite activation (Pacheco-Moisés et al. 2000) and therefore the PdF_1-ATPase and PdF_1F_O-ATPase activities could be followed along the chromatographic or density gradient fractions (de la Rosa-Morales 2005; Morales-Rios et al. 2010). The first preparations of the PdF_1 and PdF_1F_O complexes showed consistently a protein of about 11 kDa as resolved by SDS-PAGE which coincidentally co-migrated with the mitochondrial IF_1 inhibitor protein (de la Rosa-Morales 2005; Morales-Rios et al. 2010). The N-terminal of the 11 kDa protein was sequenced and this sequence could be aligned with the inhibitory domain of the mitochondrial IF_1 subunit (de la Rosa-Morales 2005; Zarco-Zavala et al. 2014). The fact that the 11 kDa subunit was consistently present in both the PdF_1 and PdF_1F_O preparations indicated that it was an integral subunit of the enzyme, and its similar features with IF_1 suggested that this could work as an inhibitory protein of the PdF_1-ATPase and PdF_1F_O-ATPase complexes. Further functional, cloning, and sequencing analyses of this 11 kDa subunit, indicated that it has a different full sequence as compared with mitochondrial IF_1 or bacterial ε subunits, but nevertheless, it preserved some identity at its N-terminal domain with the inhibitory domain of mitochondrial IF_1 (Zarco-Zavala et al. 2014). Because this 11 kDa subunit migrated in SDS-PAGE below ε (15–16 kDa) we named it as the ζ subunit of the PdF_1-ATPase, according to the Greek alphabet. This name would allow to distinguish it from the other two natural F_1-ATPase inhibitors already described (ε and IF_1). Importantly, we showed that under the conditions tested, in *P. denitrificans* the ε subunit does not function as a regulator of its F_1-ATPase activity, and it does not affect the affinity of productive binding of ζ to PdF_1 (Zarco-Zavala et al. 2014). Taken together, these results and the loss of the ATP binding pocket in the ε subunit (Fig. 7a and b) indicate that ε subunit has lost its regultatory function in *P. denitrificans*. Therefore, the ζ subunit has taken the role of the inhibitory protein in *P. denitrificans* in order to control its ATP hydrolysis activity. Importantly, it seems that the ζ subunit not only is the inhibitory subunit in *P. denitrificans* but also among most, if not all of the α-proteobacteria class as described below.

Bioinformatic analyses showed that the open reading frame (ORF) of the ζ subunit is present and conserved essentially exclusively in the α-proteobacteria class, suggesting that it should work as a novel F_1F_O-ATPase inhibitor not only in *P. denitrificans*, but all along this important bacterial class. Western-blot combined with 2D-BN-SDS-PAGE analyses showed that this protein is expressed and bound to the F_1F_O-ATP synthase of *Rhodobacter sphaeroides* (Morales-Rios et al. 2010). Further analyses with other α-proteobacteria from the order of Rhodobacterales and Rhizobiales also showed that the sequence of the ζ subunit is conserved along the α-proteobacteria (Zarco-Zavala et al. 2014). Particularly, the N-terminal domain of the ζ subunit is highly conserved, whereas the central and C-terminal domains are variable (Zarco-Zavala et al. 2014). Interestingly, the NMR structure of the ζ subunit, that we resolved in collaboration with Professor Kurt Wüthrich, showed its N-terminal domain is highly mobile and disordered, whereas the central and C-terminal domains of ζ form a 4-α-helix globular bundle (Fig. 9) (Zarco-Zavala et al. 2012). A similar structure of the ζ subunit from *Jannaschia sp*. also solved by NMR shows a very similar 4-α-helix bundle but lacks the N-terminal disordered domain (Serrano et al. 2014). Therefore, the conservation of the N-terminus, plus its high mobility strongly suggested that the N-terminal domain harboured the inhibitory portion of the protein. With this hypothesis, we constructed a $\zeta^{\Delta NT}$ mutant lacking the first 14 residues of the N-terminal domain and confirmed that upon reconstitution into the PdF_1-ATPase, this mutant had lost completely its inhibitory function although it was still able to bind to PdF_1 (Zarco-Zavala et al. 2014). Besides, this truncated protein preserved its native 4-α-helix fold, as well as the truncated ζ subunit from *Jannaschia* lacking 19 residues from its N-terminus (Zarco-Zavala et al.

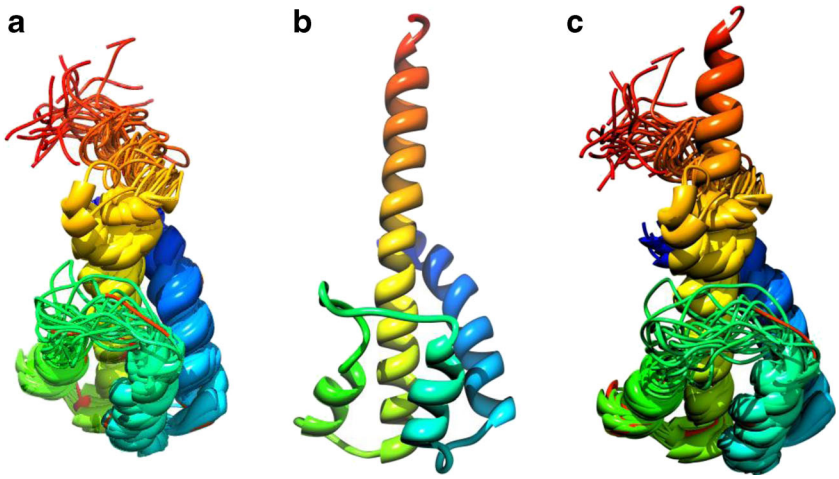

Fig. 9 Conformational change of the ζ subunit of *Paracoccus denitrificans* F_1-ATPase from N-terminal disordered to inhibitory ordered α-helical structure. **a** Structure of the ζ subunit resolved by NMR in solution (20 conformers of PDB ID 2LL0, in red the N-terminal). **b** Structure of the ζ subunit, the N-terminal structure was taken from the F_1F_O-ζ inhibited structure resolved by X-ray diffraction (PDB ID 5DN6) and the C-terminal was taken from the ζ subunit resolved by RNM in solution (PDB ID 2LL0). The N-terminal from PDB ID 5DN6 and C-terminal from PDB ID 2LL0 were aligned using UCSF Chimera. **c** Transition of Pd-ζ from solution structure (20 NMR conformers) to the inhibitory conformer of the protein bound to the F_1Fo-ATPase of *P. denitrificans* (stiff α-helix). The Inhibitory N-terminus is shown in red, and the C-terminus in blue. The structure was obtained by alignment of the NMR structure (PDB ID 2LL0) with the crystal structure (PDB ID 5DN6) using UCSF Chimera

2014). These experiments demonstrated that the first 14 N-terminal residues contained the inhibitory domain of the protein, and combined with chemical cross-linking data showing that truncation of this N-terminal portion prevented the formation of the ζ-γ adduct observed with the wild type ζ subunit (Zarco-Zavala et al. 2014); all together, these results indicated that the N-terminus of ζ interacts with the γ subunit, and the central and C-terminal domain worked as an anchoring domain contacting probably an α/β interface (Zarco-Zavala et al. 2014). More recently, it was recalled that this N-terminus of ζ preserves some identity with the inhibitory N-terminal domain of the mitochondrial IF_1 (Zarco-Zavala et al. 2014). Therefore, it was hypothesized and assessed whether this inhibitory N-terminal of ζ could bind at the same position where the IF_1 binds at the mitochondrial MF_1-IF_1 complex (García-Trejo et al. 2016). Furthermore, it was also taken into account that both, the bacterial ε and mitochondrial IF_1 inhibitors bind at the same α_{DP}/β_{DP} catalytic interface of their respective F_1-ATPases. This interface was named the Inhibition-General Core Region (here abbreviated as INGECORE) and contained residues of the stator (α_{DP}, β_{DP}) and of the rotor (γ) of the nanomotor (Shirakihara et al. 2015b), see Fig. 10. These facts raised the possibility that the N-terminus of the ζ subunit could also exert its inhibitory function by binding at the INGECORE ($\alpha_{DP}/\beta_{DP}/\gamma$) interface.

In order to assess whether the α-proteobacterial ζ subunit and the mitochondrial IF_1 inhibitors actually share the same inhibitory binding site, the inhibitory N-terminus of the ζ subunit was aligned structurally in a PdF_1 structural model raised from the MF_1-stalk structure as a template (García-Trejo et al. 2016), and the IF_1 bound to MF_1 as the guiding structure to align the N-terminus of the ζ subunit. It was found that not only the N-terminus of ζ, but the whole NMR structure of the ζ subunit could be aligned in silico with the inhibitory domain of IF_1 bound to its inhibitory site (García-Trejo et al. 2016). This strongly suggested that ζ and IF_1 actually bind to the same INGECORE interface and also lead us to predict that the mitochondrial IF_1 should inhibit the PdF_1-ATPase by binding competitively with ζ at the PdF_1 INGECORE region in an heterologous reconstitution experiment. The experiment showed clearly, for the first time, the inhibition of a bacterial F_1-ATPase by the mitochondrial IF_1, and this takes place thanks to the close identity between the F_1-ATPases of *P. denitrificans* and the mitochondrial enzyme (García-Trejo et al. 2016). For instance, it is well known that mitochondrial IF_1 does not inhibit the bacterial F_1-ATPase of *E. coli*, and this was also confirmed in these studies (García-Trejo et al. 2016). Furthermore, the inhibitory effect of IF_1 on the PdF_1-ATPase was additive with ζ and this indicated that the ζ subunit binds to the INGECORE region of the PdF_1-ATPase. The INGECORE residues as described by Shirakihara et al. (Shirakihara et al. 2015a) but in the PdF_1-ATPase portion of the PdF_1F_O complex are shown in yellow-green α-carbon sufaces of the $\alpha_{DP}\beta_{DP}\gamma$ interface in Fig. 10. Here it is shown that the INGECORE residues form part of the binding site of the inhibitory and α-helical N-terminus of ζ (shown in red in Fig. 10). In summary, this indicates that ζ binds to the PdF_1-ATPase with a bind/lock mechanism similar to that of IF_1 in the mitochondrial F_1-ATPase, in other words, IF_1 or ζ enter at the open catalytic interface (α_E/β_E), allowing the γ subunit to make two partial 120° turns induced by ATP binding (García-Trejo et al. 2016), the first transforming this catalytic interface

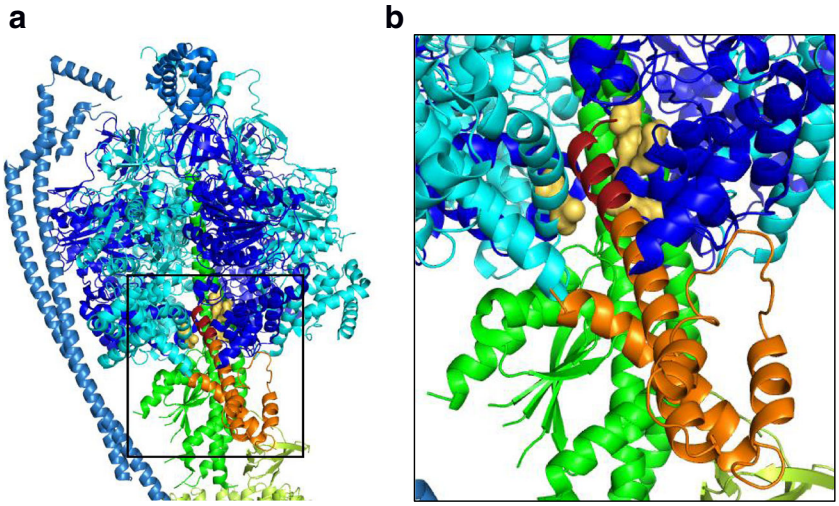

Fig. 10 The consensus INGECORE residues of the $\alpha_{DP}\beta_{DP}\gamma$ interface form part of the binding site of the inhibitory N-terminus of the ζ subunit in *Paracoccus denitrificans*. **a** The F_1-stalk part of the ATP synthase with stator subunits in shades of blue, and rotor subunits in shades of green. α subunits in cyan and β subunits in blue. The rotary γ subunit in green. The INGECORE residues as defined by Shirakihara et al. are shown in yellow α-carbon surfaces . The ζ subunit is shown in red on its N-terminal inhibitory side and in orange the globular and C-terminal domains. The black box in **a** is zoomed in **b**, where the INGECORE residues are shown forming part of the binding site of the inhibitory N-terminal domain of ζ (in red α-helix). These INGECORE residues belong to the three $\alpha_{DP}\beta_{DP}\gamma$ subunits at this interface, the same residues are preserved for the binding of mitocnodrial IF_1 and bacterial ε subunits (see text and Fig. 1). The structure shown is that of the PdF_1F_O-ζ structure that we obtained by combining the NMR (PDB ID 2LL0) and crystal structure of the PdF_1F_O complex (PDB ID 5DN6) in Mendoza-Hoffmann et al. 2018. The INGECORE residues are shown as their α-carbon surface for clarity in yellow-green

into the α_{TP}/β_{TP}, and a final 120° step locking IF_1 or ζ into the α_{DP}/β_{DP} interface contacting the γ subunit to block its further rotation (Fig. 8c) (Bason et al. 2014; García-Trejo et al. 2016). Furthermore, it is also known that mitochondrial IF_1 undergoes a conformational change from disordered to the extension of its α-helix structure as it becomes more deeply inserted in the INGECORE interface (Bason et al. 2014; Shirakihara et al. 2015b). This transition from a disordered secondary structure to an α-helix secondary structure was predicted to take place also in the ζ subunit. This was predicted because of the partial identity among the ζ-N-terminus and IF_1-N-terminus that could preserve this ordering transformation (García-Trejo et al. 2016). In the course of our finding of the inhibitory binding site of the ζ subunit at the INGECORE interface, a crystal structure of the full PdF_1F_O complex appeared simultaneously resolving the inhibitory N-terminal domain of the ζ subunit bound exactly at the INGECORE of the PdF_1F_O complex as we predicted (Morales-Rios et al. 2015). Furthermore, this N-terminus of ζ was found to acquire an α-helical structure that superimposes exactly with the IF_1 bound to the $\alpha_{DP}/\beta_{DP}/\gamma$ interface of MF_1 as we envisaged previously (Garcia-Trejo et al. 2016; Morales-Rios et al. 2015). In other words, the crystal structure of the full PdF_1F_O complex confirmed at the atomic detail the inhibitory binding site of the N-terminus of ζ in the PdF_1-ATPase and the full PdF_1F_O-ATPase complexes that we resolved previously (García-Trejo et al. 2016). The key observation here is that the N-terminus of the ζ subunit undergoes a transition from disordered as resolved in the solution structure of the isolated ζ subunit (Fig. 9a) (Serrano et al. 2014; Zarco-Zavala et al. 2012), to an ordered α-helix that blocks rotation of the γ subunit of the rotor by grabbing it through its far N-terminal residues contacting γ (Fig. 9b) (García-Trejo et al. 2016; Morales-Rios et al. 2015; Zarco-Zavala et al. 2014), and by stabilizing this α-helix interaction with residues from the α_{DP}/β_{DP} interface (García-Trejo et al. 2016; Morales-Rios et al. 2015). This ordering process is similar to the ERAHL mechanism that takes place with the mitochondrial IF_1 which extends its N-terminal α-helix during the partial rotation of γ that locks it in its terminal inhibitory position (Bason et al. 2014). The binding of the ζ subunit must be very alike to the mitochondrial IF_1 in that the N-terminal disordered sequence latter becomes progressively folded into an α-helix as observed by comparison of the three different bound states of the N-terminal of IF_1 into the α_E/β_E, α_{TP}/β_{TP} and α_{DP}/β_{DP} catalytic interfaces of the MF_1-IF_1 complex (Fig. 8c) (Bason et al. 2014). The binding of the ζ subunit then should start as a disordered N-terminal sequence and continue as a transition into an α-helix. This transition is coupled to two consecutive partial 120° rotations of the γ subunit. The two 120° rotations of the γ subunit shift the catalytic empty interface (α_E/β_E) from where ζ enters, into the catalytic tight interface (α_{TP}/β_{TP}) and finally into the catalytic loose interface (α_{DP}/β_{DP}). Once the ζ subunit is in the loose interface (α_{DP}/β_{DP}) it is going to block completely the rotation of the γ subunit. In the case of the ζ subunit, this transition is the extension of α-helix 1 that finally goes all through the N-terminus into the first loop connecting to α-helix 2 of the globular domain. The α-helix structure of the ζ subunit is rigid enough to stall further rotation of the γ subunit in the CCW direction.

Modelling the position of the full ζ subunit bound to the inactive PdF_1F_O-ATPase complex

The atomic structure of the F_1F_O complex from *P. denitrificans* resolved most of the F_1F_O subunits already resolved by high resolution Electron Microscopy in the dimeric ATP synthase of *Polytomella* (Allegretti et al. 2015), including the novel horizontal α-helixes that form the structure that separate the entry and exit half proton channels in the a/c_{12} interface (Allegretti et al. 2015; Morales-Rios et al. 2015). It also confirmed the inhibitory position of the inhibitory α-helix of the N-terminus of the ζ subunit bound to the INGECORE $\alpha_{DP}/\beta_{DP}/\gamma$ interface, which we found by structural modelling and functional heterologous reconstitution experiments with mitochondrial IF_1 (García-Trejo et al. 2016). The novel features of this structure are the confirmation of the α-helical structure of the inhibitory N-terminus of ζ, and the position of the ζ C-terminal α-helix which is in close proximity to the α subunit of the PdF_1-ATPase head (García-Trejo et al. 2016). However, the globular domain of ζ was unresolved, probably due to crystal contacts or the intrinsic conformational flexibility of this globular part of the protein. This globular portion is believed to add structural stability and contact surface to hold the N-terminal inhibitory domain in the correct orientation to bind into the INGECORE (Mendoza-Hoffmann et al. 2018). Also noteworthy, the C-terminal part of the ζ subunit contains a low-affinity nucleotide binding site that could regulate the binding affinity of ζ (Serrano et al. 2014; Zarco-Zavala et al. 2014), and could therefore work as an ATP sensor, similar to that of the ε subunit described in several like bacteria like *E. coli* and *G. stearothermophilus* (PS3) (Yagi et al. 2007).

The ζ subunit of α-proteobacteria and mitochondrial IF_1 as intrinsically disordered proteins (IDPs)

At present, there is a large number of examples of intrinsically disordered proteins (IDPs) that are partially or completely disordered when free in solution, and that become ordered or folded upon binding to a ligand to form a protein-protein complex where they will exert different biological functions (Oldfield and Dunker 2014). These functions range from signalling, toxins, chaperones, DNA binding, transcription factors, cytokines, kinase inhibitors, moonlight proteins with different functions, with some of them involved in human diseases such as prostate cancer and others (Shigemitsu and Hiroaki 2018; Sotomayor-Pérez et al. 2015). These IDPs can be water soluble or transmembrane proteins with soluble intrinsically disordered regions (IDRs). Some of these proteins have an ordered domain and at least one IDR; for instance, the mitochondrial IF_1 protein is an IDP with its N-terminal being an IDR (Gordon-Smith et al. 2001). The case of the ζ subunit is of striking detail since in this case, both the disordered as well as the ordered conformation of the N-terminal domain have been resolved by NMR (Serrano et al. 2014; Zarco-Zavala et al. 2013) and by crystallography (Morales-Rios et al. 2015), respectively. Whereas, in the case of the mitochondrial IF_1, only the ordered α-helix have been resolved by crystallography (Bason et al. 2014). The solution NMR structure of the ζ subunit shows 20 resolved conformers, and the central domain containing α-helixes 1–4 remain relatively rigid, whereas the N-terminus undergoes large movements according to the comparison of the 20 conformers (Fig. 9a). Some of these conformers actually acquire an α-helix like structure, but they do not reach the periodicity of an α-helix (Fig. 9c) (Serrano et al. 2014). The disordered N-terminus of the NMR ζ structure shows the most representative 20 conformers resolved by NMR (Fig. 9a), however a number of other structural intermediates must occur in aqueous solution which increase the entropy of the isolated protein. Upon productive binding into the final inhibitory position at the INGECORE of the F_1-ATPase of *P. denitrificans*, the decrease in entropy associated to the loss of conformational freedom upon transition into an ordered α-helix must be compensated by the stabilizing interactions with residues of the INGECORE region, namely those of the $\alpha_{DP}/\beta_{DP}/\gamma$ interface (Fig. 10) (Mendoza-Hoffmann et al. 2018; Morales-Rios et al. 2015). The final locked PdF_1-ζ or PdF_1F_O-ζ complex is unable to catalyse and/or rotate in the CCW direction since the ζ subunit is a total inhibitor leaving zero ATP hydrolysis catalytic activity after productively binding to the F_1 fraction (Zarco-Zavala et al. 2014). Therefore, the final interactions in this locked conformation stabilizes the folding and insertion of the N-terminal inhibitory α-helix of the ζ subunit, thus compensating for the entropy loss of ordering into an α-helix.

The biological role of ε, ζ, and IF_1 as natural F_1F_O-ATPase inhibitors

Knockouts of the ε subunit induce physical separation and therefore uncoupling of F_1 from F_O, thus ε knockout studies cannot be carried out to asses the inhibitory function of ε in vivo. Recently, we have demonstrated that the ζ subunit works as an unidirectional pawl-ratchet inhibitor blocking exclusively the CCW ATPase rotation, but not the CW ATP synthase turnover (Mendoza-Hoffmann et al. 2018), thus showing that the ζ subunit functions as a pawl-ratchet inhibitor favouring ATP synthesis. This was demonstrated by the first knockout mutant of any natural ATP synthase inhibitor with a clear distinctive phenotype of the Δζ mutant, different to the wild type strain by deleting the ζ gene in *P. denitrificans* (Mendoza-Hoffmann et al. 2018). Other previous knockout mutants of the mitochondrial IF_1 inhibitor did not show a clear different phenotype compared with the wild types in the organism growth, reproduction, or bioenergetics, in yeast (Lu et al. 2001), mice (Nakamura et al. 2013), or in *Caenorhabditis elegans*, (Fernandez-Cardenas et al. 2017). In contrast our

PdΔζ mutant showed a very strong growth delay exclusively in respiratoty succinate media, accompanied by a decrease in cellular ATP concentration ([ATP]) and an increase in proton-pumping PdF_1F_O-ATPase activity (Mendoza-Hoffmann et al. 2018). In consequence, our PdΔζ mutant is the first knockout of the ATP synthase's natural inhibitors showing a clear different phenotype, and indicating that the biological role of ζ and likely IF_1 and ε, is to work as unidirectional pawl ratchets, blocking the CCW-F_1F_O-ATPase activity, and thus favouring the CW-F_1F_O-ATP synthase turnover to preverve the cellular ATP (Mendoza-Hoffmann et al. 2018). This also implies that ADPMg is not the key inhibitory mechanism of the F_1F_O-ATPase in vivo, otherwise the Δζ-knockout mutant would had been inhibited in the PdF_1F_O-ATPase activity by ADPMg showing no clear phenotype. This also explains why the previous IF_1 mutants did not show a phenotype different to the wild types, the ζ gene is monogenic in *P. denitrificans*, whereas IF_1 can have up to three different genes in eukaryotes, and besides it also has two accessory and IF_1-like proteins (Stf1, Stf2) which may also work as F_1F_O-ATPase inhibitors. Thus it is likely that the previous knockout studies deleted only one IF_1 gene, and therefore the other IF_1-like genes may had complemented genetically and biochemically the single IF_1 deletion in eukaryotes. In contrast since ζ is monogenic in *P. denitrificans*, we confirmed the total absence of ζ by PCR and western-blot, and corroborated that the expression of the ATP synthase of *P. denirtificans* was not affected by the PdΔζ- deletion. Similarly, another PdΔHydΔζ mutant was described recently showing no clear differences in bacterial respiratory growth and the PdF_1F_O-ATPase/ATP synthase activities (Varghese et al. 2018); however the latter was a multiple mutant where two hydrogenase operons were deleted with a total of nine deletions including the Δζ, and thus the lack of a different phenotype of the mutant is very likely due to complementation of the putative Δζ phenotype with the ΔHyd mutations, together with low-activity enzyme preparations, as explained recently (Zarco-Zavala et al. 2018). However, both Δζ studies coincide in that ζ does not have any effect on the ATP synthase turnover, whereas it blocks the PdF_1F_O-ATPase activity, thus confirming our proposed unidirectional pawl-ratchet mechanism of ζ (Garcia-Trejo et al. 2016; Mendoza-Hoffmann et al. 2018). By preventing exclusively the F_1F_O-ATPase activity and not affecting at all the F_1F_O-ATP synthase rate, ζ, and likely ε and IF_1, work as pawl ratchets to preserve the cellular ATP (See Fig. 11). A ratchet mechanism has been proposed initially for bacterial ε

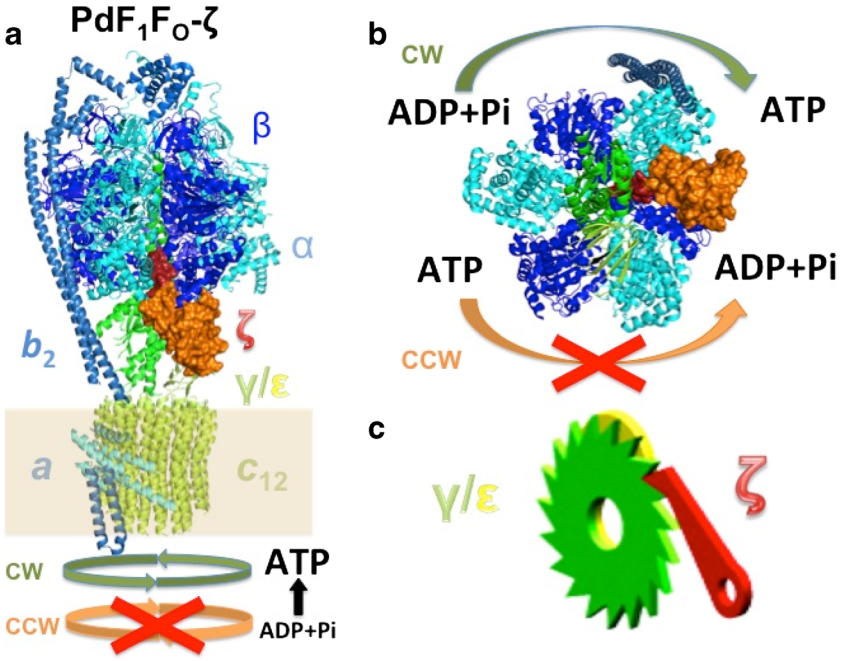

Fig. 11 Unidirectional pawl-ratchet mechanism of the ζ subunit of the ATP synthase of *Paracoccus denitrificans*. A) Model of the full PdF_1F_O-ζ complex obtained by combination of the NMR Pd-ζ structure (PDB-ID 2LL0) and the PdF_1F_O-ζ crystallographic resolution (PDB_ID 5DN6), (Mendoza-Hoffmann et al. 2018), when ζ (orange, globular domain, and red inhibitory N-terminus) is bound at the INGECORE of the $\alpha_{DP}\beta_{DP}\gamma$ interface (cyan, α; blue, β and *b* subunits; γ/ε green and yellow), the enzyme is unable to gyrate its rotor in the CCW-ATPase turnover, but is able to rotate in the CW-ATP synthase activity. B) View of the F_1-ζ complex from F_O to F_1, showing the deep insertion of the ζ N-treminus (red) into the INGECORE blocking the CCW-ATPase rotor gyration, but allowing the CW-ATP synthase rotation (the F_O- subunits were removed for clarity). C) Model of the pawl-ratchet mechanism of the ζ subunit (red) working as a pawl of a ratchet formed by γ/ε subunits (green/yellow). The ζ pawl-ratchet my operate through partial or total release of ζ (conformational pawl-ratchet) during CW-ATP synthase turnover, or by CCW rotation driven by the proton flow and susbtrate binding energies overcoming the presence of bound ζ (mechanical ratchet)

(Tsunoda et al. 2001) and unidirectional effect has been observed from the pioneering studies of mitochondrial IF_1 (Pullman and Monroy 1963a). Here, given that all three natural inhibitors ε, ζ, and IF_1 converge to bind to the INGECORE of the $\alpha_{DP}\beta_{DP}\gamma$ interface, and particularly ζ mimics IF_1 binding exactly in the same position as IF_1 and as an inhibitory folding α-helix, we propose that all three natural PdF_1F_O-ATPase inhibitors work as unidirectional pawl-ratchets inhibiting exclusively the F_1F_O-ATPase turnover to preserve cellular ATP by preventing wasterful ATP consumption.

Concluding remarks

- The F_1F_O-ATP synthase/ATPase of bacteria, mitochondria, and chloroplasts is a kinetically and thermodynamically reversible nanomotor that has to be regulated in order to favour the F-ATP synthase turnover over the F-ATPase one.
- The natural control mechanisms of the F_1F_O-ATPase activity include entrapment of an inhibitory ADPMg, and three inhibitory proteins, bacterial ε, ζ and mitohondrial IF_1.
- In some bacteria, the ε subunit works as a ratchet blocking exclusively the bacterial F_1F_O-ATPase activity by stretching two inhibitory C-terminal and α-helical α-helixes, in a manner controlled by ATP binding, besides its structural function to connect the F_1 and F_O parts of the nanomotor in the central rotary stalk.
- The mitochondrial IF_1 inhibitory protein has an intrinsically disordered inhibitory N-terminus (IDPr) that is folded upon productive bind and lock into a long α-helix by the ERAHL mechanism, blocking preferably the F_1F_O-ATPase activity by stalling the nanomotor at the INGECORE residues of the $\alpha_{DP}/\beta_{DP}/\gamma$ interface. The C-terminus of IF_1 promotes dimerization of IF_1. This ERAHL IF_1 mechanism induce the unidirectional inhibition of the F_1F_O-ATPase probably also as a pawl-ratchet.
- The ζ subunit of *P. denitrificans* is essentially exclusive of the α-proteobacteria class, and binds its IDPr into the INGECORE of the $\alpha_{DP}/\beta_{DP}/\gamma$ interface exactly at the same position as mitochondrial IF_1 but in the *P. denitrificans* PdF_1F_O complex. This inhibitor has a globular and C-terminal anchoring domain, and its biological role in vivo is to work as unidirectional pawl-ratchet blocking exclusively the PdF_1F_O-ATPase turnover but not the PdF_1F_O-ATP synthase activity, thus being essential for respiratory growth and preserving the cellular ATP.
- All three natural F-ATPase inhibitors, ε, ζ, and IF_1 converge to bind into the INGECORE of the $\alpha_{DP}/\beta_{DP}/\gamma$ interface to work probably like ζ, as pawl-ratchets of the ATP synthase nanomotor to block exclusively the wasteful consumption of cellular ATP, and thus favouring the ATP synthase activity. Since bidirectional effects have been also proposed for ε and IF_1, the mechanisms of ε and IF_1 need to be revisited in order to confirm if all natural F_1F_O-ATPase inhbitors, ε, ζ and IF_1 work as such pawl-ratchets to preserve the vital energy of cellular ATP in bacteria and mitochondria.

Acknowledgements This work was supported by grants from México, (CONACyT) Grant CB-2011-01-167622 and U.N.A.M. (DGAPA) Grant PAPIIT- IN221216 (both to J. J. G.-T.). This work is part of PhD Thesis of FMH at the "Programa de Maestría y Doctorado en Ciencias Bioquímicas de la Universidad Nacional Autónoma de México (U.N.A.M.), with JJGT as PhD advisor. FMH was supported by CONACyT Ph.D. Fellowship 277245, and MZZ by CONACyT Fund I0010, Fellowship No. 277592. The kind help to improve the main text of this review paper is gratefully acknowledged to Pattie Nelson, Oregon, and to Prof. Duncan McMillan, Delft. The ζ knockout mutant of *P. denitrificans* was constructed in collaboration with Prof. Miguel Angel Cevallos from UNAM.

References

Abrahams JP, Leslie AGW, Lutter R, Walker JE (1994) Structure at 2.8 Â resolution of F1-ATPase from bovine heart mitochondria. Nature 370:621–628

Akram M (2014) Citric acid cycle and role of its intermediates in metabolism. Cell Biochem Biophys 68:475–478

Allegretti M, Klusch N, Mills DJ, Vonck J, Kühlbrandt W, Davies KM (2015) Horizontal membrane-intrinsic α-helices in the stator a-subunit of an F-type ATP synthase. Nature 14:237–240

Allen RD (1995) Membrane tubulation and proton pumps. Protoplasma 189:1–8

Arnold I, Pfeiffer K, Neupert W, Stuart RA, Schagger H (1998) Yeast mitochondrial F1F0-ATP synthase exists as a dimer: identification of three dimer-specific subunits. EMBO J 17:7170–7178

Arselin G, Giraud MF, Dautant A, Vaillier J, Brethes D, Coulary-Salin B, Schaeffer J, Velours J (2003) The GxxxG motif of the transmembrane domain of subunit e is involved in the dimerization/oligomerization of the yeast ATP synthase complex in the mitochondrial membrane. Eur J Biochem 270:1875–1884

Arselin G, Vaillier J, Salin B, Schaeffer J, Giraud MF, Dautant A, Brethes D, Velours J (2004) The modulation in subunits e and g amounts of yeast ATP synthase modifies mitochondrial cristae morphology. J Biol Chem 279:40392–40399

Bason JV, Montgomery MG, Leslie AG, Walker JE (2014) Pathway of binding of the intrinsically disordered mitochondrial inhibitor protein to F1-ATPase. Proc Natl Acad Sci U S A 111:11305–11310

Bilyard T, Nakanishi-Matsui M, Steel BC, Pilizota T, Nord AL, Hosokawa H, Futai M, Berry RM (2013) High-resolution single-molecule characterization of the enzymatic states in Escherichia coli F1-ATPase. Philos Trans R Soc Lond Ser B Biol Sci 368:20120023

Bonora M, Patergnani S, Rimessi A, De Marchi E, Suski JM, Bononi A, Giorgi C, Marchi S, Missiroli S, Poletti F et al (2012) ATP synthesis and storage. Purinergic Signal 8:343–357

Bouchal P, Kučera I (2003) Examination of membrane protein expression in Paracoccus denitrificans by two-dimensional gel electrophoresis. J Basic Microbiol 44:17–22

Boyer PD (1997) The ATP synthase–a splendid molecular machine. Annu Rev Biochem 66:717–749

Boyer PD (2002) Catalytic site occupancy during ATP synthase catalysis. FEBS Lett 512:29–32

Boyer PD, Chance B, Ernster L, Mitchell P, Racker E, Slater EC (1977) Oxidative phosphorylation and photophosphorylation. Annu Rev Biochem 46:955–1026

Bravo C, Minauro-Sanmiguel F, Morales-Rios E, Rodriguez-Zavala JS, Garcia JJ (2004) Overexpression of the inhibitor protein IF(1) in AS-30D hepatoma produces a higher association with mitochondrial F(1)F(0) ATP synthase compared to normal rat liver: functional and cross-linking studies. J Bioenerg Biomembr 36:257–264

Cabezon E, Butler PHG, Runswick MJ, Walker JE (2000) Modulation of the oligomerization state of the bovine F1-ATPase inhibitor protein, IF1, by pH. J Biol Chem 275:25460–25464

Cabezon E, Runswick M, Leslie AGW, Walker J (2001) The stucture of bovine IF1, the regulatory subunit of mitochondrial F-ATPase. EMBO J 20:6990–6996

Cain BD, Simoni RD (1989) Proton translocation by the F1F0ATPase of Escherichia coli. Mutagenic analysis of the a subunit J Biol Chem 264:3292–3300

Capaldi RA, Schulenberg B (2000) The ϵ subunit of bacterial and chloroplast F1F0 ATPases. Structure, arrangement, and role of the ϵ subunit in energy coupling within the complex Biochim Biophys Acta 1458:263–269

Capaldi RA, Aggeler R, Turina P, Wilkens S (1994) Coupling between catalytic sites and the proton channel in F1F0-type ATPases. Trends Biochem Sci 19:284–289

Capaldi RA, Schulenberg B, Murray J, Aggeler R (2000) Cross-linking and electron microscopy studies of the structure and functioning of the *Escherichia coli* ATP synthase. J Exp Biol 203:29–33

Chandel NS, Schumacker PT (1999) Cells depleted of mitochondrial DNA (rho0) yield insight into physiological mechanisms. FEBS Lett 454:173–176

Cingolani G, Duncan TD (2011) Structure of the ATP synthase catalytic complex F(1) from Escherichia coli in an autoinhibited conformation. Nat Struct Mol Biol 18:701–707

Conway T (1992) The Entner-Doudoroff pathway: history, physiology and molecular biology. FEMS Microbiol Rev 103:1–27

Cori CF (1983) Embden and the glycolytic pathway. Trends Biochem Sci 8:257–259

Cross RL (1981) The mechanism and regulation of ATP synthesis by F1-ATPases. Annu Rev Biochem 50:681–714

Dautant A, Velours J, Giraud M-F (2010) Crystal structure of the mg·ADP-inhibited state of the yeast F1c10-ATP synthase. J Biol Chem 285:29502–29510

de la Rosa-Morales, F. (2005) "Composición de subunidades y Mecanismo de Regulación de la F1FoATP sintasa de Paracoccus denitrificans". In Posgrado en Ciencias Biologicas (Biologia Experimental), Facultad de Ciencias (Direccion General de Bibliotecas: Universidad Nacional Autonoma de Mexico (U.N.A.M.)), pp. 75

Elston T, Wang H, Oster G (1998) Energy transduction in ATP synthase. Nature 391:510–513

Entner N, Doudoroff M (1952) Glucose and gluconic acid oxidation of Pseudomonas saccharophila. J Biol Chem 196:853–862

Esparza-Moltó, P.B., and Cuezva, J.M. (2018) The Role of Mitochondrial H^+-ATP Synthase in Cancer. Front Oncol 8, eCollection

Faccenda D, Campanella M (2012) Molecular Regulation of the Mitochondrial F(1)F(o)-ATPsynthase: Physiological and Pathological Significance of the Inhibitory Factor 1 (IF(1)). Int J Cell Biol 2012:367934

Faccenda D, Tan CH, Duchen MR, Campanella M (2013) Mitochondrial IF1 preservers cristae structure to limit apoptotic cell death signaling. Cell Cycle 12:2530–2332

Faccenda D, Nakamura J, Gorini G, Dhoot GK, Piacentini M, Yoshida M, Campanella M (2017) Control of mitochondrial remodeling by the ATPase inhibitory factor 1 unveils a pro-survival relay via OPA1. Cell Rep 18:1869–1883

Feniouk BA, Mulkidjanian AY, Junge W (2005) Proton slip in the ATP synthase of Rhodobacter capsulatus: induction, proton conduction, and nucleotide dependence. Biochim Biophys Acta 1706:184–194

Feniouk BA, Suzuki T, Yoshida M (2006) The role of subunit epsilon in the catalysis and regulation of FOF1-ATP synthase. Biochim Biophys Acta 1757:326–338

Ferguson SA, Cook GM, Montgomery MG, Leslie AG, Walker JE (2016) Regulation of the thermoalkaliphilic F1-ATPase from Caldalkalibacillus thermarum. Proc Natl Acad Sci U S A 113: 10860–10865

Fernandez-Cardenas LP, Villanueva-Chimal E, Salinas LS, Jose-Nunez C, Tuena de Gomez Puyou M, Navarro RE (2017) Caenorhabditis elegans ATPase inhibitor factor 1 (IF1) MAI-2 preserves the mitochondrial membrane potential (Deltapsim) and is important to induce germ cell apoptosis. PLoS One 12:e0181984

Fillingame RH, Steed PR (2014) Half channels mediating H+ transport and the mechanism of gating in the Fo sector of Escherichia coli F1Fo ATP synthase. Biochim Biophys Acta 1837:1063–1068

Fillingame RH, Peters LK, White LK, Mosher ME, Paule CR (1984) Mutations altering aspartyl-61 of the omega subunit (uncE protein) of Escherichia coli H+ -ATPase differ in effect on coupled ATP hydrolysis. J Bacteriol 158:1078–1083

Fothergill-Gilmore LA, Michels PA (1993) Evolution of glycolysis. Prog Biophys Mol Biol 59:105–235

Gabellini N, Gao Z, Eckerskorn C, Lottspeich F, Oesterhelt D (1988) Purification of the H^+-ATPase from *Rhodobacter capsulatus*, identification of the F_1F_O components and reconstitution of the active enzyme. Biochim Biophys Acta 932:227–234

García JJ, Morales-Ríos E, Cortés-Hernandez P, Rodríguez-Zavala J (2006) The inhibitor protein (IF1) promotes dimerization of the mitochondrial F1F0-ATP synthase. Biochemistry 45:12695–12703

García-Bermúdez J, Cuezva JM (2016) The ATPase inhibitory factor 1 (IF1): a master regulator of energy metabolism and of cell survival. Biochim Biophys Acta 1857:1167–1182

García-Trejo JJ, Morales-Ríos E (2008) Regulation of the F1F0-ATP synthase rotary Nanomotor in its monomeric-bacterial and dimeric-mitochondrial forms. J Biol Phys 34:197–212

Garcia-Trejo JJ, Zarco-Zavala M, Mendoza-Hoffmann F, Hernandez-Luna E, Ortega R, Mendoza-Hernandez G (2016) The inhibitory mechanism of the zeta subunit of the F1FO-ATPase Nanomotor of Paracoccus denitrificans and related alpha-Proteobacteria. J Biol Chem 291:538–546

Gledhill JR, Montgomery MG, Leslie AGW, Walker JE (2007) How the regulatory protein, IF1, inhibits F1-ATPase from bovine mitochondria. Proc Natl Acad Sci U S A 104:15671–15676

Gómez-Puyou A, Tuena de Gómez-Puyou M, Ernster L (1979) Inactive to active transitions of the mitochondrial ATPase complex as controlled by the ATPase inhibitor. Biochim Biophys Acta 547:252–257

Gordon-Smith DJ, Carbajo RJ, Yang JC, Videler H, Runswick MJ, Walker JE, Neuhaus D (2001) Solution structure of a C-terminal coiled-coil domain from bovine IF(1): the inhibitor protein of F(1) ATPase. J Mol Biol 308:325–339

Groth G, Pohl E (2001) The structure of the chloroplast F1-ATPase at 3.2 Å resolution. J Biol Chem 276:1345–1352

Guo H, Bueler SA, Rubinstein JL (2017) Atomic model for the dimeric FO region of mitochondrial ATP synthase. Science 358:936–940

Hammad N, Rosas-Lemus M, Uribe-Carvajal S, Rigoulet M, Devin A (2016) The Crabtree and Warburg effects: do metabolite-induced regulations participate in their induction? Biochim Biophys Acta 1857:1139–1146

Hanson RW (1989) The role of ATP in metabolism. Biochem Educ 17: 86–92

Harris DA, John P, Radda GK (1977) Tightly bound nucleotides of the energy-transducing ATPase, and their role in oxidative phosphorylation. I. the Paracoccus denitrificans system. Biochim Biophys Acta 459:546–559

Harrison MA, Muench SP (2018) The vacuolar ATPase – a Nano-scale motor that drives cell biology. Subcell Biochem 87:409–459

Hashimoto T, Negawa Y, Tagawa K (1981) Binding of intrinsic ATPase inhibitor to mitochondrial ATPase–stoichiometry of binding of nucleotides, inhibitor, and enzyme. J Biochem 90:1151–1157

Hausrath AC, Grüber G, Matthews BW, Capaldi RA (1999) Structural features of the γ subunit of the Escherichia coli F1 ATPase revealed by a 4.4-Å resolution map obtained by x-ray crystallography. Proc Natl Acad Sci U S A 96:13697–13702

Iino R, Hasegawa R, Tabata KV, Noji H (2009) Mechanism of inhibition by C-terminal α-helices of the ϵ subunit of Escherichia coli FoF1-ATP synthase. J Biol Chem 284:17457–17464

John P (1987) Paracoccus as a free-living mitochondrion. Ann N Y Acad Sci 503:140–151

John P, Whatley FR (1975) *Paracoccus denitrificans* and the evolutionary origin of the mitochondrion. Nature 254:495–498

Junge W, Sielaff H, Engelbrecht S (2009) Torque generation and elastic power transmission in the rotary FOF1-ATPase. Nature 459:364–370

Kadoya F, Kato S, Watanabe K, Kato-Yamada Y (2011) ATP binding to the ϵ subunit of thermophilic ATP synthase is crucial for efficient coupling of ATPase and H+ pump activities. Biochem J 437:135–140

Kagawa Y, Racker E (1966) Partial resolution of the enzymes catalyzing oxidative phosphorylation. IX Reconstruction of oligomycin-sensitive adenosine triphosphatase. J Biol Chem 241:2467–2474

Kamerlin SCL, Sharma PK, Prasad RB, Warshel A (2013) Why nature really chose phosphate. Q Rev Biophys 46:1–132

Kato S, Yoshida M, Kato-Yamada Y (2007) Role of the ϵ subunit of thermophilic F1-ATPase as a sensor for ATP. J Biol Chem 282: 37618–37623

Klein G, Satre M, Dianoux AC, Vignais PV (1980) Radiolabeling of natural adenosine triphosphatase inhibitor with phenyl (14C)isothiocyanate and study of its interaction with mitochondrial adenosine triphosphatase. Localization of inhibitor binding sites and stoichiometry of binding. Biochemistry 19:2919–2925

Klionsky DJ, Brusilow WSA, Simoni RD (1984) In vivo evidence for the role of the epsilon subunit as an inhibitor of the proton-translocating ATPase of Escherichia coli. J Bacteriol 160:1055–1060

Knowles JR (1980) Enzyme-catalyzed phosphoryl transfer reactions. Annu Rev Biochem 1980:877–919

Koukourakis, M.I., and Giatromanolaki, A. (2018) Warburg effect, Lactate Dehydrogenase and Radio/Chemo-therapy efficacy. Int J Radiat Biol [Epub ahead of print]

Koumandow VL, Kossida S (2014) Evolution of the F0F1 ATP synthase complex in light of the patchy distribution of different bioenergetic pathways across prokaryotes. PLoS Comput Biol 10:e1003821

Krah A, Kato-Yamada Y, Takada S (2017) The structural basis of a high affinity ATP binding ε subunit from a bacterial ATP synthase. PLoS One 12:e0177907

Krah A, Zarco-Zavala M, McMillan DGG (2018) Insights into the regulatory function of the varepsilon subunit from bacterial F-type ATP synthases: a comparison of structural, biochemical and biophysical data. Open Biol 8

Krebs HA, Johnson WA (1980) The role of citric acid in intermediate metabolism in animal tissues. FEBS Lett 117:K2–K10

Lau W, Rubinstein J (2012) Subnanometre-resolution structure of the intact Thermus thermophilus H+−driven ATP synthase. Nature 481:214–218

Lightowlers RN, Howitt SM, Hatch L, Gibson F, Cox GB (1987) The proton pore in the Escherichia coli F0F1-ATPase: a requirement for arginine at position 210 of the a-subunit. Biochim Biophys Acta 894:399–406

Lu YM, Miyazawa K, Yamaguchi K, Nowaki K, Iwatsuki H, Wakamatsu Y, Ichikawa N, Hashimoto T (2001) Deletion of mitochondrial ATPase inhibitor in the yeast Saccharomyces cerevisiae decreased cellular and mitochondrial ATP levels under non-nutritional conditions and induced a respiration-deficient cell-type. J Biochem 130:873–878

Lu J, Tan M, Cai Q (2014) The Warburg effect in tumor progression: mitochondrial oxidative metabolism as an anti-metastasis mechanism. Cancer Lett 356:156–164

Maldonado E, Dreyfus G, García JJ, Gómez-Puyou A, de Gómez-Puyou MT (1998) Unisite ATP hydrolysis by soluble *Rhodospirillum rubrum* F_1-ATPase is accelerated by Ca^{2+}. Biochim Biophys Acta 1363:70–78

Margulis L, Chapman MJ (1998) Endosymbioses: cyclical and permanent in evolution. Trends Microbiol 6:342–345 discussion 345-346

Martin JL, Ishmukhametov R, Spetzler D, Hornung T, Frasch WD (2018) Elastic coupling power stroke mechanism of the F1-ATPase molecular motor. Proc Natl Acad Sci U S A 115:5750–5755

McMillan DG, Ferguson SA, Dey D, Schroder K, Aung HL, Carbone V, Attwood GT, Ronimus RS, Meier T, Janssen PH et al (2011) A1Ao-ATP synthase of Methanobrevibacter ruminantium couples sodium ions for ATP synthesis under physiological conditions. J Biol Chem 286:39882–39892

McMillan DG, Watanabe R, Ueno H, Cook GM, Noji H (2016) Biophysical characterization of a Thermoalkaliphilic molecular motor with a high stepping torque gives insight into evolutionary ATP synthase adaptation. J Biol Chem 291:23965–23977

Mendoza-Hoffmann F, Pérez-Oseguera A, Cevallos MA, Zarco-Zavala M, Ortega R, Peña-Segura C, Espinoza-Simón E, Uribe-Carvajal S, García-Trejo JJ (2018) The biological role of the ζ subunit as unidirectional inhibitor of the F1FO-ATPase of Paracoccus denitrificans. Cell Rep 22:1067–1078

Mitchell P (1961) Coupling of phosphorylation to Electron and hydrogen transfer by a Chemi-osmotic type of mechanism. Nature 191:144–148

Morales-Rios E, de la Rosa-Morales F, Mendoza-Hernandez G, Rodriguez-Zavala JS, Celis H, Zarco-Zavala M, Garcia-Trejo JJ (2010) A novel 11-kDa inhibitory subunit in the F_1F_O ATP synthase of Paracoccus denitrificans and related α-proteobacteria. FASEB J 24:599–608

Morales-Rios E, Montgomery MG, Leslie AGW, Walker JE (2015) Structure of ATP synthase from Paracoccus denitrificans determined by X-ray crystallography at 4.0 Å resolution. Proc Natl Acad Sci U S A 112:13231–13236

Muench SP, Trinick J, Harrison MA (2011) Structural divergence of the rotary ATPases. Q Rev Biophys 44:311–356

Müller V, Grüber G (2003) ATP synthases: structure, function and evolution of unique energy converters. Cell Mol Life Sci 60:474–494

Nakamura J, Fujikawa M, Yoshida M (2013) IF1, a natural inhibitor of mitochondrial ATP synthase, is not essential for the normal growth and breeding of mice. Biosci Rep 33:735–741

Nakanishi A, Kishikawa J-i, Tamakoshi M, Mitsuoka K, Yokoyama K (2018) Cryo EM structure of intact rotary H+-ATPase/synthase from Thermus thermophilus. Nat Commun 9:1–10

Noji H, Yoshida M (2001) The rotary machine in the cell, ATP synthase. J Biol Chem 276:1665–1668

Noji H, Yasuda R, Yoshida M, Kinosita K Jr (1997) Direct observation of the rotation of F1-ATPase. Nature 386:299–302

Noji H, Ueno H, McMillan DGG (2017) Catalytic robustness and torque generation of the F1-ATPase. Biophys Rev 9:103–118

Oldfield CJ, Dunker AK (2014) Intrinsically disordered proteins and intrinsically disordered protein regions. Annu Rev Biochem 2014: 553–584

Oster G, Wang H (2000) Reverse engineering a protein: the mechanochemistry of ATP synthase. Biochim Biophys Acta 1458:482–510

Pacheco-Moisés F, García JJ, Rodríguez-Zavala JS, Moreno-Sánchez R (2000) Sulfite and membrane energization induce two different active states of the Paracoccus denitrificans F0F1-ATPase. Eur J Biochem 267:993–1000

Paumard P, Vaillier J, Coulary B, Schaeffer J, Soubannier V, Mueller DM, Brethes D, di Rago JP, Velours J (2002) The ATP synthase is

involved in generating mitochondrial cristae morphology. EMBO J 21:221–230

Perez JA, Ferguson SJ (1990) Kinetics of oxidative phosphorylation in *Paracoccus denitrificans*. 1. Mechanism of ATP synthesis at the active site(s) of F_0F_1-ATPase. Biochemistry 29:10503–10518

Pogoryelov D, Krah A, Langer JD, Yildiz Ö, Faraldo-Gómez JD, Meier T (2010) Microscopic rotary mechanism of ion translocation in the Fo complex of ATP synthases. Nat Chem Biol 6:891–899

Pullman ME, Monroy GC (1963a) A naturally occurring inhibitor of mitochondrial adenosine Triphosphatase. J Biol Chem 238:3762–3769

Pullman ME, Monroy GC (1963b) A naturally Ocurring inhibitor of mitochondrial adenosine Triphosphatase. J Biol Chem 238:3762–3769

Rodgers AJ, Wilce MC (2000) Structure of the gamma-epsilon complex of ATP synthase. Nat Struct Biol 7:1051–1054

Rondelez Y, Tresset G, Nakashima T, Kato-Yamada Y, Fujita H, Takeuchi S, Noji H (2005) Highly coupled ATP synthesis by F1-ATPase single molecules. Nature 433:773–777

Sagan L (1967) On the origin of mitosing cells. J Theor Biol 14:255–274

Sánchez-Cenizo L, Formentini L, Aldea M, Ortega ÁD, García-Huerta P, Sánchez-Aragó M, Cuezva JM (2010) Up-regulation of the ATPase inhibitory factor 1 (IF1) of the mitochondrial H+-ATP synthase in human tumors mediates the metabolic shift of cancer cells to a Warburg phenotype. J Biol Chem 285:25308–25313

Schägger H, Pfeiffer K (2000) Supercomplexes in the respiratory chains of yeast and mammalian mitochondria. EMBO J 19:1777–1783

Senior AE (2012) Two ATPases. J Biol Chem 287:30049–30062

Serrano P, Geralt M, Mohanty B, Wüthrich K (2014) NMR structures of α-Proteobacterial ATPase-regulating ζ-subunits. J Mol Biol 426: 2547–2553

Shigemitsu Y, Hiroaki H (2018) Common molecular pathogenesis of disease-related intrinsically disordered proteins revealed by NMR analysis. J Biochem 163:11–18

Shirakihara Y, Shiratori A, Tanikawa H, Nakasako M, Yoshida M, Suzuki T (2015a) Structure of a thermophilic F1-ATPase inhibited by an epsilon-subunit: deeper insight into the epsilon-inhibition mechanism. FEBS J 282:2895–2913

Shirakihara Y, Shiratori A, Tanikawa H, Nakasako M, Yoshida M, Suzuki T (2015b) Structure of a thermophilic F1-ATPase inhibited by an ε-subunit: deeper insight into the ε-inhibition mechanism. FEBS J 282:2895–2913

Smith JB, Sternweis PC (1977) Purification of membrane attachment and inhibitory subunits of the proton translocating adenosine triphosphatase from *Escherichia coli*. Biochemistry 16:306–311

Sobti M, Smits C, Wong ASW, Ishmukhametov R, Stock D, Sandin S, Stewart AG (2016) Cryo-EM structures of the autoinhibited E coli ATP synthase in three rotational states. Elife 5:e21598

Sotomayor-Pérez A-C, Ladant D, Chenal A (2015) Disorder-to-order transition in the CyaA toxin RTX domain: implications for toxin secretion. Toxins (Basel) 7:1–20

Stewart AG, Sobti M, Harvey RP, Stock D (2013) Models, machine elements and technical specifications. Bioarchitecture 3:2–12

Stock D, Leslie AGW, Walker JE (1999) Molecular architecture of the rotary motor in ATP synthase. Science 286:1700–1705

Stroh A, Anderka O, Pfeiffer K, Yagi T, Finel M, Ludwig B, Schägger H (2004) Assembly of respiratory complexes I, III, and IV into NADH oxidase Supercomplex stabilizes complex I in Paracoccus denitrificans. J Biol Chem 279:5000–5007

Suzuki T, Murakami T, Iino R, Suzuki J, Ono S, Shirakihara Y, Yoshida M (2003) F0F1-ATPase/synthase is geared to the synthesis mode by conformational rearrangement of ϵ subunit in response to proton motive force and ADP/ATP balance. J Biol Chem 278:46840–46846

Suzuki T, Tanaka K, Wakabayashi C, Saita E, Yoshida M (2014) Chemomechanical coupling of human mitochondrial F1-ATPase motor. Nat Chem Biol 10:930–936

Symersky J, Pagadala V, Osowski D, Krah A, Meier T, Faraldo-Gómez JD, Mueller DM (2012) Structure of the c(10) ring of the yeast mitochondrial ATP synthase in the open conformation. Nat Struct Mol Biol 19:485–491

Tsunoda SP, Aggeler R, Noji H, Kinosita K, Yoshida M, Capaldi RA (2000) Observations of rotation within the FoF1-ATP synthase: deciding between rotation of the Foc subunit ring and artifact. FEBS Lett 470:244–248

Tsunoda SP, Rodgers AJ, Aggeler R, Wilce MC, Yoshida M, Capaldi RA (2001) Large conformational changes of the epsilon subunit in the bacterial F1F0 ATP synthase provide a ratchet action to regulate this rotary motor enzyme. Proc Natl Acad Sci U S A 98:6560–6564

Tuena de Gomez-Puyou MT, Muller U, Dreyfus G, Ayala G, Gomez-Puyou A (1983) Regulation of the synthesis and hydrolysis of ATP by mitochondrial ATPase. Role of the natural ATPase inhibitor protein. J Biol Chem 258:13680–13684

Turina P, Rumberg B, Melandri BA, Graber P (1992) Activation of the H(+)-ATP synthase in the photosynthetic bacterium Rhodobacter capsulatus. J Biol Chem 267:11057–11063

Turina P, Giovannini D, Gubellini F, Melandri BA (2004) Physiological ligands ADP and pi modulate the degree of intrinsic coupling in the ATP synthase of the photosynthetic bacterium Rhodobacter capsulatus. Biochemistry 43:11126–11134

Uhlin U, Cox GB, Guss JM (1997) Crystal structure of the ϵ subunit of the proton-translocating ATP synthase from *Escherichia coli*. Structure 5:1219–1230

Uversky VN (2016) Dancing protein clouds: the strange biology and chaotic physics of intrinsically disordered proteins. J Biol Chem 291:6681–6688

van Raaij MJ, Orriss GL, Montgomery MG, Runswick MJ, Fearnley IM, Skehel JM, Walker JE (1996) The ATPase inhibitor protein from bovine heart mitochondria: the minimal inhibitory sequence. Biochemistry 35:15618–15625

Varghese F, Blaza JN, Jones AJY, Jarman OD, Hirst J (2018) Deleting the IF1-like zeta subunit from Paracoccus denitrificans ATP synthase is not sufficient to activate ATP hydrolysis. Open Biol 8

von Ballmoos C, Wiedenmann A, Dimroth P (2009) Essentials for ATP synthesis by F1F0 ATP synthases. Annu Rev Biochem 78:649–672

Walker JE (2013) The ATP synthase: the understood, the uncertain and the unknown. Biochem Soc Trans 41:1–16

Walker JE, Dickson VK (2006) The peripheral stalk of the mitochondrial ATP synthase. Biochim Biophys Acta 1757:286–296

Watanabe R, Iino R, Noji H (2010) Phosphate release in F1-ATPase catalytic cycle follows ADP release. Nat Chem Biol 6:814–820

Wilkens S, Capaldi RA (1998) Solution structure of the epsilon subunit of the F1-ATPase from Escherichia coli and interactions of this subunit with beta subunits in the complex. J Biol Chem 273:26645–26651

Yagi H, Kajiwara N, Tanaka H, Tsukihara T, Kato-Yamada Y, Yoshida M, Akutsu H (2007) Structures of the thermophilic F1-ATPase ε subunit suggesting ATP-regulated arm motion of its C-terminal domain in F1. Proc Natl Acad Sci U S A 104:11233–11238

Yasuda R, Noji H, Yoshida M, Kinosita K Jr, Itoh H (2001) Resolution of distinct rotational substeps by submillisecond kinetic analysis of F1-ATPase. Nature 410:898–904

Yin T, Lu L, Xiong Z, Wei S, Cui D (2015) ATPase inhibitory factor 1 is a prognostic marker and contributes to proliferation and invasion of human gastric cancer cells. Biomed Pharmacother 70:90–96

Zarco-Zavala M, morales-Ríos E, Serrano-Navarro P, Wüthrich K, Mendoza-Hernández G, Ramírez-Silva L, García-Trejo JJ (2012) The ζ subunit of the α-proteobacterial F1FO-ATP synthase in Paracoccus denitrificans: a novel control mechanism of the central rotor. Biochim Biophys Acta 1817:S27–S28

Zarco-Zavala, M., Morales-Ríos, E., Serrano-Navarro, P., Wüthrich, K., Mendoza-Hernández, G., Ramírez-Silva, L., García-Trejo, J.J. (2013). Corringendum to: The ζ subunit of the α-proteobacterial F1FO-ATP synthase in Paracoccus denitrificans: A novel control mechanism of the central rotor Biochimica et Biophysica Acta 1827, 60

Zarco-Zavala M, Morales-Ríos E, Mendoza-Hernández G, Ramírez-Silva L, Pérez-Hernández G, García-Trejo JJ (2014) The ζ subunit of the F1FO-ATP synthase of α-proteobacteria controls rotation of the nanomotor with a different structure. FASEB J 28:2146–2157

Zarco-Zavala M, Mendoza-Hoffmann F, Garcia-Trejo JJ (2018) Unidirectional regulation of the F1FO-ATP synthase nanomotor by the zeta pawl-ratchet inhibitor protein of Paracoccus denitrificans and related alpha-proteobacteria. Biochim Biophys Acta 1859:762–774

Zharova T, Vinogradov A (2003) Proton-translocating ATP-synthase of *Paracoccus denitrificans*: ATP-hydrolytic activity. Biochemistry (Mosc) 68:1101–1108

Zhou A, Rohou A, Schep DG, Bason JV, Montgomery MG, Walker JE, Grigorieff N, Rubinstein JL (2015) Structure and conformational states of the bovine mitochondrial ATP synthase by cryo-EM. Elife 4

BBA - Bioenergetics 1859 (2018) 762–774

Contents lists available at ScienceDirect

BBA - Bioenergetics

journal homepage: www.elsevier.com/locate/bbabio

Unidirectional regulation of the F_1F_O-ATP synthase nanomotor by the ζ pawl-ratchet inhibitor protein of *Paracoccus denitrificans* and related α-proteobacteria☆

Mariel Zarco-Zavala[a,b], Francisco Mendoza-Hoffmann[a], José J. García-Trejo[a,*]

[a] Departamento de Biología, Facultad de Química, Ciudad Universitaria, Universidad Nacional Autónoma de México (U.N.A.M.), Delegación Coyoacán, Ciudad de México (CDMX), CP 04510, Mexico
[b] Department of Applied Chemistry, Graduate School of Engineering, The University of Tokyo, Tokyo 113-8656, Japan

ARTICLE INFO

Keywords:
ATP synthase
Unidirectional inhibitor
ζ subunit
Paracoccus denitrificans
Pawl
Ratchet

ABSTRACT

The ATP synthase is a reversible nanomotor that gyrates its central rotor clockwise (CW) to synthesize ATP and in counter clockwise (CCW) direction to hydrolyse it. In bacteria and mitochondria, two natural inhibitor proteins, namely the ε and IF_1 subunits, prevent the wasteful CCW F_1F_O-ATPase activity by blocking γ rotation at the $\alpha_{DP}/\beta_{DP}/\gamma$ interface of the F_1 portion. In *Paracoccus denitrificans* and related α-proteobacteria, we discovered a different natural F_1-ATPase inhibitor named ζ. Here we revise the functional and structural data showing that this novel ζ subunit, although being different to ε and IF_1, it also binds to the $\alpha_{DP}/\beta_{DP}/\gamma$ interface of the F_1 of *P. denitrificans*. ζ shifts its N-terminal inhibitory domain from an intrinsically disordered protein region (IDPr) to an α-helix when inserted in the $\alpha_{DP}/\beta_{DP}/\gamma$ interface. We showed for the first time the key role of a natural ATP synthase inhibitor by the distinctive phenotype of a Δζ knockout mutant in *P. denitrificans*. ζ blocks exclusively the CCW F_1F_O-ATPase rotation without affecting the CW-F_1F_O-ATP synthase turnover, confirming that ζ is important for respiratory bacterial growth by working as a unidirectional pawl-ratchet PdF_1F_O-ATPase inhibitor, thus preventing the wasteful consumption of cellular ATP. In summary, ζ is a useful model that mimics mitochondrial IF_1 but in α-proteobacteria. The structural, functional, and endosymbiotic evolutionary implications of this ζ inhibitor are discussed to shed light on the natural control mechanisms of the three natural inhibitor proteins (ε, ζ, and IF_1) of this unique ATP synthase nanomotor, essential for life.

1. Introduction

The F_1F_O-ATP synthase is a multi-protein molecular machine conserved in the three domains of life to produce most of the cellular chemical energy in the form of ATP. It is located ubiquitously in the energy-transducing membranes of bacteria, chloroplasts, and mitochondria, where it couples the energy associated to a transmembrane electrochemical ion gradient ($\Delta\tilde{\mu}_{H+}$), established by the oxidative or the photosynthetic electron transfer chains, to the chemical synthesis of ATP from ADP and Pi [1].

The physiological function of the F_1F_O complex is the "forward" reaction of ATP synthesis. Nevertheless, during the partial or total collapse of the transmembrane gradient by uncouplers, or in the absence of oxygen and/or alternative electron acceptors, this nanomotor becomes thermodynamically prone to perform the opposite reaction, in which the "reverse" ATP hydrolysis drives the associated proton pumping [2–4]. This activity represents a powerful mechanism to generate $\Delta\tilde{\mu}_{H+}$ in bacteria under anaerobic conditions and could be used to energize other essential cellular functions, such as chemotaxis and secondary transport processes. However, it could be detrimental to mitochondria or chloroplast [5, 6].

Because of the harmful risk of a futile ATP hydrolysis, a number of mechanisms to control the ATPase activity of the enzyme have evolved. One of these mechanisms is controlled by MgADP and is shared by most ATP synthases from different organisms, in which the F_1-ATPase fails to release the inhibitory MgADP from its catalytic sites, thus producing a stable entrapment where the ATPase activity is inhibited. Nevertheless, due to the particular necessities of the mitochondrial, chloroplast, and bacterial ATP synthases, each one has adopted different natural inhibitors for regulating their own ATPase activity. We will recall first the

☆ This article is part of a Special Issue entitled 20th European Bioenergetics Conference, edited by László Zimányi and László Tretter.

* Corresponding author at: Departamento de Biología, Facultad de Química, Universidad Nacional Autónoma de México (U.N.A.M.), Circuito Escolar s/n. Laboratorio 206, Edificio "F", Ciudad Universitaria, Delegación Coyoacán, Ciudad de México (CDMX), CP 04510, Mexico.
E-mail address: jjgartre@unam.mx (J.J. García-Trejo).

https://doi.org/10.1016/j.bbabio.2018.06.005
Received 7 February 2018; Received in revised form 28 May 2018; Accepted 5 June 2018
Available online 08 June 2018

basic rotor/stator architecture of the ATP synthase, and subsequently describe the natural inhibitor proteins that control the rotary mechanism of these unique nanomotors.

2. Structure and catalytic mechanism of ATP synthase

Due to its remarkable biologic importance, the basic architecture of the F_1F_O-ATP synthase has been conserved through evolution. Regardless of their origin, all F_1F_O-ATP synthases are composed of two mechanical rotary-motors; the soluble one is known as F_1 and catalyzes the synthesis or hydrolysis of ATP, and the membrane embedded sector named F_O which transports H^+ or Na^+ ions across the membrane. In the F_1F_O-complex both sectors are coupled by central and peripheral stalks, and work through a chemomechanical rotatory mechanism. However, they can be separated from each other through mild dissociation technics, remaining active in isolated forms [5]. Of course, because the absence of a proton gradient without an energy-transducing membrane, the water-soluble F_1 is unable to synthesize ATP, but is fully functional to hydrolize it.

The bacterial enzyme displays the simplest subunit composition. In this complex, the F_1 portion comprises five proteins named α, β, γ, δ and ε, while the F_O has three essential subunits named *a*, *b* and *c* (see Figs. 4A, 5, 6 and 8). This minimal composition is shared by all F_1F_O-ATP synthases. Nevertheless, depending on their origin and complexity, a different number of additional "supernumerary" subunits bind to the complex. For instance, the mitochondrial enzyme has six to eight additional subunits named d, e, f, g, F6, A6L, the inhibitor protein (IF_1), and the mitochondrial subunit ε (non homologous to bacterial ε). These subunits don't have a direct role in catalysis but fulfil other specific necessities of the enzyme [7]. As in the case of the ε and δ subunits from the mitochondrial enzyme, they are in the lower part of the F_1 fraction and do not interact with the α and β subunits, therefore they do not participate directly in the catalytic sites of the enzyme [8], rather their role is structural, stabilizing the central rotor without further functional or regulatory properties in mitochondria. This lack of regulatory function of mitochondrial ε and δ subunits prompted the evolution of a supernumerary regulatory subunit, the well-known mitochondrial inhibitor protein or IF_1.

The F_1-ATPase complex, also known as the minimum catalytic core of the enzyme, consists of three α and three β subunits, assembled alternately in a hexameric structure, with the γ subunit inserted in its central cavity and the ε subunit associated to γ (γ/ε sub-complex is known as the central stalk, see Figs. 4 and 5, 6, and 8). Each α/β interface has a nucleotide-binding site, but the catalytic activity is only held in the three interfaces where the nucleotide binding site is mainly formed by the β subunit residues. This structure exhibits an inherent asymmetry, critical for its catalytic mechanism. As predicted by Boyer [5, 9], the F_1-ATPase hydrolyzes ATP through a rotatory mechanism known as "binding-change mechanism", in which each β subunit adopts one of three alternative conformations with different nucleotide binding and catalytic properties: Tight, Loose, and Open, later identified by their nucleotide binding as β_{TP}, β_{DP}, and β_E, according to the bound nucleotide (ATP, ADP, or none) [8]. Boyer demonstrated that the catalytic sites have positive kinetic cooperativity and proposed that they alternate simultaneously through these three conformations as induced by energy input from nucleotide binding and from the proton gradient, leading to the different rotary interactions of the catalytic sites with the central stalk [10]. This mechanism proposed by Boyer [5, 9] was further supported by direct observation of the rotation of the central stalk through average multi-molecule and single-molecule experiments [11–13], which state that the simultaneous shifts of the three β reaction states are accompanied by the mechanical rotation of the central stalk in a CCW direction during ATP hydrolysis, and therefore the CW rotation is coupled to ATP synthesis (Fig. 8).

The single-molecule analysis of the *Bacillus* strain PS3 enzyme has provided a detailed comprehension of the rotatory catalytic mechanism of the bacterial F-ATPase. It revealed that every 360° rotation is composed of three steps of 120° and consumes three ATP molecules (see Fig. 5). Each 120° step can be further resolved into two sub-steps, the first one of 80° is driven by the ATP binding and the second one of 40° by the hydrolysis of bound ATP [14–16]. However, the understanding of eukaryotic enzyme at the unimolecular and experimental level has been limited until the human mitochondrial F_1 was analyzed. Mitochondrial F_1 also displays three 120° steps in each revolution, but each 120° step comprises three sub-steps of 65°, 25°, and 30°; driven by the ATP binding, phosphate release, and hydrolysis of bound ATP, respectively [17]. The differences between the bacterial and eukaryotic enzyme revealed a fine tune of the chemomechanical mechanism through evolution and exposed that more work is needed to fully understand the F_1-ATPase catalytic mechanism.

The F_O complex is the motor responsible for the ion transportation because of its transmembranal character, its detailed structure has remained elusive for a long time. It consists of a ring structure formed by the oligomerization of 8 to 15 *c* subunits (depending on the enzyme source) and a monomer of the *a*-subunit adjacent to it. The ion pore is located in the interface between *a*- and the *c*-subunits (see Figs. 6B and 8), where two aqueous half-channels connect the periplasmic and the cytoplasmic side of the membrane with a proton-binding site (carboxyl residue) strictly conserved in each c-subunit and positioned in the outer face of the ring [18]. Recent studies have substantially improved the understanding of the structure and proton-conducting mechanism of the F_O portion. In the suggested mechanism, the protonation of the conserved carboxylate of one *c*-subunit (exposed in one of the half channels), allows this *c*-subunit to rotate toward the hydrophonic lipid bilayer (away from the *a*-subunit), thus exposing a second *c*-subunit for subsequent protonation. After an almost 360° turn, the first protonated *c*-subunit encounters the second half channel which has a hydrophilic environment that promotes the deprotonation of the carboxyl residue, releasing the proton on the opposite side of the membrane [19].

During ATP synthase activity the *c*-ring rotates in a CW direction (viewed from the membrane domain towards the F_1) and ions are translocated across the membrane. The energy associated with this movement is transmitted to the F_1 portion thought the central stalk domain, inducing the conformational changes in the β subunits needed for the synthesis of ATP. Meanwhile, during the ATPase activity, the energy provided by the binding energy and hydrolysis of ATP drives the CCW rotation of the central stalk, the proton pumping and the building up of the electrochemical gradient [20, 21], see Figs. 7B and 8.

Additionally to the two rotatory motors and the central stalk, there is also another functional domain named the peripheral stalk, this portion is located contiguous to the *a*-subunit and laterally connects the transmembrane domain with the top of the $\alpha_3\beta_3$ sub-complex. Its basic composition is a dimer of *b*-subunits and the δ subunit. This portion is not involved directly in the catalytic reaction but its role is to withstand the rotation of $\alpha_3\beta_3$ with respect to the rotating element, preventing futile energy dissipation [22–25], see Figs. 6B and 8.

3. Regulation of the F_1F_O ATP synthase by its natural inhibitor proteins

As mentioned above, and like any molecular engine, the F_1F_O nanomotor is kinetically and thermodynamically reversible, this is, it gyrates both in the "forward" clockwise (CW) direction of ATP synthesis and in the "reverse" counter clockwise (CCW) direction of ATP hydrolysis (see Fig. 8). When the proton gradient $\Delta\tilde{\mu}_{H+}$ collapses either partially or fully, for instance during anoxia (*i.e.* ischemia or anaerobiosis) or uncoupling, the F_1F_O-complex tends to rotate in the reverse direction to work as a primary proton pump to re-establish the $\Delta\tilde{\mu}_{H+}$ that cannot be formed by respiratory chains [21]. Both in mitochondria and in chloroplasts, when de-energized for instance during anoxia or in the darkness, respectively, the F_1F_O-ATPase activity is essentially forbidden

since these organelles are designed to produce, but not to consume ATP; therefore the CCW F_1F_O-ATPase rotation is blocked by different mechanisms to avoid the damage of the cellular and/or organism bioenergetics by the wasteful ATP consumption. The case of chloroplasts, which are regulated by a redox-responsive disulphide bridge in the rotary γ subunit will not be discussed since it has been recently reviewed [6]. The role of other kinetic regulators of the enzyme such as inhibitory MgADP and its release by oxyanions leading to activation of the reverse F_1F_O-ATPase turnover, will not be discussed since their role are well preserved in all F-ATPases. Instead, this review will focus on the regulatory proteins of bacteria and mitochondria where the "reverse" activity of F_1F_O-ATPase may be promoted, for instance during anoxia. We will review particularly the case of facultative bacteria since in this case the ATP synthase regulation must allow both the CW and CCW rotations to carry out synthesis or hydrolysis of ATP, respectively. We will describe how it has been shown that in order to avoid the spurious F_1F_O-ATPase, nature has designed or modified some regulatory subunits of the enzyme to inhibit preferably the F_1F_O-ATPase turnover, thus favouring the F_1F_O-ATP synthase activity. In general, besides the known enzyme regulation by the $\Delta\tilde{\mu}_{H+}$ [26, 27], when the latter decreases, some subunits or inhibitory domains are structured in such a way within the enzyme that they prevent preferably the CCW rotation of the central stalk driven by ATP binding and hydrolysis [28]. Although these inhibitory proteins had been revised recently [29], some details of the mechanism, structure, and biological role of these inhibitors had just emerged and therefore these structural and functional advances are here reviewed.

4. The inhibitory ε subunit of bacterial ATP synthases

As mentioned above, the structure of the nanomotor is divided into a rotating part or rotor, formed mainly by a ring of 8–15 c subunits, which is connected to γ of the central stalk by means of the bacterial subunit ε (see Figs. 6B and 8). The main function of ε is therefore the structural coupling of F_1 and F_O by connecting γ and the c-ring of the central rotor [30–32], and this is achieved by its N-terminal β-sheet globular domain, connecting γ with the c-ring. However, besides its coupling function, in some bacteria ε also works as an intrinsic F_1-ATPase inhibitor [32, 33]. To accomplish this function, ε undergoes a large structural change to favour the CW rotation during ATP synthesis (Figs. 3C and 4A). The inhibitory domain of bacterial ε is found in the two C-terminal α-helixes of the protein, which extend to contact the stator (α/β) and rotor (γ) subunits of the enzyme and therefore inhibit the rotation of the central stalk but preferably in the CCW F_1F_O-ATPase direction [34, 35]. Therefore, the extended conformation of ε favours the CW rotation in the direction of ATP synthesis, and for this reason it has been proposed that it works as a ratchet [34]. Consequently, the compact conformation of ε (Fig. 3C, left) is a non-inhibitory conformer, in which the inhibitory C-terminal domain contracts its two α-helixes in an antiparallel hairpin interacting with the non-inhibitory N-terminal domain. In this way, when contracting its C-terminal domain, ε allows the free γ rotation in both the CCW and CW directions of hydrolysis and synthesis of ATP (Figs. 3C, left, 6B and 8). The transition of ε from its compact to the extended form must go through a semi-extended intermediate, likely similar to that firstly resolved for both the γ/ε complex [36] and the full F_1-ATPase of *E. coli* [37]. More recent structural data [35] confirms that the transition from the active to the inactive forms of the bacterial F_1-ATPase requires the insertion of the C-terminal inhibitory α-helix of ε into the $\alpha_{DP}/\beta_{DP}/\gamma$ interface of the F_1-ATPase to block γ rotation (see Figs. 3C, right and 4A).

Overall, *in vitro* studies have shown that the epsilon subunit has an inhibitory role in the ATPase activity of several bacterial enzymes, through its C-terminal domain. Nevertheless, this domain is the most variable among different bacterial species [38], probably because of a fine tuning to regulate its metabolic functions depending of their environmental demands. More studies under *in vivo* conditions are needed to completely understand the physiological importance of this subunit. For instance, under physiological conditions of *E. coli* growth, removal of the last 5 residues of the C-terminal inhibitory domain of ε decreases aerobic bacterial growth [39], thus showing that ε may play a regulatory role of the forward CW ATP synthase gyration of the enzyme, besides blocking the reverse CCW F_1-ATPase turnover.

Previous studies have stated that depending on their origin, several bacterial epsilon subunits can bind a molecule of ATP. Moreover, the conformational change of the ε subunit from *E. coli* and *Geobacillus stearothermophilus* (formerly known as *Bacillus* PS3) is dependent of the concentration of ATP. This is the case of the ε subunit from *G. stearothermophilus* [40] and *Caldalkalibacillus thermarum* [41]. Recently the structure of the ε subunit from *Mycobacterium tuberculosis* has been resolved [42]. This ε subunit doesn't bind ATP but works as a regulator of the ATPase activity [42]. Although the ε subunit from *M. tuberculosis* has a shorter sequence in its C-terminal, it is proposed to be able to reach the DELSEED region of the α subunit and therefore inhibits the ATP hydrolysis of the enzyme [42]. Ferguson et al. [41] and Joon et al. [42] had raised the question of whether or not the conformational changes of the ε subunit are regulated by the binding of an ATP molecule, as the structure of a mutant ε subunit from *C. thermarum* that doesn't bind an ATP molecule is nevertheless found in the compact conformation; it seems that the effect of ATP binding on the inhibitory function of ε is a species specific feature.

On the other hand, it has been shown that not all ε subunits preserve their inhibitory function, for instance the ε subunit of *Paracoccus denitrificans* [43] is not able to exert F_1F_O-ATPase inhibition; therefore in some cases the inhibitory role of ε has been lost somehow. Moreover, the ε subunits of *G. stearothermophilus* (*Bacillus* PS3) [44] and *Bacillus subtilis* [45] seem to exert F_1-ATPase activation rather than inhibition *in vitro*, indicating that ε does not always work as a bacterial F_1-ATPase inhibitor. On the other hand, the role of ε *in vivo* cannot be assessed by ε knockout studies because ε is a key structural subunit connecting the central γ/ε domain with the c-ring of the rotor, thus a mutant Δε induce dissociation and uncoupling of F_1 from F_O (discussed in Mendoza-Hoffmann et al., 2018 [46]). The instances where ε had lost its inhibitory role are of particular interest for this review since this inhibitory function has been transferred to other natural inhibitor proteins such as the mitochondrial IF_1 (where the homologous δ subunit and the non-homologous ε subunit are non-inhibitory) and the so-called ζ subunit in *P. denitrificans* and related α-proteobacteria, which are the main subject of this review.

5. Mitochondrial F_1-ATPase inhibitor protein IF_1

In mitochondria the δ subunit is homologue to the ε regulatory subunit of bacteria. But neither the ε or δ subunits from mitochondria seem to interact with the α and β subunits as seen in the structural model of the yeast F_1Fo-ATP synthase dimer based on subtomogram average (PDB 4B2Q), and mitochondrial δ doesn't have the ATP binding pocket that the bacterial ones have. Therefore, the δ subunit from mitochondria does not have the ability to inhibit the ATPase activity. This might be the main reason why the IF_1 inhibitory subunit arose. IF_1 is present as a regulatory subunit of mitochondrial ATP synthase from yeasts to complex eukaryotes. This inhibitor has been extensively studied, it is a protein of 10 kDa that binds to the mitochondrial F_1–ATPase with a stoichiometry of 1:1 in a pH sensitive manner and it works better as inhibitor at acidic pH [47–49], *i.e.* in conditions of collapse of the mitochondrial proton gradient that acidifies the mitochondrial matrix. From its very first isolation, IF_1 was described as an unidirectional inhibitor of the F_1F_O-ATPase, *i.e.* without exerting any effect on the ATP synthase turnover [47]; however, other studies had suggested that IF_1 might inhibit both the "forward" F_1F_O-ATP synthase and the "reverse" F_1F_O-ATPase functioning [27, 50–53]. The inhibitory domain of the IF_1 protein resides on its N-terminal side, and this interacts at cross-linking

distance with the C-terminal domain of the β subunit and also with the α subunit of the F_1 (reviewed in [21, 28, 51, 54]). This suggested that the mechanism of action of this protein was to block the catalytic conformational changes of the β subunit, binding through its inhibitory N-terminal domain at one α/β interface [55]. The binding of IF_1 to the mitochondrial F_1-ATPase requires *in vitro* some MgATP hydrolysis turnovers, and it was predicted that it blocks the catalytic turnover of the enzyme at the F_1-MgADP catalytic intermediate [56]. In order to figure out the inhibitory binding mechanism of IF_1, we contributed with the first evidence showing that IF_1, besides interfering with the catalytic β subunits, it also blocks the gyration of the γ subunit since IF_1 cross-links with the rotor subunits γ and ε in the soluble F_1 as well as in the full F_1F_O -ATP synthase [57]. In these studies, we also predicted that the inhibitory N-terminus of IF_1 should enter into the F_1-ATPase through the open catalytic site α_E/β_E [57]. This was later confirmed by the crystal structure of the F_1-IF_1 complex showing that the N-terminus of IF_1 interacts directly with the γ subunit in the central stalk [58]. Upon entrance of the inhibitory IF_1 N-terminus into the open α_E/β_E interface mitochondrial F_1-ATPase, the central rotor of the F_1-ATPase undergoes at least two partial CCW 120° rotations to transform this catalytic interface firstly into the subsequent α_{TP}/β_{TP} conformer and finally into the α_{DP}/β_{DP} conformation where IF_1 locks and blocks further γ rotation [28]. This explains why some F_1-ATPase turnovers are required to achieve the proper productive biding of IF_1 and confirms the predicted action of IF_1 into the F_1-ADP catalytic intermediate [56]. Interestingly, this bind and lock mechanism of IF_1 is also coupled to the transition of the IF_1 N-terminus from an intrinsically disordered region (IDPr) free in solution to a long α-helix when bound to F_1 (see Fig. 3B). This is depicted as an Entrance-Rotation-Alpha-Helix-Lock (ERAHL) mechanism for the α-proteobacterial ζ subunit in Fig. 5A–D, where the final inactive F_1-inhibitor complex is formed after two partial 120° γ-ε rotations, similar to the bind-lock mechanism that we proposed before for mitochondrial IF_1 [28]. The primary, secondary, and tertiary structure of IF_1 is very different from the bacterial ε inhibitory subunit, since it does not contain any β-folded structure but is, in its isolated form, a single (or dimeric) α-helix that becomes extended and structured as it is inserted into the $\alpha_{DP}/\beta_{DP}/\gamma$ interface (Fig. 3B), thus inhibiting γ rotation and further conformational changes of the catalytic interfaces α/β (see Figs. 3B and 4B,D). In essence, the mechanism of inhibition of both IF_1 and ε are similar in that both proteins interact with γ to inhibit the rotation of the central stalk; however, they do it differently since IF_1 has a larger contact surface with the α/β interface (Fig. 4B), whilst subunit ε literally wraps with subunit γ (Fig. 4A).

6. The ζ inhibitor protein of the F_1F_O-ATPase of *Paracoccus denitrificans* and related α-proteobacteria

To shed light on how the control of ATP synthase had evolved from bacteria to mitochondria, we studied the kinetics and structure of the ATP synthase of the α-proteobacterium *Paracoccus denitrificans*, which is phylogenetically related to the protoendosymbiont that gave origin to the actual mitochondria [59]. *P. denitrificans* has been used as a model to isolate and study other respiratory complexes due to its relative simplicity in subunit composition compared to mitochondrial complexes. In addition, the ATP synthase of *P. denitrificans* has the peculiarity of being the fastest ATP synthase and the slowest F-ATPase that has been described, and this is reflected in its ratio of ATP synthase/ATPase activities which is in the range of 20–60 [60–63], while the same ratio is much lower, even < 1.0, for the enzymes of bacteria or mitochondria; that is, the *Escherichia coli* and mitochondrial ATP synthases can synthesize or hydrolyze ATP at a similar rate, while the *P. denitrificans* enzyme is practically a *unidirectional* ATP synthase. Due to these antecedents, our laboratory has been interested in solving the mechanism of the ATP synthase regulation of *P. denitrificans* that allows it to synthesize ATP at high speed, essentially without hydrolyzing it.

Initial attempts to isolate the F_1-ATPase of *Paracoccus denitrificans*

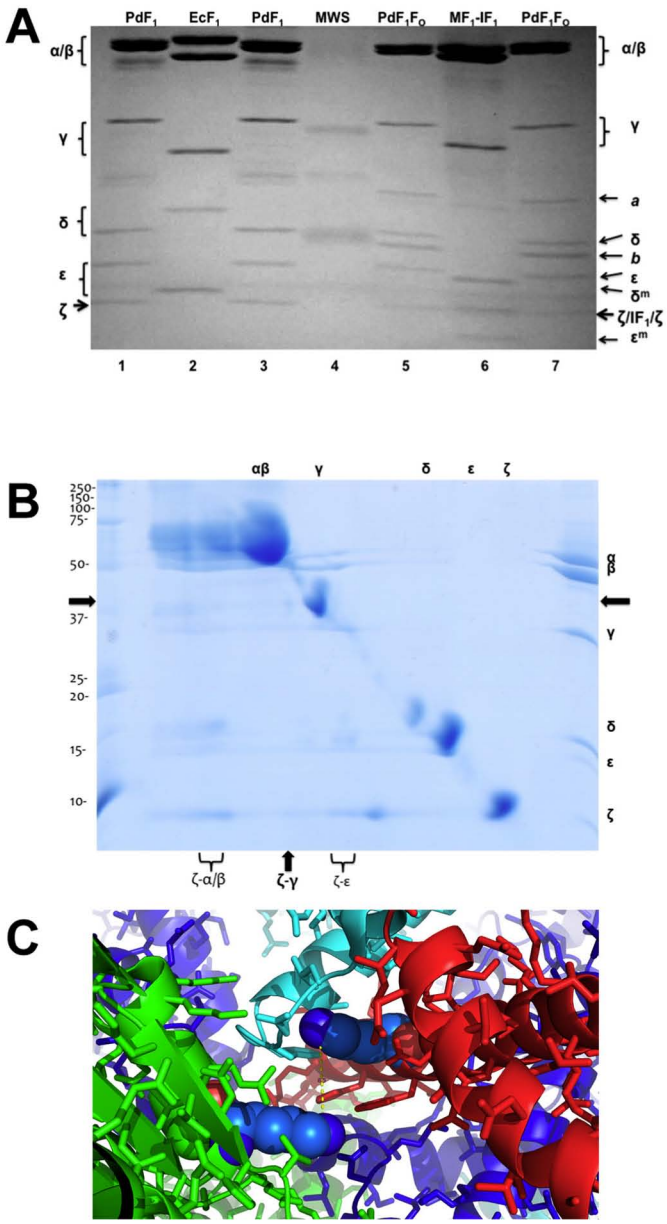

Fig. 1. SDS-PAGE of F_1 and F_1F_O complexes from *E. coli*, *P. denitrificans* and bovine heart mitochondria and γ-ζ cross-linking. A) A denaturing SDS-PAGE gel (10–22%) was loaded with 20 μg of the following preparations: 1, PdF_1-ATPase from *P. denitrificans*; 2, *E. coli* F_1-ATPase; 3, PdF_1-ATPase; 4, Molecular Weight Standards (20, 25, 30 and 50 kDa from bottom to top); 5, The F_1F_O-ATP synthase complex of *P. denitrificans*; 6 mitochondrial F_1-IF_1 complex; 7, F_1F_O from *P. denitrificans*. The mitochondrial δ and ε subunits are labelled δ^m and ε^m. The position of the ζ subunit (thick arrows) is underneath ε and co-migrates with the mitochondrial inhibitor protein, IF_1, as seen at the bottom. All preparations were obtained by Fernanda de la Rosa [65]. B) A Coomassie-stained 2D-SDS-PAGE was loaded with ≈450 μg of the ζ-reconstituted and cross-linked PdF_1-ζ complex. Crosslinking was carried out with dithiobis-succinimidyl proprionate (DSP) as described before [43]. The low-yield ζ-γ cross-linking is indicated by the black arrows and appeared as a faint γ and ζ spots aligned vertically below the diagonal formed by non-crosslinked subunits. Other ζ-ε and ζ-α/β cross-linkages of higher yield are also indicated, similar 2D gels are also shown in [43]. C) Two lysine residues (γ-K122 and ζ-K14, shown in blue spheres) are in cross-linking distance (≈9 Å) to explain the low yield ζ-γ cross-link observed in A). A number of other K residues are in cross-linking distance between ζ-α/β or between ζ-ε also explain these other higher yield cross-linkages observed in B, but are not shown. The structure shown is derived from combined crystal and NMR structures of the PdF_1F_O-ζ complex from reference, ζ is red, γ is green, α is cyan and β is blue [46].

showed a very low activity or latent F_1-ATPase [64], therefore we looked for maximal activation conditions of the F_1-ATPase turnover of this enzyme and found these in the presence of oxyanions such as sulphite [61, 62]. After finding the proper activation conditions of the enzyme to follow it during purification, the functional and stable F_1 and F_1F_O complexes from *P. denitrificans*, (PdF_1 and PdF_1F_O) were isolated for the first time [65], and hence we discovered a sixth subunit of 11 kDa associated with PdF_1 in addition to the 5 canonical subunits of bacterial F_1-ATPases (α, β, γ, δ, and ε). This protein was also found associated to the PdF_1F_O complex, which is purified by a method different from that used to isolate PdF_1, indicating that this sixth subunit of PdF_1 should be a structural or regulatory subunit of the PdF_1F_O complex [65]. Coincidentally, this protein co-migrates in denaturing gels with the inhibitory protein (IF_1) of mitochondrial ATP synthase [65] (see also Fig. 1A). This observation, together with the tight control of the ATP synthase of *P. denitrificans* that favours its "forward" synthetic activity over the "backward" hydrolytic one, led us to propose that this sixth subunit of PdF_1 could be an inhibitory protein of this bacterial F_1-ATPase [65]. Given its relatively low molecular weight and migration in denaturing gels, we named this protein as the "ζ" subunit in decreasing order of size relative to ε [66]. Before cloning ζ, we obtained an enriched preparation of the endogenous ζ from Sub-Bacterial Particles (inside-out vesicles, SBP) of *P. denitrificans* by incubation in activating conditions with sulphite, similar to the *in vitro* conditions that release IF_1 from Sub-Mitochondrial Particles (SMP) [65]. Although this crude ζ extract was not completely pure, but it was a ζ enriched preparation, it was assessed for its hypothetical inhibitory function on the PdF_1 and PdF_1F_O ATPases. As can be seen in Fig. 2A, this ζ enriched fraction exerted a partial inhibition of the PdF_1F_O-ATPase when it was added to the inside-out vesicles containing the native PdF_1F_O without pre-incubation in the presence of MgATP. This suggested that the ζ inhibition was partial because the productive inhibitory binding of ζ should require some rotary turnovers induced by pre-incubation with limited amounts of MgATP, similar to mitochondrial IF_1. Therefore, after cloning the ζ gene in *E. coli*, and purifying the ζ recombinant protein, we assessed the effect of this recombinant and highly pure ζ protein (see inset in Fig. 2B) on the ATPase activities of the PdF_1F_O ATPase of sub-bacterial particles (SBP) and in the soluble PdF_1-ATPase, after pre-incubation with ζ in the presence of MgATP. According to our regulatory hypothesis for this subunit ζ, we confirmed that this protein is a total inhibitor of the PdF_1-ATPase and PdF_1F_O-ATPase activities, even under conditions of strong activation [43, 66]. These results indicated that indeed, some PdF_1-ATPase turnovers are necessary for the proper ERAHL ζ binding mechanism to take place (Fig. 5).

Interestingly, we also found that the ε subunit does not exert an inhibitory function on the PdF_1-ATPase or the PdF_1F_O-ATPase, which strongly suggested that in *P. denitrificans* the regulatory mechanism of the ATP synthase was different in that the ε subunit does not participate [43]. It was then very likely that the ζ subunit could represent another control mechanism of the bacterial nanomotor, where the inhibitory function was transferred from ε to ζ. Remarkably, we also found that this protein exists as an open reading frame preserved exclusively along the α-proteobacteria class, and we confirmed that this ζ is expressed and bound to the ATP synthase of other α-proteobacteria such as *Rhodobacter sphaeroides* [66], among others (Mendoza Hoffmann and García-Trejo, in preparation). This implies that this new control mechanism of subunit ζ was not exclusive of *P. denitrificans*, but it exists as such in most if not all α-proteobacteria.

When we sequenced both the ζ gene and the ζ protein, it was found that it has no significant overall similarity with the other regulatory subunits of the F_1F_O nanomotor, *i.e.* ε and IF_1. However, from our very first isolations of the F_1-ATPase and the ζ subunit of *P. denitrificans* we sequenced initially the first 15 N-terminal residues by Edman degradation [65]. Intriguingly, these first residues of ζ N-terminus resulted similar to the inhibitory domain of mitochondrial IF_1 (see [43, 65] and Fig. 4C), and eventually this last similarity had a strong

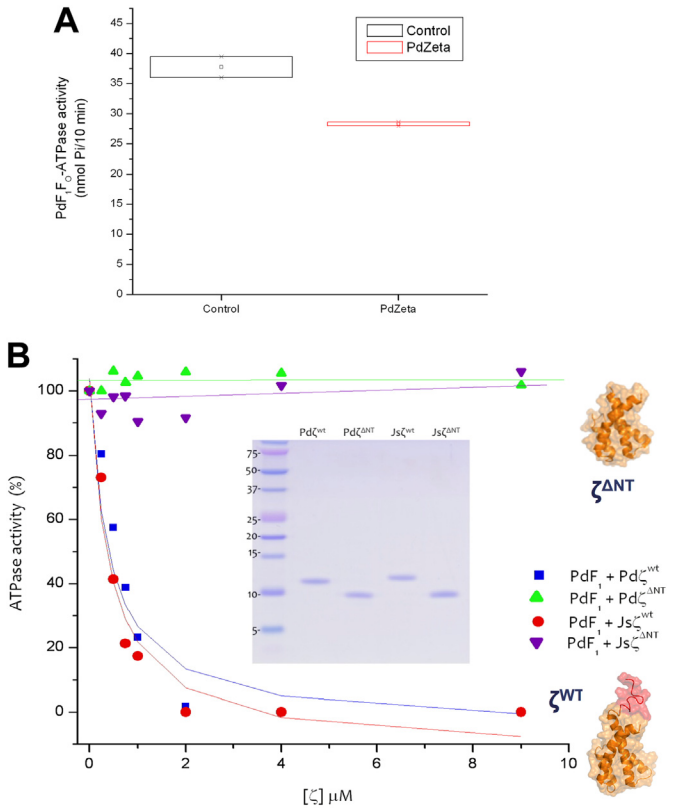

Fig. 2. Functional demonstration that the ζ subunit is a total inhibitor of the PdF_1-ATPase and that the ζ-Nterminus has the inhibitory domain. A). 20 μg of the native ζ subunit extracted from inverted vesicles (SBP) of *Paracoccus denitrificans* as in reference [65] were added to 100 μg of SBP containing the F_1F_O-ATPase, before the addition of 3 mM MgATP (red), and the initial rate of PdF_1F_O-ATPase activity (followed by Pi release as in [43]) was compared with a control where no ζ was added (black). The PdF_1F_O-ATPase was inhibited by about 30% without pre-incubation with ζ and MgATP. This experiment was the first evidence of PdF_1-ATPase inhibition by the ζ subunit, data were derived from duplicate determinations, thus no statistical deviation was calculated but the PdF_1F_O-ATPase activities of each duplicate of control without ζ (black) and experimental + ζ (PdZeta,red) duplicates are shown by the upper and lower line of each box. The average values are shown by the central spot (black square, control; red diamond, Pd-ζ. Similar results were obtained with the soluble PdF_1-ATPase (not shown). B) The PdF_1-ATPase (lacking ζ and ε subunits) was pre-incubated by about 10 min with 1 mM MgATP with increasing concentrations of the indicated *recombinant* ζ subunits: ■, Pd-ζ^{WT}; ●, Js-ζ^{WT}; ▲, Pd-$\zeta^{\Delta NT}$; ▼, Js-$\zeta^{\Delta NT}$. The PdF_1-ATPase activities obtained by Zarco-Zavala et al. [43] were re-plotted including an insert with a denaturing SDS-PAGE of ≈0.5 μg of the purified recombinant Pd-ζ^{WT}, Js-ζ^{WT}, Pd-$\zeta^{\Delta NT}$, and Js-$\zeta^{\Delta NT}$ subunits (lanes 2–5, lane 1 size markers). The gel shows the high purity of the preparations. The NMR structure of the complete Pd-ζ^{WT} (PDB 2LL0) subunit is shown at the right bottom with the N-terminal inhibitory domain in red, and the globular 4-α-helix domain in orange. At the right top, the NMR Js-$\zeta^{\Delta NT}$ (PDB 2KZC) is shown lacking the N-terminal inhibitory domain. Both structures can be superimposed very well (see Fig. 3A, left side).

significance as discussed later. However, the overall structural difference between ζ and IF_1 (Fig. 3) strongly suggests that the ζ subunit of the ATP synthase of α-proteobacteria is not an evolutionary predecessor of mitochondrial IF_1, although this difference does not rule out completely this possibility. On the other hand, what was certain was that the ζ subunit is the first supernumerary gene external to the ATP operon that is structurally and functionally integrated into the bacterial F_1F_O nanomotor.

To start unveiling this new regulatory mechanism of the bacterial F_1F_O nanomotor, and before the structural resolution of this protein, we carried out some reversible cross-linking experiments similar to those

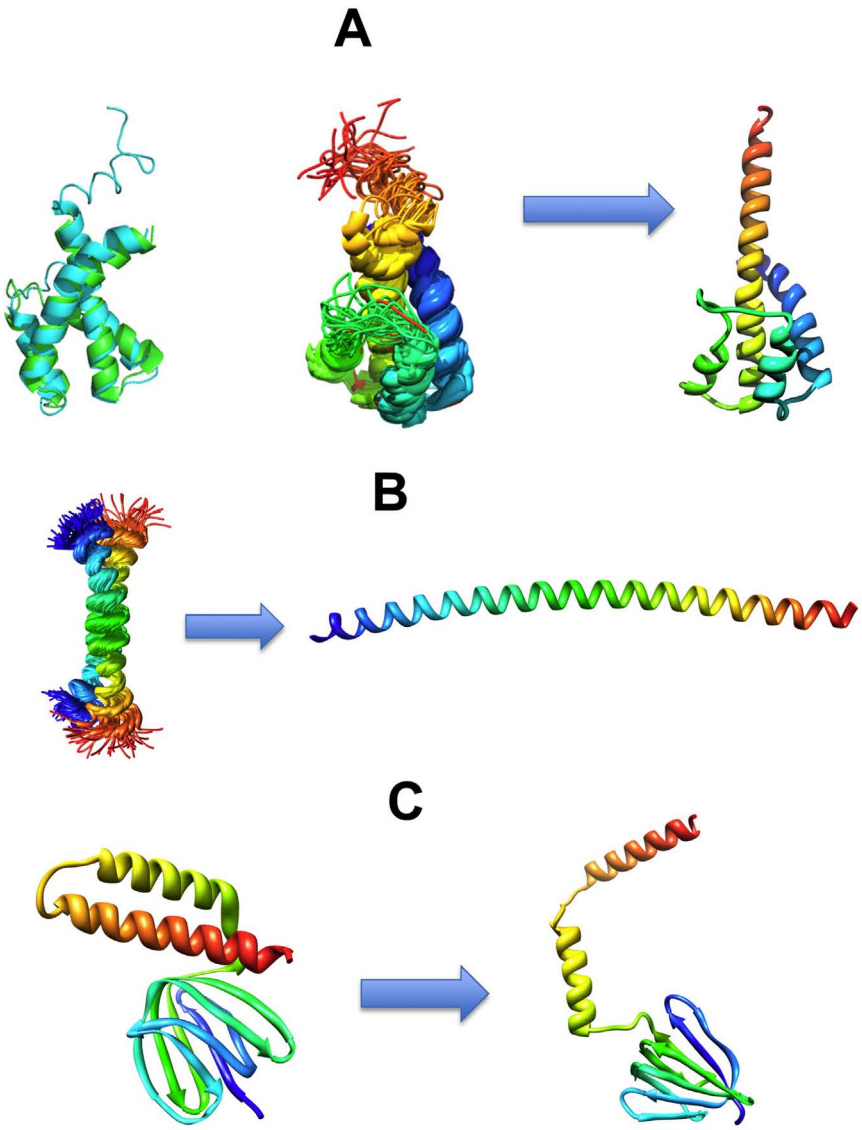

Fig. 3. Structural transitions of the three F_1-ATPase inhibitor proteins. A) Left: Superposition of Pd-ζ (PDB 2LL0, cyan) and Js-ζ (PDB 2KZC, green) subunits as resolved by NMR. Center and Right: transition of Pd-ζ from solution structure (center) to the inhibitory conformer of the protein bound to the F_1Fo-ATPase of *P. denitrificans* (far right). The Inhibitory N-terminus is shown in red, and the C-terminus in blue. The right structure was obtained by alignment of the NMR structure (PDB 2LL0) with the crystal structure (PDB 5DN6). B) Transition of the mitochondrial IF_1 from dimeric state in solution by NMR (PDB 1HF9, left) to the bound state in mitochondrial F_1-IF_1 complex (PDB 2V7Q, right). C) Transition of the *E coli* ε subunit from free in solution (PDB 1AQT, left) to the extended inhibitory form bound to EcF_1 (PDB 3OAA, right). The inhibitory C-terminal domain is shown in red and the N-terminal domain in blue.

we carried out before with the mitochondrial F_1-IF_1 complex, and in which we contributed with the first direct evidence showing that IF_1 is in close proximity to γ and ε subunits of the central rotor, thus indicating that IF_1 inhibits γ-rotation [57]. Accordingly, we succeeded in the observation of a low yield ζ-γ adduct in addition to the higher yield ζ-α/β and ζ-ε cross-linkages (see reference [43] and Fig. 1B), reminiscent of those we observed before in the mitochondrial F_1-IF_1 complex [57]. This suggested that the low yield ζ-γ adduct could be formed with the unique ζ-K14 residue of the ζ-N terminus and the γ-K122 of the γ subunit (shown as blue spheres in Fig. 1C), whereas the more extensive ζ-α/β and ζ-ε adducts were likely formed thanks to a larger number of K residues present in ζ and γ subunits (not shown). Eventually, the atomic structure of the PdF_1F_O-ζ complex showed that these two lysines (in blue spheres) are in good cross-linking distance (Fig. 1C) thus explaining the ζ-γ adduct shown in Fig. 1B and reference [43]. Notwithstanding that this was a low yield ζ-γ crosslink, the data was reproducible and indicated that similar to IF_1 [57], ζ should also be at close proximity to the γ subunit of the central rotor, thus blocking the γ-ε rotation of the PdF_1-ATPase.

Once stated that ζ blocks the γ-ε rotation in PdF_1, we determined the secondary structure content of the recombinant ζ subunit by circular dichroism finding that it is > 90% α-helix [43], and subsequently we resolved its tertiary structure in solution by Nuclear Magnetic Resonance (NMR) thanks to a kind collaboration with Prof. Kurt Wüthrich [43, 67]. We resolved 20 conformers of the ζ-subunit showing a protein with > 90% α-helix as we observed initially by circular dichroism, containing 4 α-helices folded in a globular domain and the N-terminus protruded as an intrinsically disordered protein region (IDPr) with high mobility (see ref. [43, 67] and Fig. 3A). It is worth to mention that this highly mobile N-terminus of ζ was also the most conserved domain of the protein along the class of α-proteobacteria [43]. The tertiary structure of the protein is totally different from those of ε and IF_1 (Fig. 3). Experiments of limited proteolysis, chemical cross-linking (Fig. 1B), together with the high mobility and conservation of this N-terminal domain of ζ, suggested that the inhibitory domain of this protein should be found in its N-terminus that protrudes from the globular domain (red in Figs. 2B, 3A, 5,6 and 8), with the latter resulting structurally identical to that resolved from the related α-proteobacteria *Jannaschia* sp. (PDB 2KZC; [68]), see Fig. 3A (left side, green).

In order to confirm that the ζ N-terminus contained the inhibitory domain of the protein, we constructed a $Pd\zeta^{\Delta NT}$ mutant truncated from the first 15 N-terminal residues, the same that were highly mobile and conserved (red in Figs. 2B, 3A, 5,6 and 8). Clearly, we observed that removal of the ζ N-terminus abolished completely the functional inhibitory capacity of the protein [43] (see also Fig. 2B). Besides, removal

of these residues did not affect the folding of ζ because the truncated protein was able to bind to the PdF_1-ATPase [43], and moreover, the similar N-terminus truncated protein from *Jannaschia* sp., was also unable to inhibit the PdF_1-ATPase, whereas the WT ζ from *Jannaschia* (Js-ζ) was as good inhibitor as the Pd-ζ (see Fig. 2B and reference [43]). Furthermore, and as mentioned above, the structure of the Js-$\zeta^{\Delta NT}$ truncated protein (PDB 2KZC, ref. [68], green in Fig. 3A and orange in Fig. 2B) superimposed very well to that of the full Pd-ζ (cyan in Fig. 3A and orange/red in Fig. 2B), thus confirming that the folding of the ΔNT mutants was not affected by the ΔNT truncation. Taken together, these results confirmed that the first 15 residues conformed the inhibitory N-terminal domain of ζ (red in Figs. 2B, 3A, 5, 6 and 8).

7. The N–terminal domain of ζ mimics IF_1 and binds to the same $\alpha_{DP}/\beta_{DP}/\gamma$ interface

In order to resolve the inhibitory binding site of the N-terminus of ζ in the PdF_1-ATPase, functional, crystallographic and structural modelling approaches were carried out. Our first collaborative efforts to crystallize the native PdF_1-ATPase resulted in a high resolution structure, but of a single catalytic α/β pair lacking the central rotor and ζ subunits [69]. Therefore, in order to resolve this issue, a homology model of the PdF_1-ATPase was constructed that was of high quality given the strong identity between the F_1-ATPases of bovine heart mitochondria and that of *P. denitrificans* [70]. This high identity, supports, by the way, the endosymbiotic origin of mitochondria as derived from the α-proteobacteria class [59]. Once the PdF_1 model was obtained as supported by cross-linking and limited proteolysis data, an extended conformer of the ζ subunit was docked into the open interface of the catalytic PdF_1-ATPase [70]. As we observed before for the mitochondrial IF_1 by similar approaches [28, 57], the ζ subunit enters into the PdF_1-ATPase through the open α_E/β_E interface, and two partial 120° γ/ε rotations driven by ATPMg hydrolysis are coupled to the final lock of ζ into its final inhibitory destination (Fig. 5). The cross-linking (Fig. 1B, and ref. [43]) and ΔNT truncated mutants indicated that the ζ N-terminus should enter somehow into a catalytic interface to block rotation [43]. However, the key element to find the final inhibitory position of ζ was the similarity between the ζ N-terminus and that of the mitochondrial IF_1 [43, 65, 70], Fig. 4C). This allowed us to make a structural alignment in 3D of the N-terminus of ζ with IF_1 bound to its inhibitory position in mitochondrial F_1-ATPase ([70], Fig. 4D). This successful structural alignment indicated that both, ζ and IF_1 bind to the same inhibitory position at the $\alpha_{DP}/\beta_{DP}/\gamma$ interface of their respective F_1-ATPases, and this was confirmed by functional competition assays with both inhibitors binding to the $\alpha_{DP}/\beta_{DP}/\gamma$ interface of the F_1-ATPase of *P. denitrificans* [70]. The similarity between ζ and IF_1 also allowed us to predict that the ζ N-terminus could shift from an IDPr to an α-helix if the ζ binding structure and mechanism was similar enough to that of IF_1 [70], which also undergoes such an IDPr-α-helix transition [71]. This ζ binding site and shift from IDPr to α-helix were predicted and appeared on line just before the release on the PDB of the atomic coordinates of the crystallographic resolution of the full F_1F_O-ATPase of *P. denitrificans,* which confirmed this binding site [72]; since we had no access to the atomic coordinates of the 5DN6 structure, the appearance of our structural, modelling, cross-linking, and functional studies [70] just before the PDB 5DN6 release, validated further that our own clues gave us the right insights to resolve the IF_1-like ζ binding site in the $\alpha_{DP}/\beta_{DP}/\gamma$ interface of the PdF_1-ATPase, independently of the release of the PdF_1F_O crystal structure. In summary both ζ and IF_1 inhibitors contain N-terminal domains as IDPr free in solution, which acquire a folded α-helical structure upon productive binding to their respective F_1-ATPases. The transition from IDPr to α-helix of the ζ N-terminus is more easily seen in Fig. 3A, where the highly mobile N-terminus of ζ found in solution is shifted to a stiff α-helix that can be perfectly superimposed to that of mitochondrial IF_1. Thus ζ and IF_1 can be added to the large family of Intrinsically Disordered Proteins (IDPs) [73, 74]. The final inhibitory position of ζ is shown in our PdF_1-ζ model [70] as stereo view in Fig. 6A, with the ζ-N-terminus in red. This position is very similar to that observed for the ζ subunit in the full PdF_1F_O in the crystal structure [72]. However, the latter lacked the globular domain of ζ, since it resolved only the N- and C-terminal ζ α-helixes; thus we constructed a more complete structural model of the PdF_1F_O-ζ complex [46] by structural alignment of the ζ NMR structure [43, 67, 68] (PDBs 2LL0) with the crystallographic N- and C-terminal α-helixes of ζ [72] (PDB 5DN6). The combined and refined structure shows that the N-terminal α-helix of ζ (red in Figs. 6B and 8), blocks rotation of γ, while the globular domain (orange in Figs. 6B and 8) holds ζ bound to the α_{DP}/β_{DP} interface [46]. This position of ζ raises the question of whether it is a bidirectional inhibitor of CW and CCW γ rotation, thus inhibiting both the PdF_1F_O-ATPase as well as the PdF_1F_O-ATPase. Alternatively, ζ could be a unidirectional inhibitor of the CCW PdF_1F_O-ATPase, thus favouring the overall "forward" ATP synthase turnover. In the latter case, ζ should work as a pawl-ratchet blocking selectively the CCW γ rotation.

8. The biological role of ζ as unidirectional pawl-ratchet PdF_1F_O-ATPase inhibitor

In order to ascertain the role and mechanism of ζ, we constructed recently a ζ null mutant in *P. denitrificans* (PdΔζ) that allowed us to assess the effect of ζ removal on both the bacterial physiology and on the relative ATP synthase/ATPase rates of the PdF_1F_O complex [46]. The construction was successful thanks to a recombinant suicidal plasmid that removed the full ζ gene thus leaving an antibiotic resistance cassette for selection, and the total removal of ζ was confirmed by PCR and anti-ζ western-blots [46]. Interestingly, this resulted in the first clear distinctive phenotype of a knockout of any natural ATP synthase inhibitor, because previous IF_1 knockouts failed to give a significantly different phenotype compared to the WT in yeast [75], mice [76], or *C. elegans* [77], where the slight effects of lacking IF_1 are only seen under very extreme stress conditions. The lack of major effects of the ΔIF_1 mutations is probably due to complementation with other copies of the IF_1 gene or by homologous genes that encode for assembly factors that may also work as F_1 inhibitors [78, 79]. In contrast to mitochondrial IF_1, the ζ subunit is monogenic in *P. denitrificans*, and therefore the PdΔζ mutant was severely affected in its growth in succinate ([46] see Fig. 7A) which is a strictly respiratory medium. This was accompanied by a significant increase in the PdF_1-ATPase and proton-pumping PdF_1F_O-ATPase activities (Fig. 7B), but failed to affect at all the ATP synthase activity [46]. In parallel, the intracellular concentration of ATP ([ATP]) decreased in succinate to about half in the mutant due to an increased PdF_1F_O-ATPase activity, in concordance with a much slower growth rate compared with the WT Pd1222 [46]. Genetic complementation with recombinant WT Pd-ζ by an exogenous plasmid induced the recovery of both parameters, *i.e.* the bacterial growth rate and the cellular [ATP], showing that the observed phenotypic differences of the mutant are exclusively due to the Δζ mutation and not to non-specific mutations or changes [46]. Furthermore, the reconstitution of excess ζ into the PdΔζ membranes of *P. denitrificans* failed to exert any effect on the steady state PdF_1F_O-ATP synthase rate, but inhibited fully the proton-pumping PdF_1F_O-ATPase [46]. In parallel, another recent report of a ζ knockout from others showed, in apparent contrast to our results, no significant effects of the ζ deletion on the respiratory growth of *P. denitrificans* and a limited activation the PdF_1 and PdF_1F_O-ATPase activities [80]. At first sight, the latter study seemed contrary to our findings on the key biological role of ζ as unidirectional PdF_1-ATPase inhibitor in respiratory growth [46]; however, a closer look to this report of Hirst and colleagues show several differences with our ζ knockout: 1) firstly, their Δζ knockout is not a single mutation but a multiple mutant constructed in addition to 8 deletions of genes encoding for proteins belonging to hydrogenase operons (ΔHy) of *P. denitrificans* [80]; in contrast, our Δζ mutant was constructed on the

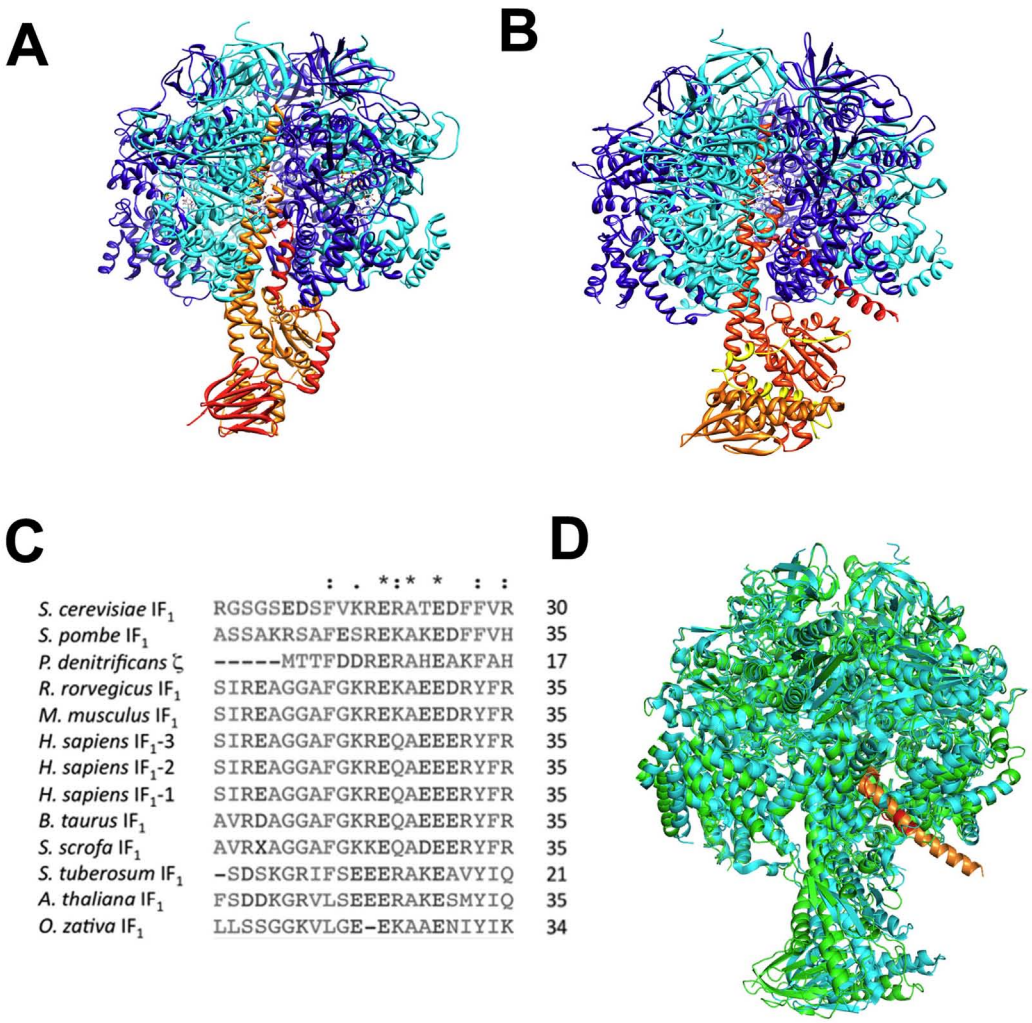

Fig. 4. Structures of the bound inhibitory proteins of the F_1-ATPase. A) The ε subunit (red) in its inhibitory extended structure of the EcF_1-ATPase wrapped to the γ subunit (orange), PDB 3OAA. B) The mitochondrial IF_1 (red) bound to the mitochondrial F_1-ATPase (PDB 2V7Q). C) Alignment of the ζ subunit of *P. denitrificans* with several mitochondrial IF_1 proteins, original alignments reported in references [43, 65]. D) Structural alignment of the ζ N-terminus (red) with the mitochondrial IF_1 (orange) of the aligned PdF_1-ATPase (green) with mitochondrial F_1-IF_1 complex (green. PDB 2V7Q), see also [70]. In A) and B), α and β are in cyan and blue, γ in orange and ε in yellow.

WT Pd1222 genetic background as a single deletion (PdΔζ) [46]. Therefore the lack of a respiratory growth phenotype in their study could be a result of a possible compensation of the Δζ slow growth phenotype in succinate media [46] by the multiple ΔHy mutations. This compensation or revertant-like phenotype could operate in their ΔHyΔζ mutant because hydrogenases compete for the quinone pool with succinate dehydrogenase (particularly in succinate media), and besides, these hydrogenases release protons into the cytoplasmic side of *Paracoccus denitrificans* [81], opposite to the chemiosmotic protons pumped into the periplasmic space by the respiratory chain or by the "reverse" CCW- PdF_1F_O-ATPase (Fig. 7B). Therefore, one possible scenario of how the ΔHy deletions could compensate the Δζ respiratory deficient phenotype is as follows: the ΔHy deletions may improve succinate oxidation by removing competing electron and/or proton flows derived from the hydrogenases, thus complementing the Δζ mutation by producing a higher $\Delta\tilde{\mu}_{H+}$ that will drive back the "reverse" CCW-PdF_1F_O-ATPase induced by the Δζ mutation, into the "forward" CW-PdF_1F_O-ATP synthase turnover, therefore restoring OxPhos and growth of the PdΔζ mutant in respiratory media, and in the absence of ζ. Furthermore, their ΔHy and Δζ constructions lose the antibiotic resistance for Kanamycin [80], whereas our PdΔζ construction preserves the Kanamycin resistance cassette for proper selection, and the complemented Δζ + ζ strain also have Gentamycin resistance [46]. We therefore confirmed the identity of each strain (WT Pd1222, PdΔζ, and PdΔζ + ζ) by their respective antibiotic sensitivity (Francisco Mendoza-Hoffmann and Jose J. Garcia-Trejo, unpublished observations). Secondly, 2) their PdF_1-ATPase and PdF_1F_O-ATPase activities are several-fold lower than the ones we obtained; for instance our $PdF_1^{\Delta\zeta}$–ATPase reached an specific activity of 20–30 μmol/min·mg in the presence of activators (LDAO and sulphite), and 0.87 μmol/min·mg in the absence of activators [46]; in contrast, their respective specific activities with and without activators are 5.12 μmol/min·mg and 0.047 μmol/min·mg, respectively [80]; *i.e.* on average their PdF_1-ATPase activities are 5–20 fold lower than the ones reached by our PdF_1 preparations. This discrepancy emerged probably because we measure the specific activities of freshly eluted PdF_1-ATPase preparations, otherwise the enzyme becomes partially inactivated by freezing or storing before activity determinations. Thus the lack of a higher activation by the genetic ζ removal by Hirst and colleagues [80] is likely due to an underestimation of their PdF_1 activities, given that their PdF_1 preparations were frozen after elution until used [80]. On the other hand, some results that are in concordance between both deletion studies are that their PdF_1F_O-ATPase activities obtained in SBP from *P. denitrificans* [80] are similar to our own determinations, and both studies show no effects of ζ on the "forward" ATP synthase turnover, but a 2-fold activation of the "reverse" PdF_1F_O-ATPase after ζ removal [46]. In their case, they assume that this 2-fold activation of the PdF_1F_O-ATPase is not significant [80]; however, we demonstrated that this apparently low 2-fold activation *in vitro* is actually important *in vivo* as shown by a higher proton pumping and a lower intracellular [ATP] in response to the ζ deletion [46]. In addition, it could also be considered that the fold of PdF_1F_O-ATP activation by ζ removal *in vivo* could be higher than the 2-fold observed *in vitro*; for instance, our 6-fold activation of the isolated PdF_1-ATPase by ζ removal in the absence of other activators show the actual effect of the ζ deletion

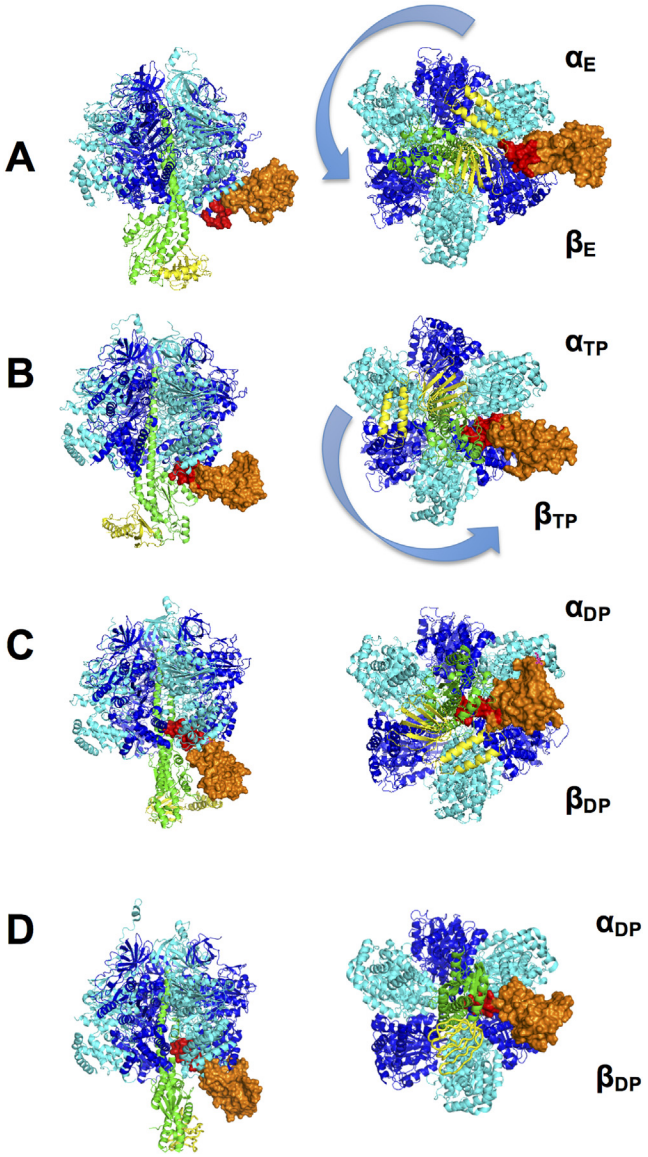

Fig. 5. Bind and lock mechanism of the ζ subunit to block CCW PdF_1-ATPase rotation. The PdF_1 structures shown (ribbons) are viewed from aside (left panels) or the F_O channel towards the F_1-ATPase (right panels), with γ/ε rotor subunits in the center. Color code: α, cyan; β, blue; γ, green; ε, yellow. The atomic surface of ζ subunit of *Paracoccus denitrificans* is shown in orange with its inhibitory N-terminus in red. The binding of the ζ subunit is coupled to rotation of the γ/ε central stalk subunits and therefore to some MgATP binding/hydrolysis turnovers; a putative binding and lock process of ζ named Entrance-Rotation-Alpha-Helix-Lock (ERAHL) is depicted as follows: *A)* ζ enters through an open and empty $\alpha_E\beta_E$ interface with productive binding promoted by the entrance of the disordered ζ N-terminus directed towards the γ/ε rotor. A first partial 120° CCW rotation step of γ/ε coupled to MgATP binding/hydrolysis (not shown), promotes the $\alpha_E\beta_E \rightarrow \alpha_{TP}\beta_{TP}$ shift shown in *B)* and here the ζ N-terminus is further inserted into the $\alpha_{TP}\beta_{TP}$ interface. A second 120° CCW γ/ε rotation coupled to MgATP/binding hydrolysis prompts the shift of the ζ-occupied $\alpha_{TP}\beta_{TP}$ interface to the $\alpha_{DP}\beta_{DP}$ conformation shown in *C*). In parallel, the disordered ζ N-terminus shifts from an IDPr to an α-helix coupled to the γ/ε rotation and to the conformational changes of the catalytic interface occupied by ζ (see Fig. 1A). Finally, in the transition from *C*) to *D*), the ζ subunit is locked into its final inhibitory conformation as shown in the NMR-Crystal structural model of Fig. 5B [46], where only the PdF_1 portion is shown. In this position the CCW rotation driven by MgATP binding and hydrolysis is totally blocked, thus preventing further consumption of the cellular ATP. The CW rotation is allowed somehow and thus the ζ subunit works as a pawl-ratchet, inhibiting exclusively the CCW rotation, but not the ATP-synthesis coupled CW γ/ε rotation [46]. Panels A–C were constructed with the PdF_1-ζ model [70] and the panel D with the crystal(PDB 5DN6)-NMR(PDB 2LLO) structural model of the PdF_1F_O-ATPase. See Figs. 5–6 and the text for further details.

on the PdF_1-ATPase turnover [46], if this several-fold activation by ζ removal holds *in vivo*, the "reverse" PdF_1F_O-ATPase activation by ζ removal could be higher than 2-fold, leading to the observed higher proton pumping and lower intracellular [ATP] [46]. Finally, the effects of our Δζ knockout showing a slower respiratory growth, a lower [ATP], and a higher proton-pumping CCW-PdF_1F_O-ATPase were in our case fully restored by complementation with recombinant ζ expressed *in trans* [46]. This demonstrates that the distinctive phenotype of our Δζ mutant is not the result of non-specific changes or mutations exerted by our knockout strategy, but exclusively due to the absence of ζ [46]. Taken together, it seems that rather than leading to contrary conclusions, the Δζ deletion studies ([46, 80]) confirm that ζ is a unidirectional inhibitor of the "reverse" CCW-PdF_1F_O-ATPase activity.

In summary, our PdΔζ mutant [46] has shown clearly and for the first time as derived from a full knockout study, that the natural F_1F_O-ATPase inhibitors actually have a very important role for cell bioenergetics, and on the other hand this mutant was useful to demonstrate that the ζ subunit is an unidirectional inhibitor of the PdF_1F_O-ATPase because it does not exert any inhibition whatsoever on the CW-PdF_1F_O ATP synthase turnover [46]. This is in concordance with the recently observed heterogeneous population of "forward" ATP synthase and reverse "ATPase" isoforms of the enzyme of *P. denitrificans* [82] since this heterogeneity may be due to a fraction of enzymes containing and another lacking the ζ subunit. Accordingly, we had observed that the exogenously added recombinant ζ subunit is able to inhibit the PdF_1F_O and PdF_1 ATPases as isolated in their native form containing the endogenously expressed ζ subunit [65, 66], thus indicating that there is a fraction of enzymes inactivated as ATPase by the endogenous ζ and another fraction functionally rotating in the reverse CCW ATPase direction because of the lack of ζ [65, 66]. Furthermore, we had determined the content of the endogenous ζ subunit by quantitative western blotting relative to that of the F_1F_O-ATP synthase in *P. denitrificans* whole cells, membranes, and in the isolated PdF_1F_O and PdF_1 ATPase preparations, and observed a sub-stoichiometric relation of ζ/F_1F_O (Carlos Chávez and José J. García-Trejo, unpublished observations), in concordance with the location of the ζ gene outside the two ATP operons in *P. denitrificans* and related α-proteobacteria [65, 66], a proper place for a regulatory, non-essential, and supernumerary subunit of the enzyme. This indicates that when *P. denitrificans* is grown in succinate media in respiratory conditions, a fraction of ATP synthases are inhibited by its bound ζ, whereas another fraction is actually lacking its natural ζ inhibitor, thus likely explaining the heterogeneity of the F_1F_O-ATPsynthase/ATPase recently observed in *P. denitrificans* [82]. In this context, the ζ containing enzymes will be prone to rotate exclusively in the "forward" CW ATP synthase direction, whereas the ζ lacking fraction of enzymes will be able to rotate in both directions CW and CCW, as explained in our recent Δζ knockout studies [46]; see also Figs. 7 and 8, where the *P denitrificans* WT cells will therefore actually be a mixture of Fig. 7B of the left "WT" together with right "PdΔζ" phenotypes with a fraction of CCW-ATPase inactive enzymes containing ζ, and another fraction CCW-ATPase active enzymes lacking its endogenous ζ subunit.

On the other hand, these results also suggest that all natural inhibitors of the ATP synthase ε, ζ, and IF_1 may work as unidirectional pawl-ratchets, as suggested by previous studies [34, 47, 70]. However, other studies indicate that IF_1 may also inhibit the "forward" ATP synthase turnover in mitochondria, thus it seems that the unidirectional or bidirectional effects of IF_1 need to be revisited [27, 50–53]. The clear phenotypic effects of our Δζ mutant in respiratory media suggest that

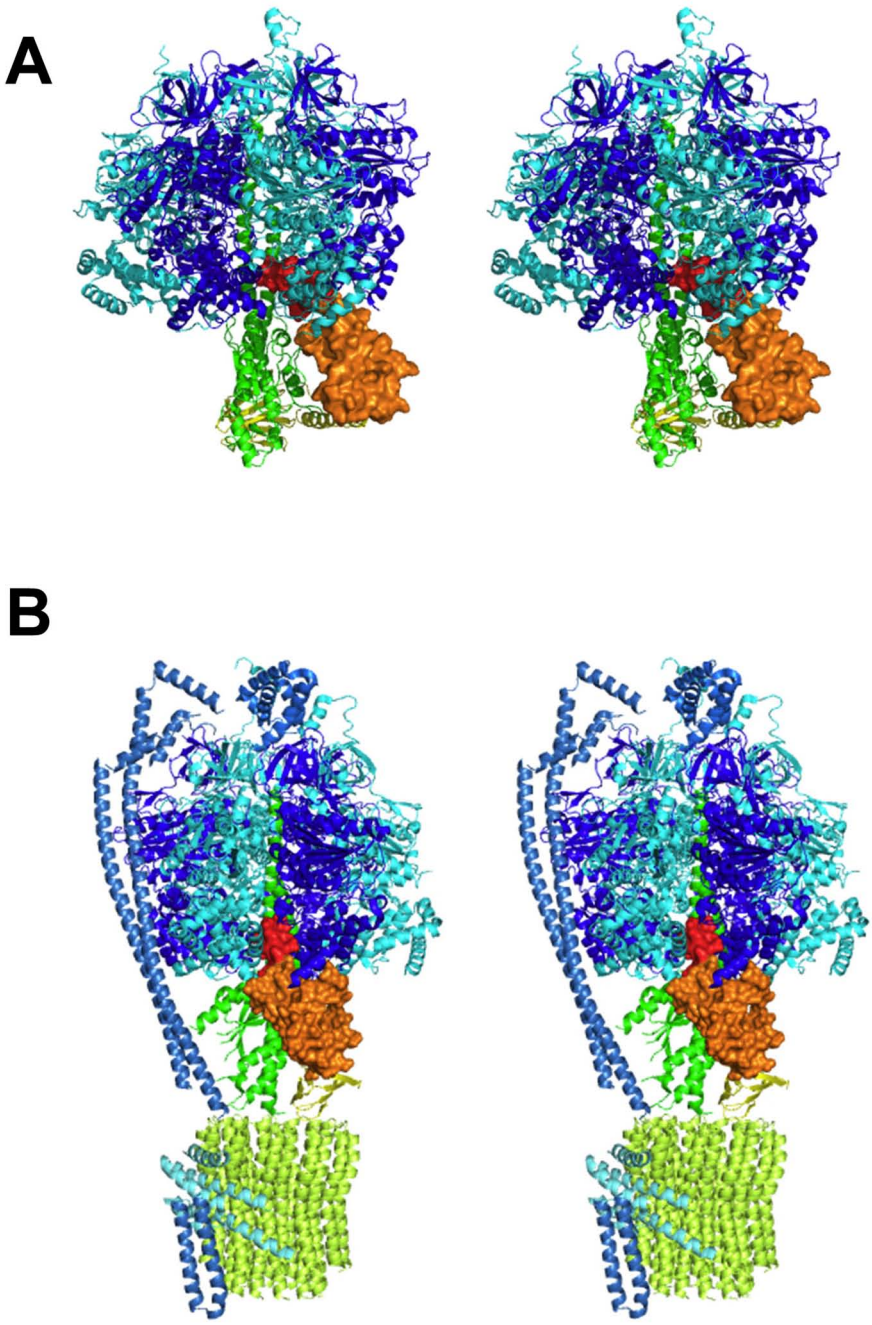

Fig. 6. Structure of the PdF_1-ζ and PdF_1F_O-ζ complexes. A) The PdF_1-ζ model in stereo view, with α and β shown in cyan and blue, γ in green and ε in yellow. The inhibitory domain of ζ is in red and its globular domain in orange. The ζ subunit is shown modelled by structural alignment with IF_1 and refinement in the $\alpha_{DP}/\beta_{DP}/\gamma$ interface. B) The PdF_1F_O-ζ model obtained by structural alignment and combination of NMR (PDB 2LL0) and crystal (PDB 5DN6) structures (see ref. [46]). The color code is the same as in A), rotor subunits are shown in shades of green and stator subunits in shades of blue. The N-terminus of ζ (red) acquires an α-helical structure and is inserted deeply into the $\alpha_{DP}/\beta_{DP}/\gamma$ interface. The globular domain of ζ (orange) interacts with the α_{DP}/β_{DP} interface to hold ζ in its inhibitory place [46].

the lack of a clear phenotype of the previous ΔIF_1 knockouts [75–77] could be due to compensating inhibitory functions by other copies of IF_1 genes, or by complementation with homologous stabilizing factors such as Stf1 which also has F_1-ATPas inhibitory properties [78, 79]. Thus, the slow respiratory phenotype of our PdΔζ knockout [46] sheds light on the important biological role of all natural ATP synthase's inhibitors, probably more related to mitochondrial IF_1 since it shares the same binding site, N-terminal structure, and mechanism with this mitochondrial inhibitor [43, 70, 72]. Accordingly, the emerging broad roles of IF_1 in cell metabolism [53, 83–85] could be related to a similar key unidirectional inhibitory mechanism as the analogous ζ inhibitor of α-proteobacteria.

In order to give a structural rationale to account for such unidirectional effects of ζ, our PdF_1F_O-ζ structural model has been instrumental. As shown in Figs. 6 and 8, the position of the ζ N-terminus, deeply inserted in the $\alpha_{DP}/\beta_{DP}/\gamma$ interface (red), shows how ζ may work as a pawl-ratchet blocking exclusively the CCW-γ rotation; this could be achieved by either: A) a *conformational* ratchet mechanism (left) where the ζ N-terminus is partially or totally released by the proton gradient and ADP/Pi binding energies (see red arrow); or B) by a *mechanical* ratchet where the ζ subunit is held at its inhibitory position while the γ subunit rotates thanks to the energy input from the proton gradient and the ADP/Pi binding energies [21]. Both possibilities had been proposed recently [46], and the partial exposure of ζ and IF_1 upon membrane energization observed by others [86] and by ourselves [61] suggests that the conformational pawl-ratchet could be the actual mechanism. However, further studies are necessary to ascertain if ζ is a conformational or mechanical pawl-ratchet. Nevertheless, it is worth to note that the close similarity between ζ and IF_1, and the shared binding site of ε at this $\alpha_{DP}/\beta_{DP}/\gamma$ interface suggest that all three natural inhibitors ζ, ε and IF_1 may work as unidirectional pawl-ratchets. Indeed, the first report of IF_1 indicated that it worked as unidirectional PdF_1-ATPase

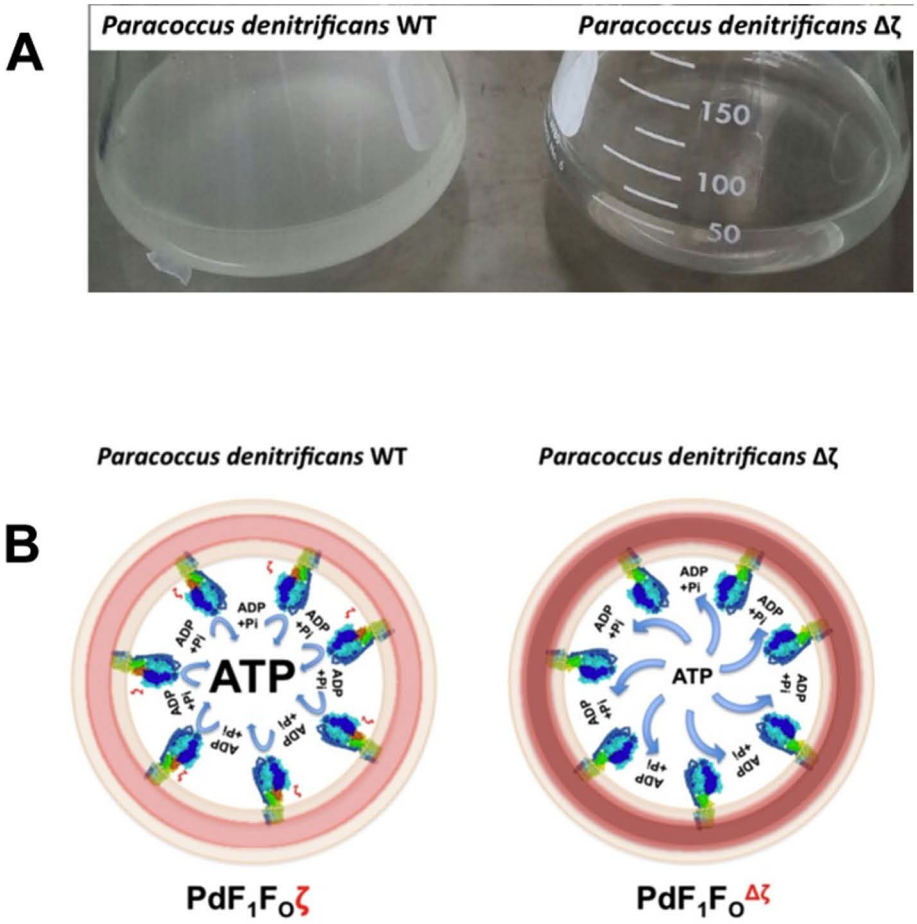

Fig. 7. Effect of the PdΔζ mutation on respiratory bacterial growth and bioenergetics. A) The PdΔζ mutant (right) fails to grow efficiently overnight in succinate media, whereas the PdWT strain grows normally well, for details see [46]. B) Effect of the Δζ knockout on bacterial bioenergetics: the proton pumping PdF_1F_O-ATPase is enhanced in the PdΔζ mutant (dark red = high proton pumping into the bacterial periplasm, right side), whereas the [ATP] is decreased, thus resulting in the slow growth phenotype in succinate seen above. In contrast, the PdWT strain grows normally because the ζ subunit is a unidirectional inhibitor of the PdF_1F_O-ATPase activity, thus it enhances the steady state rate of ATP synthesis and therefore increases the internal [ATP] and the respiratory cell growth, with a lower ATP-driven proton pumping into the periplasm (light red, left side).

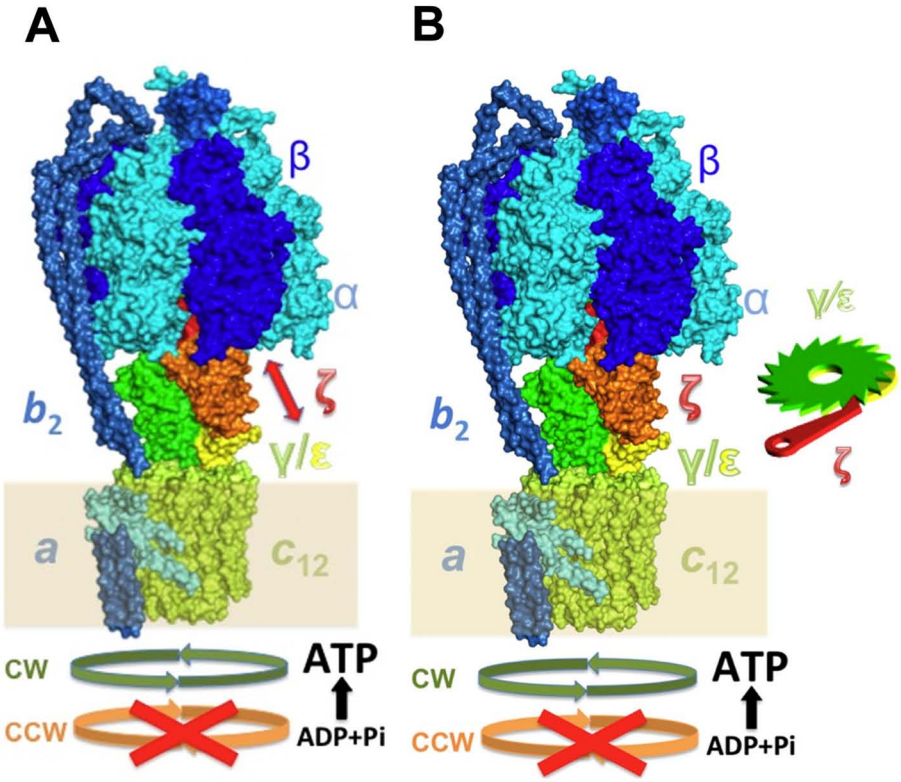

Fig. 8. The pawl-ratchet mechanism of ζ to favour the unidirectional PdF_1F_O-ATP synthase turnover. A) The *conformational* pawl-ratchet: the N-terminal inhibitory domain of ζ (red), and the globular and C-terminal domain of ζ (orange), bound into the $\alpha_{DP}/\beta_{DP}/\gamma$ interface. The F_1-stator complex ($\alpha_3/\beta_3/\delta/b_2/a$) is shown in shades of blue. The $\gamma/\varepsilon/c_{12}$ rotor (in shades of green and yellow) is unable to rotate in the Counter Clock Wise (CCW) direction driving ATP hydrolysis, but is able to rotate in the Clock Wise (CW) direction of ATP synthesis due to partial release of the inhibitory ζ-N-terminus; B) The *mechanical* pawl-ratchet: ζ is blocking rotation of the $\gamma/\varepsilon/c_{12}$ rotor only in the CCW direction without removal or release of the inhibitory ζ N-terminus (red). In this case, CW rotation is driven by the proton gradient and ADP/Pi binding energies; on the contrary, the single MgATP binding energy is not enough to drive the CCW rotation in the presence of ζ. In either case the ζ subunit favours ATP synthesis, and therefore oxidative bacterial growth, by working as a pawl-ratchet or unidirectional PdF_1F_O-ATPase inhibitor, and thus making of the PdF_1F_O-ζ complex an unidirectional ATP synthase. The mechanical ratchet cartoon of the right panel was modified from the original created by Vigneshwaran I (https://grabcad.com/library/ratchet-mechanism-1).

inhibitor [47] and in the case of ε, the ratchet mechanism was proposed from its unidirectional effects on the F_1F_O-ATPase of *Escherichia coli* (EcF_1F_O) by the groups of Roderick Capaldi and Masasuke Yoshida [34]. Similar to our deletion studies with the ζ subunit of *P. denitrificans*, some partial deletion mutants in the C-terminal domain of *E. coli* ε had shown a decreased growth in respiratory media [39], associated to the role of this ε domain in the control of the enzyme activity [87]. These results indicate further similarities among ε, ζ, and IF_1 inhibitors that suggest a common pawl-ratchet inhibitory mechanism for the three natural F_1-ATPase inhibitor proteins. Furthermore, it is worth to recall that the release [50, 88] or relocation [27, 86] of mitochondrial IF_1 as induced by the proton gradient, had been previously observed in sub-mitochondrial particles, suggesting a similar conformational ratchet mechanism for ζ and IF_1. Oncoming studies will resolve in more detail if ζ, ε, and IF_1 converge at a similar conformational or mechanical pawl-ratchet mechanics, as the actual data suggest. Our recent studies with mitochondrial IF_1 indicate this inhibitor it is partially released from mitochondrial F_1F_O by establishment of a proton gradient (Margarita López-Tovar and José J. García-Trejo, unpublished observations); therefore, it is likely that the functionally homologous ζ subunit will also be released by membrane energization as a conformational pawl-ratchet in the *P. denitrificans* membranes (Fig. 8A), however this is being actually studied in our laboratory.

In summary, we had discovered and resolved the ζ subunit of *Paracoccus denitrificans*, which resulted in another important natural F_1F_O-ATPase inhibitor, aside from bacterial ε and mitochondrial IF_1; but beyond that, ζ is a good bacterial protein model to resolve not only its own pawl-ratchet mechanics, but also to shed light on the actual biological role and mechanisms of all ATP synthase's natural inhibitors.

Transparency document

The http://dx.doi.org/10.1016/j.bbabio.2018.06.005 associated with this article can be found, in online version.

Acknowledgements

This work was supported by grants from México, (CONACyT) Grant CB-2011-01-167622 and U.N.A.M. (DGAPA) Grant PAPIIT- IN221216 (both to J. J. G.-T.). This work is part of PhD Thesis of FMH at the "Programa de Maestría y Doctorado en Ciencias Bioquímicas de la Universidad Nacional Autónoma de México" (U.N.A.M.), with JJGT as PhD advisor. FMH was supported by CONACyT Ph.D. Fellowship 277245, and MZZ by CONACyT Fund I0010, Fellowship No. 277592. We thank Pattie Nelson, English and Spanish teacher of the Lane Community College of Eugene, Oregon, for reviewing the proper writing of this paper. The improvement of this paper by editors and reviewers is deeply acknowledged.**Dedication**

This paper is dedicated to the admired memory of Prof. Paul D. Boyer (1918-2018), as the main authority in the ATP synthase field, Nobel Laureate in Chemistry for being the one that discovered the rotary mechanism of the ATP synthase nanomotor, besides his many contributions to biochemistry and bioenergetics, and as one of the greatest scientists of all times.

References

[1] P. Mitchell, Coupling of phosphorylation to electron and hydrogen transfer by a chemi-osmotic type of mechanism, Nature 191 (1961) 144–148.
[2] J. St-Pierre, M.D. Brand, R.G. Boutilier, Mitochondria as ATP consumers: cellular treason in anoxia, Proc. Natl. Acad. Sci. U. S. A. 97 (2000) 8670–8674.
[3] P.C. Maloney, E.R. Kashket, H.T. Wilson, A protonmotive force drives ATP synthesis in bacteria, Proc. Natl. Acad. Sci. U. S. A. 71 (1974) 3896–3900.
[4] I.D. Scott, D.G. Nicholls, Energy transduction in intact synaptosomes. Influence of plasma-membrane depolarization on the respiration and membrane potential of internal mitochondria determined in situ, J. Biochem. 186 (1980) 21–33.
[5] P.D. Boyer, The ATP synthase—a splendid molecular machine, Annu. Rev. Biochem. 66 (1997) 717–749.
[6] W. Junge, N. Nelson, ATP synthase, Annu. Rev. Biochem. 84 (2015) 631–657.
[7] J.J. Garcia, C. Bravo, F. Minauro-Sanmiguel, Mitochondrial F1FOI-ATP synthase: structure, function, assembly, and a topography model of human subunit 6, in: J.J. García-Trejo (Ed.), Recent Research Developments in Human Mitochondrial Myopathies, Research Signpost, Place Published, 2002, pp. 127–150.
[8] J.P. Abrahams, A.G.W. Leslie, R. Lutter, J.E. Walker, Structure at 2.8 Å resolution of F1-ATPase from bovine heart mitochondria, Natue 370 (1994) 621–628.
[9] M.J. Gresser, J.A. Myers, P.D. Boyer, Catalytic site cooperativity of beef heart mitochondrial F1 adenosine triphosphatase. Correlations of initial velocity, bound intermediate, and oxygen exchange measurements with an alternating three-site model, J. Biol. Chem. 257 (1982) 12030–12038.
[10] P.D. Boyer, Energy, Life, and ATP (Nobel Lecture), Angew. Chem. Int. Ed. Engl. 37 (1998) 2296–2307.
[11] T.M. Duncan, V.V. Bulygin, Y. Zhou, M.L. Hutcheon, R.L. Cross, Rotation of subunits during catalysis by *Escherichia coli* F1-ATPase, Proc. Natl. Acad. Sci. U. S. A. 92 (1995) 10964–10968.
[12] D. Sabbert, S. Engelbrecht, W. Junge, Intersubunit rotation in active F-ATPase, Nature 381 (1996) 623–625.
[13] H. Noji, R. Yasuda, M. Yoshida, K. Kinosita Jr., Direct observation of the rotation of F1-ATPase, Nature 386 (1997) 299–302.
[14] H. Noji, M. Yoshida, The rotary machine in the cell, ATP synthase, J. Biol. Chem. 276 (2001) 1665–1668.
[15] H. Noji, H. Ueno, D.G.G. McMillan, Catalytic robustness and torque generation of the F1-ATPase, Biophys. Rev. 9 (2017) 103–118.
[16] R. Watanabe, H. Noji, Chemomechanical coupling mechanism of F(1)-ATPase: catalysis and torque generation, FEBS Lett. 587 (2013) 1030–1035.
[17] T. Suzuki, K. Tanaka, C. Wakabayashi, E. Saita, M. Yoshida, Chemomechanical coupling of human mitochondrial F1-ATPase motor, Nat. Chem. Biol. 10 (2014) 930–936.
[18] R.H. Fillingame, P.R. Steed, Half channels mediating H(+) transport and the mechanism of gating in the Fo sector of *Escherichia coli* F1Fo ATP synthase, Biochim. Biophys. Acta 1837 (2014) 1063–1068.
[19] H. Guo, S.A. Bueler, J.L. Rubinstein, Atomic model for the dimeric FO region of mitochondrial ATP synthase, Science 358 (2017) 936–940.
[20] J.J. Garcia, R.A. Capaldi, Unisite catalysis without rotation of the gamma-epsilon domain in *Escherichia coli* F1-ATPase, J. Biol. Chem. 273 (1998) 15940–15945.
[21] J.J. Garcia, The F_0F_1-ATP Synthase: Binding Energy, Coupling and Rotational Catalysis, First ed., Transworld Research Network, Place Published, 2000.
[22] S. Wilkens, R.A. Capaldi, ATP synthase's second stalk comes into focus, Nature 393 (1998) 29.
[23] I. Ogilvie, S. Wilkens, A.J. Rodgers, R. Aggeler, R.A. Capaldi, The second stalk: the delta-b subunit connection in ECF1F0, Acta Physiol. Scand. Suppl. 643 (1998) 169–175.
[24] S.B. Claggett, M. O'Neil Plancher, S.D. Dunn, B.D. Cain, The b subunits in the peripheral stalk of F1F0 ATP synthase preferentially adopt an offset relationship, J. Biol. Chem. 284 (2009) 16531–16540.
[25] A. Wachter, Y. Bi, S.D. Dunn, B.D. Cain, H. Sielaff, F. Wintermann, S. Engelbrecht, W. Junge, Two rotary motors in F-ATP synthase are elastically coupled by a flexible rotor and a stiff stator stalk, Proc. Natl. Acad. Sci. U. S. A. 108 (2011) 3924–3929.
[26] S. Fischer, P. Graber, P. Turina, The activity of the ATP synthase from *Escherichia coli* is regulated by the transmembrane proton motive force, J. Biol. Chem. 275 (2000) 30157–30162.
[27] A. Gomez-Puyou, M.T. de Gomez-Puyou, L. Ernster, Inactive to active transitions of the mitochondrial ATPase complex as controlled by the ATPase inhibitor, Biochim. Biophys. Acta 547 (1979) 252–257.
[28] J.J. Garcia-Trejo, E. Morales-Rios, Regulation of the F1F0-ATP synthase rotary nanomotor in its monomeric-bacterial and dimeric-mitochondrial forms, J. Biol. Phys. 34 (2008) 197–212.
[29] A. Krah, Linking structural features from mitochondrial and bacterial F-type ATP synthases to their distinct mechanisms of ATPase inhibition, Prog. Biophys. Mol. Biol. 119 (2015) 94–102.
[30] R.A. Capaldi, R. Aggeler, P. Turina, S. Wilkens, Coupling between catalytic sites and the proton channel in F1F0-type ATPases, Trends Biochem. Sci. 19 (1994) 284–289.
[31] R.A. Capaldi, B. Schulenberg, The epsilon subunit of bacterial and chloroplast F(1)F(0) ATPases. Structure, arrangement, and role of the epsilon subunit in energy coupling within the complex, Biochim. Biophys. Acta 1458 (2000) 263–269.
[32] D.J. Klionsky, W.S. Brusilow, R.D. Simoni, In vivo evidence for the role of the epsilon subunit as an inhibitor of the proton-translocating ATPase of *Escherichia coli*, J. Bacteriol. 160 (1984) 1055–1060.
[33] P.C. Sternweis, J.B. Smith, Characterization of the inhibitory (epsilon) subunit of the proton-translocating adenosine triphosphatase from *Escherichia coli*, Biochemistry 19 (1980) 526–531.
[34] S.P. Tsunoda, A.J. Rodgers, R. Aggeler, M.C. Wilce, M. Yoshida, R.A. Capaldi, Large conformational changes of the epsilon subunit in the bacterial F1F0 ATP synthase provide a ratchet action to regulate this rotary motor enzyme, Proc. Natl. Acad. Sci. U. S. A. 98 (2001) 6560–6564.
[35] G. Cingolani, T.M. Duncan, Structure of the ATP synthase catalytic complex (F(1)) from *Escherichia coli* in an autoinhibited conformation, Nat. Struct. Mol. Biol. 18 (2011) 701–707.
[36] A.J. Rodgers, M.C. Wilce, Structure of the gamma-epsilon complex of ATP synthase, Nat. Struct. Biol. 7 (2000) 1051–1054.
[37] A.C. Hausrath, R.A. Capaldi, B.W. Matthews, The conformation of the epsilon- and gamma-subunits within the *Escherichia coli* F(1) ATPase, J. Biol. Chem. 276 (2001) 47227–47232.
[38] B.A. Feniouk, T. Suzuki, M. Yoshida, The role of subunit epsilon in the catalysis and

regulation of FOF1-ATP synthase, Biochim. Biophys. Acta 1757 (2006) 326–338.
[39] N.B. Shah, T.M. Duncan, Aerobic growth of *Escherichia coli* is reduced, and ATP synthesis is selectively inhibited when five C-terminal residues are deleted from the subunit of ATP synthase, J. Biol. Chem. 290 (2015) 21032–21041.
[40] H. Yagi, N. Kajiwara, H. Tanaka, T. Tsukihara, Y. Kato-Yamada, M. Yoshida, H. Akutsu, Structures of the thermophilic F1-ATPase ε subunit suggesting ATP-regulated arm motion of its C-terminal domain in F1, Proc. Natl. Acad. Sci. 104 (2007) 11233–11238.
[41] S.A. Ferguson, G.M. Cook, M.G. Montgomery, A.G.W. Leslie, J.E. Walker, Regulation of the thermoalkaliphilic F1-ATPase from *Caldalkalibacillus thermarum*, Proc. Natl. Acad. Sci. 113 (2016) 10860–10865.
[42] S. Joon, P. Ragunathan, L. Sundararaman, W. Nartey, S. Kundu, M.S.S. Manimekalai, N. Bogdavonic, T. Dick, G. Grüber, The NMR solution structure of *Mycobacterium tuberculosis* F-ATP synthase subunit ε provides new insight into energy coupling inside the rotary engine, FEBS J. 285 (2018) 1111–1128.
[43] M. Zarco-Zavala, E. Morales-Rios, G. Mendoza-Hernandez, L. Ramirez-Silva, G. Perez-Hernandez, J.J. Garcia-Trejo, The zeta subunit of the F1FO-ATP synthase of alpha-proteobacteria controls rotation of the nanomotor with a different structure, FASEB J. 28 (2014) 2146–2157.
[44] Y. Kato, T. Matsui, N. Tanaka, E. Muneyuki, T. Hisabori, M. Yoshida, Thermophilic F1-ATPase is activated without dissociation of an endogenous inhibitor, epsilon subunit, J. Biol. Chem. 272 (1997) 24906–24912.
[45] J. Mizumoto, Y. Kikuchi, Y.H. Nakanishi, N. Mouri, A. Cai, T. Ohta, T. Haruyama, Y. Kato-Yamada, Epsilon subunit of *Bacillus subtilis* F1-ATPase relieves MgADP inhibition, PLoS One 8 (2013) e73888.
[46] F. Mendoza-Hoffmann, A. Pérez-Oseguera, M.A. Cevallos, M. Zarco-Zavala, R. Ortega, C. Peña-Segura, E. Espinoza-Simón, S. Uribe-Carvajal, J.J. García-Trejo, The biological role of the ζ subunit as unidirectional inhibitor of the F1FO-ATPase of *Paracoccus denitrificans*, Cell Rep. 22 (2018) 1067–1078.
[47] M.E. Pullman, G.C. Monroy, A naturally occurring inhibitor of mitochondrial adenosine triphosphatase, J. Biol. Chem. 238 (1963) 3762–3769.
[48] G. Klein, M. Satre, A.C. Dianoux, P.V. Vignais, Radiolabeling of natural adenosine triphosphatase inhibitor with phenyl (14C)isothiocyanate and study of its interaction with mitochondrial adenosine triphosphatase. Localization of inhibitor binding sites and stoichiometry of binding, Biochemistry 19 (1980) 2919–2925.
[49] T. Hashimoto, Y. Negawa, K. Tagawa, Binding of intrinsic ATPase inhibitor to mitochondrial ATPase—stoichiometry of binding of nucleotides, inhibitor, and enzyme, J. Biochem. 90 (1981) 1151–1157.
[50] G. Lippe, M.C. Sorgato, D.A. Harris, Kinetics of the release of the mitochondrial inhibitor protein. Correlation with synthesis and hydrolysis of ATP, Biochim. Biophys. Acta 933 (1988) 1–11.
[51] K. Schwerzmann, P.L. Pedersen, Regulation of the mitochondrial ATP synthase/ATPase complex, Arch. Biochem. Biophys. 250 (1986) 1–18.
[52] J. Garcia-Bermudez, M. Sanchez-Arago, B. Soldevilla, A. Del Arco, C. Nuevo-Tapioles, J.M. Cuezva, PKA phosphorylates the ATPase inhibitory factor 1 and inactivates its capacity to bind and inhibit the mitochondrial H(+)-ATP synthase, Cell Rep. 12 (2015) 2143–2155.
[53] J. Garcia-Bermudez, J.M. Cuezva, The ATPase inhibitory factor 1 (IF1): a master regulator of energy metabolism and of cell survival, Biochim. Biophys. Acta 1857 (2016) 1167–1182.
[54] J.J. García, F. Minauro-Sanmiguel, C. Bravo, Mitochondrial ATP synthase: structure, function, assembly, and a topography model for human subunit 6, in: J.J. Garcia (Ed.), Recent Research Developments in Human Mitochondrial Myopathies Research Signpost, Trivandrum, 2002, p. 21.
[55] P.J. Jackson, D.A. Harris, The mitochondrial ATP synthase inhibitor protein binds near the C-terminus of the F1 beta-subunit, FEBS Lett. 229 (1988) 224–228.
[56] M.T. Tuena de Gomez-Puyou, U. Muller, G. Dreyfus, G. Ayala, A. Gomez-Puyou, Regulation of the synthesis and hydrolysis of ATP by mitochondrial ATPase. Role of the natural ATPase inhibitor protein, J. Biol. Chem. 258 (1983) 13680–13684.
[57] F. Minauro-Sanmiguel, C. Bravo, J.J. García, Cross-linking of the endogenous inhibitor protein (IF1) with rotor (gamma, epsilon) and stator (alpha) subunits of the mitochondrial ATP synthase, J. Bioenerg. Biomembr. 34 (2002) 433–443.
[58] E. Cabezon, M.G. Montgomery, A.G. Leslie, J.E. Walker, The structure of bovine F1-ATPase in complex with its regulatory protein IF1, Nat. Struct. Biol. 10 (2003) 744–750.
[59] L. Margulis, M.J. Chapman, Endosymbioses: cyclical and permanent in evolution, Trends Microbiol. 6 (1998) 342–345 (discussion 345–346).
[60] J.A. Perez, S.J. Ferguson, Kinetics of oxidative phosphorylation in *Paracoccus denitrificans*. 1. Mechanism of ATP synthesis at the active site(s) of F0F1-ATPase, Biochemistry 29 (1990) 10503–10518.
[61] F. Pacheco-Moises, J.J. Garcia, J.S. Rodriguez-Zavala, R. Moreno-Sanchez, Sulfite and membrane energization induce two different active states of the *Paracoccus denitrificans* F0F1-ATPase, Eur. J. Biochem. 267 (2000) 993–1000.
[62] F. Pacheco-Moises, F. Minauro-Sanmiguel, C. Bravo, J.J. Garcia, Sulfite inhibits the F1F0-ATP synthase and activates the F1F0-ATPase of *Paracoccus denitrificans*, J. Bioenerg. Biomembr. 34 (2002) 269–278.
[63] T.V. Zharova, A.D. Vinogradov, Proton-translocating ATP-synthase of *Paracoccus denitrificans*: ATP-hydrolytic activity, Biochemistry (Mosc) 68 (2003) 1101–1108.
[64] D.A. Harris, P. John, G.K. Radda, Tightly bound nucleotides of the energy-transducing ATPase, and their role in oxidative phosphorylation. I. The *Paracoccus denitrificans* system, Biochim. Biophys. Acta 459 (1977) 546–559.
[65] F. de la Rosa-Morales, Composición de subunidades y Mecanismo de Regulación de la F1FoATP sintasa de Paracoccus denitrificans, Posgrado en Ciencias Biologicas (Biologia Experimental), Facultad de Ciencias., Universidad Nacional Autonoma de Mexico (U.N.A.M.), Direccion General de Bibliotecas, (2005), p. 75.
[66] E. Morales-Rios, F. de la Rosa-Morales, G. Mendoza-Hernandez, J.S. Rodriguez-Zavala, H. Celis, M. Zarco-Zavala, J.J. Garcia-Trejo, A novel 11-kDa inhibitory subunit in the F1FO ATP synthase of *Paracoccus denitrificans* and related alpha-proteobacteria, FASEB J. 24 (2010) 599–608.
[67] M. Zarco-Zavala, E. Morales-Ríos, P. Serrano-Navarro, K.§. Wüthrich, G. Mendoza-Hernández, L. Ramírez-Silva, J.J. García-Trejo, Corringendum to: the ζ subunit of the α-proteobacterial F1FO-ATP synthase in *Paracoccus denitrificans*: a novel control mechanism of the central rotor, Biochim. Biophys. Acta 1827 (2013) 60.
[68] P. Serrano, M. Geralt, B. Mohanty, K. Wuthrich, NMR structures of alpha-proteobacterial ATPase-regulating zeta-subunits, J. Mol. Biol. 426 (2014) 2547–2553.
[69] E. Morales-Rios, M.G. Montgomery, A.G.W. Leslie, J.J. Garcia-Trejo, J.E. Walker, Structure of a catalytic dimer of the α- and β-subunits of the F-ATPase from Paracoccus denitrificans at 2.3 A resolution, Acta Crystallogr. Sect. F 71 (2015) 1307–1309.
[70] J.J. Garcia-Trejo, M. Zarco-Zavala, F. Mendoza-Hoffmann, E. Hernandez-Luna, R. Ortega, G. Mendoza-Hernandez, The inhibitory mechanism of the zeta subunit of the F1FO-ATPase nanomotor of *Paracoccus denitrificans* and related alpha-proteobacteria, J. Biol. Chem. 291 (2016) 538–546.
[71] J.V. Bason, M.G. Montgomery, A.G. Leslie, J.E. Walker, Pathway of binding of the intrinsically disordered mitochondrial inhibitor protein to F1-ATPase, Proc. Natl. Acad. Sci. U. S. A. 111 (2014) 11305–11310.
[72] E. Morales-Rios, M.G. Montgomery, A.G. Leslie, J.E. Walker, Structure of ATP synthase from *Paracoccus denitrificans* determined by X-ray crystallography at 4.0 A resolution, Proc. Natl. Acad. Sci. U. S. A. 112 (2015) 13231–13236.
[73] V.N. Uversky, Dancing protein clouds: the strange biology and chaotic physics of intrinsically disordered proteins, J. Biol. Chem. 291 (2016) 6681–6688.
[74] A.L. Darling, V.N. Uversky, Intrinsic disorder and posttranslational modifications: the darker side of the biological dark matter, Front. Genet. 9 (2018) 158.
[75] Y.M. Lu, K. Miyazawa, K. Yamaguchi, K. Nowaki, H. Iwatsuki, Y. Wakamatsu, N. Ichikawa, T. Hashimoto, Deletion of mitochondrial ATPase inhibitor in the yeast *Saccharomyces cerevisiae* decreased cellular and mitochondrial ATP levels under non-nutritional conditions and induced a respiration-deficient cell-type, J. Biochem. 130 (2001) 873–878.
[76] J. Nakamura, M. Fujikawa, M. Yoshida, IF1, a natural inhibitor of mitochondrial ATP synthase, is not essential for the normal growth and breeding of mice, Biosci. Rep. 33 (2013).
[77] L.P. Fernandez-Cardenas, E. Villanueva-Chimal, L.S. Salinas, C. Jose-Nunez, M. Tuena de Gomez Puyou, R.E. Navarro, Caenorhabditis elegans ATPase inhibitor factor 1 (IF1) MAI-2 preserves the mitochondrial membrane potential (Deltapsim) and is important to induce germ cell apoptosis, PLoS One 12 (2017) e0181984.
[78] T. Hashimoto, Y. Yoshida, K. Tagawa, Binding properties of 9K protein to F1-ATPase: a counterpart ligand to the ATPase inhibitor, J. Biochem. 102 (1987) 685–692.
[79] T. Hashimoto, Y. Yoshida, K. Tagawa, Simultaneous bindings of ATPase inhibitor and 9K protein to F1F0-ATPase in the presence of 15K protein in yeast mitochondria, J. Biochem. 108 (1990) 17–20.
[80] F. Varghese, J.N. Blaza, A.J.Y. Jones, O.D. Jarman, J. Hirst, Deleting the IF1-like zeta subunit from *Paracoccus denitrificans* ATP synthase is not sufficient to activate ATP hydrolysis, Open Biol. 8 (2018).
[81] J. Doussiere, F. Porte, P.M. Vignais, Orientation of hydrogenase in the plasma membrane of *Paracoccus denitrificans*, FEBS Lett. 114 (1980) 291–294.
[82] T.V. Zharova, A.D. Vinogradov, Functional heterogeneity of Fo.F1H(+)-ATPase/synthase in coupled *Paracoccus denitrificans* plasma membranes, Biochim. Biophys. Acta 1858 (2017) 939–944.
[83] D. Faccenda, M. Campanella, Molecular regulation of the mitochondrial F(1)F(o)-ATPsynthase: physiological and pathological significance of the inhibitory factor 1 (IF(1)), Int. J. Cell Biol. 2012 (2012) 367934.
[84] D. Faccenda, J. Nakamura, G. Gorini, G.K. Dhoot, M. Piacentini, M. Yoshida, M. Campanella, Control of mitochondrial remodeling by the ATPase inhibitory factor 1 unveils a pro-survival relay via OPA1, Cell Rep. 18 (2017) 1869–1883.
[85] D. Faccenda, C.H. Tan, A. Seraphim, M.R. Duchen, M. Campanella, IF1 limits the apoptotic-signalling cascade by preventing mitochondrial remodelling, Cell Death Differ. 20 (2013) 686–697.
[86] G. Dreyfus, A. Gomez-Puyou, M. Iuena de Gomez-Puyou, Electrochemical gradient induced displacement of the natural ATPase inhibitor protein from mitochondrial ATPase as directed by antibodies against the inhibitor protein, Biochem. Biophys. Res. Commun. 100 (1981) 400–406.
[87] M. D'Alessandro, P. Turina, B.A. Melandri, S.D. Dunn, Modulation of coupling in the *Escherichia coli* ATP synthase by ADP and Pi: role of the epsilon subunit C-terminal domain, Biochim. Biophys. Acta 1858 (2017) 34–44.
[88] G. Lippe, M.C. Sorgato, D.A. Harris, The binding and release of the inhibitor protein are governed independently by ATP and membrane potential in ox-heart submitochondrial vesicles, Biochim. Biophys. Acta 933 (1988) 12–21.

THE JOURNAL OF BIOLOGICAL CHEMISTRY VOL. 291, NO. 2, pp. 538–546, January 8, 2016

The Inhibitory Mechanism of the ζ Subunit of the F_1F_O-ATPase Nanomotor of *Paracoccus denitrificans* and Related α-Proteobacteria*[S]

Received for publication, August 27, 2015, and in revised form, November 2, 2015 Published, JBC Papers in Press, November 6, 2015, DOI 10.1074/jbc.M115.688143

José J. García-Trejo[‡1], Mariel Zarco-Zavala[‡], Francisco Mendoza-Hoffmann[‡], Eduardo Hernández-Luna[‡], Raquel Ortega[‡], and Guillermo Mendoza-Hernández[§]

From the [‡]Departamento de Biología, Facultad de Química, and the [§]Departamento de Bioquímica, Facultad de Medicina, Universidad Nacional Autónoma de México, Ciudad Universitaria, Delegación Coyoacán, D.F., CP 04510, México

The ζ subunit is a novel inhibitor of the F_1F_O-ATPase of *Paracoccus denitrificans* and related α-proteobacteria. It is different from the bacterial (ε) and mitochondrial (IF_1) inhibitors. The N terminus of ζ blocks rotation of the γ subunit of the F_1-ATPase of *P. denitrificans* (Zarco-Zavala, M., Morales-Ríos, E., Mendoza-Hernández, G., Ramírez-Silva, L., Pérez-Hernández, G., and García-Trejo, J. J. (2014) *FASEB J.* 24, 599–608) by a hitherto unknown quaternary structure that was first modeled here by structural homology and protein docking. The F_1-ATPase and F_1-ζ models of *P. denitrificans* were supported by cross-linking, limited proteolysis, mass spectrometry, and functional data. The final models show that ζ enters into F_1-ATPase at the open catalytic α_E/β_E interface, and two partial γ rotations lock the N terminus of ζ in an "inhibition-general core region," blocking further γ rotation, while the ζ globular domain anchors it to the closed α_{DP}/β_{DP} interface. Heterologous inhibition of the F_1-ATPase of *P. denitrificans* by the mitochondrial IF_1 supported both the modeled ζ binding site at the $\alpha_{DP}/\beta_{DP}/\gamma$ interface and the endosymbiotic α-proteobacterial origin of mitochondria. In summary, the ζ subunit blocks the intrinsic rotation of the nanomotor by inserting its N-terminal inhibitory domain at the same rotor/stator interface where the mitochondrial IF_1 or the bacterial ε binds. The proposed pawl mechanism is coupled to the rotation of the central γ subunit working as a ratchet but with structural differences that make it a unique control mechanism of the nanomotor to favor the ATP synthase activity over the ATPase turnover in the α-proteobacteria.

The F_1F_O-ATP synthase is the ubiquitous nanomotor that fuels life by producing vital chemical energy through the condensation of ADP and P_i to form ATP during oxidative phosphorylation or photophosphorylation. This process occurs in the energy-transducing inner membranes of bacteria, mitochondria, and chloroplasts. The core structure of the F_1F_O-ATP synthase nanomotor is conserved through evolution. This nanomotor has a stator plus a rotor that gyrates clockwise (viewed from F_O to F_1) to synthesize ATP. The process is fueled by the proton flow through F_O and the trans-membranous proton gradient established by respiratory or photosynthetic electron transfer chains of energy-transducing membranes. However, during partial or total collapse of the transmembrane proton gradient, the nanomotor will turn in the opposite counterclockwise direction and therefore act to hydrolyze the ATP. This reversal of direction of the F_1F_O-ATPase activity is detrimental in mitochondria and chloroplasts, but it could be advantageous for bacteria in the absence of oxygen or alternative electron acceptors, where the F-ATPase pumps protons to energize secondary transporters under anaerobic or non-respiring conditions. In order to prevent the reverse F_1F_O-ATPase activity, a couple of natural inhibitors have evolved: the eubacterial ε subunit and the mitochondrial inhibitor protein (IF_1)[2] (reviewed in Ref. 1). Both inhibitors act to hinder predominantly the counterclockwise rotor gyration of the F_1F_O-ATPase (F_1-ATPase turnover) by interacting differently with the γ, α, and β subunits (2–4). A recent study found that the inhibitory domains of bacterial ε and mitochondrial IF_1 bind at the same interface of their respective bacterial or mitochondrial F_1-ATPases, contacting the γ subunit at a common $\alpha_{DP}/\beta_{DP}/\gamma$ interface named the "inhibition-general core region" (5).

We recently discovered a third, natural, and potent inhibitor of the bacterial F_1F_O-ATPase in *P. denitrificans* and related α-proteobacteria (6, 7). This new inhibitor is different in structure from the bacterial ε and mitochondrial IF_1 and is conserved exclusively in the α-proteobacteria class. We named this inhibitor the ζ subunit because it is smaller than ε and showed that the N-terminal side harbors the inhibitory domain of the protein. The other side of ζ, containing four α-helixes, works as a globular anchoring domain (7). These studies also showed cross-linking of ζ with the α and β subunits of the F_1-ATPase stator and with the γ and ε subunits of the rotor, indicating that ζ blocks rotation of the central stalk in a similar way to the mitochondrial IF_1, which also blocks the intrinsic rotation of

* This work was supported by México (CONACyT) Grant CB-2011-01-167622 and U.N.A.M. (DGAPA) Grant PAPIIT-IN211012 (to J. J. G.-T.). The authors declare that they have no conflicts of interest with the contents of this article.

This work is dedicated to the memory of Prof. Armando Gómez-Puyou for his major contributions to the fields of bioenergetics and protein structure and function.

[S] This article contains supplemental data.

[1] To whom correspondence should be addressed: Dept. de Biología, Facultad de Química, Universidad Nacional Autónoma de México (U.N.A.M.), Laboratorio 206, Edificio "F", Circuito Escolar, s/n Ciudad Universitaria, Delegación Coyoacán, D.F., CP 04510, México. Tel./Fax: 5255-56223899 (ext. 44449); E-mail: jjgartre@unam.mx.

[2] The abbreviations used are: IF_1, inhibitor protein of mitochondrial F_1-ATPase; $BhMF_1$- or MF_1-ATPase, F_1-ATPase of bovine heart mitochondria; DSP, dithiobis(succinimidyl propionate); EcF_1-ATPase, F_1-ATPase of *E. coli*; PdF_1-ATPase, F_1-ATPase complex of *P. denitrificans*.

TABLE 1

Identities among the subunits of the F_1-ATPase resolved by x-ray crystallography and the PdF_1-ATPase

The identities of each subunit of the PdF_1-ATPase resolved by x-ray crystallography compared with the subunits of the PdF_1-ATPase (IDvsPd) were determined by structural alignment with Swissmodel. The highest identities were observed in the first line with the MF_1-stalk structure (Protein Data Bank entry 2WSS). For this reason, the 2WSS structure was chosen as the template to construct the PdF_1-ATPase model.

	Chain							
Template	A (α1) IDvsPd	B (α2) IDvsPd	C (α3) IDvsPd	D (β1) IDvsPd	E (β2) IDvsPd	F (β3) IDvsPd	G (γ) IDvsPd	H (ϵ) IDvsPd
2WSS (*Bos taurus*)	68.04	69.58	70.45	78.37	78.54	78.54	41.15	25.58
2JDI (*B. taurus*)	70.02	69.58	70.02	78.37	78.17	78.54	26.63	15.91
3FKS (*Saccharomyces cerevsiae*)	67.15	67.43	67.36	76.34	76.66	76.17	33.21	24.14
3OAA (*E. coli*)	59.33	59.37	59.45	71.33	71.33	71.33	37.59	23.19

the mitochondrial F_1-ATPase (8). The ζ subunit also has a low affinity ATP binding site that seems to control its inhibitory capacity (7, 9). In order to resolve the inhibitory mechanism of ζ before the structural data becomes available, we constructed a homology model of the PdF_1-ATPase complex of *P. denitrificans* to dock the NMR structure of ζ at its inhibitory binding site. Together with previous and new biochemical data, the final model shows how the ζ subunit blocks rotation of the F_1F_O-ATPase of *P. denitrificans* and related α-proteobacteria, by a "pawl" mechanism on a ratchet (10) formed by the γ subunit. This is somehow a hybrid mechanism between mitochondrial IF_1 and bacterial ϵ but with structural differences giving it a uniqueness on the control of the α-proteobacterial F_1-ATPase nanomotor.

Materials and Methods

PdF_1-ζ Model Construction—A homology model of the PdF_1-ATPase was constructed by using the most complete mitochondrial F_1-ATPase structure available as a template. The mitochondrial F_1-stalk structure (Protein Data Bank entry 2WSS) was chosen because it showed the highest identity after structural alignment of the sequences of PdF_1-ATPase with several available bacterial, yeast, and mitochondrial F_1-ATPase structures (Table 1). The mitochondrial second stalk and ϵ subunits were removed from the template before the construction of the PdF_1-ATPase model. Thus, the final PdF_1-ATPase model contained only the subunits α_3, β_3, γ_1, δ_1, and ϵ_1 (with the indicated stoichiometries). A model of each subunit was constructed separately by the Swissmodel server, and subsequently all of the subunits were then assembled into a model of the full PdF_1-ATPase complex in Swissmodel (deep view). The quality of each subunit model was confirmed by manual checking of the full alignment in Swissmodel and Chimera, with an upper limit of main chain root mean square deviation of around 0.2 Å. The raw model obtained was subjected to several rounds of three-dimensional fitting using the template 2WSS structure. Afterward, the model was refined by correction of clashes and incorrect atom positions by several energy minimizations in Chimera, Swissmodel, and by evaluation of the model with Molprobity (11–13). The final model fitted to each subunit of the 2WSS template (Fig. 1) with an average root mean square deviation of ≤0.2 Å. Some small regions of the γ subunit that were not resolved in the template (2WSS) were modeled in order to obtain a higher accuracy. Special care was taken with the PdF_1-ϵ subunit, which had the lowest identity; therefore, this model was further evaluated using a combination of biochemical data together with other bacterial ϵ templates.

PdF_1-ATPase, ζ Subunit, and IF_1 Purifications—The PdF_1-ATPase was purified by chloroform extraction and chromatography as described before (7). The recombinant ζ and IF_1 subunits were overproduced and purified as described elsewhere (7, 14).

Cross-linking Analyses—Cross-linking analyses were carried out as described previously with dithiobis(succinimidyl propionate) (DSP) by incubating the PdF_1-ATPase with or without recombinant ζ subunit (or the $\zeta^{\Delta NT}$ construct) (7) for 30 min at room temperature in 20 mM KH_2PO_4 buffer at pH 7.4. The cross-linking reaction was arrested by the addition of excess L-lysine (20 mM), and the samples were immediately loaded into SDS-polyacrylamide gels (15) to analyze cross-linking products.

Limited Proteolysis of the PdF_1-ζ Complex—The PdF_1-ATPase containing its endogenous ϵ and ζ subunits was incubated for limited proteolysis with trypsin in a ratio (w/w) of 1:20 (trypsin/PdF_1) at room temperature as described before (6, 7). The limited proteolysis was stopped with excess PMSF (5 mM), together with a 4× supplement of the complete mixture of protease inhibitors (Roche Applied Science). Sequencing of the protein fragments was done by mass spectrometry as described before (7).

Other Procedures—The PdF_1-ATPase activity was measured by the coupled ATPase assay as described before (7, 14, 16) in the presence of 0.15% of lauryldimethylamine oxide detergent, 1 mM sulfite, pH 6.9. Protein concentrations were measured by the modified TCA-Lowry method (17), and Western blots were carried out as before (7).

Results and Discussion

Attempts to crystallize the PdF_1-ATPase had resulted in non-diffracting or unstable PdF_1-ATPase preparations that dissociate upon crystallization and produced diffracting crystals of a single α/β catalytic pair, thus lacking the γ, ϵ, and ζ subunits (18). In order to obtain a suitable structural model of the PdF_1-ζ complex, an initial homology model for the PdF_1-ATPase was constructed using the most similar and complete crystallographic structure of the F_1-ATPase available (Protein Data Bank entry 2WSS). According to the endosymbiotic theory (19–22), it was found that the most similar F_1-ATPase structure was that of the mitochondrial enzyme, rather than the eubacterial form, such as that of *Escherichia coli* (Table 1). By using the 2WSS structure to construct the PdF_1-ATPase model, it was possible to obtain a homology model with a very high superposition of tertiary and quaternary structures of the α, β, γ, and ϵ subunits (see Fig. 1*A*). After energy minimizations and

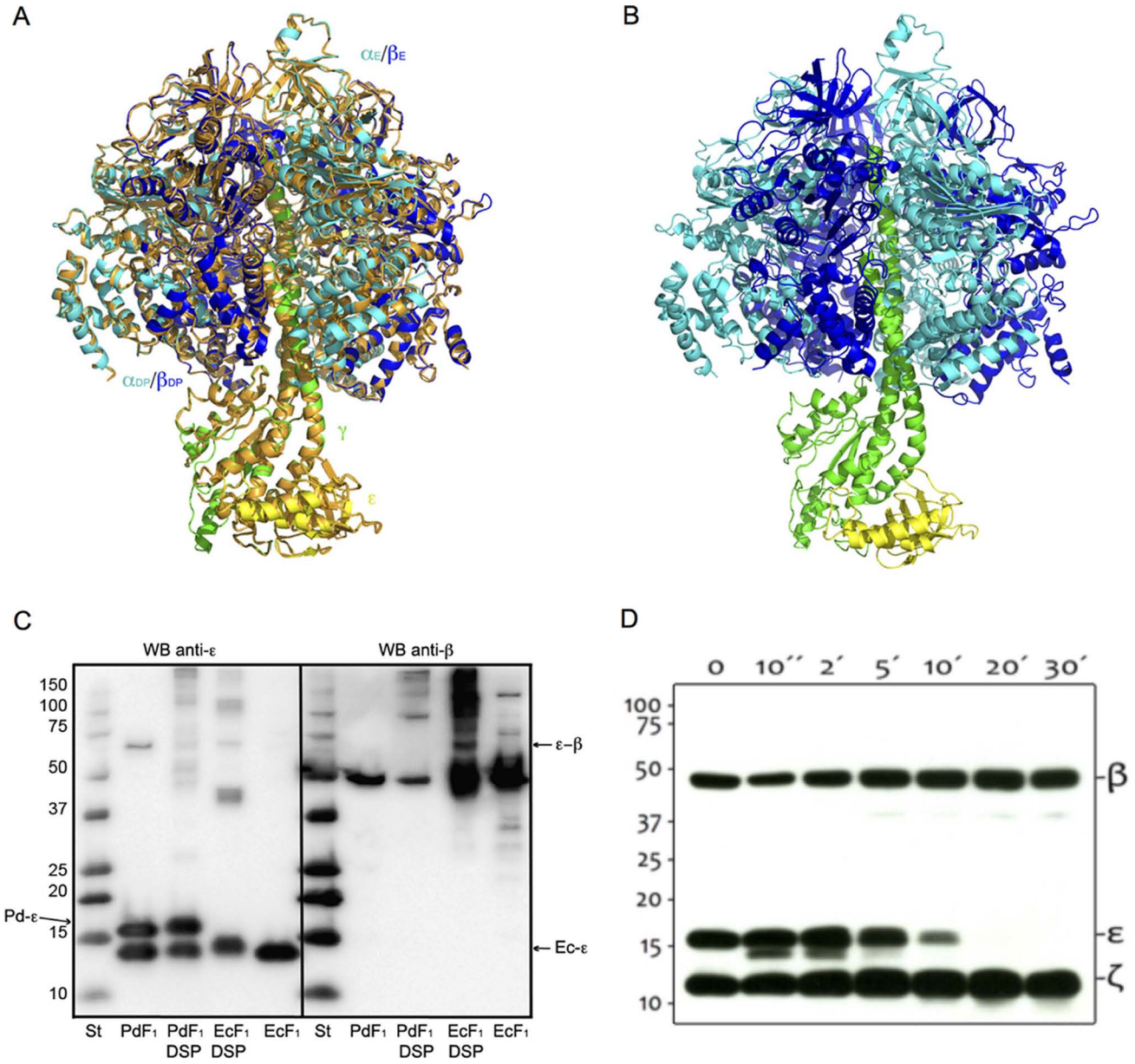

FIGURE 1. **Homology structural model of the F_1-ATPase of *P. denitrificans*.** The structure of PdF_1-ATPase was modeled by homology using the structure of the bovine F_1-stalk structure resolved by x-ray crystallography (Protein Data Bank entry 2WSS) as a template. The model was constructed with Swissmodel, Chimera, and PyMOL as described under "Materials and Methods." *A*, the model (α (*cyan*), β (*blue*), γ (*green*), and ϵ (*yellow*)) matched very well the overall main chain structure of the template (Protein Data Bank entry 2WSS, *orange*) after superposition, with an average root mean square deviation of 0.128 Å. The positions of the α_E/β_E and α_{DP}/β_{DP} interfaces, together with γ and ϵ subunits, are indicated; the $\alpha_{TP}\beta_{TP}$ interface is not indicated because it is located "behind" and therefore it is not clearly visible from this view. *B*, "side view" of the final PdF_1-ATPase model with the characteristic folding of the central rotor containing the γ/ϵ heterodimer at the center of the $\alpha_3\beta_3$ heterohexamer. The three conformations observed in most F_1-ATPases of the catalytic α/β interfaces as the empty (α_E/β_E), ADP (α_{DP}/β_{DP}), and ATP (α_{TP}/β_{TP}) heterodimers are conserved. No nucleotides are included in the model. *C*, cross-linking with DSP of the PdF_1-ATPase and EcF_1-ATPase, as revealed by anti-ϵ and anti-β Western blot (*WB*). The PdF_1- and EcF_1-ATPases were incubated for cross-linking with DSP as indicated under "Materials and Methods." The cross-linking products were resolved by loading the samples in the same SDS-polyacrylamide gel and revealed by Western blotting after immunotransfer and cutting of the PVDF membrane in the middle (indicated by the *central line*). The *left half* of the membrane was developed with anti-ϵ primary antibodies, and the *right side* of the membrane was developed with anti-β primary antibodies. The immunoblots showed the presence of ϵ-γ (45 kDa) and ϵ-β (65 kDa) cross-linking products in the EcF_1-ATPase (EcF_1-DSP) and their absence in the PdF_1-ATPase (PdF_1-DSP). These results support the compact conformation of ϵ of the PdF_1-ATPase model shown above (see "Results and Discussion"). *D*, limited proteolysis of the PdF_1-ATPase carried out with trypsin and developed by Western blot with anti-β, anti-ϵ, and anti-ζ antibodies as described under "Materials and Methods." The ζ subunit was totally resistant to limited proteolysis with the cleavage sites occluded in the PdF_1-ζ complex as shown in Fig. 4. The ϵ subunit was cleaved initially at the C-terminal α-helices that are exposed in the PdF_1-ATPase model above; the first fragment that appeared below ϵ corresponded to ϵ(1–103), according to mass spectrometry analyses.

refinements (see "Materials and Methods"), the final PdF_1-ATPase model lowered its average root mean square deviation after superposition with the bovine template from 0.2 to 0.128 Å. The resulting structure of the modeled PdF_1-ATPase was, as expected, very similar to the mitochondrial enzyme with the γ subunit in the center of the α_3/β_3 hexamer, which had the expected conformation of three different interfaces, one open (α_E/β_E) and two closed interfaces (α_{DP}/β_{DP} and α_{TP}/β_{TP}) (Fig.

1*B*). The folding of the Pd-ϵ model was fitted to the compact conformer of bacterial ϵ resolved before (23), and this conformation was supported by limited proteolysis and cross-linking experiments together with its lack of inhibition (6, 7), as described below.

Two experimental approaches supported the presence of the compact conformer of ϵ in the PdF_1-ATPase. First, in order to explore the putative compact conformation of Pd-ϵ, it was assessed whether the endogenous ϵ subunit was able or not to cross-link with the β subunits in the PdF_1-ATPase complex (see Fig. 1*C*). In the PdF_1-ATPase model, the compact Pd-ϵ (Fig. 1*B*) is at a distance of about 29 Å to the closest β C terminus, whereas the cross-linker (DSP) has a shorter distance of 12 Å. In the extended conformation, the two C-terminal α-helixes of ϵ make close contacts with α, β, and γ subunits (2, 5, 24). Therefore, in the compact conformation, Pd-ϵ should be unable to form the ϵ-β and ϵ-γ adducts with DSP, whereas in the extended conformation, Pd-ϵ should form ϵ-β and ϵ-γ cross-linkages. In order to determine the presence or absence of the ϵ-β adduct in the PdF_1-ATPase, control experiments were also carried out with the F_1-ATPase isolated from *E. coli*. As expected, the latter enzyme showed both the ϵ-β (Fig. 1*C*, *left* and *right*, *EcF_1-DSP*, 65 kDa band) and the ϵ-γ cross-linkings (Fig. 1*C*, *left*, *EcF_1-DSP*, 45 kDa) previously identified by two-dimensional SDS-PAGE (7). These results show that in *E. coli*, the extended conformation of ϵ promotes the ϵ-β cross-linking of 65 kDa, which immunoreacted with both anti-ϵ and anti-β antibodies (Fig. 1*C*, *EcF_1-DSP*, *left* and *right*). In contrast, in the PdF_1-ATPase, there are some faint ϵ-adducts (Fig. 1*C*, *left*, *PdF_1-DSP*), but none of these are ϵ-β adducts, as shown by the absence of the 65 kDa band in the anti-β blot (Fig. 1*C*, *right*, *PdF_1-DSP*). A 65 kDa anti-ϵ band in the control non-cross-linked sample (PdF_1) seems to be an ϵ aggregate or a nonspecificity (Fig. 1*C*, *left PdF_1 lane*), which is also present in the PdF_1-DSP cross-linked sample (Fig. 1*C*, *left*). Taken together, the absence of the ϵ-β adduct in PdF_1-ATPase and its presence in F_1-ATPase of *E. coli* (EcF_1) support the finding that the endogenous Pd-ϵ prefers to adopt the compact conformation, as shown in the PdF_1-ATPase model (Fig. 1*B*). This preferred compact conformation of Pd-ϵ explains why this subunit does not work as an endogenous inhibitor of the PdF_1-ATPase and putatively should not work in the other α-proteobacteria. The Pd-ϵ subunit does not seem to be able to acquire the extended inhibitory conformation, and it is therefore unable to block γ rotation. This leaves this inhibitory role to the ζ subunit.

The two C-terminal α-helixes of ϵ were accessible to limited proteolysis in the PdF_1-ATPase (see Fig. 1*D*). This accessibility to the protease is more likely to take place in the compact conformation of ϵ, as shown in Fig. 1*B*, than in the extended conformation of ϵ, where the two inhibitory C-terminal α-helixes are inserted and mostly buried within the α/β/γ interface (2). In the extended conformation, the C-terminal α-helixes of ϵ should be inaccessible to limited proteolysis in the F_1-ATPase complex. Our limited proteolysis (Fig. 2) and MS results of the PdF_1-ATPase (supplemental data) showed a tryptic ϵ fragment of 11 kDa, among other α and γ fragments, migrating just below the intact ζ subunit and containing the N-terminal peptide $\epsilon_{Met1-Arg13}$ (see Fig. 2, *A–D*, and supplemental data). Therefore, the protease cleaved the two C-terminal α-helixes of ϵ, leaving an 11-kDa fragment consisting of $\epsilon_{Met1-Arg103}$ (Fig. 2*D*). These results strongly suggest that the two C-terminal ϵ α-helixes are exposed in the PdF_1-ATPase and therefore most probably in the compact ϵ conformation (Fig. 1, *B* and *D*). These results seem to be opposite to those of Wilkens and Capaldi (23). They found that the isolated ϵ subunit from the F_1-ATPase of *E. coli* (Ec-ϵ) is relatively resistant to trypsin in its compact soluble conformation as resolved by NMR (23). Therefore, we analyzed the trypsin sensitivity of the isolated ϵ subunit from *P. denitrificans* (Pd-ϵ), and in contrast to that of *E. coli* (23), we observed an extensive cleavage of the Pd-ϵ subunit at trypsin/Pd-ϵ ratios of 1:5–1:100 (w/w) (Fig. 2*B*). The trypsin/Ec-ϵ ratio used by Wilkens and Capaldi (23) was in the same range (1:80), and the isolated Ec-ϵ was resistant to the protease for about 8 min, whereas our Pd-ϵ subunit was extensively cleaved at the same 1:80 ratio after only 3 min of limited proteolysis, clearly producing the 11-kDa $\epsilon_{Met1-Arg103}$ fragment among other peptides (Fig. 2*B*). These results indicate that the trypsin sensitivities of the isolated Ec-ϵ and Pd-ϵ subunits are different, probably due to intrinsic sequence differences or to different proteolysis conditions, and therefore, their trypsin sensitivities are not comparable with each other. In consequence, given the high sensitivity of the isolated Pd-ϵ to trypsin, the formation of the $\epsilon_{Met1-Arg103}$ fragment by limited trypsinolysis of the full PdF_1-ATPase indicates that the two C-terminal α-helixes of the endogenous Pd-ϵ are exposed and most likely in the compact conformation as shown in the PdF_1-ATPase model (Fig. 1, *A* and *B*).

Once the PdF_1-ATPase model was completed, the most represented average structure of the 20 conformers of Pd-ζ that were resolved was docked with Chimera into the α/β interfaces following the previously observed high cross-linking interaction of ζ with PdF_1-ATPase (6, 7). The most probable α/β pair to provide the first interaction surface for ζ was the open α_E/β_E interface, because this allowed an easier docking of the ζ subunit than the other two closed interfaces. We already showed that the N terminus of ζ is the inhibitory domain (*red* in Fig. 3*A*) and that there is a high yield of ζ cross-linking with α and β subunits and a lower yield with γ and ϵ subunits (6, 7). Therefore, the disordered N-terminal domain of ζ was oriented toward the γ subunit, and its globular part, which works as an anchoring domain, was oriented to the C termini of the α_E/β_E interface (Fig. 3*B*). This orientation is also supported by cross-linking data because the cross-linkers used previously (2-iminothiolane and DSP) were specific for lysines, and most of these lysines (4 of 6) are on the globular ζ domain, compared with only 2 lysines in the N-terminal side. This suggests that the high ζ-α and ζ-β cross-linking yields (7) result from interaction of the globular part of ζ with the α/β interface, whereas the lower ζ-γ cross-linking yield (7) is due to the N-terminal inhibitory domain of ζ interacting with subunit γ. In order to test this putative orientation, we took advantage of our Pd-$\zeta^{\Delta NT}$ construct lacking the first 14 N-terminal residues (7). The overall model predicts the interaction of the N-terminal inhibitory domain of ζ with the γ subunit to inhibit rotation. If this is the case, the Pd-$\zeta^{\Delta NT}$ construct lacking the inhibitory N-terminal domain should decrease its cross-linking yield with γ after its reconstitution in conditions that promote its effective binding

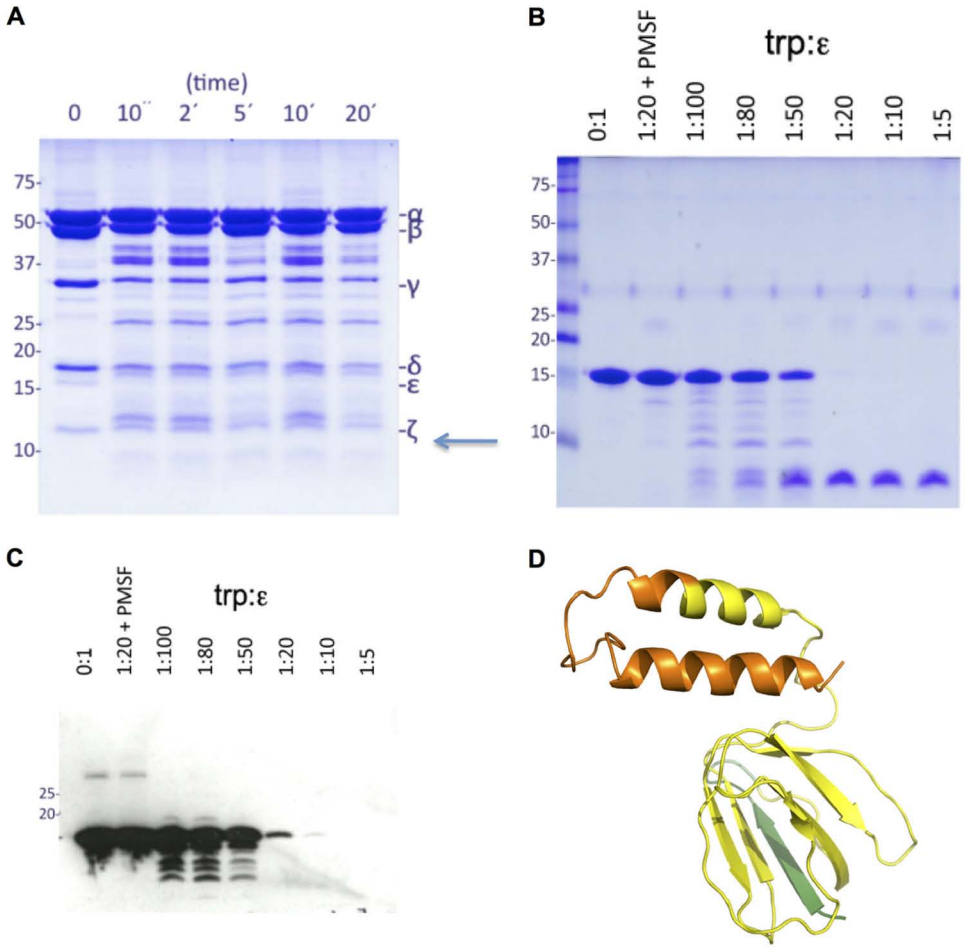

FIGURE 2. **Limited trypsinolysis of the PdF_1-ATPase and the isolated ϵ subunit.** *A*, SDS-polyacrylamide gel of the trypsinized PdF_1-ATPase. Trypsin and the PdF_1-ATPase were mixed in reconstitution buffer at a ratio of 1:20 Trp/PdF_1-ATPase (w/w) at 25 °C, and the cleavage reactions were arrested by 5 mM PMSF at the times indicated (in minutes). The *blue arrow* indicates the position where the N-terminal Met^1–Arg^{13} peptide of ϵ was found by mass spectrometry (see supplemental data and *panel D*). At t_0, PMSF was present before the addition of trypsin. *B*, limited trypsinolysis of the isolated Pd-ϵ subunit. The recombinant Pd-ϵ subunit was subjected to limited trypsinolysis at the indicated Trp/Pd-ϵ ratios by 3 min at 25 °C in reconstitution buffer, and the reactions were arrested as before loading the samples onto the SDS-polyacrylamide gel as shown. *C*, Western blot against the ϵ subunit of *P. denitrificans* of the same samples shown in *A* but loaded with 3-fold lower amounts of protein. *D*, observed limited trypsinolysis fragment of the endogenous ϵ subunit bound to the PdF_1-ATPase. The model of ϵ subunit of *P. denitrificans* is shown, indicating in *green* the N-terminal Met^1–Arg^{13} peptide sequenced by MS from the proteolytic ϵ fragment of 11 kDa (*A* and *B*). Given this 11 kDa size, the most probable cleavage position is the first of three arginine residues (Arg^{103}) in the C-terminal α-helixes of ϵ, corresponding to the inhibitory domain of the protein in other eubacteria. The trypsin-cleaved segment is shown in *orange*, and therefore, the proteolytic fragment is $\epsilon_{Met1\text{-}Arg103}$. The C-terminal domain of ϵ is therefore exposed and accessible to the protease in the intact PdF_1-ATPase (*A* and Fig. 1) as well as in the isolated ϵ subunit (*B*).

to the PdF_1-ATPase (7) and where we had previously shown that the reconstitution of the full ζ^{WT} subunit increases the ζ-γ cross-linking yield (7). For this experiment, most of the endogenous ζ subunit of the PdF_1-ATPase complex was removed by immunoaffinity columns as described before (7), and then the Pd-$\zeta^{\Delta NT}$ construct was reconstituted. Excess free Pd-$\zeta^{\Delta NT}$ was removed by gel filtration. As revealed by Western blot, the DSP cross-linking showed a decrease in the yield of the ζ-γ cross-link instead of an increase (Fig. 3*C*, *right lane*), as expected if the N-terminal extreme of ζ is the domain interacting with γ blocking its rotation. However, we also observed a decrease in the ζ-β adduct and an increase in high molecular weight unidentified adducts (Fig. 3*C*, *right lane*). The latter could result from extensive Pd-$\zeta^{\Delta NT}$-α/β cross-linking derived from a lower accessibility of Pd-$\zeta^{\Delta NT}$ to cross-link with ζ. Alternatively, because the Pd-$\zeta^{\Delta NT}$ construct was reconstituted in excess amounts relative to PdF_1, the truncated ζ subunit could probably bind to two or three α/β interfaces, similar to the reconstituted mitochondrial F_1-$(IF_1)_2$ and F_1-$(IF_1)_3$ complexes (2–4). If this is the case with the Pd-$\zeta^{\Delta NT}$ construct, the larger molecular adducts are probably derived from extensive ζ-α-β cross-linkages formed after reconstitution into the PdF_1-ATPase. On the other hand, the low yield ζ-γ cross-link observed after Pd-$\zeta^{\Delta NT}$ reconstitution (Fig. 3*C*, *right lane*) is probably due to small amounts of remanant endogenous Pd-ζ^{WT} that could not be removed by immunoaffinity columns, as observed previously (7). In summary, the lack of the N-terminal inhibitory domain in the Pd-$\zeta^{\Delta NT}$ construct decreased the ζ-γ cross-linking yield, suggesting that this is in close proximity to or in direct contact with γ to block its rotary function.

After finding that the final PdF_1-ATPase structure is compatible with the cross-linking and limited proteolysis data, we therefore proceeded to accommodate the NMR structure of the ζ subunit into its putative inhibitory site on the PdF_1-ATPase model. In order to achieve this, the N-terminal domain of ζ was oriented toward the γ subunit, and the globular and C-terminal

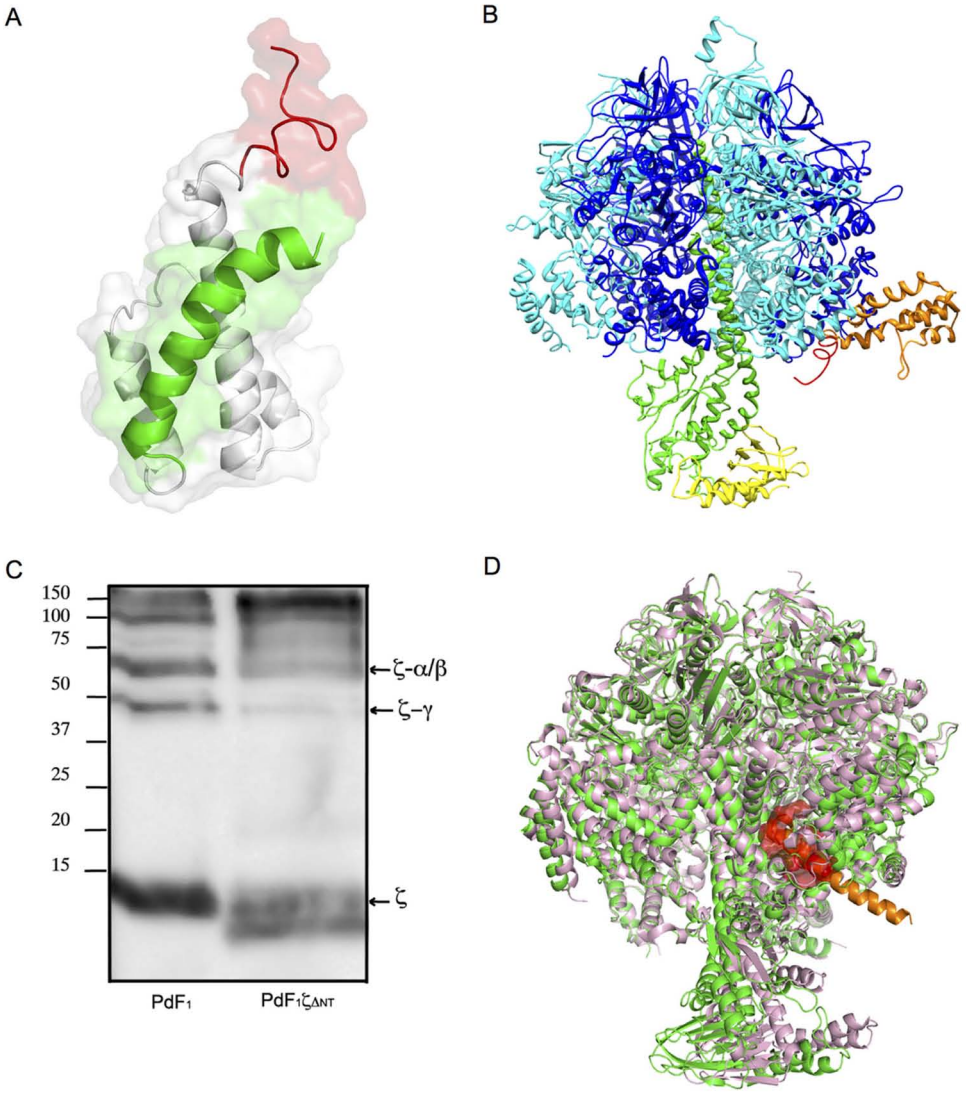

FIGURE 3. **Structural and functional evidence indicating that ζ and IF_1 bind to the same $\alpha_{DP}/\beta_{DP}/\gamma$ interface to inhibit rotation and F_1-ATPase activity.** *A*, the NMR structure of the ζ subunit of *P. denitrificans* (Protein Data Bank entry 2LL0) (7, 9, 28) is shown in *different colors*; the disordered and highly mobile N-terminal inhibitory domain that is cleaved by trypsin (7) is shown in *red*; the C-terminal α-helix 4, which is also cleaved by trypsin, is shown in *green*, and the globular domain of ζ that is resistant to trypsin containing α-helices 1–3 is shown in *white*. *B*, the initial entrance site of Pd-ζ into PdF_1-ATPase was more easily modeled by docking the C-terminal α-helix of ζ (*orange*) into the α_E/β_E interface, with the inhibitory N-terminal domain of ζ (*red*) pointing toward the central γ/ϵ rotor. Subunit *color codes* are the same as in Fig. 1. *C*, Western blot anti-ζ revealing the ζ cross-linking products of control PdF_1-ATPase (*left lane*) and the PdF_1-ATPase (lacking most of the endogenous ζ) reconstituted with the Pd-$\zeta^{\Delta NT}$ construct (*right lane*). The same amounts of protein (10 μg) were loaded on both *lanes*. The ζ-γ cross-linking yield decreased with the reconstitution of the Pd-$\zeta^{\Delta NT}$ construct, whereas other higher adducts increased probably because of extensive ζ-α/β cross-linkages. *D*, the PdF_1-ATPase model (*green*) was aligned and fitted to the structure of the mitochondrial F_1-IF_1 complex (Protein Data Bank entry 2V7Q, *light pink*) with PyMOL; the alignment is not as good as in the non-inhibited MF_1-PdF_1-ATPase alignment shown above (Fig. 1) because of differences in the rotor positions induced by IF_1 or stalk subunits, respectively. IF_1 is shown in *orange*, and the slightly similar (7) inhibitory N-terminal domain of ζ is shown in *red* with a *semitransparent surface*. The alignment indicates that both ζ and IF_1 are probably bound to the same inhibitory site.

domains were bound to the α/β interface. The N-terminal domain and the C-terminal α-helix of the ζ subunit extend together on one side of ζ and make together a continuous contact surface to interact with the α/β interface (*red* N terminus and *green* C terminus in Fig. 3*A*). In accordance with limited proteolysis assays, these regions were protected from limited trypsinization in the intact PdF_1-ζ complex, indicating that N and C termini of ζ are occluded in the native PdF_1. In contrast, both proteolytic sites on the N and C termini of Pd-ζ (*red* and *green* in Fig. 3*A*) are exposed in the isolated subunit (6). The ζ subunit was therefore inserted in the α_E/β_E interface, which opens the more accessible entrance site, with the N terminus approaching the γ subunit and the C-terminal α-helix of ζ occluded at the α_E/β_E interface (Fig. 3*B*).

This initial entrance of the ζ subunit does not seem to be the final inhibitory position because the productive interaction of ζ with PdF_1-ATPase is enhanced by the catalytic turnover of the enzyme, similar to the mechanism described for the mitochondrial IF_1. In this mechanism, some ATP hydrolysis turnovers are required for the proper binding of the inhibitor into its final inhibitory position (6, 7, 25). It has been found that two 120° partial rotations of the γ subunit are required for the accommodation of IF_1 in its final inhibitory binding $\alpha_{DP}/\beta_{DP}/\gamma$ interface in a binding lock mechanism (3, 4). Therefore, it was con-

sidered that ζ could work through an IF_1-like mechanism because we also found previously that the N-terminal inhibitory domain of ζ has a limited but convergent similarity with the corresponding inhibitory domain of IF_1 (7). This hypothesis was further supported by the recent finding that the inhibitory α-helixes of ϵ and IF_1 interact with the homologous $\alpha_{DP}/\beta_{DP}/\gamma$ interface of their respective F_1-ATPases of *E. coli*, *PS3*, and mitochondria, at a common inhibitor-binding pocket named the "inhibition general core region," which includes residues from the C terminus of α/β subunits and some catch residues of γ (5).

Taken together, these antecedents supported the possibility that the inhibitory N-terminal domain of the ζ subunit will also bind to the same $\alpha_{DP}/\beta_{DP}/\gamma$ interface as the inhibitory domains of ϵ and IF_1. In order to assess this hypothesis, the N-terminal inhibitory domain of ζ (ζ-NT) was aligned structurally with the mitochondrial IF_1 bound in its inhibitory position in the mitochondrial IF_1. Afterward, the PdF_1-ATPase model was aligned and superimposed on the MF_1-IF_1 and ζ-NT structures. The small similarity between both inhibitory domains of ζ and IF_1 (7) allowed a structural alignment in PyMOL (Fig. 3*D*). This structure of the PdF_1-ATPase model with the ζ-NT (*red* in Fig. 3*D*) aligned to IF_1 was used as a guide for the fitting of the ζ subunit into the $\alpha_{DP}/\beta_{DP}/\gamma$ interface of the PdF_1-ATPase model. The final structural alignment showed that the N-terminal inhibitory domain of ζ very likely binds to the common inhibitor-binding region of the PdF_1-ATPase at the $\alpha_{DP}/\beta_{DP}/\gamma$ interface (Fig. 3*D*) in a similar fashion to the way mitochondrial IF_1 binds to MF_1-ATPase (3, 26).

One of the main predictions of this model is that if ζ and IF_1 share a common binding site with their N-terminal inhibitory domains interacting similarly with their respective F_1-ATPases, this raises the possibility that the mitochondrial IF_1 could exert heterologous inhibition on the F_1-ATPase of *P. denitrificans*, albeit with a lower affinity than that of the Pd-ζ during homologous reconstitution. Therefore, the putative inhibitory effect of mitochondrial IF_1 on the PdF_1-ATPase was assayed, in parallel to the known inhibitory action of ζ, by carrying out titration curves of IF_1 and ζ on the PdF_1-ATPase activity. In accordance with the present model of the interaction of ζ with PdF_1, it was clearly observed that the mitochondrial IF_1 exerted a partial inhibition of the PdF_1-ATPase. In contrast, the ζ subunit exerted a stronger total inhibition (Fig. 4*A*). As expected, the affinity of IF_1 to inhibit the PdF_1-ATPase was lower than that of ζ, because the IC_{50} of IF_1 was about 50-fold higher than that of Pd-ζ (Fig. 4*A*). We also observed that after adding IF_1 in amounts close to its IC_{5O} in order to produce 50% inhibition, the subsequent addition of ζ showed an additive effect and reached total inhibition (Fig. 4*B*). This suggests that both inhibitory proteins interact at the same binding site. To our knowledge, this is the first evidence of inhibition of a bacterial F_1-ATPase by the mitochondrial IF_1. It is well known that IF_1 does not inhibit the EcF_1-ATPase. We confirmed this and found that IF_1 showed no inhibition of the EcF_1-ATPase at all (Fig. 4*A*); however, it produced a 93% inhibition of the mitochondrial F_1-ATPase as a positive control (Fig. 4*B*). The endosymbiotic theory proposes that mitochondria arose from α-proteobacteria (19–22). Given the close similarity between PdF_1-ATPase

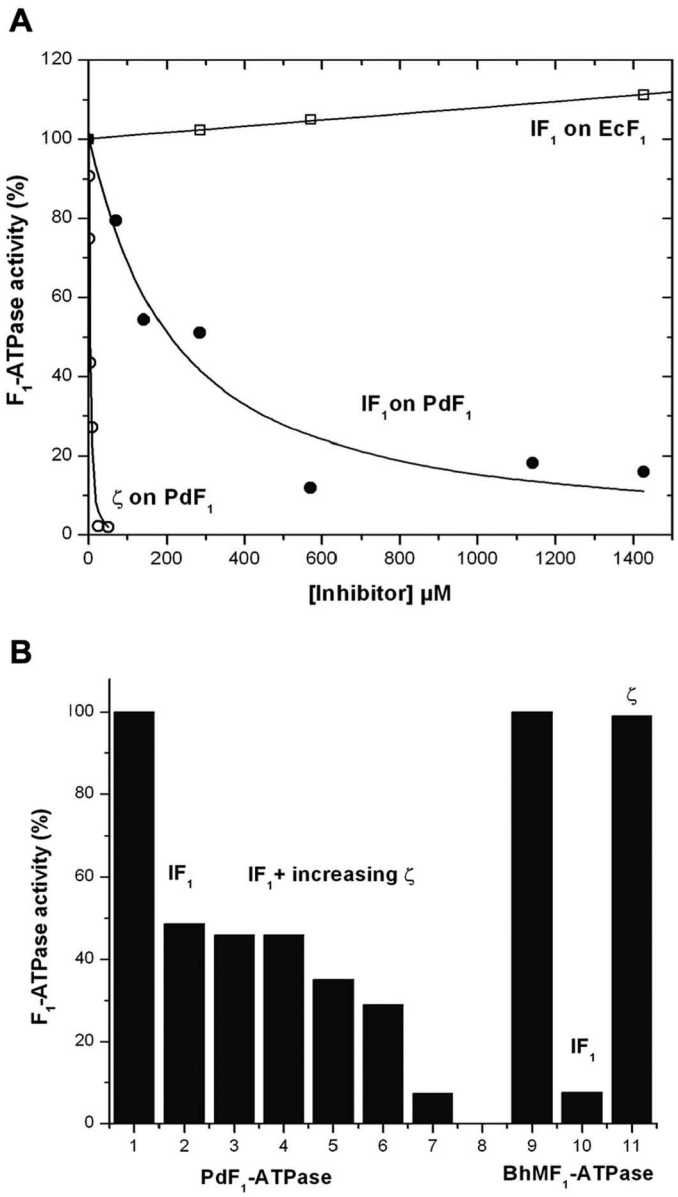

FIGURE 4. **Heterologous inhibition of the PdF_1-ATPase by the mitochondrial IF_1 inhibitor.** *A*, effect of ζ (○) and IF_1 (●) on the PdF_1-ATPase. The PdF_1-ATPase (21 μg) was preincubated in 20 μl with the indicated concentrations of recombinant ζ or IF_1 proteins purified as described under "Materials and Methods" in the presence of 1 mM MgATP in reconstitution buffer at pH 7.0. After 20 min preincubation at room temperature, the full mixture was added to a 1-ml reaction cells at 37 °C containing the coupled ATPase assay buffer as described under "Materials and Methods." 100% of PdF_1-ATPase activity corresponds to 4.99 μmol/min·mg for the ζ titration curve and 4.019 μmol/min·mg for the IF_1 titration curve and 41.5 μmol/min·mg for the EcF_1-ATPase (□). The plot shows the fitting to a non-linear Hill inhibitory equation giving an IC_{50} of ζ = 4.76 μM and IC_{50} of IF_1 = 208.6 μM carried out with Origin version 7.5. *B*, the additive effects of IF_1 and ζ were assayed by preincubation of the PdF_1-ATPase (4 μg) with 50 μg of purified bovine heart IF_1 as indicated above to obtain about 50% inhibition of the PdF_1-ATPase (*bar 2* indicated as IF_1). Increasing amounts of the ζ subunit (0.25, 0.5, 1, 2, and 5 μg) were added in addition to IF_1 to samples 3–7 for preincubation as described above, before measurement of the PdF_1-ATPase activity as described under "Materials and Methods." Control samples were preincubated in the absence of IF_1 and ζ inhibitors and showed a PdF_1-ATPase activity of 7.7 μmol/min·mg protein. In the last samples (9–11), the activity of BhF_1-ATPase was measured, and the effects of preincubation of 3.8 μg of $BhMF_1$-ATPase with 25 μg of IF_1 and 22 μg of ζ were assayed on the $BhMF_1$-ATPase activity. The control activity of the $BhMF_1$-ATPase was 14.7 μmol/min·mg protein; this activity is relatively lower than those reported before, probably because the ATPase assay was carried out at pH 6.9, and the optimal pH of the mitochondrial enzyme is 8.0. Only IF_1, but not ζ, exerted a strong inhibitory effect on the $BhMF_1$-ATPase.

and MF_1-ATPase (Table 1), it may not be a coincidence that the PdF_1-ATPase is inhibited by IF_1, whereas the EcF_1-ATPase is not (Fig. 4*A*). In other words, the selective heterologous inhibition of PdF_1-ATPase by mitochondrial IF_1 is in concordance with the α-proteobacterial origin of mitochondria because the N-terminal inhibitory domains of ζ and IF_1 are slightly similar (7). In addition, the "inhibition general core region" at the $\alpha/\beta/\gamma$ interface should be more conserved between the *P. denitrificans* and mitochondrial PdF_1-ATPases than between the mitochondrial F_1-ATPase and EcF_1-ATPase. This closest similarity between *Paracoccus* and mitochondrial F_1-ATPases allowed the productive binding of mitochondrial IF_1 into the inhibitor general domain of the $\alpha/\beta/\gamma$ interface of the PdF_1-ATPase (Fig. 4*A*). The reciprocal experiment to assess the effect of ζ on the mitochondrial $BhMF_1$-ATPase showed no inhibition (Fig. 4*B*). However, the experiment was carried out with 22 μg of ζ, so it remains to be explored with larger amounts of ζ to confirm whether or not it inhibits the mitochondrial F_1-ATPase. Taken together, these results strongly suggest that the inhibitory mechanisms and therefore the binding sites of IF_1 and ζ are very similar and support the model described above. This indicates that the limited but converging similarity between the N-terminal inhibitory domains of the ζ subunit and IF_1 promote their binding to the common inhibitor binding region at the $\alpha_{DP}/\beta_{DP}/\gamma$ interface to block rotation of the PdF_1-ATPase.

Taking all of the results together, the overall inhibitory mechanism of binding of the ζ subunit to the PdF_1-ATPase is most likely as follows: 1) the ζ subunit enters through the open α_E/β_E interface with its N-terminal inhibitory domain pointing forward to interact with the rotary γ subunit, with its globular part working as an anchoring domain (Fig. 5, *A* and *B*); 2) one partial 120° counterclockwise rotation of γ as induced by ATP binding (27) transforms the α_E/β_E interface into the α_{TP}/β_{TP} conformation (Fig. 5, *C* and *D*); 3) a second ATP binding and 120° counterclockwise rotation of γ locks the N-terminal inhibitory domain of ζ into the $\alpha_{DP}/\beta_{DP}/\gamma$ interface known as the "inhibitor general core region," whereas the globular domain of ζ holds the inhibitor bound to the C terminus of the α_{DP}/β_{DP} interface (Fig. 5, *E* and *F*). This model explains the mechanism of inhibition of γ rotation exerted by ζ, which acts to block the PdF_1-ATPase activity. Presumably, this is preserved in most if not all α-proteobacteria. In summary, ζ works similarly to IF_1 and ϵ by working as a pawl (*i.e.* by blocking preferably the counterclockwise gyration of γ, which rotates as a ratchet) (10). In the final modeled inhibitory position of ζ, the N-terminal inhibitory domain of the protein is partially inserted in the "inhibition general core region" of the $\alpha_{DP}/\beta_{DP}/\gamma$ interface (Fig. 5, *E* and *F*), in a similar way to IF_1 in the mitochondrial enzyme. This position of ζ explains why the Pd-$\zeta^{\Delta NT}$ construct binds but does not inhibit the PdF_1-ATPase (7). Removal of the N-terminal inhibitory domain will allow the rotation of the γ-ϵ rotor because the Pd-$\zeta^{\Delta NT}$ construct will not be able to work as a pawl to hinder γ rotation. A further induced fit of the PdF_1-ζ interface should lead to a deeper insertion of the N terminus of ζ to reach γ as it is proposed in Fig. 3*D*. This would result in a closer interaction of ζ with the γ subunit to block rotation. If the inhibitory mechanisms of ζ and IF_1 are similar enough, the disordered N-terminal domain of ζ (Fig. 3*A*) will probably fold into an extended α-helical conformation upon reaching its final locked position in PdF_1, as the mitochondrial IF_1 does in MF_1-ATPase (4). Our model also considers that the ζ subunit may turn its globular anchoring domain upon reaching its final locked position. Some of these finer details of the Pdζ-PdF_1 interaction will have to wait for the atomic resolution of the structure; nonetheless, the overall inhibitory mechanism of ζ

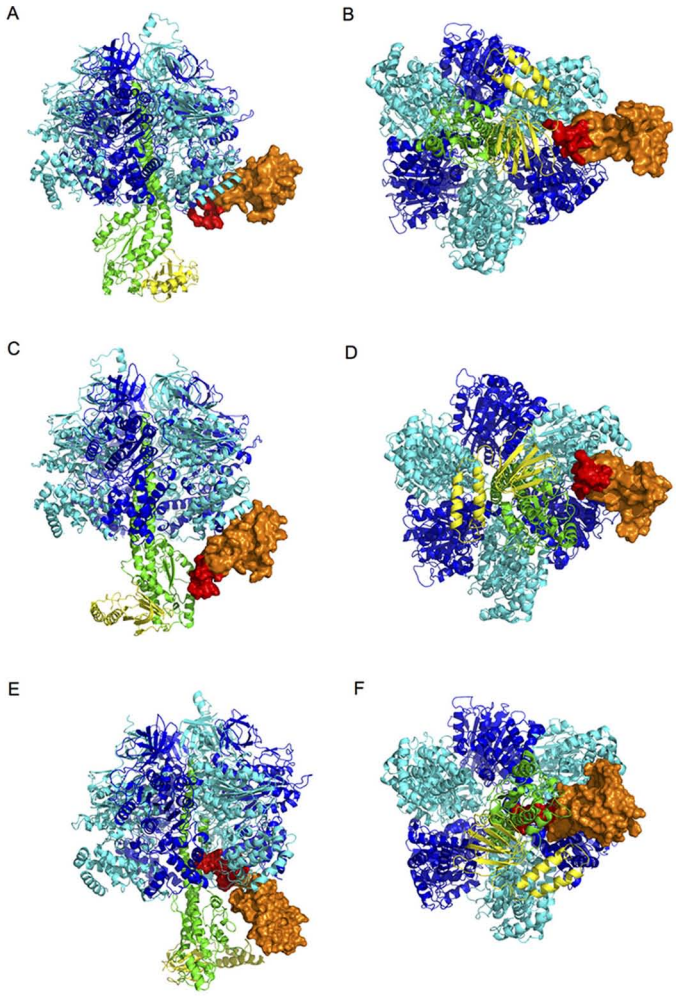

FIGURE 5. **Model for the inhibitory interaction of the ζ subunit to inhibit rotation of the PdF_1-ATPase nanomotor.** *A* and *B*, the open α_E/β_E interface of the PdF_1-ATPase model was the most accessible first interaction surface to dock the ζ subunit structure. Because the N-terminal domain (*red*) of the ζ subunit is the inhibitory domain and this should interact with the γ subunit to inhibit rotation, this domain was directed through the open α_E/β_E interface by accommodating the C-terminal α-helix of the globular part of ζ as a binding surface. *C* and *D*, after the initial entrance of ζ at the empty interface, a 120° rotation of the central rotor induced by ATP binding changes the conformation of the α_E/β_E interface to the α_{TP}/β_{TP} conformer and promotes a closer interaction of the globular domain of ζ with this interface, whereas the N-terminal inhibitory domain is presented to interact with the γ subunit. *E* and *F*, a final ATP binding step promotes a second 120° partial gyration of the γ/ϵ rotor; therefore, the catalytic interface interacting with the ζ subunit shifts to the α_{DP}/β_{DP} conformation, making a closer interaction with the globular domain of ζ, whereas the inhibitory N-terminal domain (*red*) is inserted through the α_{DP}/β_{DP} interface or "inhibitor general region," similarly to mitochondrial IF_1 bound to MF_1. The N-terminal side of ζ is now in position to hinder the further rotation of the γ subunit, thus inhibiting fully the PdF_1-ATPase activity. A deeper insertion of the N-terminal extreme of ζ might occur in order to align completely with the IF_1 binding position of MF_1-ATPase as in Fig. 2. Presumably, this ζ interaction inhibits preferably the counterclockwise rotation of the PdF_1-ATPase. See "Results and Discussion" for details.

was resolved here. On the other hand, the globular domain of ζ has additional ϵ-like features, such as a low affinity nucleotide binding site that may regulate the inhibitory capacity of ζ (7). Analyses are ongoing to assess this putatively regulatory ATP binding site and also the proposed pawl mechanism of ζ on the γ ratchet.

Author Contributions—J. J. G.-T. designed the research, constructed the PdF_1-ATPase and PdF_1-ζ models, carried out the functional inhibitory titration experiments, purified the EcF_1- and $BhMF_1$-ATPases, carried out cross-linking and Western blot analyses, and wrote the paper. M. Z.-Z. carried out cross-linking, Western blotting, and limited proteolysis experiments; purified the PdF_1-ATPase and the recombinant ζ and IF_1 proteins; and helped with the manuscript preparation. F. M.-H. and E. H.-L. carried out SDS-PAGE for cross-linking and Western blot analyses and protein concentration determinations. R. O. made the bacterial cultures and helped with SDS-PAGE and cross-linking experiments and overexpression and purification of ζ and IF_1 recombinant proteins. G. M.-H. carried out the mass spectrometry analyses.

Acknowledgments—The monoclonal antibodies against the β subunit of bovine heart mitochondrial F_1-ATPase were kindly provided by Professors Michael Marusich and Roderick A. Capaldi (University of Oregon, Eugene, OR). The helpful discussions with Heliodoro Celis (Universidad Nacional Autónoma de México) and Blanca Barquera (Rensselaer Polytechnic Institute, Troy, NY) are gratefully acknowledged. The suggestions and corrections for English style by Isla Ogilvie, Katherine G. Mezic, and Pattie Nelson are gratefully acknowledged. The excellent comments and suggestions from reviewers and editors to improve this paper are also gratefully acknowledged.

References

1. García-Trejo, J. J., and Morales-Ríos, E. (2008) Regulation of the F_1F_0-ATP synthase rotary nanomotor in its monomeric-bacterial and dimeric-mitochondrial forms. *J. Biol. Phys.* **34,** 197–212
2. Cingolani, G., and Duncan, T. (2011) Structure of the ATP synthase catalytic complex (F1) from *Escherichia coli* in an autoinhibited conformation. *Nat. Struct. Mol. Biol.* **18,** 701–707
3. Gledhill, J. R., Montgomery, M. G., Leslie, A. G., and Walker, J. E. (2007) How the regulatory protein, IF_1, inhibits F_1-ATPase from bovine mitochondria. *Proc. Natl. Acad. Sci. U.S.A.* **104,** 15671–15676
4. Bason, J. V., Montgomery, M. G., Leslie, A. G., and Walker, J. E. (2014) Pathway of binding of the intrinsically disordered mitochondrial inhibitor protein to F_1-ATPase. *Proc. Natl. Acad. Sci. U.S.A.* **111,** 11305–11310
5. Shirakihara, Y., Shiratori, A., Tanikawa, H., Nakasako, M., Yoshida, M., and Suzuki, T. (2015) Structure of a thermophilic F_1-ATPase inhibited by an ϵ-subunit: deeper insight into the ϵ-inhibition mechanism. *FEBS J.* **282,** 2895–2913
6. Morales-Ríos, E., de la Rosa-Morales, F., Mendoza-Hernández, G., Rodríguez-Zavala, J. S., Celis, H., Zarco-Zavala, M., and García-Trejo, J. J. (2010) A novel 11-kDa inhibitory subunit in the F_1F_0 ATP synthase of *Paracoccus denitrificans* and related α-proteobacteria. *FASEB J.* **24,** 599–608
7. Zarco-Zavala, M., Morales-Ríos, E., Mendoza-Hernández, G., Ramírez-Silva, L., Pérez-Hernández, G., and García-Trejo, J. J. (2014) The ζ subunit of the F_1F_0-ATP synthase of α-proteobacteria controls rotation of the nanomotor with a different structure. *FASEB J.* **28,** 2146–2157
8. Minauro-Sanmiguel, F., Bravo, C., and García, J. J. (2002) Cross-linking of the endogenous inhibitor protein (IF1) with rotor (γ, ϵ) and stator (α) subunits of the mitochondrial ATP synthase. *J. Bioenerg. Biomembr.* **34,** 433–443
9. Serrano, P., Geralt, M., Mohanty, B., and Wüthrich, K. (2014) NMR structures of α-proteobacterial ATPase-regulating ζ-subunits. *J. Mol. Biol.* **426,** 2547–2553
10. Tsunoda, S. P., Rodgers, A. J., Aggeler, R., Wilce, M. C., Yoshida, M., and Capaldi, R. A. (2001) Large conformational changes of the ϵ subunit in the bacterial F_1F_0 ATP synthase provide a ratchet action to regulate this rotary motor enzyme. *Proc. Natl. Acad. Sci. U.S.A.* **98,** 6560–6564
11. Pettersen, E. F., Goddard, T. D., Huang, C. C., Couch, G. S., Greenblatt, D. M., Meng, E. C., and Ferrin, T. E. (2004) UCSF Chimera: a visualization system for exploratory research and analysis. *J. Comput. Chem.* **25,** 1605–1612
12. Guex, N., Peitsch, M. C., and Schwede, T. (2009) Automated comparative protein structure modeling with SWISS-MODEL and Swiss-PdbViewer: a historical perspective. *Electrophoresis* **30,** S162–S173
13. Chen, V. B., Arendall, W. B., 3rd, Headd, J. J., Keedy, D. A., Immormino, R. M., Kapral, G. J., Murray, L. W., Richardson, J. S., and Richardson, D. C. (2010) MolProbity: all-atom structure validation for macromolecular crystallography. *Acta Crystallogr. D Biol. Crystallogr.* **66,** 12–21
14. García, J. J., Morales-Ríos, E., Cortés-Hernandez, P., and Rodríguez-Zavala, J. S. (2006) The inhibitor protein (IF1) promotes dimerization of the mitochondrial F_1F_0-ATP synthase. *Biochemistry* **45,** 12695–12703
15. Schägger, H., and von Jagow, G. (1987) Tricine-sodium dodecyl sulfate-polyacrylamide gel electrophoresis for the separation of proteins in the range from 1 to 100 kDa. *Anal. Biochem.* **166,** 368–379
16. Ogilvie, I., and Capaldi, R. A. (1999) Mutation of the mitochrondrially encoded ATPase 6 gene modeled in the ATP synthase of *Escherichia coli*. *FEBS Lett.* **453,** 179–182
17. Lowry, O. H., Rosebrough, N. J., Farr, A. L., and Randall, R. J. (1951) Protein measurement with the Folin phenol reagent. *J. Biol. Chem.* **193,** 265–275
18. Morales-Rios, E., Montgomery, M. G., Leslie, A. G. W., García-Trejo, J. J., and Walker, J. E. (2015) Structure of a catalytic dimer of the α- and β-subunits of the F-ATPase from *Paracoccus denitrificans* at 2.3 Å resolution. *Acta Crystallogr. F Struct. Biol. Commun.* **71,** 1309–1317
19. Sagan, L. (1967) On the origin of mitosing cells. *J. Theor. Biol.* **14,** 255–274
20. Margulis, L., and Chapman, M. J. (1998) Endosymbioses: cyclical and permanent in evolution. *Trends Microbiol.* **6,** 342–345; discussion 345–346
21. John, P., and Whatley, F. R. (1975) *Paracoccus denitrificans* and the evolutionary origin of the mitochondrion. *Nature* **254,** 495–498
22. Ku, C., Nelson-Sathi, S., Roettger, M., Sousa, F. L., Lockhart, P. J., Bryant, D., Hazkani-Covo, E., McInerney, J. O., Landan, G., and Martin, W. F. (2015) Endosymbiotic origin and differential loss of eukaryotic genes. *Nature* **524,** 427–432
23. Wilkens, S., and Capaldi, R. (1998) Solution structure of the epsilon subunit of the F_1-ATPase from *Escherichia coli* and interactions of this subunit with β subunits in the complex. *J. Biol. Chem.* **273,** 26645–26651
24. Rodgers, A. J., and Wilce, M. C. (2000) Structure of the γ-ϵ complex of ATP synthase. *Nat. Struct. Biol.* **7,** 1051–1054
25. Tuena de Gómez-Puyou, M. T., Muller, U., Dreyfus, G., Ayala, G., and Gómez-Puyou, A. (1983) Regulation of the synthesis and hydrolysis of ATP by mitochondrial ATPase. Role of the natural ATPase inhibitor protein. *J. Biol. Chem.* **258,** 13680–13684
26. Cabezón, E., Montgomery, M. G., Leslie, A. G., and Walker, J. E. (2003) The structure of bovine F_1-ATPase in complex with its regulatory protein IF1. *Nat. Struct. Biol.* **10,** 744–750
27. García, J. J., and Capaldi, R. A. (1998) Unisite catalysis without rotation of the γ-epsilon domain in *Escherichia coli* F_1-ATPase. *J. Biol. Chem.* **273,** 15940–15945
28. Zarco-Zavala, M., Morales-Ríos, E., Serrano-Navarro, P., Wüthrich, K., Mendoza-Hernández, G., Ramírez-Silva, L., García-Trejo, J. J. (2013) Corringendum to: The ζ subunit of the α-proteobacterial F_1F_0-ATP synthase in *Paracoccus denitrificans*: a novel control mechanism of the central rotor. *Biochim. Biophys. Acta* **1827,** 60